ANALYSIS METHODOLOGY, DISTRIBUTION, AND HEALTH RISK ASSESSMENT OF SIZE-SEGREGATED AIRBORNE MICRO(NANO)PLASTICS

PhD Dissertation

Parisa AKBARI DANA

Eskişehir 2025

ANALYSIS METHODOLOGY, DISTRIBUTION, AND HEALTH RISK ASSESSMENT OF SIZE-SEGREGATED AIRBORNE MICRO(NANO)PLASTICS

Parisa AKBARI DANA

PhD DISSERTATION

Department of Environmental Engineering

Supervisor: Prof. Dr. Kadir GEDİK

(Co-Supervisor: Prof. Dr. Eftade GAGA)

Eskişehir

Eskişehir Technical University

Institute of Graduate Programs

June 2025

This thesis has been supported by TÜBİTAK (No: 121Y142) and ESTÜ-BAP (No:24ADP056).

FINAL APPROVAL FOR THESIS

This thesis titled "ANALYSIS METHODOLOGY, DISTRIBUTION, AND HEALTH RISK ASSESSMENT OF SIZE-SEGREGATED AIRBORNE MICRO(NANO)PLASTICS" has been prepared and submitted by "Parisa AKBARI DANA" in partial fulfillment of the requirements in "Eskişehir Technical University Directive on Graduate Education and Examination" for the Degree of Doctor in Environmental Engineering Department has been examined and approved on 27.06.2025.

Committee Members	**Title, Name and Surname**	**Signature**
Member	Prof. Dr. Kadir GEDİK	
Member	Prof. Dr. Tuncay DÖĞEROĞLU	
Member	Prof. Dr. Mustafa ODABAŞI	
Member	Prof. Dr. Mehmet KODAL	
Member	Prof. Dr. Sema YURDAKUL	

Prof. Dr. Harun BÖCÜK

Director of the Institute of Graduate Programs

27/06/2025

SUPERVISOR APPROVAL

PhD student Parisa AKBARI DANA, whom I supervise, has completed this thesis titled "ANALYSIS METHODOLOGY, DISTRIBUTION, AND HEALTH RISK ASSESSMENT OF SIZE-SEGREGATED AIRBORNE MICRO(NANO)PLASTICS". According to my inspections, the work is scientifically and ethically appropriate for the student to the thesis defense exam.

Supervisor

Prof. Dr. Kadir GEDİK

ABSTRACT

ANALYSIS METHODOLOGY, DISTRIBUTION, AND HEALTH RISK ASSESSMENT OF SIZE-SEGREGATED AIRBORNE MICRO(NANO)PLASTICS

Parisa AKBARI DANA

Department of Environmental Engineering

Eskişehir Technical University, Institute of Graduate Programs, June 2025

Supervisor: Prof. Dr. Kadir GEDİK

(Co-Supervisor: Prof. Dr. Eftade GAGA)

The objective of this study is to investigate airborne micro(nano)plastics (MNPs) that were collected from industrial, rural, and urban areas using a high-volume size-segregated sampler. A sample pretreatment and the optimization of the sampling parameters (a flow rate of 40 cfm for eight hours) were conducted, and the slotted Teflon filter, which was placed in both the five-stage and the glass fiber in the nano-fraction stage, was analyzed without pretreatment by particle (μ-Raman and SEM-EDX) and mass-based analysis (Pyr-GC/MS). The distribution of MNPs was found to vary according to geographical location, with concentrations observed in the industrial (1.8±3.1 μg/m³), urban (2.2±4.4 μg/m³), and rural/suburban (1.5±2.4μg/m³) regions. The majority of these particles (approximately 95%) were found to be in the form of fragments, while the remaining 5% were classified as fibers with a chemical identity of carbon black in particle-based analysis. Of the polymers analyzed by the mass-based approach (i.e., PE, PET, PP, PVC, PS, PC, SBR, and NR), results revealed that tire-derived rubbers (SBR, NR), along with PE, were the predominant polymers, with urban areas exhibiting substantial contributions from tire and brake wear in the nano-fraction stage. The results indicated that levels of MNP were elevated during daytime hours in urban areas and during winter months in rural regions. A subsequent statistical analysis revealed moderate correlation (R^2=0.64) between PM (<0.49 μm) and MNPs abundance in backup stage. An exposure assessment was conducted according to particle-based and mass-based data, indicating that smaller MNPs, particularly during urban nights and rural winter days, pose a heightened risk to pulmonary health. The findings underscore the importance of implementing standard procedures and specific strategies to address the pervasive presence and health effects of airborne MNPs for better air quality management and policy development.

Keywords: Air pollution, Plastic particles, Active sampling, Particle-based analysis, Mass-based analysis.

ÖZET

HAVADAKİ BOYUT AYRIMLI MİKRO(NANO)PLASTİKLERİN ANALİZ METODOLOJİSİ, DAĞILIMI VE SAĞLIK RİSKİ DEĞERLENDİRMESİ

Parisa AKBARI DANA

Çevre Mühendisliği Anabilim Dalı

Eskişehir Teknik Üniversitesi, Lisansüstü Eğitim Enstitüsü, Haziran 2025

Danışman: Prof. Dr. Kadir GEDİK

İkinci Danışman: Prof. Dr. Eftade GAGA

Bu çalışmanın amacı, yüksek hacimli boyut ayrıştırmalı bir örnekleyici kullanılarak endüstriyel, kırsal ve kentsel alanlardan toplanan havadaki mikro(nano)plastiklerin (MNP'ler) incelenmesidir. Numune ön arıtım ve örnekleme parametrelerinin optimizasyonu (sekiz saat boyunca 40 cfm akış hızı) gerçekleştirilmiş, beş kademeli ayrıştırıcılara yerleştirilen oluklu Teflon filtre ve nano-fraksiyon kademesine yerleştirilen cam elyaf filtre, parçacık (μ-Raman ve SEM-EDX) ve kütle bazlı yaklaşım (Pyr-GC/MS) ile ön işlem yapılmadan analiz edilmiştir. MNP dağılımının coğrafi konuma göre endüstriyel (1.8±3.1 μg/m³), kentsel (2.2±4.4 μg/m³), ve kırsal/yarı-kentsel (1.5±2.4 μg/m³) bölgelerde değiştiği tespit edilmiştir. Parçacık bazlı analizlerde, örneklenen partiküller karbon karası olarak tanımlanmış, çoğunluğu (yaklaşık %95) parça şeklinde ve kalan %5'lik kısım lif olarak sınıflandırılmıştır. Kütle bazlı yaklaşımla analiz edilen polimerlerden (PE, PET, PP, PVC, PS, PC, SBR ve NR) elde edilen bulgular, lastik türevi maddelerin (SBR, NR) PE ile birlikte baskın polimerler olduğunu ve kentsel bölgelerin nano fraksiyon kademesine lastik ve fren aşınmasından kaynaklanan önemli katkılar sergilediğini ortaya koymuştur. Bulgular, MNP seviyelerinin kentsel bölgelerde gündüz saatlerinde, kırsal bölgelerde ise kış aylarında yükseldiğini göstermiştir. Devamında yapılan istatistiksel analiz, son kademedeki (backup) PM (<0,49 μm) ile MNP arasında orta düzeyde anlamlı bir korelasyon (R^2=0.64) olduğunu ortaya koymuştur. Parçacık ve kütle bazlı verilere göre yapılan maruziyet değerlendirmesi, özellikle kentsel gecelerde ve kırsal kış günlerinde daha küçük MNP'lerin akciğer sağlığı için daha yüksek bir risk oluşturduğunu göstermiştir. Sonuçlar, hava kalitesi yönetimi ve politika geliştirilmesi için havadaki MNP'lerin varlığını, dağılımını ve sağlık etkilerini ele almak üzere standart prosedürlerin ve özel stratejilerin uygulanmasının önemini vurgulamaktadır.

Anahtar Sözcükler: Hava kirliliği, Plastik partiküller, Aktif örnekleme, Partikül bazlı analiz, Kütle bazlı analiz.

ACKNOWLEDGEMENTS

I would like to express my deepest gratitude to my professors for their invaluable guidance, unwavering support, and insightful feedback throughout the course of this research, which has been instrumental in the successful completion of this thesis.

Special thanks to: Prof. Dr. Kadir GEDİK, and Prof. Dr. Eftade GAGA

Prof. Dr. Tuncay DÖĞEROĞLU (Eskişehir Technical University)

Prof. Dr. Mustafa ODABAŞI (Dokuz Eylül University)

Prof. Dr. Mehmet KODAL (Kocaeli University)

Prof. Dr. Sema YURDAKUL (Süleyman Demirel University)

Doç. Dr. Yasemin ÇELİK (Eskişehir Technical University)

Prof. Dr. Servet TURAN (Eskişehir Technical University)

Doç. Dr. Sinem BAŞKUT (Eskişehir Technical University)

Prof. Dr. Ender SUVACI (Eskişehir Technical University)

Dr. Öğr. Üyesi Gül İpek SELİMOĞLU (Eskişehir Technical University)

Öğr. Gör. Dr. Mehmet Ali IŞIKOĞLU (Eskişehir Technical University)

Dr. Öğr. Üyesi İlker BALCILAR (Eskişehir Technical University)

Prof. Dr. Serdar GÖNCÜ (Eskişehir Technical University)

Doç. Dr. Rafig GURBANOV (Bilecik Şeyh Edebali University)

Doç. Dr. Gökhan DİKMEN (Eskişehir Osmangazi University)

Prof. Dr. Onur KOYUNCU (Eskişehir Osmangazi University)

Finally, I sincerely thank Doç. Dr. Nuray GEDİK for her invaluable guidance in scientific research and academic writing, which greatly contributed to the quality and success of this work.

Parisa AKBARI DANA

27/06/2025

STATEMENT OF COMPLIANCE WITH ETHICAL PRINCIPLES AND RULES

I hereby truthfully declare that this thesis is an original work prepared by me; that I have behaved in accordance with the scientific ethical principles and rules throughout the stages of preparation, data collection, analysis and presentation of my work; that I have cited the sources of all the data and information that could be obtained within the scope of this study, and included these sources in the references section; and that this study has been scanned for plagiarism with "scientific plagiarism detection program" used by Eskişehir Technical University, and that "it does not have any plagiarism" whatsoever. I also declare that, if a case contrary to my declaration is detected in my work at any time, I hereby express my consent to all the ethical and legal consequences that are involved.

Parisa AKBARI DANA

CONTENTS

LIST OF TABLES

LIST OF FIGURES

GLOSSARY OF SYMBOLS AND ABBREVIATIONS

ABS	:	Acrylonitrile-butadiene-styrene
AC	:	Acceptable concentration
Al	:	Aluminum
BWPs	:	Brake wear particles
Ca	:	Calcium
CCN	:	Cloud condensation nuclei
Cfm	:	cubic feet per minute
EC	:	Exposure concentration
EPA	:	Environmental protection agency
Fe	:	Iron
HQI	:	Hit quality index
ICRP	:	International Commission on Radiological Protection
LOD	:	Limit of detection
MPs	:	Microplastics
MNPs	:	Micro(nano)plastics
Na	:	Sodium
NGOs	:	Non-governmental organizations
NOAECs	:	No observed adverse effects concentrations
NR	:	Natural rubber
PA66	:	Polyamide 66
PAHs	:	Polycyclic aromatic hydrocarbons
PC	:	Polycarbonate
PE	:	Polyethylene
PET	:	Polyethylene Terephthalate

PMMA	:	Polymethyl methacrylate
PP	:	Propylene
PTR-MS	:	Proton-Transfer Reaction-Mass Spectrometry
PS	:	Polystyrene
PTFE	:	Polytetrafluoroethylene
PVC	:	Polyvinyl chloride
Pyr-GC/MS	:	Pyrolysis gas chromatography mass spectrometry
RfC	:	Reference of concentration
ROS	:	Reactive Oxygen Species
S	:	Sulfur
SBR	:	Styrene butadiene rubber
SEM-EDX	:	Scanning electron microscope energy dispersive X-ray spectroscopy
Si	:	Silicon
SNR	:	Signal to noise ratio
TSP	:	Total suspended particles
TWPs	:	Tire wear particles
Zn	:	Zinc

1. INTRODUCTION

1.1. General Overview

In the ongoing endeavor to record and understand the changes occurring within the Earth's ecosystem, the scientific community has recently introduced a new term, the 'Anthropocene' (Waters and Turner, 2022). In the Anthropocene, the considerable and pervasive impact of human activity on Earth's ecosystems is evident in a multitude of ways. Anthropogenic airborne particles are those which have been produced by human activities, including industrial processes, transportation, and the combustion of fuels. These particles impact air quality, harm human health (e.g., causing respiratory and cardiovascular issues), affect ecosystems, and influence climate by either cooling (e.g., sulfates reflect sunlight) or warming (e.g., black carbon absorbs heat). The reduction of emissions through the implementation of cleaner technologies and the enactment of more stringent regulations represents a crucial strategy for the mitigation of their effects (Smichowski and Gómez, 2024).

One of the most notable characteristics of the Anthropocene is the exponential growth of plastic pollution, which has reached a point where it is now one of the most ubiquitous materials on the planet (Rangel-Buitrago et al., 2024). Plastics, derived from petrochemicals, are characterized by their durability, versatility, and low cost, which has led to their becoming an integral part of modern life (Waters and Turner, 2022). The earliest known human-made plastic was nitrocellulose, a substance known as Parkesine. This was first synthesized in 1862 and subsequently became the first completely synthetic plastic, namely a phenolic resin with the trade name Bakelite. The latter invention was credited to Leo Baekeland in 1907 (Crawford and Quinn, 2016). Figure 1.1 illustrates the evolution of plastic production over time. It has been estimated that approximately 8.3 billion metric tons of plastic have been manufactured since the 1950s, with approximately 60% of this amount discarded in landfills or the natural environment (Tsakona, 2021). In the course of 2021, the highest production amounts ever achieved were reached, with 390.7 million tons produced (Borase, 2023).

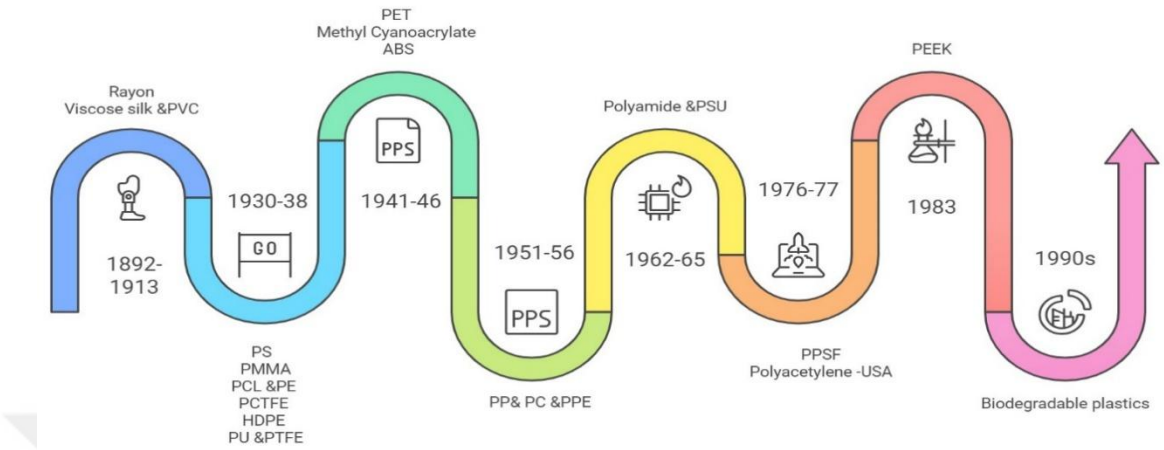

Figure 1.1. *Appearance and development of major plastic types and products. PEEK, poly (aryl ether ether ketone); PPSF, polyphenylethersulphone; PSU, polysulphone; PI, polyimide;PPE, polyphenylene ether; POM, polyformaldehyde; PC, polycarbonate; PP, polypropylene; ABS, acrylonitrile butadiene styrene; PET, polyethylene terephthalate; PTFE, polytetrafluoroethylene; PU, polyurethane; HDPE, high-density polyethylene; PA, polyamide; PCTFE, polychlorotrifluoroethylene;PCL, polycaprolactone; PE, polyethylene; LDPE, low-density polyethylene; PMMA, poly(methyl methacrylate); PS, polystyrene; PAN, polyacrylonitrile; PVC, polyvinyl chloride.*

The global spread of the Covid-19 virus has led to a significant increase in the demand for plastic and single-use plastic products (SUPs), which have become one of the three most widely produced materials in the world, alongside steel and cement (Kibria et al., 2023). The advent of the global pandemic caused by the COVID-19 has resulted in an estimated doubling of the quantity of plastic waste generated. Projections indicate that the total volume of global plastic waste could reach approximately 630 million tons in 2020 alone, representing a significant increase from the approximately 380 million tons of plastic waste produced globally in 2018, the year preceding the pandemic (Rai et al., 2023).

It is notable that over the past 50 years, the volume of plastic waste has increased in parallel with the growth in plastic production, given that a significant proportion of plastic products are designed for single use. It is estimated that approximately 22 million tons of plastics (comprising 19.4 million tons of macro and 2.6 million tons of micro plastic particles) were released into the global environment in 2019. In the absence of new policy measures, it is anticipated that the generation of plastic waste could exceed 800 million tons

by 2050, with this quantity increasing twofold by 2060 (Ilyas et al., 2024; Rai et al., 2023). The pivotal role of polymeric particles in the conceptualization and comprehension of the Anthropocene has prompted the proposition that the time interval be alternatively designated the Plasticene (Haram et al., 2020).

The term 'microplastics (MPs)' was first coined by Thompson et al. (2004) to describe the small plastic particles that have become a significant environmental concern on a global scale. These particles were first identified in plankton samples dating back to the 1960s, and their abundance has increased significantly over time (Ostle et al., 2019). When discarded in the environment, plastics undergo a gradual process of decomposition or fragmentation into MPs (with a diameter of less than 5 mm) as a result of mechanical wear, weathering, solar radiation, and the activity of microorganisms (Evangeliou et al., 2020; Hale et al., 2020). This phenomenon gives rise to what is known as secondary MPs, (the release of small particles intended for specific applications and the degradation of larger plastics) which are subject to further investigation (Evangeliou et al., 2020; Hale et al., 2020). In the meantime, the MPs (e.g., cosmetic additives) that are produced and released directly into the environment represent the primary source of MPs (Hale et al., 2020; Y. Zhang et al., 2020). It is possible for MPs to undergo further decomposition, resulting in the formation of nanoplastics (NPs) with a diameter typically ranging from 1 nanometer (nm) to 1 micrometer (μm) in size (Lai et al., 2022; Ng et al., 2018). They have been detected in terrestrial, aquatic, and atmospheric systems across the globe. The detection of micro(nano)plastics (MNPs) across a range of environmental matrices, including water, sediments, soil, biota and air, demonstrates their pervasive presence and the associated ecological risks. The pervasive contamination highlights the necessity for the establishment of uniform sampling techniques and comprehensive monitoring strategies to ascertain the full extent of MNPs pollution and its impact on ecosystems and human health.

1.2. The Background of the Study

Following the inception of the term "microplastic" in 2004, scientific studies on micro-sized plastic waste demonstrated a gradual development, with an average of fewer than 1 publication per year until 2010. A steady growth phase ensued (average >35 publications per

year) until 2016, after which a rapid development process (average >300 publications per year) has been observed (X. Zhang et al., 2022). On the other hand, a comprehensive study conducted through the Web of Science Core Collection, which analyzed 1,039 papers, provided insights into the distribution and characteristics of MNPs in diverse environmental compartments (Wang et al., 2024). In terms of distribution, the soil contains a notable quantity of MNPs, with an average concentration of 12,107.42 items/kg dw. In comparison, water bodies have an average concentration of 97,271.18 items/m^3 (97.27118 item/l). The atmospheric presence of MNPs also contributes to the overall pollution load, although specific concentration data in the atmosphere were not detailed in the study (Wang et al., 2024). The study of atmospheric MNPs is a relatively nascent field of research, particularly in comparison to the extensive body of work that has been conducted on marine and terrestrial MNPs. A substantial proportion of MP studies (>96%) pertain to marine and aquatic ecosystems (Xu et al., 2020). Consequently, the air medium has remained unexplored in the field of MP research, which has a history of about 20 years. As a result, the comparison and interpretation of MNP pollution has become difficult due to the fact that the quantitative findings obtained (such as numbers instead of mass) are not obtained within a certain standard (X. Zhang et al., 2022). As scientists begin to elucidate the prevalence and effects of these particles, it becomes evident that a comprehensive understanding of their role in atmospheric processes is essential for a full assessment of the overall environmental impact (Haque and Fan, 2023).

A significant obstacle to the establishment of standardized methodologies is the absence of harmonization in the current sampling and analytical techniques employed. A significant proportion of scientists (78.4%) identify this as a major challenge in MPs research, as indicated by recent findings (Prata et al., 2024). MNPs are not uniformly distributed in the environment; this variability presents a challenge for the development of a universal sampling method, as different environments may necessitate the implementation of bespoke approaches to ensure accurate results (Lv et al., 2021). The plethora of analytical techniques available for MNPs analysis introduces further complications to the process of standardization. The application of diverse methodologies, including visual analysis, spectroscopy (i.e., FTIR, μ-FTIR or Raman and μ- Raman), and mass spectrometry, has been

observed to yield disparate outcomes contingent upon the specific approach employed. The combination of methodological diversity, environmental variability, contamination challenges, resource limitations, and evolving research needs has resulted in the absence of standardized sampling methods for MNPs. Ongoing efforts by international bodies and research communities are aimed at addressing these challenges through collaborative initiatives and the establishment of comprehensive guidelines. The implementation of standardized sampling and analytical procedures ensures consistency and minimizes variability in data collection techniques, thereby facilitating more reliable comparisons of MNPs concentrations and types across diverse environmental contexts. The standardization of MNPs sampling methods is a crucial step in enhancing the reliability and comparability of research findings. It enhances the accuracy of data, facilitates regulatory efforts, addresses contamination issues, and promotes best practices within the scientific community. As awareness of MNPs pollution continues to grow, the establishment of standardized methodologies will be critical for the development of effective monitoring and management strategies (Prata et al., 2024).

The current methods used to detect MNPs in the atmosphere employ a range of sophisticated techniques and technologies with the objective of evaluating exposure levels and elucidating potential human health risks. Active sampling methods, such as high-volume air samplers, are frequently employed to collect airborne MNP particles. Such samplers draw substantial volumes of air through filters that are specifically designed to capture particulate matter, including MNPs (Han et al., 2024). The current research indicates that atmospheric MNPs may interact with other pollutants and climate factors in complex ways that are not yet fully understood. For instance, atmospheric MNPs have the potential to act as cloud condensation nuclei (CCN), which are essential for cloud formation. Research has demonstrated that these particles can impact the formation of ice crystals at temperatures that are warmer than would typically occur in the absence of the particles, which may result in alterations to precipitation patterns (Aeschlimann et al., 2022). Conversely, the inhalation of airborne MNPs represents a direct health risk, as these particles can be inhaled by humans and animals alike. Research findings indicate that individuals may potentially inhale considerable quantities of MNPs on a daily basis, which gives rise to concerns regarding

respiratory health and systemic exposure to toxic substances adsorbed onto these particles (Bourzac, 2022). These findings underscore the necessity for additional research to be conducted on such interactions.

The research objectives were designed with the intention of successfully achieving the study's overall aims. The study's innovative approach centered on identifying characteristics of inhalable MNPs less than 10 microns that are captured by a size-segregated high-volume sampler. This sampler is based on six different levels of aerodynamic particle size that have the potential to remain in the atmosphere for extended periods of time. Consequently, in order to collect suspended MNPs, it was necessary to develop a suitable filter membrane for the sampling process and preparation of samples, taking into account the specific size of airborne MNPs. In addition, we would like to propose the use of microscopic and thermal identification techniques for the purpose of comparing their results. The objectives that we have outlined are as follows:

- ✓ To establish a method that encompasses the separation and identification of MNPs < 10 μm in the atmosphere. This method should be specific to this field and should form part of a broader methodological approach.
- ✓ To determine the presence of airborne MNPs in samples with varying size distributions, additionally, morphological characterization, and chemical identification through microscopy (optical), μ-Raman, pyrolysis-GC/MS, and SEM/EDX analysis.
- ✓ To determine the distribution of MNPs in diurnal and nocturnal, spatial (urban, rural, industrial), seasonal (summer, winter) cycles, based on particle (μ-Raman) and/or mass-based (pyrolysis-GC/MS) analysis.
- ✓ To carry out risk assessment of respiratory human health based on the number and mass concentration of airborne MNP particles.

2. LITERATURE REVIEW

2.1. An Overview of Environmental Micro(nano)plastics

It is a common characteristic of traditional plastic materials to demonstrate a high level of resistance to degradation. Based on the properties inherent to plastics and the surrounding environmental conditions, the lifespan of these materials can be expected to span hundreds or even thousands of years (Zhang et al., 2021). Despite the slow rate at which it occurs, environmental weathering continues to deteriorate plastics, leading to alterations in polymer properties due to a combination of abiotic and biotic processes (Debroas et al., 2017). The general processes of plastic degradation are illustrated in Figure 2.1.

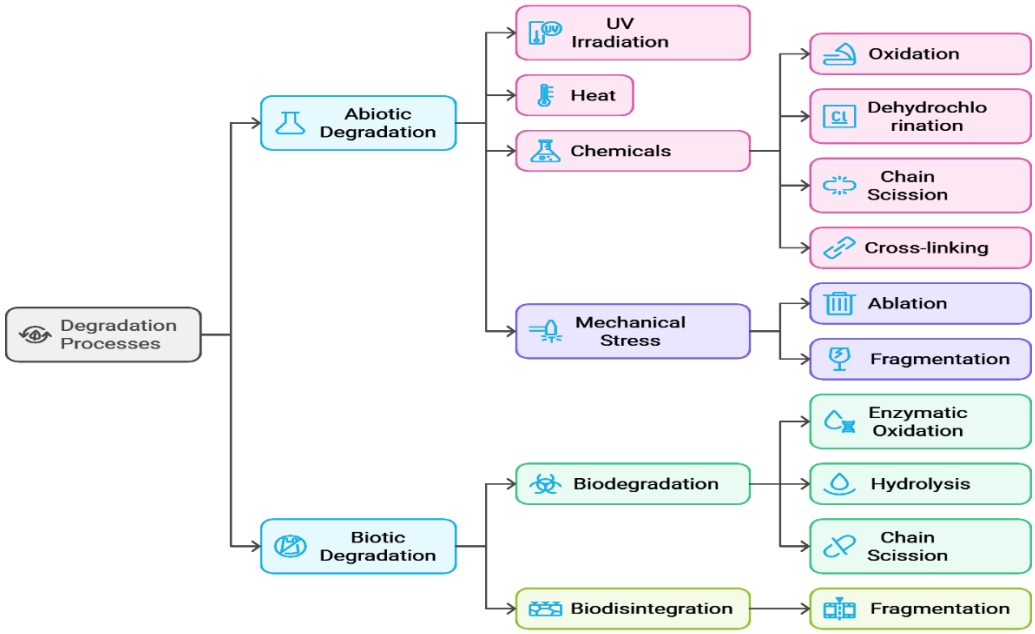

Figure 2.1. *The schematic diagram illustrates the principal processes involved in the degradation of plastics(Debroas et al., 2017).*

Abiotic degradation of plastics encompasses alterations in the physical and chemical properties of these materials due to factors such as light, temperature, air, water, and mechanical forces. It can be anticipated that abiotic degradation will typically precede biodegradation, given the limited bioavailability of plastics (Bergmann et al., 2015). The

process of biotic degradation of plastics refers to the deterioration of plastics caused by organisms. This can occur either physically, whereby the plastic is degraded by the organisms biting, chewing or digesting it, or chemically, whereby the plastic is degraded by the action of enzymes produced by the organisms (Cau et al., 2020; Mateos-Cárdenas et al., 2020).

It is widely acknowledged that MNPs represent a pervasive contaminant, occurring in a multitude of environmental settings across the globe. Their pervasive presence has been documented in a multitude of ecological compartments, including the atmosphere, hydrosphere, lithosphere, and even within human tissues (Moyo, 2022). It has been established that a considerable quantity of plastic waste is transported into the marine environment via continental sources. This is predominantly conveyed by rainwater runoff in freshwater, industrial discharge, urban wastewater, resuspension from coastal sediments and agricultural runoff (Yubo Li et al., 2020). The density of MNPs determines whether they will float or sink in water. MNPs with low densities, such as polypropylene and polyethylene, are more prone to floating on water. Conversely, polyethylene terephthalate, polyvinyl chloride and polystyrene are high-density MP fragments that are inclined to sink in water (Patidar et al., 2024). Recent research has revealed the existence of key mechanisms through which marine low-density MNPs that float in surface water are transported from the ocean into the atmosphere (Patidar et al., 2024).

The majority of research to date has concentrated on MNPs in marine environments. However, there is still a paucity of knowledge regarding the hydrosphere, geosphere, and atmosphere (Allen et al., 2020). In studies conducted by researchers from Princeton and Cornell University, it was estimated that approximately 100,000 metric tons of MNPs may be emitted into the atmosphere as a result of the bursting bubbles process (Shiu et al., 2022). In recent times, there has been a growing interest in the study of MNPs in the atmosphere, particularly as a constituent of particulate matter in the smaller particle size ranges.

There are a number of interconnected environmental issues currently facing us, including the link between airborne MNPs pollution, climate change, and biodiversity loss (Cau et al., 2020). The correlation can be readily substantiated on the grounds of the considerable production of greenhouse gases during the manufacture of plastic -based products, which rely on fossil fuels (K. Li et al., 2024). While the majority of the academic

community concentrates its attention on the impact of MNPs on human health, this ultimately has the potential to disrupt the ecosystem as a whole, leading to the loss of species and diversity. Such alterations are irreversible, rendering the ecosystem unable to revert to its original state (Bergmann et al., 2015). It is imperative that further research be conducted into the sources, concentrations, and long-term effects on human health and the planet's climate systems of this emerging pollutant, which is a significant threat to public health and environmental sustainability.

2.2. Airborne Micro(nano)plastics

Nowadays, air pollution has emerged as a significant concern for the international community (such as the United Nations Environment Programme (UNEP), World Health Organization (WHO), and Environmental Protection Agency (EPA), etc.), largely due to its detrimental environmental impact and the concomitant increase in anthropogenic activities. This has led to a rise in MNPs particle production, driven by an expanding human population and industrialization. Airborne MNPs have been identified as one of the most significant recent air pollutants, attracting considerable attention from researchers, public media outlets, non-governmental organizations (NGOs), governmental bodies, and numerous other scientists worldwide (Amobonye et al., 2021). The pervasive dispersion of sources for airborne MNPs intensifies the environmental exposure to this pollutant. The predominant sources for primary MNPs encompass city dust resuspension, abrasion of synthetic rubber tires and roads (Dris et al., 2015). Further sources of contamination may include construction materials, poorly managed landfills, waste incineration (Liu et al., 2019a), fragments from clothing and house furniture (Klein and Fischer, 2019), industrial emissions, sewage sludge (Hatinoğlu and Sanin, 2021), and synthetic particles (Marnane et al., 2006). Particles used in horticultural soils (for example, polystyrene peat), tumble dryer exhaust, car seats' outer surfaces, obsolete garments (Marnane et al., 2006), and plastics recycling processes (X. Wang et al., 2020) have been identified as sources.

There is a paucity of studies that have identified traffic MNPs as a significant source of environmental MNPs (Baensch-Baltruschat et al., 2020). In a study, Järlskog et al. (2020) found tire and bitumen MNPs in samples collected from the road surface, stormwater, and

sweeper sediment. Their findings highlight the significant contribution of these MNPs to the overall emission levels. The analysis of environmental samples from roadside drains in Plymouth, UK, revealed that the wear aggregates from tires constitute a significant source of metal-related pollution in the drainage system (Knight et al., 2020). The MP levels in London's outdoor air have been estimated to be 20 times higher than in any remote rural location, which implies the influence of local sources such as people or vehicular movements (Wright et al., 2020). Similarly, MPs can also be released from brake wear particles, which are mainly composed of metals and plastics (fibers, binders, fillers, etc., from the brake lining). Grigoratos and Martini (2015) demonstrated that a frictional connection generated by the contact between a brake disk and pad, as well as the road surface and tire, produces heat and shear in the tires when a vehicle is in motion. The combination of these processes results in the formation of tire wear particles, which are subsequently released into the surrounding environment.

Kole et al. (2017) identified a number of factors that contribute to the formation of traffic MPs, including the structure and composition of tires, age, driving speed, climate, mode and nature of contact, as well as the type and condition of the road surface (pavement), define traffic MPs' size and amount. Panko et al.(2013) reported that tire wear and tear particles constituted up to 0.84% of PM_{10}, while Grigoratos and Martini (2014) and Kole et al. (2017) concluded that 0.1–10% of PM_{10} and 3–7% of atmospheric $PM_{2.5}$ are composed of tire wear and tear particles. Moreover, Ketzel et al.(2007) demonstrated that between 50 and 85 % of traffic-emitted PM_{10} particles have a non-exhaust origin.

2.2.1. Morphological characteristics

The morphology, size, color, shape, and surface mechanical wear of individual MNPs can be characterized by visual observation (i.e., stereo microscope), irrespective of the collection method employed, whether passive or active. Moreover, the implementation of automated image analysis processing software has the potential to the size of particles that can be measured in a single analysis session. Nevertheless, stereoscopic microscopy is unable to detect particles with a diameter of less than 100 μm, which fall within the accepted detection limit of optical instruments (Silva et al., 2018). Scanning electron microscopy

(SEM) was used to detect and characterize MNPs with smaller particle sizes (< 100 μm) in various studies (Abbasi et al., 2019; Yaowei Li et al., 2020; Löber et al., 2024). SEM enables the generation of a high-resolution image of the particle by directing a high-intensity electron beam onto the surface of the sample. This allows for the clear observation of the surface of MNPs and the determination of their microstructure (Shao et al., 2022a).The combined application of SEM and energy-dispersive X-ray spectroscopy (EDX) has been employed to analyze MNPs in the atmosphere. It is noteworthy that SEM-EDX represents a powerful means of individual particle analysis, can provide detailed qualitative information regarding the elements that constitute MNPs. Additionally, it can observe the surface morphology of MNPs, including features such as grooves, pits, cracks, and flakes (Shao et al., 2021; Shao et al., 2022b).

A variety of shapes and forms of airborne MNPs have been identified Figure 2.2, reflecting the diverse origins and behaviors of these particles in the atmosphere (AkbariDana et al., 2024a)

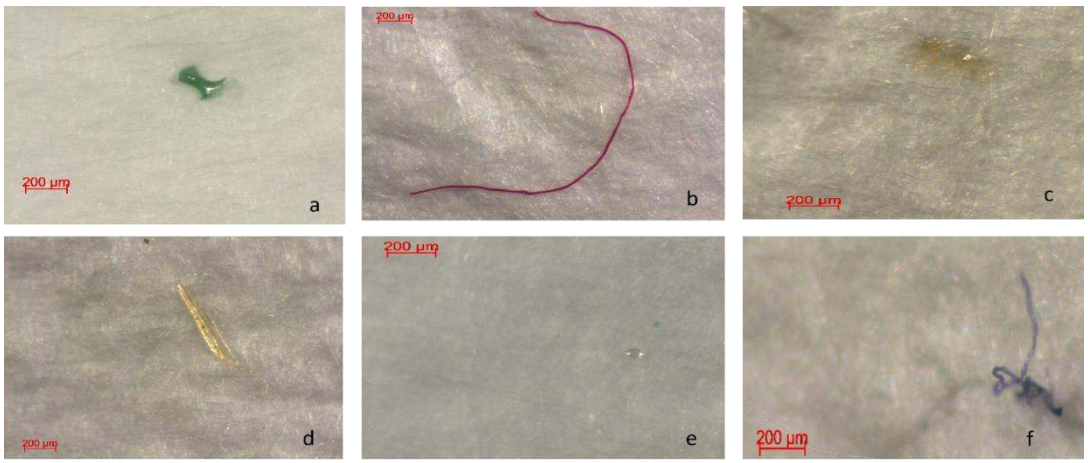

Figure 2.2. *Different shapes and colors of microplastics, a) fragment, b) fiber, c) film, d) filament, e) pellet, f) clump fiber (AkbariDana et al., 2024a).*

The shapes of these particles are contingent upon the original form of the primary MNPs, the degradation and erosion processes of the plastic particle surface, and the length of time that the particles have been in the environment (Rocha-Santos and Duarte, 2017). In urban centers such as Dongguan, Shanghai, Yantai, and Paris, fiber constitutes the majority

of atmospheric MNPs, representing over 60% of the total number of particles. In Hamburg (Germany), the dominant shape of atmospheric MNPs was fragmented, which accounted for 95% of the total particle numbers, with fibers representing only 5% (Klein and Fischer, 2019). In Iran, the most prevalent shapes of MPs in street dust were fibrous (33.5%) and granule (65.9%) types (Allen et al., 2019; Dehghani et al., 2017). The diverse shapes of MNPs may influence the transport of this pollutant through the environment. For example, films may be particularly thin and flat, thereby offering a greater surface area for atmospheric conveyance in comparison to fragments of an equivalent mass (Allen et al., 2019). Furthermore, particular shapes or dimensions of MNPs may exhibit enhanced potential to inflict physical harm upon biological systems. Smaller angular particles are observed to traverse membrane barriers with greater ease than particles exhibiting regular surfaces or extended edges (Rochman et al., 2019; Y. Zhang et al., 2020). Airborne MNPs were sampled through aircraft (air sampling within and above the planetary boundary layer), and the results demonstrated that urban air was commonly polluted by fragments, while rural/sub-rural air was predominantly polluted by fibers (González-Pleiter et al., 2021).

The size of plastic particles is a significant determinant of the way in which they interact with biota and the fate of their environment (Besseling et al., 2017). In general, a broad range of MP sizes, which are typically considered to be between 1 μm and 5 mm in length, and the limits for MP size are defined operationally based on the sampling and analysis method (Hartmann et al., 2019). The majority of airborne MPs are in the smallest size range, indicating a significant number of particles below the minimum limit size (typically <10 μm) (Allen et al., 2019; Bergmann et al., 2019). The consensus was that the enlargement of the MPs in question has resulted in a reduction in their overall abundance (Bergmann et al., 2017).

Dahl et al. (2006) identified a tire wear/tear size range of 15–50 nm (mean: 27 nm) in relation to the road, with mineral oils and carbon black fragments representing a significant portion of the particles. Kreider et al. (2010) employed a road simulator to assess the dimensions of particles and their interaction with the road surface, that they observed that the most of tire wear and tear particles ranged in size from 5 to 25 μm, with the overall distribution of particle sizes spanning from 4 to 350 μm. The objective of the study conducted

by Mathissen et al. (2011) was to determine the presence of airborne particles in the range of 6–562 nm in size during the processes of acceleration, braking, and cornering when driving. The findings revealed that the particles resulting from tire wear and tear fell within the size range of 30–60 nm. In a further study, a road simulator was constructed with the objective of indicating the number and size of particles within the range of 0.3–20 nm. Additionally, runoff samples were collected from the instrument and the walls for use as prototypical samples. The results indicated that the majority of PM_{10} particles were within the 0.3–1 μm range, with a weight-to-number ratio of particles ≤10 μm of less than 0.1% (Kaul and Sharma, 2009).

The MNPs identified in different environmental matrices have been observed to exhibit a range of colors. It has been established that the various colors of MNPs may reflect the numerous stages of degradation and/or the sources from which they originate (Enyoh et al., 2019). The following attributes have been made: opaque items have been attributed to LDPE, white items to PE, and transparent and clear items to PP (Rocha-Santos and Duarte, 2017). Nevertheless, color alone is not a reliable indicator of source and polymer type for MNPs, as analytical bias may occur (Rochman et al., 2019). The use of colorants can influence the photoaging process of plastics, as well as the adsorption and degradation of MNP pollutants (Zhao et al., 2022). Furthermore, UV degradation can be utilized to regulate the release of specific colorants, such as cadmium, from cadmium-colored MNPs (H. Liu et al., 2020). Cadmium is one of the heavy metals used as an inorganic MNP pigment. The leaching of these metals from MNPs into the environment is identified as one of the most significant environmental impacts of MNPs. The research literature on atmospheric MPs has focused on specific colors for identified plastics.

The fallout MNPs samples collected from Lake Donghu (China) were found to be mainly transparent (64.4%), blue (18.6%), and red (9.5%)(Xia et al., 2020). The analysis of air samples from Christchurch (New Zealand) revealed the presence of black, red, clear, and blue fibrous MPs. In contrast, snow samples deposited near Demon Lake in the Italian Carnic Alps showed the presence of light blue PET, representing the only identified type of MPs (Knobloch et al., 2021). The analysis of suspended dust samples from the urban region of Bushehr port (Iran) revealed the presence of MNPs with a variety of colors, including black

(21%), grey (12%), white/transparent (39%), orange (8%), and red (20%) (Akhbarizadeh et al., 2021). While the presence of black MPs is more prevalent in urban samples than in remote samples, the high proportion of these particles in both categories underscores the need for regulating the most common sources of MNPs, such as tire wear particles (TWPs) and brake wear particles (BWPs). However, black MNPs are less prone to long-range atmospheric transport than other colors under examination, they are susceptible to short-distance biotic and abiotic transport pathways (Lwanga et al., 2022). The underlying mechanism that governs this phenomenon is attributed to the highlight absorption and low UV transmittance characteristics of the particles, which result in accelerated settling and diminished fragmentation. Consequently, this reduces their atmospheric residence time (Zhao et al., 2022). Nevertheless, these particles remain vulnerable to local redistribution by biological and physical processes. Consequently, short-distance biotic and abiotic transport pathways are significant for determining their environmental fate (Schefer et al., 2025). There is significant concern regarding the impact of dark-colored MNPs on the surface albedo in cryosphere regions. Research has shown that they have a positive net radiative effect, similar to that of carbon black, which increases the melting rate of snow and ice (Y.-L. Zhang et al., 2022).

2.2.2. Chemical identification

The chemical composition of environmental MNPs can be identified using a combination of advanced analytical techniques including particle-based (Raman, FTIR) and mass-based (Pyr-GC/MS) methods. Pyrolysis coupled with gas chromatography mass spectrometry (Pyr-GC/MS) is a thermochemical technique that has been widely adopted for the characterization of airborne MNPs (Hermabessiere et al., 2018). Pyr-GC/MS is a destructive technique that analyzes pyrolysis spectra of a polymer's decomposition products and compares them to the system's library in order to identify the composition of the MNPs (Löder and Gerdts, 2015). The numerous benefits of this technique, including the use of a very small quantity of samples, the ability to detect particles of a very small size, minimal contamination risks, high sensitivity, and a short measurement time, have led to Pyr-GC/MS being recognized as a promising technique for the analysis of airborne MNPs (Dümichen et

al., 2019; Picó and Barceló, 2020). The primary challenge associated with these methods (micro-Raman and Pyr-GC/MS) is the mandatory recognition of the sample matrix, which is necessary for potential assessments of the m/z ratio or vibration bands (Goedecke et al., 2020). A recent study by Peñalver et al. (2021) employed TGA-MS to analyze PM_{10}'s PS-MPs fraction in atmospheric samples from Cartagena (Spain). The average PS-MPs concentration was estimated to be 35.97 ng/m³, affirming the technique's ability to investigate MNPs from different environmental matrices. A recent study revealed that the limits of detection for different polymers varied considerably. For instance, the study found that the detection limit for polyurethane was 0.1 μg, while for polyethylene it was 9.1 μg. This highlights the significant variability in detection capabilities depending on the specific polymer being analyzed (Santos et al., 2023). In a further study, the Pyr-GC/MS method demonstrated an impressive limit of quantitation (LOQ) of just 0.005 mg/g (5 μg), highlighting its effectiveness in detecting MNPs at low concentrations in complex environmental matrices (Akoueson et al., 2021).

To identify the functional groups and structures of MNP polymers and determine the compositions of these materials, Fourier Transform Infrared Spectroscopy (FTIR), micro-FTIR, and Raman, μ-Raman spectroscopy techniques were employed (Luo et al., 2022). Micro-FTIR can detect MP particles (>10 μm) (Suaria et al., 2020), another technique employed to identify MPs in a sample is Raman spectroscopy. This technique involves using a laser light source to interact with molecular vibrations, which causes the laser photons to emit or absorb energy, showing a specific molecular vibration mode. However, it should be noted that particles below 10 μm in size cannot be analyzed effectively using this method due to the potential for destructive effects caused by the laser energy (Y. Zhang et al., 2020). It is, therefore, important to consider the potentially damaging effects of laser light sources on MPs.

Allen et al. (2019) used a 25% intensity laser light source, and no obvious damage to MNPs was observed, along with an improved spectral profile. In recent study, the combination of Raman spectroscopy and microscopy (i.e. μ-Raman) has enabled the chemical identification of MNPs with diameters less than 1 μm (Löder and Gerdts, 2015).

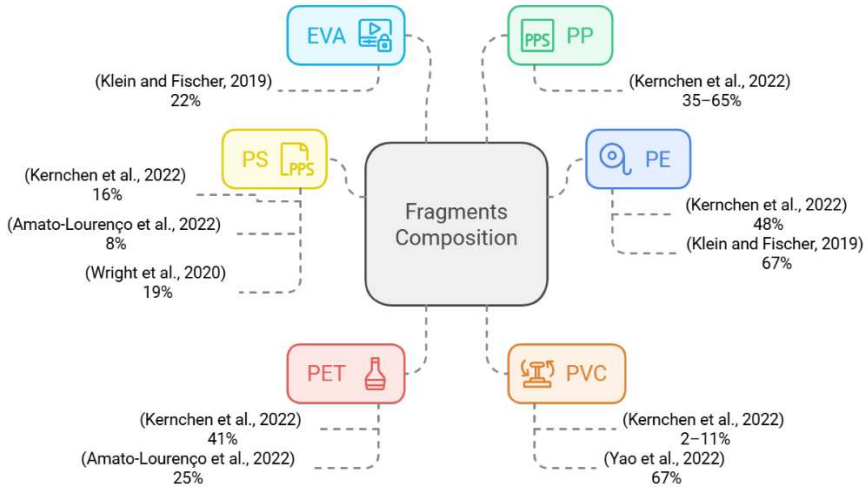

Figure 2.3. *The percentage of different polymer types in relation to the total number of fragment-MPs in the atmosphere (Amato-Lourenço et al., 2022; Sarmite Kernchen et al., 2022; Klein and Fischer, 2019; Wright et al., 2020; Y. Yao et al., 2022).*

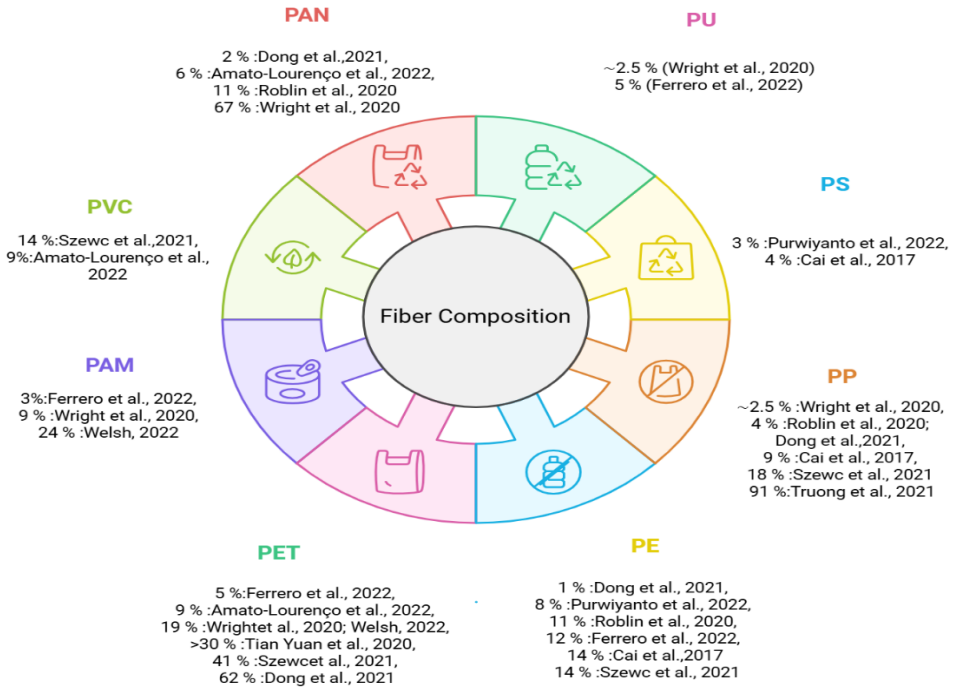

Figure 2.4. *The percentage of different polymer types in relation to the total number of fiber-MPs in the atmosphere (Amato-Lourenço et al., 2022; Cai et al., 2017; Dong et al., 2021; Ferrero et al., 2022; Purwiyanto et al., 2022; Roblin et al., 2020; Strady et al., 2021; Szewc et al., 2021; Welsh et al., 2022; Wright et al., 2020).*

The application of surface-enhanced Raman spectroscopy (SERS) is being explored as a potential solution to overcome this obstacle. SERS is a technique that can enhance otherwise weak Raman signals, and it has already demonstrated effectiveness in detecting particles as small as 350 nm (Mikac et al., 2023). Prior research has identified the composition of MPs as comprising two primary shapes: fibers and fragments, which the chemical composition of these shapes is illustrated in Figure 2.3 and Figure 2.4. At last, Carriera et al. (2024) have demonstrated that μ-Raman spectroscopy is suitable for particles larger than 0.45 μm.

It is estimated that up to 84% of the plastics in the air may be the result of the re-suspension of MNPs on roads (Brahney et al., 2021). The tire tread may undergo abrasion or thermal degradation (Evangeliou et al., 2020) into tire wear particles in a range of sizes, from less than 2.5 μm up to 350 μm, and in both fiber and fragment shapes (Abbasi et al., 2019), the resulting particles have a density of 1.7–2.1 g/cm³. It is recognized that the use of synthetic rubber in tires, including styrene-butadiene copolymers and polymers employed in bitumen formulations and road marking paints, can contribute to the presence of MNPs in settled road dust. Consequently, there is a hypothesis that these particles may become suspended in the ambient air (Kitahara and Nakata, 2020; Yukioka et al., 2020). A study by Manoli et al. (2002) found that 28% of fine particles (<10 μm) are resuspended in the air by road dust. Additionally, approximately 5% of tire wear emissions become airborne (Wik and Dave, 2009).

In the USA, research indicates that 1% of all PM_{10} is derived from road emissions, with tires contributing 15% of this amount. In high traffic areas, concentrations of airborne tire wear are typically in the range of 2–5 μg/m³ (Panko et al., 2013). A calculation of approximately 146 k tons of MNPs in tire wear per annum could be aerosolized. Furthermore, Evangeliou et al. (2020) calculated airborne emissions of tire wear to be 29,07k tons globally per annum, including 2,88k tons of PM_{10} and 29k tons of $PM_{2.5}$. Irrespective of the differing estimates, the airborne emissions of tire wear and resuspended road dust particles represent a significant source of MNPs in the atmospheric environment.

2.3. Atmospheric Transport of Micro(nano)plastics

It is acknowledged that MNP particles have the potential to undergo significant atmospheric transport over vast distances, including to elevated snow-covered mountainous regions, polar latitudes, and other remote locations (Allen et al., 2019; Bergmann et al., 2019; Brahney et al., 2020; Evangeliou et al., 2020; Materić et al., 2020; Revell et al., 2021). It is possible for MNPs to travel considerable distances through atmospheric transport, with $PM_{2.5}$ particles having a residence time of up to 28 days (Allen et al., 2019). The transport dynamics of airborne MNPs are influenced by a number of environmental factors, including wind patterns, air turbulence and atmospheric conditions (Chen et al., 2023).

It is yet unknown how well different sized and shaped MNPs would travel (Chen et al., 2023). The smaller the particle, the greater the likelihood that it will be lifted by an updraft and carried by the wind, thereby increasing the potential for long-range transport of pollutants. The enhanced buoyancy of these particles facilitates their long-range transport, enabling them to be transported by wind or water currents to distant locations (Kumar et al., 2021). It is estimated that a compact PVC fragment will settle at a speed of between 1.3 and 1.5 m/s. Therefore, it is less probable that it will be lifted into the atmosphere unless there are strong upward winds (Chen et al., 2023). Updraft winds play a pivotal role in the ascent of MNPs particles into the atmosphere, exerting a considerable influence on their transport dynamics and overall environmental impact. Updraft winds, in particular those with vertical components ranging from 1 to 1.5 m/s, have the potential to effectively lift MNPs from the surface into the atmosphere (Chen et al., 2023). When wind speeds exceed the sedimentation speed of MNPs particles, these particles become airborne and remain suspended in the atmosphere for extended periods (Chen et al., 2023).

MNPs fibers approximately 1 mm have the potential to be transported over long distances to the stratosphere, where they can facilitate the transfer of persistent organic pollutants (POPs) (Chen et al., 2023). In contrast, larger particles exhibit a greater tendency to settle more rapidly and are less likely to be transported over significant distances from their point of origin (Tatsii et al., 2023). Furthermore, the density of a substance can be considered another factor. For instance, PVC has a density of around 1.4 g/cm^3, which results in a sedimentation speed that can impede its atmospheric mobility (Chen et al., 2023; Gouin,

2021). On the other hand, lower density MNPs (e.g., polyethylene, density around 0.91–0.94 g/cm^3) exhibit greater buoyancy and are capable of remaining suspended in the air or water for extended periods (Allen et al., 2022; Boisseaux et al., 2024).

The extensive surface area and hydrophobic nature of airborne MNPs enables them to adsorb a diverse range of chemicals, including POPs, and transport them to regions distant from the initial source of pollution (Gouin, 2021; Marathe et al., 2021). The release of MNPs into the atmosphere may also exert an influence on climate dynamics, as they have the potential to interact with cloud formation processes and, as a consequence, affect weather patterns (Oehlschlägel et al., 2024). The occurrence, long-range atmospheric transport, and deposition of MNPs remain unquantified in the context of the oceanic atmosphere. Previous studies have primarily focused on the oceanic transport of MNPs (Caracci et al., 2023).

2.4. Health Risk of Micro(nano)plastics

The inhalation of airborne MNPs represents a significant health risk to humans, with this exposure pathway representing a particular concern (Din et al., 2024). It has been estimated that the inhalation of MNPs by humans' results in exposure of between 0 and 3.0 × 10^7 items per person per year (Feng et al., 2023). In a study conducted by Dris et al.(2016), the concentrations of inhalable MNPs were found to range from 0.3 to 1.5 particles per cubic meter indoors and from 0.4 to 56.5 particles per cubic meter outdoors. While Vianello et al. (2019) demonstrated that an individual with sedentary habits can inhale up to 272 MP particles per day, Prata (2018) calculated that the average person inhales between 26 and 130 MP particles per day. As previously stated by Kelly and Fussell (2012) and Valavanidis et al. (2013), MNPs have the potential to cause lung tissue to become inflamed.

Prata (2018) suggests that MNPs may result in long-term pulmonary irritation. Based on the findings, both the acute and chronic inhalation of MNPs may be linked to granulomatous and inflammatory alterations in bronchial tissues, along with rapid asthma-like bronchial reactions. These changes have the potential to result in chronic pneumonia and extrinsic allergic alveolitis. It is, therefore, evident that inhaling a high quantity of airborne MNP particles may have a detrimental impact on a vulnerable individual's respiratory system.

A significant mechanism through which MNPs particles exert their influence on the respiratory system is via the induction of oxidative stress. Inhalation of MNPs can result in their deposition within the lung airways, which may subsequently elicit an inflammatory response. The inflammatory response is primarily driven by the production of reactive oxygen species (ROS), which are chemically reactive molecules containing oxygen. The presence of ROS can result in substantial cellular damage, including lipid peroxidation, DNA damage, and protein oxidation (Saha and Saha, 2024; Vattanasit et al., 2023). Furthermore, the inflammatory response initiated by airborne MNPs involves activating diverse immune cells, including macrophages and neutrophils, which subsequently contribute to oxidative stress. Such cells then release additional ROS and pro-inflammatory cytokines, exacerbating the inflammatory process and potentially leading to chronic respiratory conditions (Saha and Saha, 2024; Vattanasit et al., 2023).

As posited by Prata (2018), the most significant sources of airborne MNPs can be attributed to the deterioration of synthetic textiles and the abrasion of synthetic rubber tires. The primary source of information for the main MNPs with regard to traffic and transportation is followed by brake wear, road markings, and airplane tires (Kole et al., 2017). Accordingly, the mineralogical composition of road wear particles is a significant factor in determining their inflammatory potential. In vitro cell studies have demonstrated that mylonite, for instance, exhibits a greater potency than quartz, basalt, and feldspar (Nosratabadi et al., 2023). It has been demonstrated that the inhalation of tire wear MNPs can result in pulmonary fibrotic injury. Tire wear MNPs are notably small, frequently measuring less than 100 nm in diameter. As stated by Lehner et al.(2019), the alveolar surface area of the human lung is 150 m^2, with a tissue boundary of less than 1 μm, which facilitates nanoparticle penetration. Their small size enables them to evade the respiratory system's intrinsic defenses, thus facilitating penetration of lung tissue and subsequent entry into the bloodstream (Saha and Saha, 2024). Such exposure may result in direct contact with vital organs, including the brain, as the particles may traverse the blood-brain barrier. In studies conducted on mice, exposure to these particles has been shown to cause restricted ventilatory function and fibrotic changes in lung tissue. The underlying mechanism appears to involve epigenetic alterations, specifically the downregulation of microRNA (miR-1a-3p), which

plays a role in regulating cytoskeletal proteins that are essential for lung cell function (Li et al., 2022).

3. MATERIALS AND METHODS

3.1. Materials

In the sampling section of the present study, a slotted filter comprising hydrophobic Teflon (polytetrafluoroethylene, PTFE) with a pore size of 0.22 µm and Al slotted filters measuring 14.29 x 13.65 cm and comprising ten 12 cm-long slots was utilized. These filters were positioned in a cascade plates (Tisch Scientific), as illustrated in Figure 3.1**.**The glass fiber filter (25 x 20 cm) with a pore size of 0.3 µm, manufactured by Tisch Scientific, was positioned in the backup stage. In the pretreatment section, circle glass fiber filters (47 mm, 0.45 µm pore size glass fiber, Whatman, China) were employed in the filtration process. H_2O_2 30% and 10% were utilized for digestion, manufactured by Carlo Ebra, France. Pure water (18.2 MΩ·cm) was utilized in all experiments and was produced by the Milli-Q gradient system (Millipore, Billerica, MA). In the characterization stage, eight polymers were examined in this study, which are commonly used plastics that account for over 80% of global plastic production and consumption (Pilapitiya and Ratnayake, 2024) and are frequently detected in the atmosphere, meaning they represent the main MNPs in urban air. A group of polymers was compiled, including polyethylene (PE), polypropylene (PP), polystyrene (PS), polyvinylchloride (PVC), polyethylene terephthalate (PET), polycarbonate (PC), natural rubber (NR), and styrene butadiene rubber (SBR).

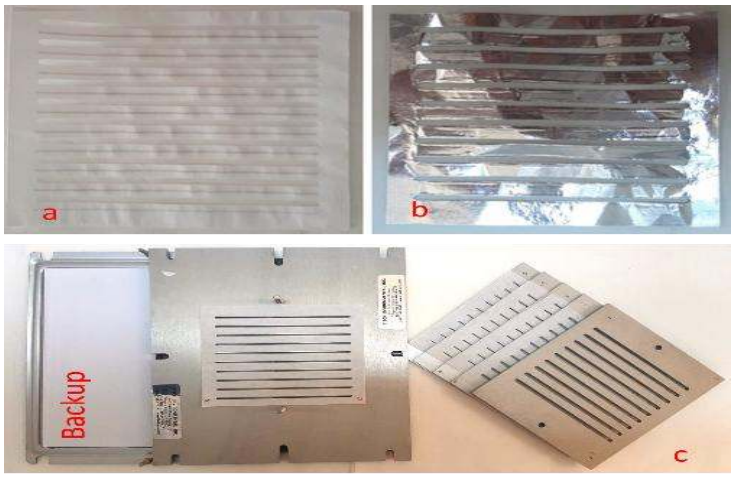

Figure 3.1. *Filters were performed in this study. a) Slotted Teflon filter, b) Slotted Al filter, c) Glass fiber filter in backup stages.*

These polymers were industrially available in the form of pellets or granules in Turkey. During the instrumental analysis, a dichloromethane (99.9%, Merck KGaA, Germany), n-hexane (98%, Merck KGaA, Germany), and tetrahydrofuran (99.9%, Merck KGaA, Germany) was used in standard preparation for Pyr-GC/MS calibration.

3.2. Methodological Approach

Given the absence of an established approach for sampling airborne MNPs utilizing diverse strategies, including random, bulk, or pooled sampling (ISO, 2020), an experimental process design contingent on the environmental context or material was devised (Figure 3.2).

The sampling of air was conducted in three distinct geographical areas, designated as background/suburban), urban, and industrial. In this context, the Eskişehir Technical University campus (background/suburban), the Eskişehir Technical University Porsuk campus (urban), and the Eskişehir Organized Industrial Zone (industrial) were identified as the most appropriate locations for the study. Meteorological data (including temperature, humidity, wind direction, and speed) were obtained from the National Centers for Environmental Information website (https://www.ncei.noaa.gov/node) for the relevant sampling periods. The airborne MNPs sampling method was classified into two principal categories: suspended particles, which were collected using active samplers, and atmospheric depositions, which were captured by passive collectors. Airborne MNPs were collected using an active sampler based on size-segregated particles. Active sampling methods utilizing high-volume, constant-air suction units, which are already in use and have a robust basis for sampling PM_{10}, $PM_{2.5}$ and $PM_{1.0}$, can be employed to sample MNPs (Pfeiffer, 2005). Passive sampling techniques may be utilized for the monitoring of particle levels, with a range of MPs from 5 mm to an aerodynamic diameter exceeding 10 μm. The establishment of standardized protocols, particularly in regard to the utilization of a cascade impactor is of paramount importance in order to guarantee the consistency and comparability of results across disparate studies. It is of the utmost importance to strike a balance between the capture of a wide size range and the practical considerations of processing time and filter replacement frequency. It is essential to give careful consideration to the filtration techniques employed

during the interpretation of data. Using different filter types and pore sizes may result in discrepancies in the collected data, which could affect the interpretation of the findings. The utilization of the filters in cascade impactors offers considerable benefits. It permits the fractionation of MPs into diverse size categories, thereby facilitating crucial insights into their distribution in the atmosphere. This approach enables the analysis of specific size ranges, each potentially having different environmental impacts and behaviors. It ensures precision in capturing a broad spectrum of particle sizes, thereby leading to a detailed and accurate analysis of the particle number, nature and size distribution in the collected samples. While using filters in a cascade impactor offers numerous advantages, it also presents a number of challenges. The use of smaller pore sizes increases the risk of clogging, particularly when sampling over extended periods with high flow rates. Furthermore, standardizing procedures for using slotted filters is essential. Establishing standardized protocols allows for the accurate interpretation and comparison of results, contributing to a more comprehensive understanding of atmospheric MNPs and their implications for the environment and human health (Logvina et al., 2024).

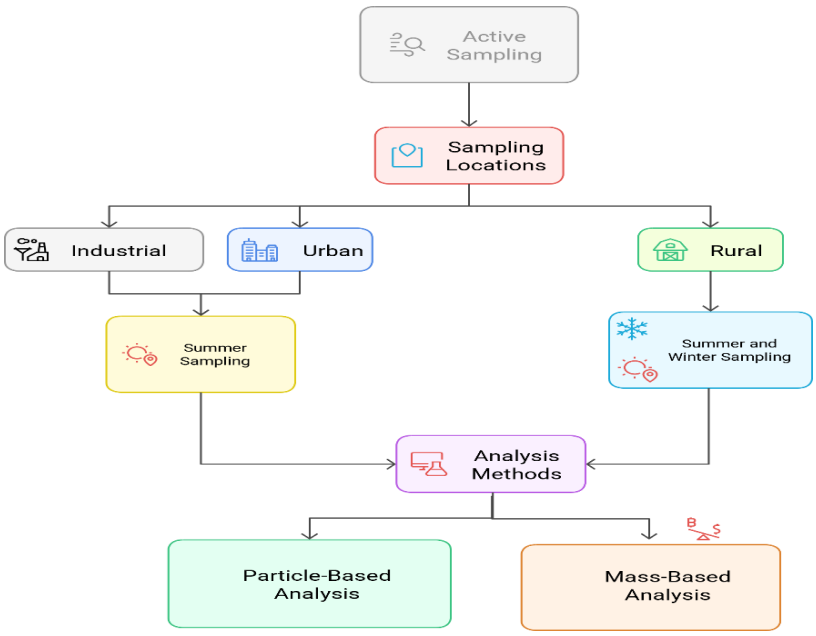

Figure 3.2. *General overview of methodological approach.*

3.3. Sampling Methodology

Active sampling was conducted in the summer at three sampling locations (industrial, urban and rural) for 15 days at a flow rate of 1.13 m^3/min (40 cfm) for 8 hours (9 a.m. to 5 p.m.), from 25/07/2023 to 07/09/2023 (weather conditions are shown in Table A.1, Appendix, after references) (Figure 3.3). Furthermore, two samples were collected in each zone over the course of two nights, from 9 p.m. to 5 a.m., with the objective of assessing the nighttime MNP level and comparing it with the daytime MNPs. However, the winter sampling was conducted exclusively in the rural zone (19/12/2023 to 01/01/2024, 14 days and 1-night samples) due to the malfunction of the sampler pump.

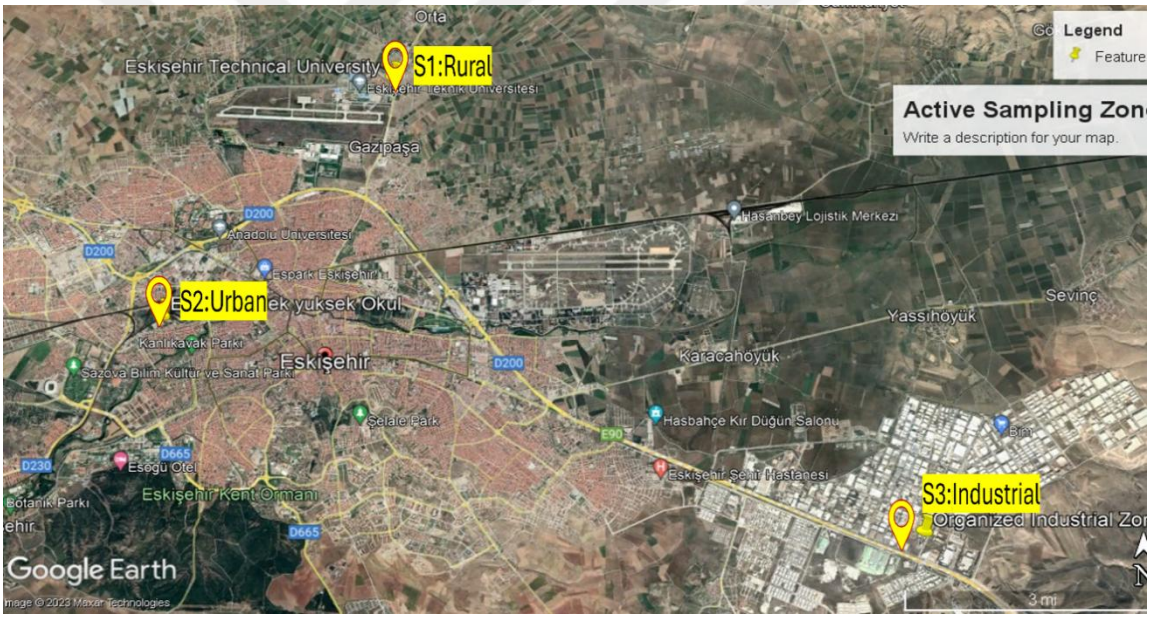

Figure 3.3. *Map of active sampling in three regions (S1: Rural, S2: Urban, S3: Industrial) in 15 days for 8 hours at flow rate of 40 cfm in the summer and winter (winter sampling was performed in rural zone).*

The sampling sets were conducted using a high-volume air sampler (Thermo VFC), which was fitted with a 5-stage cascade impactor system (Tisch TE-235 series), with a sixth stage serving as a backup. The flow rate cut-off limits were 40 cfm (1.13 m^3/min), with the following stage cut-offs: 7.2 µm > (Stage 1), 3 µm > (Stage 2), 1.5 µm > (Stage 3), 0.95 µm > (Stage 4) and 0.49 µm > (Stage 5), and 0.49 µm < backup stage. The Impactor stages are

composed of aluminum plates with external dimensions of 15.24 cm × 17.78 cm. All Impactor plates are clearly anodized in order to prevent corrosion and to reduce the likelihood of collection substrates adhering to the plates. The Impactor stages 1, 2, 3, 4, and 5 are equipped with 10 parallel slotted impaction jets. The maximum nominal cut-off size is 10 microns (Figure 3.4). This stage is primarily responsible for the collection of larger mechanically generated particles. The substrates are thin, flat sheets with ten perforations, through which the slots are exposed in each stage. The particles that traverse the slotted jets in the impactor stages collide with the collection substrates, resulting in deposition or collection. Furthermore, the collection substrates serve the additional function of forming a vacuum seal between the impactor stages. The collection substrates have dimensions of 14.29 cm × 13.65 cm and can be readily accommodated within standard micro-balances without the necessity for folding the paper. The minimal adsorption of gaseous pollutants thus enhances the accuracy of the measurements. Subsequently, each type of filter is correctly positioned within the cascade impactor. This involves orientating the filter with the rough side facing upwards on the stainless-steel screen. Afterward, the substantial base plate is positioned over the filter paper. The slots on each successive impactor stage are positioned in a staggered configuration, with each slot situated above an impaction plate and not in alignment with an adjacent slot.

In order to remove the impurities, all slotted filters were employed in different parts of this research, wrapped in aluminum foil, and baked at specific temperatures. For example, the Teflon filter (Polytetrafluoroethylene, PTFE) was backed at 60°C for four hours in an oven. Prior to sampling, glass fiber filters were baked at 550°C for three hours in a muffle furnace (Li et al., 2023). The slotted aluminum (Al) filter was utilized in its original state. Subsequently, the samples were transferred to a dedicated container at room temperature and left for 24 hours. Prior to and following the sampling process, the filters were weighed at a constant temperature and humidity using a KERN 870 semi-micro balance in order to obtain accurate measurements.

The subsequent phase of the process is the calibration of the high-volume sampler motor, which serves to guarantee that the displayed flow rate is an accurate reflection of the

actual flow rate. The calibration was conducted in accordance with the instructions provided in the specialized kit supplied by the Tisch Company.

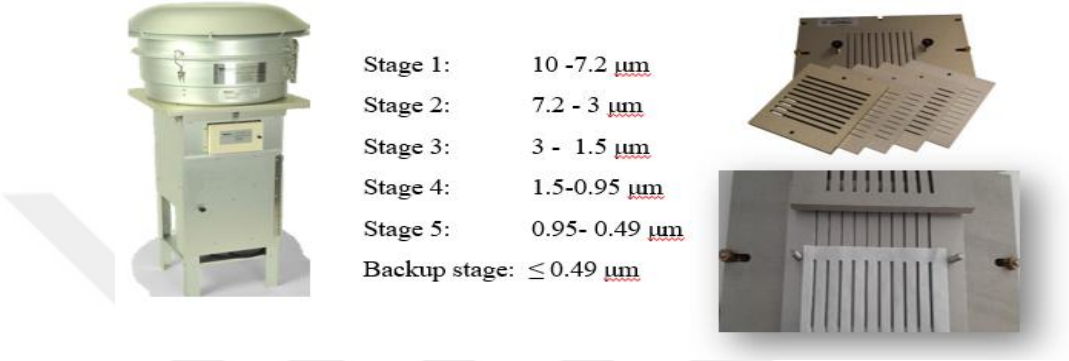

Figure 3.4. *High volume air sampler (Thermo VFC) with cascade impactor (Tisch TE-235 series).*

The specifications of the orifice are clearly delineated in the provided illustration. In order to enhance the precision and accuracy of the calibration process, it was conducted on four separate occasions. The results of the calibration are presented in the following section. The calibration tables indicate that two factors are of particular significance: (1) the corrected chart response and (2) the correlation coefficient. In regard to the column-corrected chart response, if the desired flow rate is 40 cfm, the device must be set to 65 cfm. Moreover, the correlation coefficient illustrates the precision of the operator's calibration procedures.

3.3.1. Selection of the substrate filter

Two sets of sampling were conducted at a flow rate of 1.13 m^3/min (40 cfm) for 24-hours sampling at the Eskişehir Technical University campus in Eskişehir, Türkiye, To investigate the usability of different filters/substrates: the first set using a slotted aluminum (Al) filter and glass fiber filter placed in backup stage, on July 3, 2022 (weather conditions Table A.2), while the second set was conducted a PTFE (Polytetrafluoroethylene) or Teflon filter on 18 July 2022 (weather conditions Table A.2). The particles are collected at each slot on the filter surface in the form of a thin line situated in the center of the slot (Figure 3.1).

With regard to the glass fiber filter situated in the backup stage, it was observed that the entire surface of the filter had accumulated particles.

A visual inspection of the filter structures and particles collected on the filters was conducted to investigate the morphological characteristics and thus determine an efficient substrate for further investigation. Accordingly, slotted Al and PTFE filters were employed to identify an appropriate substrate for size-segregated sampling. For this purpose, 2 cm^2 of each slotted filter was excised and analyzed without any sample pretreatment using a microscope (Carl Zeiss, Axioscope 5, Germany). The particles collected at each stage and the backup were examined at different magnifications (10x, 20x, and 50x) in accordance with the aerodynamic size segregation. In order to gain a more comprehensive understanding, particles from the Al filters were also transferred to glass fiber filters. Four series of subsamples were prepared, comprising 2 cm^2 from a slotted Al filter in stage 1, which was cut and placed in clean tubes containing 10 ml of prefiltered deionized water. Each subsample was then subjected to vortexing (5 min, 16 rpm), and ultrasonic bathing (40 kHz for 10 min at room temperature around 25°C), the process was then repeated with mixed of vortexing and ultrasonic bathing, and finally, the samples were washed five times with deionized water. Consequently, the efficiency of the PM transfer was evaluated in terms of the number of particles retained on the filter surface, with 2 cm^2 of Al filters analyzed once again with the Axioscope 5 microscope.

In order to address the significant analytical challenges presented by stages 5 and the backup, which were characterized by high loading and particle overlap, a scanning electron microscope was employed for the investigation of the morphological characterization of particles collected in these stages. For this purpose, a 1 cm^2 section of the Teflon filter with slotted openings from stage 5 (particles with a diameter greater than 0.49 μm) and the glass fiber filter from the backup stage (particles with a diameter less than 0.49 μm) were examined by SEM.

3.3.2. Sample preparation and pre-treatment

Pretreatment procedures were conducted with the objective of isolating MNPs from other airborne particles and organic/inorganic contaminants, employing physical or chemical

techniques. In the chemical approach, the sample was subjected to digestion in order to remove any organic substances that might interfere with the subsequent analysis (Ivleva et al., 2017). For this purpose, 2 cm^2 of slotted Teflon filters were cut from each of the five sampling stages conducted on 18 July 2022 and placed in tubes containing 10 ml of 30% H_2O_2 (Carlo Erba, extra pure, France). Henceforth, the tubes were maintained at room temperature for 48 hours, after which the samples were filtered through a glass fiber filter (47 mm, 0.75 µm pore size glass fiber, Whatman, China) for visual inspection. The aforementioned process was repeated using 30% and 10% hydrogen peroxide, with a 24-hour exposure time, in order to optimize oxidative digestion.

On the other hand, the density separation technique may be employed to remove inorganic matter from plastic particles, given that the density of inorganic particles is typically greater than that of MPs (Shao et al., 2022a). The theoretical aspects of physical pretreatment were considered in relation to the physicochemical properties of airborne particles < 10 µm, based on data gathered from the relevant literature. The sample processing employed in this study was illustrated in the following figure (Figure 3.5). The objective is to provide a comprehensive overview of the procedures conducted in order to facilitate a more detailed understanding.

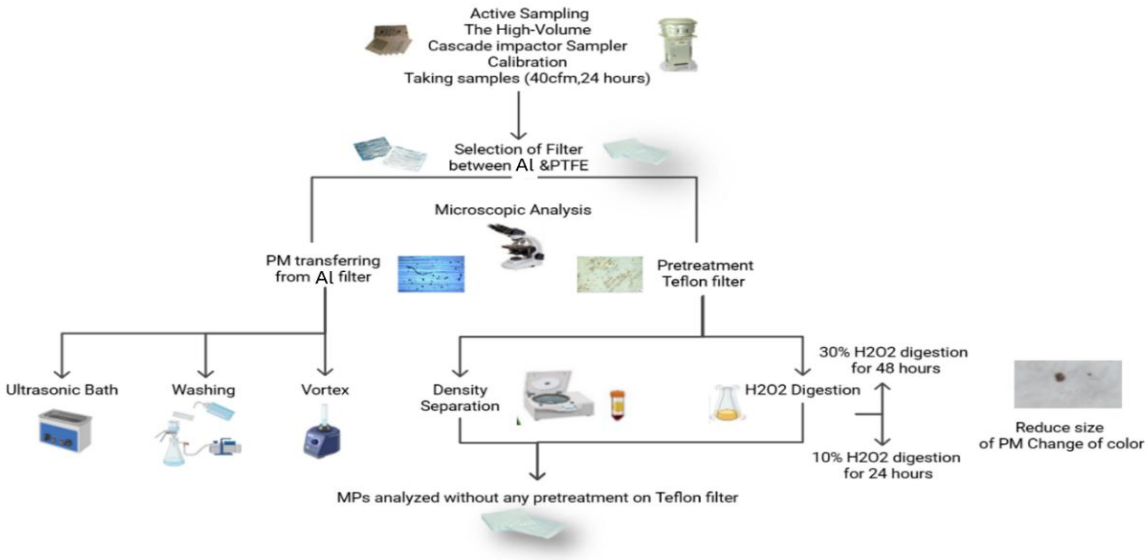

Figure 3.5. *The details of air sampling and sample processing.*

3.3.3. Selection of an appropriate subsample

The chemical characterization of airborne particles is achieved through the use of μ-Raman spectroscopy, which is a sophisticated technique that does not require sample treatment. However, this method is time-consuming and limits the analysis of the entire filter surface area (De Frond et al., 2023). Therefore, an efficient subsample should be selected on the basis of the homogeneity of the MNP distribution between different slots of a filter, which can be determined by spectrometric analysis. Accordingly, filter pieces measuring 5 x 1 cm^2 were cut from the stage 1 of Teflon filter at an oblique angle and 20 to 40 particles were randomly selected for analysis using a μ-Raman InVia spectrometer (Renishaw Plc, Wotton-under-Edge, U.K.) (Figure 3.6).

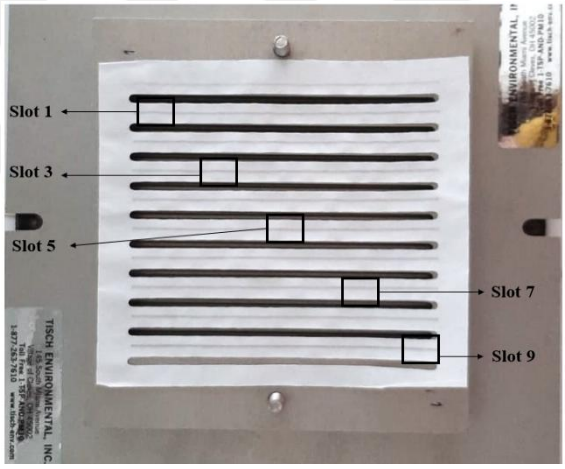

Figure 3.6. *The examination of MPs distribution between different slots of a Teflon filter.*

3.3.4. Evaluation of sampling parameters

The initial sampling phase was undertaken with the objective of controlling all of the sampling conditions and determining the most appropriate analysis procedure for MNPs, as well as the most effective identification methods. The airborne particles were collected at a flow rate of 1.13 m^3/min (40 cfm) over a period of 24 hours, on June 21, 2023 (weather conditions Table A.1). As indicated in the initial sampling phase, which is presented in the Results and Discussion section, it was necessary to evaluate the sampling conditions in order to ensure the highest possible accuracy in the particle-based analysis of airborne MNPs.

To assess the sampling procedure and parameters, the second set of samples was collected on 12/07/2023 and 13/07/2023 (weather conditions Table A.1), respectively, with flow rates set at 40 cfm and 20 cfm (The aerodynamic limits for a flow rate of 20 cfm are as follows: Stage #1: 10.2 µm, Stage #2: 4.2 µm, Stage #3: 2.1 µm, Stage #4: 1.3 µm, Stage #5: 0.69 µm, and backup < 0.69 µm) for the two groups. Table for weather conditions

In the context of sampling conditions, it is essential to consider not only the air flow rate but also the sampling duration; these factors have a significant impact on the quality of the sample collection process. Consequently, the second sampling sets were conducted in two flow rate groups (40 cfm and 20 cfm) and four different periods (4, 8, 12, and 24 hours) for comparison and final decision. Accordingly, in order to determine an appropriate sampling time, the two Teflon filter slots from each of the five stages were excised at 4 hours, 8 hours, 12 hours, and 24 hours, respectively (Figure 3.7).

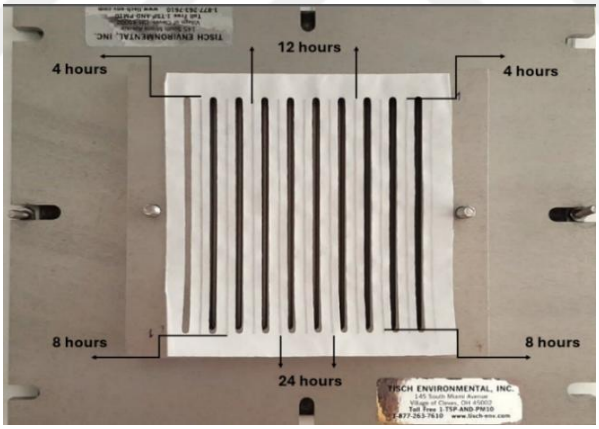

Figure 3.7. *A representative for cascade filters and slots processed in the subsequent analysis.*

In order to investigate the morphology and distribution of particles collected in the slot of the Teflon filter, a 1 cm² piece of the filter used in the initial set of sampling was randomly selected from each of the five stages and analyzed directly with a microscope (Carl Zeiss, Axioscope 5, Germany). The second set of samples was then subjected to an examination in order to assess the sampling conditions. For this purpose, a 1 cm² section of the Teflon filter slot was cut from the various stages of flow rate groups (40 cfm and 20 cfm) and sampling

times (4, 8, 12, and 24 h) for qualitative analysis of particle collection efficiency using an optical microscope (Carl Zeiss, Axioscope 5, Germany) and spectrometric analysis with μ-Raman InVia spectrometer (Renishaw Plc, Wotton-under-Edge, U.K.). The particles collected at various stages were examined at different magnifications (5x, 10x, 20x and 50x) in accordance with their aerodynamic size cut off ranges. The sampling optimization methodologies employed in this study are illustrated in the following figures (Figure 3.8). The objective is to provide a comprehensive overview of the procedures conducted in order to facilitate a more detailed understanding.

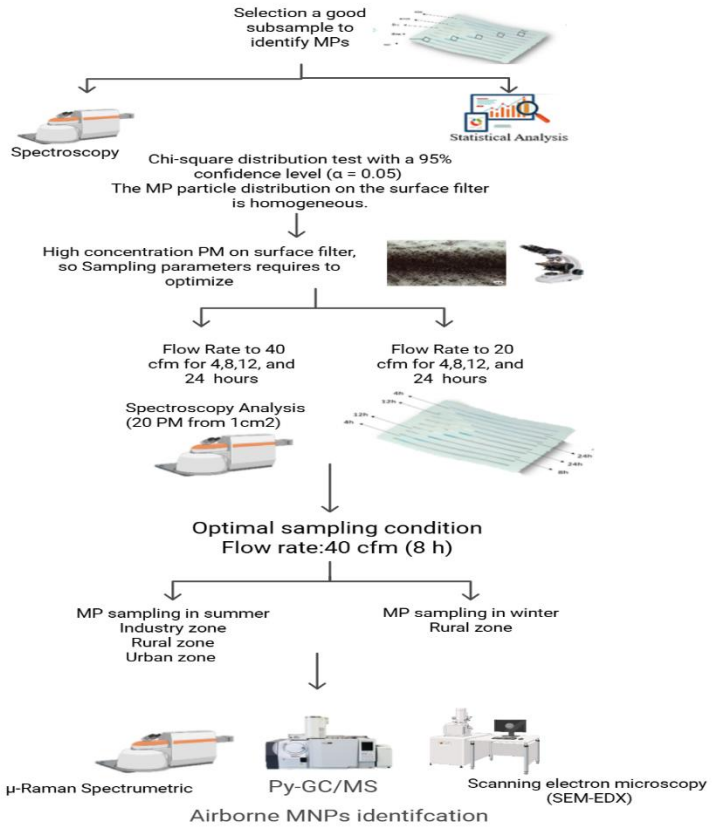

Figure 3.8. *The optimization of sampling parameters.*

3.4. Particle-based Analysis of Micro(nano)plastics

3.4.1. Optical microscope analysis

In this study, the optical microscope was employed for a brief period of time. This was due to the fact that the objective of this study was to focus on MNPs <10 μm, and thus the microscope was used to examine the distribution of particles on the surface of the filter, as well as to assess sampling parameters. The Axioscope 5 (Carl Zeiss, Germany) optical microscope was utilized for this purpose. The Axioscope 5 is furnished with high-quality optics, which facilitate the clear imaging of minute particles. It is recommended that the Axiocam camera, which is integrated with the Axioscope 5, be employed for the purpose of high-resolution image capture. The Axioscope 5 incorporates Smart Microscopy, which enables the automatic adjustment of camera settings, including white balance, contrast, and exposure time. This feature facilitates the imaging process, enabling researchers to concentrate on their samples without the necessity for extensive technical expertise or additional software, which is often a prerequisite with alternative systems. The utilization of ZEN core imaging software facilitates automated image analysis, which can assist in the quantification and classification of MNPs based on size and morphology.

3.4.2. Micro-Raman analysis

The chemical characterization of individual particles using Raman spectroscopy represents a powerful technique for improving aerosol characterization. Raman spectroscopy constitutes a valuable method that does not require sample treatment (Munno et al., 2020). However, the time-consuming nature of this method renders it unfeasible for the analysis of the entire filter surface (De Frond et al., 2023). As an illustration, the examination of 18 mm^2 by μ-Raman microscopy necessitates an average of 43±4 hours (Cabernard et al., 2018). In this study, a μ-Raman microscope was employed due to the fact that the collected particles are < 10 μm in size, with the μ-Raman microscope capable of identifying particles as small as 1 μm. In contrast, μ-FTIR is an effective technique for particles ranging in size from 10 to 20 μm (De Frond et al., 2023).

The acquisition of the spectra was conducted using Leica 50X and 100X magnification of long-range objectives. The microscope was coupled to a Prior Scientific motorized stage

(XYZ), which was controlled by a joystick. In order to detect MNPs from other airborne particles and identify their chemical composition or polymer types, 20 particles were randomly selected from 1 cm^2 filter pieces. When selecting MNPs for μ-Raman analysis, several key morphological properties should be considered, including size, shape, and color (Luo et al., 2022). This facilitated focusing and searching for points of interest. The movement of the joystick on 1 cm^2 of the Teflon filter resulted in the filter area being subdivided into four parts, with approximately five particles selected for MP examination from each part. Furthermore, the instrument is equipped with a 532 nm laser, which is within the visible range and is recommended for use with carbon materials (Smith and Dent, 2005).

When employing μ-Raman spectroscopy to detect polymeric particles, it is of the utmost importance to prevent the burning of the particles in question, as this will ensure the accuracy and reliability of the results obtained. This can be achieved by optimizing the laser power in accordance with the requisite specifications. The conditions for optimization included an extended grating scan type (400–4000 Raman cm^{-1}) and a direct correlation between the signal strength of Raman spectra and the laser power (D. Liu et al., 2020). It is recommended that the laser power settings be adjusted to a lower level in order to minimize the risk of thermal damage to the particles. It is only necessary to increase the laser power in instances where it is not possible to obtain a sufficient signal-to-noise ratio at lower laser power levels (Munno et al., 2020). In order to achieve the aforementioned objective, the study employed a laser intensity range of 0.0001 mW to 1 mW, an exposure time of 10 seconds, and an acquisition time of 1 second. In the context of the spectral acquisition setup and range, the exposure time is fixed at 10 exposure times in the extended scan grating type. In contrast, the exposure time can be modified in the case of a static scan grating type.

In the present study, the utilization of a Teflon filter, due to its polymer structure, rendered the map scanning method with a micro-Raman microscope, an unsuitable technique for identifying MNPs. The Teflon filter, which serves as the substrate, is a type of polymer (polytetrafluoroethylene) that, when employed in mapping scanning techniques, can also demonstrate pronounced interference with the μ-Raman spectra. This impairs the ability to distinguish the peaks from the collected particles, thereby hindering the detection of MNPs.

Consequently, a point-by-point or particle-by-particle analysis technique was employed to prevent any interference that would necessitate a greater investment of time (Table A.3).

The spectrometric peaks obtained from a μ-Raman microscope were examined using Wiley's KnowItAll spectroscopy software with the objective of identifying similarities with standard polymer peaks. In this study, the μ-Raman spectrum was accepted with a hit quality index (HQI) or matching ratio of greater than 70%. The majority of studies employing μ-Raman spectroscopy for MP analysis accept matches with an HQI of 70% or above as the threshold for acceptance (Wright et al., 2023). Subsequently, the FIJI (ImageJ) software was used to ascertain and record the morphology and dimensions (Feret diameter) of the MNPs.

3.4.3. SEM-EDX analysis

The use of scanning electron microscopy (SEM) allows for the imaging of particles as small as 1 nm, providing exceptional resolution. The high magnification enables researchers to observe the minute details of MNPs, including their surface morphology, which is vital for identifying different types of plastics and understanding their degradation processes (Huang et al., 2023). The capacity to capture high-resolution images permits the quantitative analysis of MNPs abundance and distribution within samples, thereby enabling researchers to assess environmental concentrations with greater precision than would be possible with lower-resolution techniques (Huang et al., 2023). When used in conjunction with Energy Dispersive X-ray Spectroscopy (EDX), SEM can perform elemental analysis, thereby enabling the identification of the chemical composition of MNP particles. This is particularly useful for the detection of specific elements associated with various plastic types, such as chlorine in PVC or other additives, including titanium dioxide (Girão, 2022).

In this research, the 1 cm^2 of filter (specific to study glass fiber filter that placed in the backup stage < 0.49μm) component was affixed to an aluminum sample holder for scanning electron microscopy (SEM) using conductive and adhesive carbon tape. All samples were coated with 5 nm gold to enhance the absorption of electrons. Secondary electron imaging was employed to conduct scanning electron microscopy (SEM) analysis at 20 kV with a working distance selected according to the particle size collected on a filter surface (in this study, the range was often adjusted to a value between 7 and 9 mm). The elemental

composition of the particles was identified through the utilization of energy-dispersive X-ray spectroscopy (EDX-SEM, Oxford Instruments, INCA) techniques within the scanning electron microscope (SEM, Zeiss, SUPRA 50 V P). During the EDX analyses, a surface area of five particles was randomly selected for a region scan. This enabled the monitoring of different elements for a period of 20 seconds, with quantitative values obtained automatically from the software (Table A. 3).

3.5. Mass-based Analysis of Micro(nano)plastics

3.5.1. Polymer standards and preparation for calibration

Prior to the analysis of the polymers in the Pyr-GC/MS system, it is essential to carry out analytical method development studies. Eight polymers were examined in this study, which are commonly used plastics that account for over 80% of global plastic production and consumption (Pilapitiya and Ratnayake, 2024) and are frequently detected in the atmosphere, meaning they represent the main MNPs in urban air. The high degree of complexity inherent in the matrix of environmental samples renders the selection of an internal standard a challenging task. Consequently, the external standard method was selected for utilization in the present study.

Uncertainty was minimized during the weighing process, and low calibration concentrations relevant to atmospheric concentrations of MNPs were achieved by using polymer standards as documented in Table 3.1**.** In the preparation of calibration standards from polymers in solid form, analytical capacity of the balance is a significant parameter in determining the lowest concentration in the calibration (e.g., <1 µg). It is imperative that the solid polymer be in powder form to the greatest extent possible in order to facilitate the weighing process. It is evident that polymers in pellet form must undergo a reduction process to achieve powder form. To facilitate this process, which can be carried out with the assistance of a grinder, polymers with a glass transition temperature of Tg < 0°C must initially be maintained in liquid nitrogen or, if feasible, ground in a cryogenic grinder. Conversely, polymers with a glass transition temperature greater than 0°C must be stored in the freezer compartment of a refrigerator or at -80°C and subsequently ground into powder.

Moreover, calibration standards may be prepared in liquid form by dissolving solid polymers in a solvent, as illustrated in Table 3.1.

Table 3.1 *The polymers for calibration.*

Solid Polymer	Tg, (°C) *	Grinding	Solid/Liquid
PE (Polyethylene)	-110	Liquid nitrogen	Solid
PP (Polypropylene)	-20	Liquid nitrogen	Solid
PS (Polystyrene)	90	Freezer	Liquid
PVC (Polyvinylchloride)	60	Freezer	Solid
PET (Polyethylene terephthalate)	73	Freezer	Solid
PC (Polycarbonate)	150	Freezer	Liquid
NR (Natural rubber)	70	Freezer	Liquid
SBR (Styrene butadiene rubber)	(-55)/ (-35)	Liquid nitrogen	Liquid

**Glass transition temperature*

Additionally, calibration standards may be prepared in liquid form by dissolving solid polymers in a solvent, as illustrated in Table 3.2. Calibration can be conducted by diluting stock solutions, which have been prepared in liquid form.

Table 3.2. *Conditions that convert solid polymer to liquid form.*

Polymer	Solvent	Additional condition	Application
PE	1,2,4-trichlorobenzene (TCB)	Allow at least 20 minutes at 120-150°C.	≈ 25 mg polymer + 5 mL solvent
PP			
PS	Tetrahydrofuran (THF)	-	≈ 25 mg polymer + 2-3 mL solvent, 5 mL volumetric flask
PVC			
PC			
PET	3-hexafluoro-2-propanol (HFIP) OR Chloroform + Phenol (1:1)	-	20/25 mg polymer + 2-3 mL solvent, 10/5 mL volumetric flask
NR	Hexane/Dicholoromethane (1:1)	-	≈ 25 mg polymer + 2-3 mL solvent, 5 mL volumetric flask
SBR	Chloroform	48 hours with stirring at 40°C	≈ 25 mg polymer + 5 mL solvent

3.5.2. Pyr-GC/MS analysis and validation

The Pyr-GC/MS analyses were carried out employing a Pyroprobe, a one-shot Pyrolyzer, and a high-resolution gas chromatograph Shimadzu GCMS-QP2010, Ultra-

quadrupole mass spectrometer Shimadzu GCMS-QP2010 Ultra (Table 3.3). Separation was performed with a Rtx 5MS column (30 m × 0.25 mm, 0.25 μm film thickness; Shimadzu Technologies), and ionization was conducted in electron ionization mode. The pyrolysis temperature was set at 550°C. The temperatures of both the Pyr/GC interface and the GC injector were set at 300°C. The injection was operated in split mode with a split ratio of 1:20. These settings were implemented to prevent peak shape distortion and to improve reproducibility. The temperature program that was implemented for the gas chromatograph (GC) oven is outlined below: Initially, the oven was set to a temperature of 40°C for a duration of five minutes. Thereafter, the temperature was increased at a rate of 20°C/minute until it reached 320°C. Subsequently, the oven was maintained at this temperature for a period of 20 minutes. The total runtime of the entire analysis was 29 minutes. The mass spectrometer was operated in electron ionization (EI) positive mode, with a mass range of 30 to 500 and a scan rate of 0.3 scans per second. The Pyr-GC/MS operating conditions, including the pyrolysis temperature, heating rate, and carrier gas flow rate, were optimized as previously outlined in a preceding publication (Lou et al., 2022; Matsueda et al., 2021; Matsui et al., 2020).

In the present study, Day and night samples were taken from each zone, and also two samples based on weather conditions (min and max PM_{10} index) were selected to analyze with Pyr-GC/MS. First, a piece of Teflon filter (around10 μg) was cut from the middle of the slot (from which particles were collected) at five stages. Furthermore, all samples were subjected to analysis with Pyr-GC/ms in accordance with the established backup stages (aerodynamic diameter < 0.49 μm). Following the identification of the products through mass spectra, the integration of their chromatographic peak areas was undertaken for the purpose of quantitative analysis. Shimadzu GC/MS re-analysis software offers three modes of peak integration: automatic integration based on peak area, automatic integration based on peak height, and an integration method involving the setting of detailed parameters. The judicious selection of integration mode, in conjunction with the precise calibration of integration parameters, wields a profound influence on the separation of disparate peaks as well as on the determination of their starting and falling points. These, in turn, exert a substantial impact on the quantitative outcomes derived from peak area measurements.

Table 3.3. *Pyr-GC/MS Method approach.*

Apparatus	Parameters	Settings
One Shot Pyrolyzer PY-2020IS	Furnace temperature	550°C
	Interface temperature	320°C
	Reaction tube	Eco-cup 
Gas Chromatograph Shimadzu GCMS-QP2010 Ultra	Carrier gas	Helium
	Injector mode	Split
	Split ratio	1/20
	Injector port temperature	300 °C
	Pressure	49.5 kPa
	Total flow	27 mL/min
	Column flow	1 mL/min
	Column	Rtx 5MS, 30 m × 0.25 mm (0.25 µm film thickness)
	Temperature program	40 °C (5 min hold) → 320 °C (20 min hold) at 10 °C /min
Mass Spectrometer Shimadzu GCMS-QP2010 Ultra	Ionization energy	70 eV
	Ion source temperature	230 °C
	Scan rate	0.3 sec
	Scan range	*m/z* 30 ~ 500

The Pyr-GC/MS system was subjected to a minimum of a five-point external calibration, with the limit of detection (LOD) for peaks with a signal-to-noise ratio greater than three to one determined (>3/1). In the calibration process, indicator compounds listed in the table below are employed for each polymer type in order to minimize potential interferences that may arise from natural organic matter or other contaminants present in the sample (Table 3.4).

It is of paramount importance to guarantee the verification of the analytical methodology employed in the Pyr-GC/MS system. The validation of polymer standards can be demonstrated by Pyr-GC/MS analysis of a polymer mixture of a known quantity in solid or liquid form, conducted entirely within laboratory conditions, without consideration of any potential interferences that may arise from the samples (Table 3.5).

It is of paramount importance to guarantee the verification of the analytical methodology employed in the Pyr-GC/MS system. The validation of polymer standards can be demonstrated by Pyr-GC/MS analysis of a polymer mixture of a known quantity in solid or liquid form, conducted entirely within laboratory conditions, without consideration of any

potential interferences that may arise from the samples. To this end, an intermediate polymer mixture standard is prepared, and the recovery rates are examined as a result of Pyr-GC/MS analysis.

Table 3.4. *Characteristic pyrolyzates in Pyr-GC/MS.*

Polymer	Amount (µg)	Characteristic pyrolyzate (P1-P2)	m/z	Reference
PE	20,40, 50, 60,90	P_1 = 1,13-tetradecadiene	55	(W. Fan et al., 2022)
		P_2=1-Heneicosene (1-tetradecene)	41	(Morioka et al., 2024)
PP	20,30, 40, 60,70, 80	P_1 = 2,4-Dimethyl-1-heptene	70	(Morioka et al., 2024)
		P_2 = 2,4,6,8-tetramethyl-1-undecene	69	(W. Fan et al., 2022)
PS	0. 25, 0. 5, 1, 2, 3	P_1 = 2,4-Diphenyl-1-butene (3-butene-1,3-diyldibenzene)	91	(Morioka et al., 2024)
		P_2 = 2,4,6-Triphenyl-1-hexene (5 hexene-1,3,5-triyltribenzene)		(W. Fan et al., 2022)
PVC	10,30, 50, 60,80	P_1 = Naphthalene	128	(Morioka et al., 2024)
		P_2 = Benzene	78	(Kaal et al., 2023)
PET	10,20, 50, 60,80	P_1 = Benzophenone	182	(Morioka et al., 2024)
		P_2 = Ethan-1,2-dyilbenzoate	105	(Kaal et al., 2023)
PC	0. 5, 1.25, 2.5, 3.75, 5	P_1 = *p*(4)-Isopropenylphenol	134	(Morioka et al., 2024)
		P_2 = phenol	241,256,133	(Gnoffo and Frache, 2023)
NR	0. 625, 1.25, 2.5, 3.75, 5	P_1 = Dipentene	68,136	(Seeley and Lynch, 2023)
		P_2 = D limonen	39,68	(Seeley and Lynch, 2023)
SBR	0. 625, 1.25, 2.5, 3.75, 5	P_1 = 4-vinyl-cyclohexene	54(79,93,108)	(Seeley and Lynch, 2023)
		P_2 = 4-Phenylcyclohexene	104(158)	(Morioka et al., 2024)

The efficacy of the approach for direct analysis of airborne samples was evaluated to ensure the validation of the analytical methodology employed in the mass-based analysis. The calibration curve with the determination coefficient (R^2) for polymer standards typically exhibits a high degree of linearity, with reported values frequently exceeding 0.97 and often reaching 0.99.

Table 3.5. *Calibration data.*

Polymer	Indicator compound(P_1-P_2)	Indicator ion (m/z)	Calibration equation	R^2	LOD (µg)
PE	P_1 = 1,13-tetradecadiene	55	Y = 3.144568e+007X + 29594.16	0.995	2
	P_2=1-Heneicosene (1-tetradecene)	41	Y = 1.721374e+007X - 67179.32	0.987	5
PP	P_1 = 2,4-Dimethyl-1-heptene	70	Y = 2.120558e+008X - 1472157	0.998	0. 08
	P_2 = 2,4,6,8-tetramethyl-1-undecene	69/43	Y = 1.851557e+007X - 21117.12	0.998	0. 03
PET	P_1 = 2,4-Diphenyl-1-butene (3-butene-1,3-diyldibenzene)	182	Y = 1.326353e+007X - 50926.21	0.999	0. 4
	P_2 = 2,4,6-Triphenyl-1-hexene (5 hexene-1,3,5-triyltribenzene)	105	Y = 8.559819e+008X + 5197327	0.999	1
PVC	P_1 = Naphthalene	128	Y = 3.470573e+007X + 78103.41	0.997	0. 2
	P_2 = Benzene	78	Y = 1.511268e+008X - 33413.24	0.998	0. 4
PS	P_1 = Benzophenone	91/207	Y = 4616.857X + 35700.7	0.997	0. 025
	P_2 = Ethan-1,2-dyilbenzoate	91	Y = 794.4222X - 29908.89	0.999	0. 05
PC	P_1 = *p*(4)-Isopropenylphenol	134	Y=1956.967X - 23099.28	0.998	0. 125
	P_2 = phenol	94	Y = 2495.06X + 204203.1	0.987	0. 05
NR	P_1 = Dipentene	68	Y = 927.6019X- 5916.573	0.992	0. 125
	P_2 = D limonen	68	Y = 124.1699X + 654.4268	0.998	0. 125
SBR	P_1 = 4-vinyl-cyclohexene	54	Y = 166.2231X + 1590.06	0.999	0. 05
	P_2 = 4-Phenylcyclohexene	104	Y = 1479.213X + 89359.44	0.998	0. 005

Accordingly, the mean recovery ratio for the polymers examined was as follows: PE and PP exhibited 98.5%, while other types of polymers demonstrated 99% (Figure 3.9 and Table 3.5).

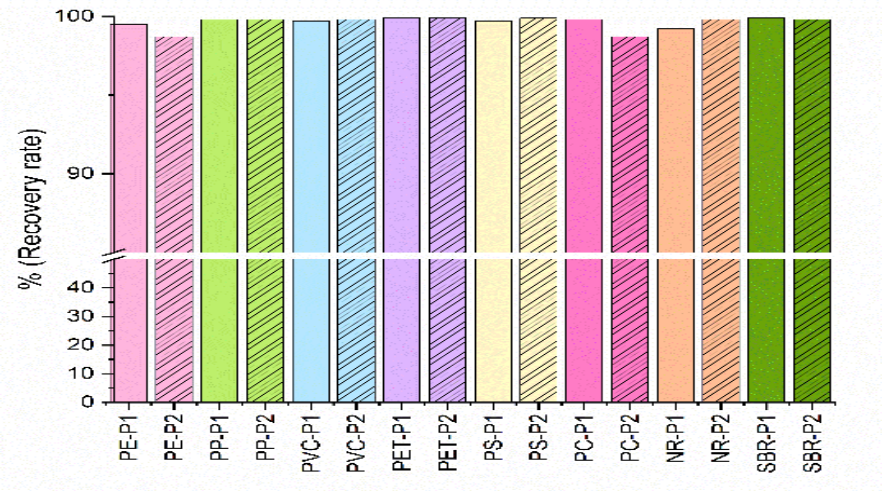

Figure 3.9. *The average recovery for each type of polymer.*

3.5.2.1. Reproducibility

In order to ascertain the reproducibility of Pyr-GC/MS analyses, a mid-point standard was analyzed on different days, with the instrument performance indicated by the peak areas (Table 3.6). Furthermore, the runs have exhibited high repeatability with RSD values ranging from 5% to 20%, typically in the range of 2–12% at moderate to high concentrations and up to 24% at lower concentrations, depending on polymer type and method specifics in different studies regarding airborne MNPs. An RSD of less than 20% is often considered acceptable with respect to repeatability and intermediate precision, as indicated by ISO standards (Hermabessiere et al., 2018).

Morioka et al. (2024) repeated measurements of the plastic standard samples were performed at concentrations approximately ten times the signal-to-noise ratio to confirm the accuracy of the repeatability and to determine the instrumental detection limit (IDL), which is three times the standard deviation, and the instrumental limit of quantification (LOQ), which is ten times the standard deviation. The coefficients of variation ranged from 1% to 20%.

Table 3.6. *Reproducibility.*

Polymer	Amount (µg)	Peak area of indicator compounds			RSD%
		Run 1	Run 2	Run 3	
PE	40-P1	1,129,711	703,885	874,179	23.7
	40-P2	444,536	388,242	375,434	9.13
PP	20-P1	365,269	392,054	374,305	3.61
	20-P2	2,714,632	2,729,399	3,360,028	12.6
PVC	80-P1	2,406,919	2,508,802	2,795,481	7.84
	80-P2	4,258,442	3,294,315	4,260,351	14.2
PET	50-P1	475,134	386,964	447,401	10.3
	50-P2	41,275,847	43,065,058	40,111,018	3.59
PS	2.5-P1	2,425,206	2,273,251	2,657,873	6.02
	2.5-P2	2,379,209	2,647,982	2,620,616	5.80
PC	1.25-P1	218,331	221,866	200,721	5.30
NR	2.5-P1	583,974	519,238	508,754	7.58
	2.5-P2	58,112	53,197	56,957	4.58
SBR	2.5-P1	82,952	63,224	59,089	18.6
	2.5-P2	536,500	485,676	632,644	13.5

According to the literature, solid mixtures possess the advantage of being unconstrained by the solubility of the polymers. Conversely, solution mixtures offer enhanced reproducibility, particularly if the reference solid polymers are available in diverse forms, such as powders, pellets, and films. Some of the most prevalent polymers, including polyethylene and polypropylene, are recognized for their extreme insolubility, a property that is only overcome under conditions that are themselves extreme.

3.5.2.2. Interference

Table 3.7 illustrates the outcome of an investigation into the potential for interference arising from the filter. As previously noted, this study employed a Teflon filter, which is one of the polymers that has the potential to induce interference. Therefore, the selection of indicators for the desired polymer was based on the absence of common indicators between the filters (Teflon and glass fiber) and the eight polymers utilized in this study. During the slotted Teflon filter mass-based analysis, PP could create interference. Subsequent Raman spectrometry of the face and back of the Teflon filter revealed that the back structure of the Teflon filter included PP with a 92% similarity ratio, while the face of the filter exhibited a PTFE cover layer with a 72% similarity ratio. Consequently, PP was removed from the list

of polymers for the analysis of 5 stages, but it was subjected to examination in the backup stage, given that the glass fiber filter was placed in this stage (Figure A. 1).

Table 3.7. *Interferences in the presence of slotted Teflon filter material.*

Polymer	Indicator compound	Occurrence
PE	P1	not detected
	P2	not detected
PP	P1	detected
	P2	detected
PVC	P1	not detected
	P2	not detected
PET	P1	not detected
	P2	not detected
PC	P1	not detected
	P2	not detected
PS	P1	not detected
	P2	not detected
NR	P1	not detected
	P2	not detected
SBR	P1	not detected
	P2	not detected

3.5.2.3. Selection of an appropriate subsample

As previously mentioned, particles with a given cutoff size that traversed the nozzle's stage were amassed as a thin line in the center of the Teflon filter slot. Accordingly, an efficient subsample should be selected on the basis of the homogeneity of the MNP distribution between different slots of a filter, which can be determined by mass-based analysis. While particles were distributed uniformly on the backup stage, an examination of the particle distribution pattern on the glass fiber filter was not necessary. Therefore, filter pieces measuring 3 x 1 cm^2 were excised (with a weight of 20 µg) from a slot of Teflon filter and another 3 x 1 cm^2 at an oblique angle from different slots (Figure 3.10). They were then injected into Pyr-GC/MS in order to detect the types of MNPs polymers and their concentration (Table A. 3).

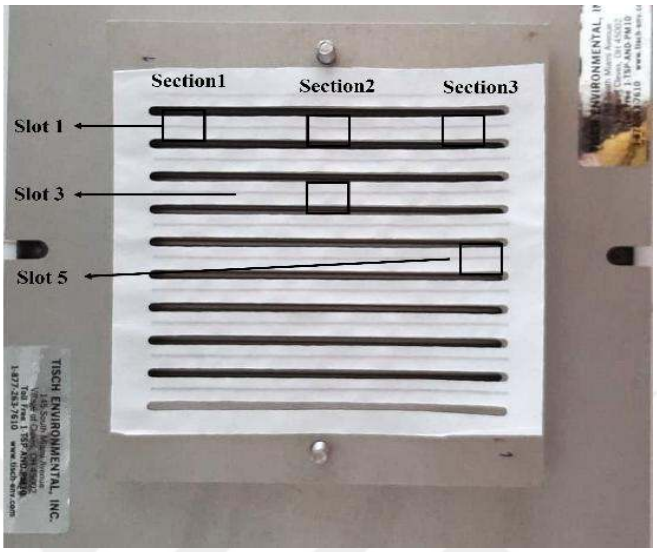

Figure 3.10. *Randomly selected subsamples for mass-based analysis.*

3.6. Statistical Analysis

A thorough investigation was conducted into the homogeneity of the MNP particles present within the filter's various slots and the subsampling approach. To this end, the results of the spectrometry analysis were subjected to a chi-square test, a statistical software program (SPSS, version 21), with the objective of investigating the homogeneity of the MNP particles in the various slots of a filter.

Determining the concentrations and sources of MNP in the air in industrial, urban and rural areas is essential for researchers to develop more effective sampling strategies and ultimately gain a better understanding of human and environmental exposure risks. Statistical analyses of the normal distribution of airborne MNPs among sampling locations were performed using SPSS software (SPSS Version 21.0). The deviation of kurtosis and skewness values from zero indicates a shift in the distribution's tendency from normality. The distribution of MNPs across each group at the sampling points was examined using the Shapiro-Wilk normality test. This test indicates whether the data sets are normally ($p > 0.05$) or log normal ($p < 0.05$) distributed. Subsequently, an independent t-test was employed to compare the levels of MNPs for data sets that exhibited normal distribution, such as those from industrial and urban areas. In the event that $p \leq 0.05$, it was concluded that there was a

significant difference in MNP concentrations. If $p > 0.05$, it can be deduced that sufficient evidence was absent to substantiate a difference.

3.7. Exposure Assessment of the Respiratory System

3.7.1. Particle-based analysis

A variety of dosimetry models have been employed in the past to estimate the deposition of inhaled particles in the lungs. Among the aforementioned models, the ICRP model is regarded as one of the most promising for the estimation of lung deposition (Guha et al., 2014). The International Commission on Radiological Protection (ICRP) model was developed in 1994 for the purpose of calculating radiation doses in humans (Stefaniak et al., 2017). The model employs empirical equations derived from experimental data and theoretical principles to estimate deposition (Laube et al., 2017). The method is capable of calculating region-specific deposition, including that occurring in the head airway, tracheobronchial, and alveolar regions. Although the model is relatively simple, it employs a holistic approach to deposition in the lungs that is as efficient as that of more complex models (Hofmann, 2011).

The equations require two components inhalation fraction and particle diameter. Inhalation fraction (IF) is the ratio of aerosol inhaled to the total aerosol in the airflow. It is affected by the entry point, the flow rate and particle diameter (Wang et al., 2009).

where,

IF= Inhalation Fraction d_p = Diameter of Particle (μm).

$$IF = 1 - O.5(1 - (1/(\ 1 + 0.00076\ dp\text{^}2.8)) \quad (3.1)$$

The ICRP model uses empirical equations to give

Head Airway (3.2)

$$DFHA = IF\left(\frac{1}{1 + \exp(6.84 + 1.183\ lndp)}\right) + (1/(1 + exp\ (0.924 - 1.885\ lndp))$$

Tracheobronchial Region (3.3)

$$DFTB = (0.00352/dp)\,(exp\,(-0.234(ln\,dp + 3.4)\text{^}2)) + (63.9\,exp\,(-0.819\,(lndp - 1.61)\text{^}2))$$

Alveolar Region (3.4)

$$DFAL = (0.0155/DP)(\,EXP\,(-0.416(ln\,dp\, +\, 2.84)\text{^}2)) +\, (\,19.11\,exp(-0.482(lndp\, -\, 1.362)\text{^}2))$$

3.7.2. Mass-based analysis

Particulate matter (PM) risk assessment using the Risk Framework Criteria (RfC) method is based on a systematic evaluation of the potential hazards and consequences associated with exposure to fine particulate matter ($PM_{2.5}$) and larger particles (PM_{10}) (EPA, 2001). The following is a structured approach. In the context of environmental health risk assessment, the risk equation represents a straightforward quantitative methodology for evaluating the potential for adverse health effects associated with exposure to specific contaminants, such as PM and MNPs (Equation 5).

$$\text{Hazard Quotient (HQ)} = \frac{\text{Exposure Concentration (EC)}}{\text{Reference Concentration (RfC)}} \quad (3.5)$$

This ratio is crucial for determining whether the measured exposure concentration exceeds the acceptable risk concentration (AC) threshold established by the Environmental Protection Agency (EPA, 2001).

EC: It signifies the actual concentration of PM (e.g., PM $_{2.5}$ or PM_{10}) to which a population or individual is exposed to the environment. (In most cases, the measurement is expressed in micrograms per cubic meter ($\mu g/m^3$)).

RfC: A threshold value that represents the concentration of a pollutant that is deemed safe over a specified exposure duration. Such determinations are typically made by regulatory agencies, such as the United States Environmental Protection Agency (EPA), the World Health Organization (WHO), or local environmental authorities.

The effective communication of risks and the guidance of regulatory decisions for the protection of public health can be achieved by the utilization of a combination of quantitative measures and qualitative descriptors (Table 3.8) (Epa, 1989).

Table 3.8. *Risk levels.*

Range EC/RfC	Risk level	Implications
0 < EC /RfC <0.1	Negligible Risk	No significant effects: safety margin is high.
0.1 < EC /RfC <1	Low Risk	Acceptable, but monitoring is advisable.
1 < EC /RfC <10	Moderate Risk	Health effects are likely; mitigation is needed.
EC /RfC >10	High Risk	Unacceptable

3.8. Quality Assurance and Control

In order to guarantee precise and dependable outcomes when examining MNPs, it is of paramount importance to implement rigorous contamination control measures. It is imperative that a white cotton lab coat be worn during all sampling and analysis procedures to prevent the contamination of samples by airborne MNPs. In conducting the experiments, all chemicals, including deionized water (Milli-Q water), were filtered through a 47 mm filter with a pore size of 0.45 μm, composed of glass fiber sourced from Whatman in China. All glassware, sampling funnels, tweezers, Petri dishes, and components of the vacuum filtration devices were rinsed with pre-filtered deionized water. The three blanks field (industrial, urban, and rural) were subjected to a comprehensive examination employing both particle and mass-based analysis methodologies. In the present study, no polymer was identified in the field blank. This outcome can be attributed to the implementation of slotted Teflon filters in cascade impactors, which were executed in a timely manner. Furthermore, the Teflon filter surface is distinguished by its smoothness, which impedes the adhesion of airborne particles, particularly those measuring less than 10 microns, through a passive process on its surface. Additionally, the filters were analyzed immediately after receipt, without undergoing any treatment, and spectroscopic analysis was conducted using the micro-Raman Renishaw model, with the sample placed in a closed chamber. In the context of studies employing blanks, contamination is often identified, with fibers being the most prevalent contaminant. However, in this particular study, the presence of fibers was detected only in a limited number of cases (Blair et al., 2019). To prevent contamination and ensure the accuracy of the Pyr-GC/MS experiment, emptying transfer lines, particularly those employed in gas

chromatography, is critical. Strict quality control measures were taken in every step of the analysis.

The preparation of the samples and the filtration processes were conducted in accordance with standard biosafety protocols within a clean laminar flow hood. To prevent contamination, personnel wore no latex gloves during the sampling and experimental phases of the study. This decision was based on the observation of latex particles in some samples (procedural blanks), which were subsequently confirmed to be the source of contamination through the use of μ-Raman spectroscopy.

Table 3.5 defines two indicators, designated P_1 and P_2. By calculating the P_2/P_1 ratio (Table A.4) of the corresponding indicator compounds in the calibrated polymer standards, it is possible to ascertain whether they originate from different impurities in the actual samples (Albignac et al., 2023). For all types of polymers, the formation of several decomposition products in significant proportions was observed. Consequently, a second indicator compound was recorded, and the ratio (P_2/P_1) was employed as an additional validation criterion. The ratio P_2/P_1, representing the ratio of two pyrolysis indicators of polymers, was evaluated during calibration for various polymers in Pyr-GC/MS analysis of MNPs. Key findings include, for most polymers except polystyrene (PS), polyethylene terephthalate (PET), and polycarbonate (PC), the P_2/P_1 ratio remained remarkably stable throughout the calibration process, with relative standard deviation (RSD) values consistently below 15% when analyzing pure polymers. For PS, monitoring the styrene dimer-to-trimer ratio (which corresponds to P_1 and P_2) is particularly important because matrix effects can significantly alter this ratio. Despite these effects, the ratio showed acceptable stability with an RSD of about 22%. Additional PET and PC reference materials were tested, but the variability observed in their P_2/P_1 ratios was not fully rationalized, indicating more complex behavior or matrix interactions for these polymers. In the analysis of airborne samples, the P_2/P_1 ratio for PS exhibited greater variability (~13%), which is considered favorable as it reflects the method's sensitivity to environmental matrix effects and sample heterogeneity. This stability and variability pattern of the P_2/P_1 ratio across polymers and sample types highlights its utility as a quality control and interference indicator in Py-GC/MS analysis, especially for PS where matrix interferences are more pronounced,

this ratio is a critical parameter for ensuring reliable polymer identification and quantification by Pyr-GC/MS, especially when dealing with complex environmental samples

4. RESULTS AND DISCUSSION

4.1. Particle-based Analysis of Micro(nano)plastics

4.1.1. Selection of the substrate filter

Visual assessment is a fundamental yet subjective component of MNP investigations. It serves as a preliminary step in determining the presence and location of potential MNPs in the filter, as well as facilitating the subsequent identification of particles. The examination of particles in such a chemical cocktail, comprising hydrocarbons, salts, and other compounds emitted by vehicles and industrial sources, as well as naturally occurring components such as silicate dust and microorganisms or PM itself, represents a significant challenge in the field of atmospheric aerosol research. This issue was not addressed in sufficient detail, particularly in light of the existing studies on airborne MNPs, which tend to focus on total suspended particles (TSPs) or PM_{10} samples. In this study, airborne particles are sampled by a cascade impactor into six size fractions, thereby reducing the potential for interference from cocktail components during visual investigation. This approach allowed for a more efficient analysis process, as it enabled physical separation of particles by size at the sampling stage. Size segregated airborne particles can be collected by cascade impactors using a variety of slotted collection substrates.

Despite the variety of filters currently available, there are limited types of slotted filters (aluminum and Teflon are surface filters; quartz and glass fiber filters are depth filters) that can be used depending on the sampler manufacturer. In order to identify MNPs from collected particles, surface filters were chosen over depth filters. The penetration of particles through the interior fiber structure can lead to difficulties in particle identification by microscopes, particularly μ-Raman microscopes, or may negatively affect particle transfer or isolation from other particles contained in the filter for subsequent experimental procedures. To illustrate, the microscopy images (stereo and SEM) of particles collected on glass fiber filters are presented in Figure 4.1. As can be observed, the fibrous strands of glass fiber filters positioned on the particles may impede the reception of the laser beam by a single particle during point-by-point analysis using μ-Raman spectrometry, which presents a significant challenge for identification.

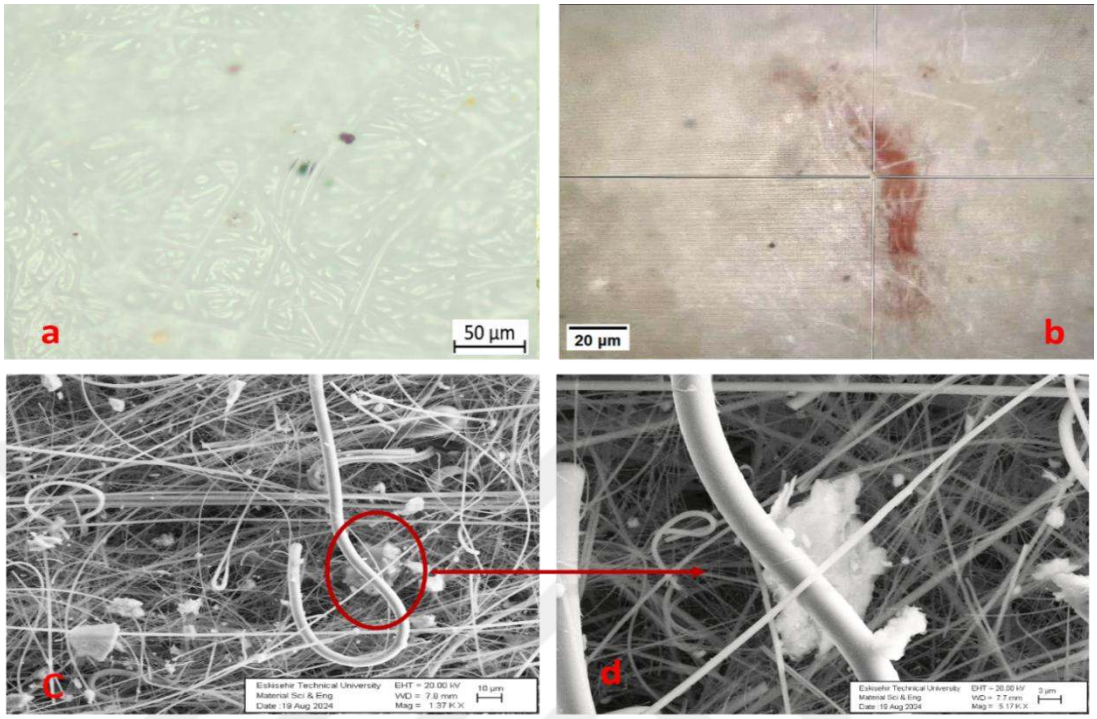

Figure 4.1. *Particles trapped in glass fiber filter (depth filter), a) fragments-stereo and b) fiber-stereo, c) fragment-SEM (scale bar: 10 µm), d) fragment-SEM (scale bar: 3 µm).*

A slotted Al filter was initially used to collect airborne MNP samples, due to the absence of any polymeric material within the filter structure. The analysis of 2 cm^2 of a slotted Al filter using an Axioscope 5 microscope (Figure 4.2a) revealed that all particles collected on the surface of the filter appeared dark and black in color. This observation renders a visual assessment of Al filters inappropriate for microscopic and subsequent spectroscopic analysis. Such an approach is frequently employed by researchers to select a specific particle from a multitude of particles based on its morphological properties, allowing for the rapid distinction of MNPs from other particles (Boakes et al., 2023). Therefore, it is exceedingly challenging to differentiate between likely MNPs and other airborne particles collected on the Al filter surface based on their morphological characterization. In addition, images from the slot edge of the Al filter were not clear due to the vacuum applied during sampling, which deformed the structure of the edge, so that particles deposited in this area could not be examined (Figure 4.2b).

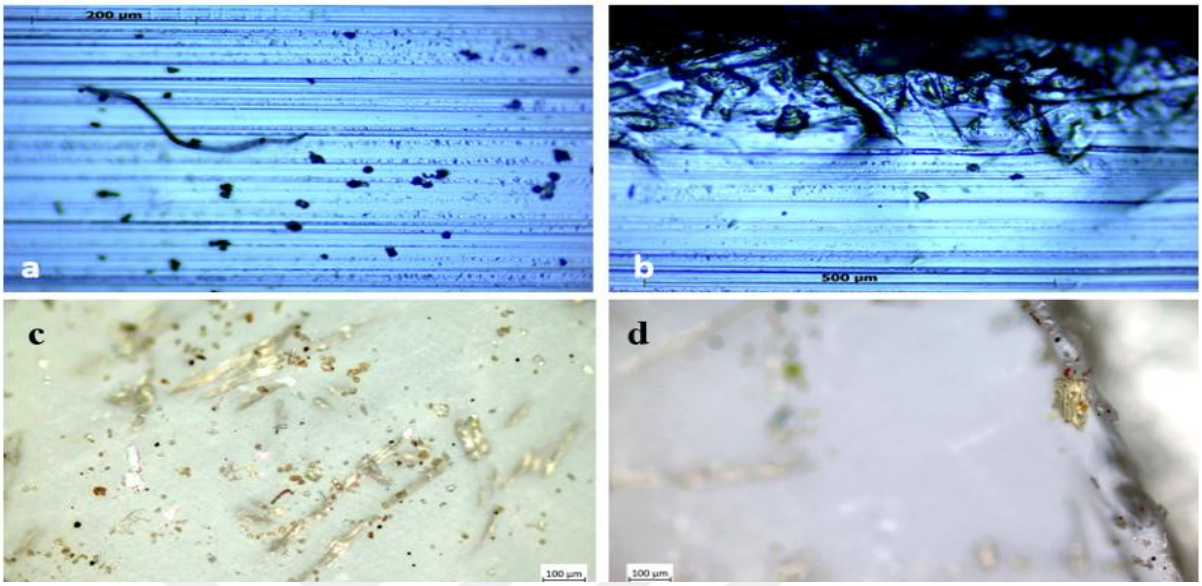

Figure 4.2. *Visual analysis of particles in stage 1 slotted filters a) middle/center zone of Al filter, b) the edge of Al filter, c) middle/center zone of slotted Teflon filter, d) the edge slot of Teflon filter.*

To investigate the morphological characterization of the particles collected on the surface of the Al filter, the particles must be transferred to a filter with a white and transparent surface. Of the three methods used, the Al filter was damaged during the ultrasonic bath technique (caused the corrosion of the structure of the Al filter, Figure B. 1); the vortex approach had the lowest efficiency (almost all of the particles remained on the filter, and about 10% of the particles were transferred from the Al filter); and deionized water washing had the highest efficiency (with an estimated amount lower than 20% of all particles retained on the filter), but this technique could not transfer all the particles collected on the filter. The results of the transfer procedures indicated that particles that may be polymeric may be lost during the transfer process, which could result in an underestimation in further analysis.

The particle transfer approach has been pursued in the literature for cascade filters, primarily to increase the number of MNPs per unit volume required for pyrolysis-GC/MS analysis (Mizuguchi et al., 2023b; Morioka et al., 2024), rather than for visual or spectroscopic examination. This led to the use of a surface filter, namely a slotted Teflon filter, for sample collection. Visually, the Teflon filter has a smooth and transparent surface; therefore, the particles collected on the Teflon surface could be distinguished by shape and color (Figure 4.2c), and even particles located at the edge of the slot were easily detected

(Figure 4.2d). Accordingly, Wright et al. (2019) reported that the morphological identification of particles (or likely microplastics) on the Teflon surface can be readily accomplished without the necessity of dislodging the particles for further examination (Wright et al., 2019).

The proportion of particulate matter (PM) identified as polymer remains inconclusively determined across all studies, thus precluding any definitive conclusions. A recently published study has indicated that 38 % of particles in the total suspended particulate (TSP) sample were determined to be MPs, followed by $PM_{2.5}$ (32%) and then PM_{10} (30%)(Jannah et al., 2024). Moreover, automotive wear and tear from car tires is acknowledged as a source of MNPs in the atmosphere (Kole et al., 2017), estimated to contribute between 0.8 and 8.5% of the PM_{10} mass fraction and between 1 and 10% of the $PM_{2.5}$ fraction (Panko et al., 2019). The observed variability in these percentages can be attributed to a number of factors, including the presence of local pollution sources, traffic density, and seasonal changes in atmospheric conditions (Amato-Lourenço et al., 2020). Consequently, the primary objective of studies examining airborne MNPs should be the minimization of sampling artifacts for particle-based analysis, despite the long history of microscopic analysis of airborne particles.

As will be discussed in subsequent sections, this issue can be addressed through the use of size-fractionated sampling. For example, our experience has shown that particles collected on stage 2 (>3 μm) and partially stage 3 (> 1.5 μm) exhibit comparable morphological characteristics when examined at lower cut-offs than stage 1 (>7.2 μm). As a transitional stage, particles smaller than 3 μm with a distinct morphology and formation mechanism may exhibit different behavior and may include particles that are typically present in the fine size range. Stages 4 and 5 have similar characteristics in that the particles collected on the surface are densely populated (hundreds of particles per mm^2), making visual inspection of the particles almost impossible. Considering the backup filter (Figure 4.3), which is a depth filter, the high loading of particles <0.49 μm, including likely NPs, hinders the particle-based identification of single micron or nano-sized particles by visual inspection and spectroscopy. Consequently, stages other than stage 1 are not subject to qualitative evaluation in this context. Therefore, mass-based analysis techniques such as pyrolysis-GC/MS should be employed to

determine MNP concentration for particles smaller than 3 µm (i.e., stage 4/5 and the backup) to provide a basis for future investigations.

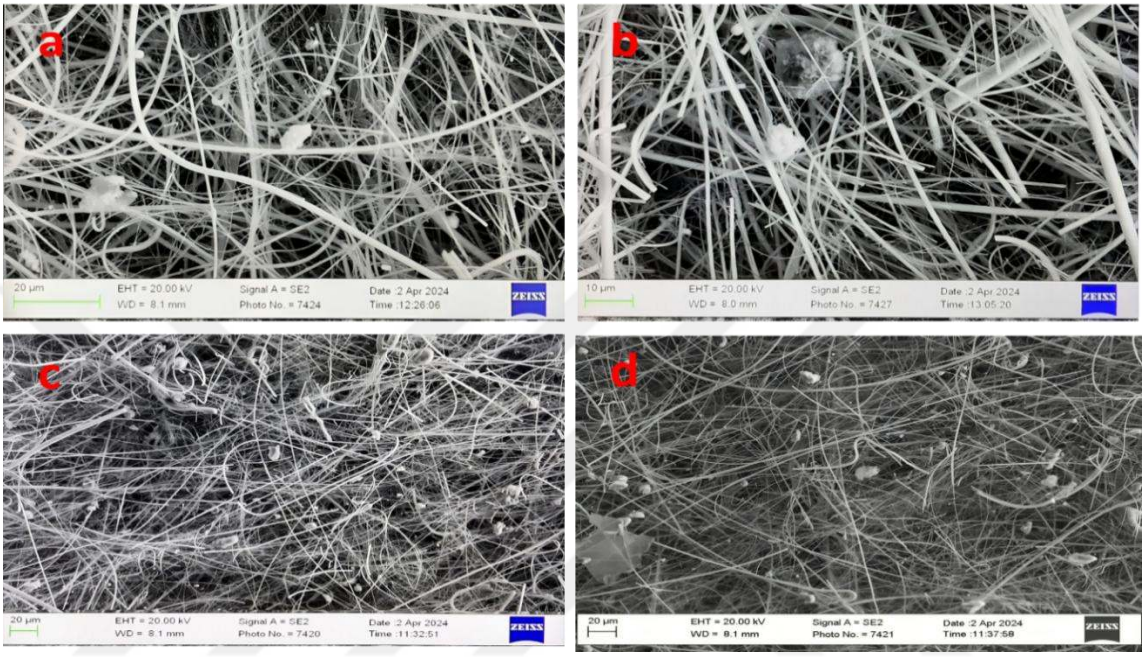

Figure 4.3. *SEM images of particles collected on the surface of a glass fiber filter (back-up). a, b) 667X, c, d) 881X.*

Employing spectroscopy microscopes for detecting tiny MNPs (< 20 µm) underscores the critical importance of particle isolation by filtration onto a filter and the selection of an appropriate filter material for effective MNP analysis (Käppler et al., 2015; Oßmann et al., 2017; Pittroff et al., 2021). In most studies, metal-coated polycarbonate (PC) membranes, such as those coated with gold (Cabernard et al., 2018; Schymanski et al., 2018), or aluminum-coated with various pore sizes ranging from 1.0 µm to 10 µm (Oßmann et al., 2017) have been used as the filter material for Raman analysis. A fabricated silicon (Si) membrane is a suitable filter for both µ-FTIR and µ-Raman analysis, as suggested by Käppler et al. (Käppler et al., 2015). On the other hand, some studies have suggested the use of aluminum oxide membranes (e.g., Anodisc 25 mm, Whatman, U.K.) (Löder et al., 2017) or, for counting larger particles (>100 µm), glass-fiber filters (Pittroff et al., 2021).

In this study, Teflon filter was selected as a suitable sampling medium for a high-volume cascade impactor sampler because the distinct Raman spectrum of PTFE shows clear

differentiation from the majority of common plastic materials in the characteristic spectral region of the polymers (C-H bands: 2800-3150 cm^{-1}).

In addition, the Teflon filter shows numerous interferences in the range of 290-1400 cm^{-1} (e.g., notable peaks at 735 cm^{-1} and 1380 cm^{-1}) but lacks any Raman bands in the characteristic C-H stretching bond region of polymers, specifically between 2800 and 3150 cm^{-1}. Consequently, this study suggests that a slotted Teflon filter can be used to detect MNPs when particles <10 µm are to be examined by Raman spectroscopy.

4.1.2. Pre-treatment of airborne samples

When studying MNPs in environmental samples, there are limitations due to the presence of natural organic and inorganic substances that cause interference (Ivleva et al., 2017). Previous studies have attempted to propose a valid pretreatment method for MNPs analysis but have often focused on MPs >10 µm. They typically used chemical digestion techniques, including acids, bases, oxidation, or enzymatic reagents, to remove organic particles from the sample (Hurley et al., 2018). However, among the methods, H_2O_2 digestion under controlled conditions has been introduced as a more effective technique, especially since this technique is used in the majority of airborne MPs studies (Y. Zhang et al., 2020). Accordingly, chemical digestion using 30% H_2O_2 for 48 hours at room temperature was adopted to remove organic constituents. The digestion of a 2 cm^2 piece from each of the five stages of the Teflon filter showed that the color and size of the particles revealed a transformation (Figure 4.4), regardless of their origin (i.e., synthetic or natural organic).

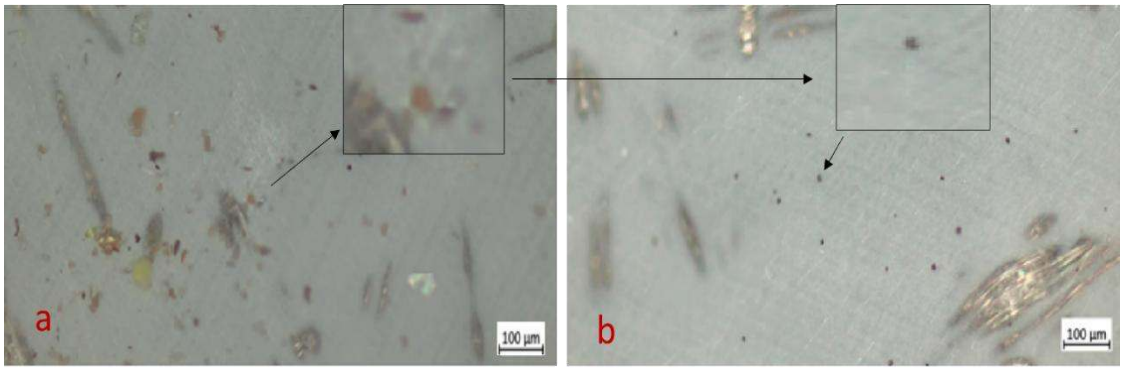

Figure 4.4. *Visual analysis of particles on PTFE filter a) before H_2O_2 digestion, b) after H_2O_2 digestion.*

This can be interpreted as oxidation of colored organics but some previous studies have also reported the similar effects of H_2O_2 digestion on the morphological properties of MPs (often larger than 10 microns), so to optimize this approach, it has also been suggested to use 10% H_2O_2 and reduce the exposure time to 24 hours (Al-Azzawi et al., 2022; Barceló et al., 2023; De Frond et al., 2023; Rahman et al., 2021). This time, the results indicated that 10% H_2O_2 can reduce the size of some particles (1-10 μm), and most of the particle color changed to black. It appears that these smaller particles, with a higher surface area to mass ratio, may be more susceptible to the negative effects of chemical digestion than their larger counterparts (Al-Azzawi et al., 2022). This is despite the fact that the H_2O_2 and Fenton has been fine-tuned and confirmed for a range of MPs (1-330 μm), particularly in wastewater effluents (Al-Azzawi et al., 2022). Hu et al. (2023) found that exposure to 30% H_2O_2 caused damage to the MPs; as the digestion time increased, the size of MNPs decreased (the size of 5 μm and 20 μm sized microplastics decreased by 7.7±2.3% and 4.5±1.0%, respectively); while this treatment may not have a noticeable effect on the size of larger MPs, a small loss of surface material could significantly affect the size of sub-micron particles (Barceló et al., 2023). O'Brien et al. (2023) stated that H_2O_2 (30%) digestion may cause discoloration in polyethylene terephthalate and polypropylene and may result in observable changes in polyamide and polycarbonate (De Frond et al., 2023; Logvina et al., 2024; Okoffo et al., 2019). Hurley et al. found that while treatment with H_2O_2 may not noticeably affect the size of larger microplastics (>100 μm), even a small loss of surface material could notably influence the size of sub-micron particles (Hurley et al., 2018). A further challenge in using Raman spectroscopy for the identification of plastics embedded in organic materials is fluorescence. Many organic materials show intense fluorescence when stimulated by the Raman laser. This can result in masking of the Raman signals from plastics, leading to misidentification (Liu et al., 2023). Consequently, some researchers, such as Rahman et al. (Rahman et al., 2021), decided to continue the analysis without any pretreatment. It can be reasonably deduced that the degradation of particles and the impact of each digestion technique on plastic particles may potentially influence the reported concentrations, size distributions and polymer compositions (as an indicator of weathering or environmental degradation), especially when analyzed using Raman spectroscopy. The findings of the

present study suggest that H_2O_2 digestion may be an appropriate pretreatment method for larger particles, including likely MPs, in other environmental matrices.

On the other hand, some studies have also used the density separation technique together with chemical digestion to isolate MNPs from other inorganic materials using different types of salt solutions in airborne MNP studies (Liu et al., 2022). Floatation, or density separation, is based on the difference in density between MNPs and other particles, causing MNPs to float on the surface of the solution. In this context, the theoretical aspects of physical pretreatment are discussed in relation to the physicochemical properties of airborne particles, based on data gathered from the existing literature. The data set includes a number of particles with varying densities resulting from atmospheric sampling (Figure 4.5). A closer examination of the density of airborne particles <10 μm in the literature suggests that there does not appear to be a significant density difference between the various types of particles collected and the density of virgin MNPs to confirm this hypothesis. Although virgin MNPs are not a direct indicator of environmentally aged and contaminated MPs (i.e., with organics, inorganics, or microorganisms), a reasonable comparison can be made given the density ranges of particles in atmospheric samples. The data presented in Table B. 1 indicates that the mean density of components gathered under PM_{10} is 1.8±0.8 (g/cm^3), while the mean density of polymer particles is 1.4±0.4 (g/cm^3). In the region between 1 and 1.5 g/cm^3 in Figure 4.5, which encompasses commodity plastics (PE, PP, PS) and particulates such as black carbon/soot from incomplete combustion or exhaust emissions in the fine size (<2.5 μm)(Tang et al., 2024), separation may prove challenging due to the reduction in particle size. Even in consideration of the effective separation solutions, namely sodium iodide (NaI, 1.67 g/cm^3) and zinc chloride ($ZnCl_2$, 1.6-3.02 g/cm^3), particles smaller than 10 μm may not be separated unselectively, irrespective of the type, due to the close density together with surface tension of liquid (Wang et al., 2015). Therefore, density separation may not be an efficient step when also considering the limitations of controlled experimentation conducted on such a small size (≤10 μm) for airborne MNPs.

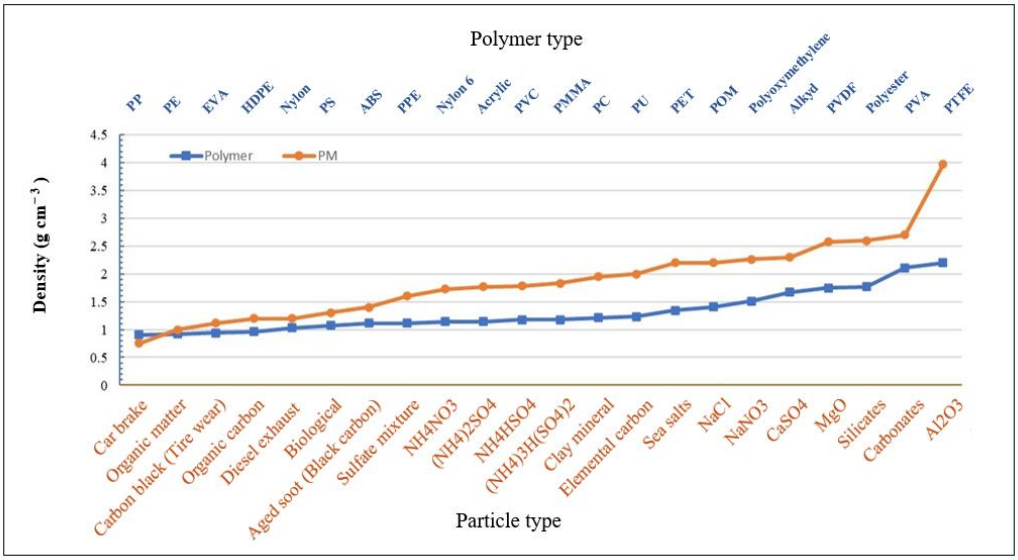

Figure 4.5. *A comparison of the densities of virgin MPs and PM constituents (PM<10 μm).*

In sum, as the MPs in samples decrease in size, there is no established procedure or clear consensus regarding the use of density separation by using solutions or chemical digestion as a pretreatment method prior to subsequent analysis. The recent trend in airborne MP studies has been to analyze samples directly through various microscopes without any pretreatment (Aliff et al., 2020; Cunningham et al., 2022; Dris et al., 2017; Gaston et al., 2020; S. Kernchen et al., 2022; Lai et al., 2019; D. Liu et al., 2020; Trainic et al., 2020; Uddin et al., 2022; T. Wang et al., 2020).

4.1.3. Selection of an appropriate subsample

Performing a microscopic analysis, especially a spectroscopic analysis, on the entire filter surface is a labor-intensive and time-consuming process that can take anywhere from a few days to a few weeks per filter, depending on the number/amount and size range of the particles involved (Pittroff et al., 2021). In previous studies, the particle size distribution showed a noticeable increase in smaller diameters in both samples and blanks. The number of particles may be observed to increase further when examining plastic particles at the single-micron level (Pittroff et al., 2021; Pivokonsky et al., 2018; Schymanski et al., 2018). For practical reasons, only a portion of the filtered area is typically inspected, ranging from

0.1 to 30 percent (Cabernard et al., 2018; Schymanski et al., 2018). Therefore, it is inevitable to select an efficient subsample for quantitative analysis of MPs and their distribution on the surface of the filter slots for particle-based investigations. The number of particles counted in the 20×20 μm^2 aperture was approximately 15±4 (n=5), which was extrapolated to yield an estimated 1,800,000 particles across the entire Teflon filter. A total of 20 particles in 1 cm^2 were selected as a subsample, representing 0.001% of the total number of particles collected on the filter (4800 mm^2) and 0.83% of the filter surface area. In accordance with the findings of a previous study, which indicated that at least 0.1% of particles must be analyzed (Cabernard et al., 2018; Schymanski et al., 2018), the examination of 1,800 particles by micro-Raman exceeds the feasible number for analysis. Moreover, as evidenced by research that employed particle-by-particle or point-by-point µ-Raman analysis (Gaston et al., 2020), a random subsample of 20 particles was selected". Accordingly, 20 to 40 particles were randomly selected to examine and distinguish MPs from 1 cm^2 pieces of the Teflon filter in different slots diagonally (odd slots from 1 to 9) of the first stage (stage 1). A random spectrometric analysis of 20 particles indicated that 40% of the PMs were identified as MPs in slots 3, 5, and 9 (8 out of 20 particles), 13 MPs were detected in slot 1 (65% of 20 particles) and 14 MPs were found in slot 7 (70%). Consequently, the results demonstrated that an average of 51±15% of the particles across slots were identified as polymeric in nature (Table B. 2).

To assess the homogeneity of the distribution of MPs among the different slots in the slotted Teflon filter, a chi-squared test with a 95% confidence level ($\alpha = 0.05$) was employed. The critical value based on the standard chi-squared table, degrees of freedom (df), and ($\alpha = 0.05$) were determined to be 9.49, and the calculated chi-squared value was obtained as 3.6, indicating that the critical chi-squared value was greater than the calculated chi-squared value. In this case, the hypothesis of homogeneous distribution of MPs in different slots in a Teflon filter can be accepted at the 95% confidence level. The distribution of plastic particles among the slots gives an idea of the selection of slot 5 (the slot in the center of the filter), which yielded a near average distribution percentage to reduce the time and cost of further analysis. Meanwhile, during the spectrometric analysis of the particles collected in stage 5, the particles may overlap and cause interference (Figure 4.6), which can increase the analysis

time. Therefore, scanning electron microscopy (SEM) was selected to investigate particles collected in stage 5 and the backup. The results of the SEM-EDX analysis will be delineated in the scanning electron microscope section with greater particularity.

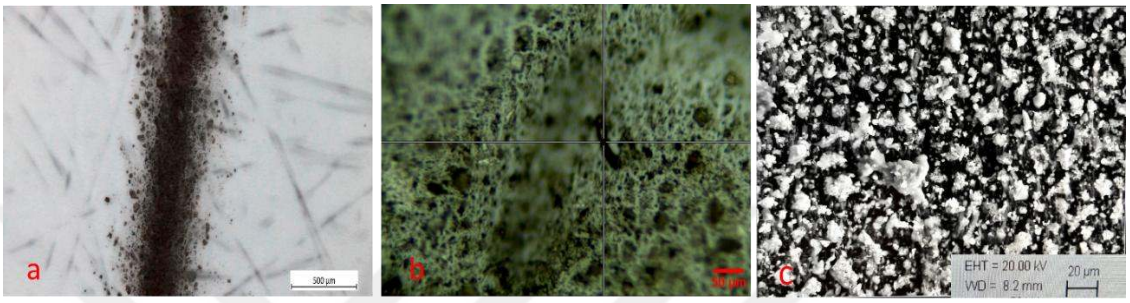

Figure 4.6. *Particles collected in stage 5 with flow rate 40 cfm in the 24 hours, a) Microscope image (5X, scale bar: 500 µm), b) Raman image (20X, scale bar: 50 µm), c) SEM image (1.79 kx, scale bar: 20 µm).*

To statistically evaluate the number of particles that were randomly selected to detect MPs, the number of particles was increased to 40 particles and analyzed in slot 5 of different stages. The results yielded 13 MPs (33%) in stage 5, 18 MPs (45%) in stage 3, and 25 MPs (62%) in stage 1, with an average of 47±15% of the particles being polymeric across all stages. This suggests no significant difference between the 20 and 40 particles, and that time savings can be achieved during µ-Raman analysis. In addition, the point by point Raman identification took about 2 hours to analyze only 20 particles on a 1 cm^2 slot (0.83% of the filter area), whereas in a previous study, the time required to analyze particles down to 5 µm was reported to be 4 to 8 days for analyzing only 22.1% of the filter area (25 mm diameter) to find particles and 1.4% for Raman imaging results (Pittroff et al., 2021). Consequently, the statistical validity of the findings can be ensured by randomly selecting 20 particles from a 1 cm^2 area on the diagonal path of a slotted filter. In a recent study, (Zhu et al., 2021) employed uniform methodologies to obtain comparable airborne MNP data in Chinese megacities, with an analysis of around 20 particles on a glass fiber filter utilizing µ-FTIR to verify the distinction between plastic and nonplastic particles. In light the size limitations of µ-FTIR, this study contributes to the recent literature with a systematic counting methodology, extending down to single-micron particles, via Raman microscope (Levermore et al., 2020).

Morphological examination of a total of 51 particles identified as polymeric revealed that 86% of the MPs can be classified as belonging to the fragment group (2.8-24.8 μm) and 14% to the fiber group (28.6-212 μm) in stage 1 (Figure B. 3) (cascade impactor of stage1, size range >7.2 μm) (Figure B. 4). Moreover, the shape of the collected particles was irregular, suggesting secondary MPs as a source. Furthermore, the size of the particles retained did not conform to the cut-off limits in stage 1, indicating the elastic behavior of plastic particles. The use of cascade sampling can be susceptible to the effects of particle bounce and re-entrainment, which could potentially contribute to the observed lack of conformity (Elmes and Gasparon, 2017). Cascade impactors separate particles based on size using inertial impaction. Inertial force propels particles through nozzles, separating them by size. Larger particles have greater inertia and impact collection surfaces more. If particles are propelled at a high velocity or through optimal flow conditions, they may bypass impaction sites and continue through the nozzle (Kwon et al., 2003; Romay and García-Ruiz, 2023). The interaction between airflow and particles is complex and not fully understood. This can also be attributed to the size of particles measured as ferret diameter using the ImageJ software. The cascade impactor limits are based on the aerodynamic diameter (a spherical particle with a density of 1 g/cm^3 (i.e. the density of water) settling in still air at the same velocity as the particle in question). The range of particles measured is larger than the cut-off size at various stages of the cascade impactor because the aerodynamic diameter is much smaller than the ferret diameter of the particle. For instance, the long fiber wraps around itself with a Brownian motion at high speed due to the air flow and can pass through the cascade impactor nozzles, so the fiber bundles are often seen swinging on the surface of the filter. Particle behavior near the cut-off size may be unpredictable, leading to misclassification (Copley and Scientific, 2008).

To sum up, the number of polymer particles per m^3 of air was estimated based on particle-based quantification (random selection of 20 particles) and filter characteristics, yielding 452±134 MPs /m^3 of air in the mean size range of 10.5±5.52 μm for fragments and 96.9±86.2 μm for fiber (considering only stage 1). Of the few studies in the literature that focused on size-segregated plastic particles, the size of MPs analyzed by μ-Raman spectroscopy was around 4 μm, and the average concentration of MPs was 91±47 MP/m^3 (S.

Kernchen et al., 2022). On the other hand, in another study collecting particles on a polycarbonate filter using low-volume sampler reported the presence of inhalable-sized airborne MPs with about 192±127 MPs/m^3 from the analysis of 50 particles in ambient aerosol (Yoo et al., 2023). In studies based on particle-based analysis, the reported uncertainty of concentrations was often considerable. This was due to the inability to examine all of the particles, and the random selection of particles for identification. Nevertheless, the degree of uncertainty regarding MPs concentration in this study was found to be less pronounced than in the aforementioned studies.

The polymer composition of the particles detected in the samples was 92% as carbon black (47 particles; two major peaks were found at D band:1350 cm^{-1} and G band:1590 cm^{-1}) and 8% as polypropylene (PP) (4 particles; the 2962 cm^{-1} peak was more intense and the second set of peaks were placed at 973 cm^{-1}) (Figure B. 5), with the similarity percentages set at >75%. PP is a lightweight polymer with a low density, which allows particles to remain airborne for longer. PP particles are small and light, which helps them stay suspended in the air and travel long distances. They can also gain an electrostatic charge, which affects how they move in the air and contributes to their prevalence in smaller sizes (Kernchen et al., 2024). Kernchen et al. found that polypropylene (PP) was the most common airborne MP polymer. The majority of sampling sites showed a high prevalence of PP, reaching 65% in the suburban region specifically in areas with a concentration of airborne MPs > 4 μm (Sarmite Kernchen et al., 2022). Another study found that polypropylene particles were the most prevalent, representing 62% and 54% of particles > 11 μm in wet and dry samples. Raman imaging with a 0.5 μm $pixel^{-1}$ step size of three 100×100 $μm^2$ quadrants did not identify plastic particles in the submicron range. The submicron particles were identified as quartz, calcite, soot, and likely amylose or another polysaccharide (Kernchen et al., 2024). Carbon black is produced by the decomposition of rubber fractions in scrap tires, and industrial combustion and has been identified as airborne MPs in settled road dust (Figure 4.7).

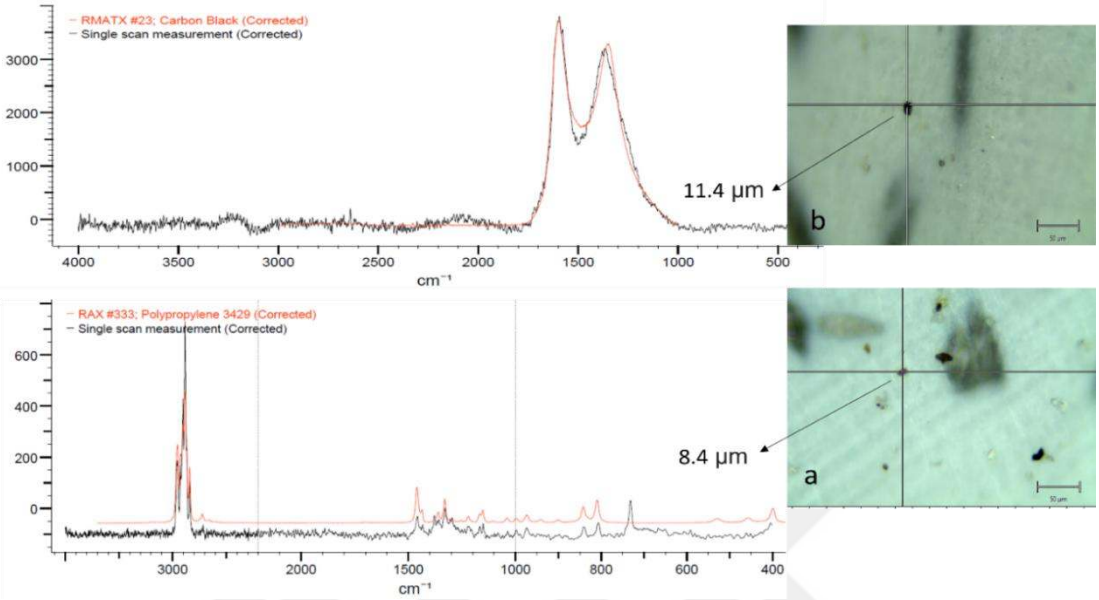

Figure 4.7. *Chemical identification of MPs by micro- Raman, a) Polypropylene and b) Carbon black spectrometric peaks.*

A diversity of particles can be present in an airborne sample depending on the meteorological conditions or the sampling methodology employed. As the use of size-segregated sampling indicates nearly homogenous distribution of particles on the filter, one should be careful during identification process. It was necessary to consider multiple lines of evidence to characterize the composition of particles using the microscopic and spectroscopic methods due to small particle size. In this study, we followed a method for quantifying airborne MPs from size-fractionated samples by combining visual analysis (microscope, SEM-EDX) and Raman spectroscopy. In cases where the results were inconclusive, we employed pyrolysis-GC/MS to obtain additional confirmation. In the visual approach, particular attention was paid to the morphological characterization (Luo et al., 2022) of randomly selected particles for analysis by spectrometry. An attempt was made to select a single particle and to prevent the selection of a cluster of particles that were adhering together (Figure 4.8 and Figure B. 6). Moreover, the majority of the black particles were identified and classified as carbon black, which is manufactured commercially via controlled combustion, exhibiting an irregular and single particle structure. In contrast, the particles identified as black carbon or soot, which are undesired byproducts of incomplete combustion,

formed a cluster comprising a number of spheres that were sticky to a certain degree (W. Li et al., 2024b). A total of 33 SEM-EDX spectra from stage 1 were examined, of which nine exhibited a high carbon content (87.7±9%), while 24 demonstrated carbon content of 43.3±10.7%. These findings indicated that the high-carbon particles were analogous to the polymer particles (Long et al., 2013).

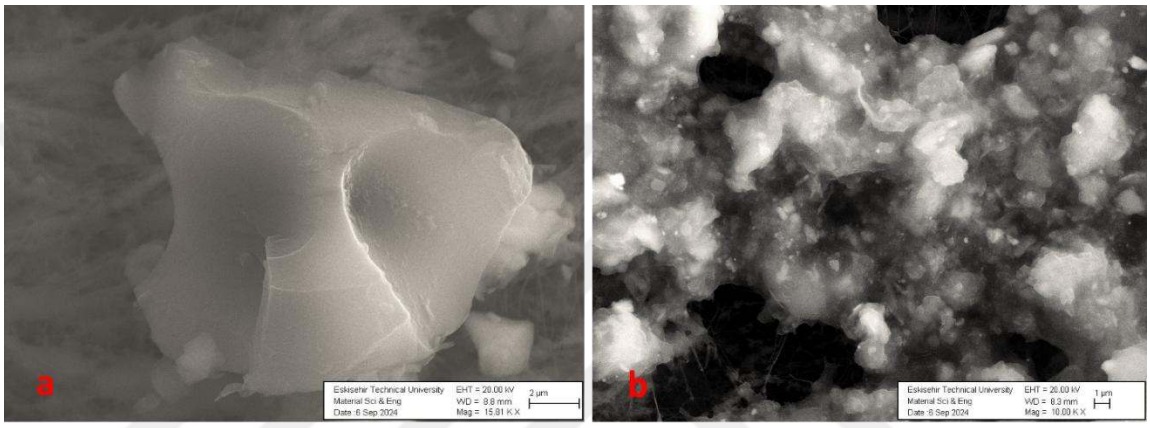

Figure 4.8 *a) A single particle to select for chemical identification with spectrometry analysis, b) A cluster of particles that were not selected for spectrometry.*

In Raman analysis, the ratio of intensity between the D and G band may serve as additional evidence indicating that the source of black particles is carbon black exiting the tire, rather than exhaust emissions (soot). The results of the peak spectrum analysis of carbon black indicated that the intensity of the G band was greater than that of the D band ($I_D<I_G$). However, this observation is inconsistent with the typical patterns observed in soot spectra, where the G band at approximately 1600 cm^{-1} and the D band at 1350 cm^{-1} are prominent, and the D band intensity was greater than G band(Haller et al., 2019; Lenz et al., 2015; Marina-Montes et al., 2023).

As evidenced by the findings of Gillibert et al. (2019), in the low-frequency region (800 cm^{-1}), amorphous carbon exhibits the following characteristics: The spectrum is weak and devoid of features, indicative of the absence of coherent vibrational modes. In the high-frequency region (>2000 cm^{-1}), the absence of overtone and combination bands is attributed to the absence of well-defined graphitic domains. The vibrational modes of additives and structural features present in carbon black from tires, including carbon aggregates, can be

observed in the low-frequency region, which reflects the material's origins. Overtones around 2700 cm^{-1} are more defined than in amorphous carbon, but weaker.

To further confirm that the tire-wear particles are indeed the source of the carbon black particles present in the samples, a piece of filter from the center across the same/different slots was subjected to pyrolysis-GC/MS analysis using a standard natural rubber (NR) and styrene butadiene rubber (SBR) as reference materials. To this end, isoprene and dipentene are employed as markers for NR, whereas 4-phenylcyclohexene and 4-vinylcyclohexene are used as SBR markers in calibration curves exhibiting linearity ($R^2 > 0.999$) for the quantification. The preliminary results of this analysis, which are not presented here, confirm the presence of particles resulting from tire-wear in varying slots of samples. On the other hand, the literature on outdoor MNPs have confirmed the overabundance of carbon black in air samples (Rahman et al., 2021). The production of carbon black from rubber waste, particularly tires, contributes to the MP pollution problem. As tires wear out, they release MNP particles, including carbon black, into the environment (De Frond et al., 2023). In a previous study, 50 particles with a mean size of 6.13 μm were analyzed by Raman spectroscopy, of which 66% were tire /road wear particles and 34% were other types (PS, PE, PET, ABS) of MNP. These tire wear particles are a significant source of MNP pollution, with estimates suggesting that they account for a substantial fraction of MNP emissions to air, lakes, and oceans. Friction between tires and the road surface during driving results in the emission of these particles, which can have harmful effects on both human health and the environment (De Frond et al., 2023). Efforts are being made to address this issue, including carrying out research to detect and remove these particles from the environment and implementing regulations to reduce tire wear and other plastic pollution. Researching ways to detect and remove these particles from the environment and implementing regulations to reduce tire wear and other plastic pollution are among the efforts being made to address this issue.

Environmental MNPs exhibit a wide range of shapes (fragment, fiber, etc.) and sizes (<1 μm to 5 mm), as well as varying densities. This complexity makes a one-size-fits-all solution, particularly for airborne particulate size ranges, impractical. The differentiation and identification of particles in sizes below 10 μm, particularly 2.5 μm, present significant

challenges for those engaged in MNP research. Consequently, standardized methodologies have been developed for specific media in order to enhance the reliability of findings. Despite the numerous analytical attempts at characterizing polymeric particles in this study, further knowledge may be gained through the use of transmission electron microscopy or EC/OC analysis. Nevertheless, it is crucial to acknowledge the limitations imposed by the destructive nature of such techniques, particularly with regard to the simultaneous analysis of identical areas within a filter slot.

4.1.4. Evaluation and optimization of sampling parameters

The initial sampling was conducted with the objective of controlling the sampling and determining the efficacy of the MNP identification procedure, as well as to establish a baseline for subsequent sampling. Accordingly, the 5×1 cm^2 pieces of filters, which had been randomly cut from the five stages of primary sampling set, were examined under an optical microscope (5x, 10x, 20x, and 50X). The optical microscope results demonstrated that the examination of particles collected in stages 1 and 2 could be conducted with relative ease (Figure B. 7). A sufficient quantity of particles was distributed on the surface of the slotted filter (stages 1 and 2) to permit both detection and morphological analysis. The analysis of particles captured in stage 3 (Figure B. 8), to some extent in stage 4 (Figure B. 9), and specifically stage 5 (Figure 4.9), presented a significant challenge due to the high density of the collected particles and their small size.

Moreover, the predominant size of the particles that were collected in the backup stage was frequently less than 1 μm (Huang et al., 2023), rendering microscopic examination impractical. Furthermore, a point-by-point trial was conducted using a Raman microscope to ascertain the quality of the selected particle and to prevent potential interference that could lead to issues. The overlapping particles prevented the laser beam from being received by a single particle, thereby preventing the identification of the quality of the given particle. Consequently, it was not feasible to determine whether the particles were polymeric or of another nature, particularly through spectrometric analysis, microscopic analysis techniques, or morphological examination. These findings illustrate the necessity for optimization of sampling parameters to enhance the precision and accuracy of the analytical methodology.

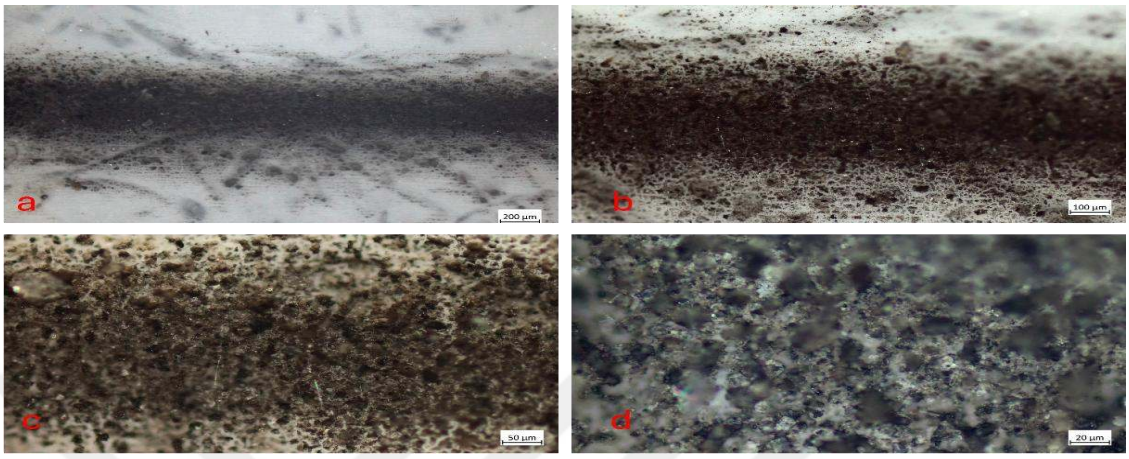

Figure 4.9. Particles collected in stage 5 with flow rate 40 cfm in the 24 hours, a) x5 (scale bar 200 µm), b) x10 (scale bar 100 µm), c) x20 (scale bar 50 µm), d) x50 (scale bar 20µm) objective.

4.1.4.1. Collection efficiency

The implementation of a multi-stage size-fractionated cascade impactor enables the initial separation of airborne particles at the sampling stage, thereby facilitating an in-depth analysis of the resulting fractions. The flow rate and sampling time are regarded as critical variables that exert a considerable influence on the efficacy of the collection efficiency of airborne MNPs. Smaller MPs, particularly those less than 10 µm, are challenging to collect due to their size. High flow rate samplers can improve the capture of these fine particles by maintaining a high air velocity, which increases the likelihood of impact on the collection surface (Ju et al., 2023). With high volume impactor sampling, it is possible to collect enough samples at every stage to be analytically detectable for 12- or 24-hour sampling. Each strip can also be used to analyze different types of pollutants if required (Arı et al., 2020). However, this can be a disadvantage when particle-based analyses such as micro-Raman are required (Azari et al., 2023). On the other hand, this phenomenon can be attributed to the fact that lower flow rates permit particles to interact with the filter for a longer duration, thereby enhancing the probability of capture through mechanisms such as inertial impaction and Brownian motion (Lindstrom et al., 2024; Wright et al., 2021a). The efficacy of flow rates is contingent upon the dimensions of the MNPs in question. At higher flow rates, smaller particles are more likely to bounce off due to their ability to be carried away by the

airflow. Conversely, larger particles may be effectively captured even at higher flow rates. It is thus imperative to assess flow rates in accordance with the intended particle size in order to guarantee sampling (Trainic et al., 2020; Wright et al., 2021b). Additionally, high flow rates can present complications, such as filter loading, which may impact the accuracy of the sampled air volume. In the event that filters become overloaded, they may exhibit a resistance to airflow, which could result in an underestimation of the volume of air sampled and an overestimation of the actual mass of particles collected (Oehlschlägel et al., 2024; Wright et al., 2021a). Furthermore, as flow rates increase, the pressure drop across the filter can also increase, potentially resulting in a reduction in airflow and compromised sampling efficiency (Rosso et al., 2023a).

In samplers with mass flow controllers, this problem can be avoided to a certain extent. Therefore, balancing flow rate with filter type and sampling duration is crucial to avoid these issues. Hence, research has demonstrated that PTFE filters (e.g., 47 mm with a pore size of 0.2 μm) exhibit an excellent collection efficiency (>93%) for particles ranging in size from the nanometer to the micrometer, including airborne particles, bacteria and viruses that are comparable in size to MNPs (Burton et al., 2007; Chow et al., 2022; Lindstrom et al., 2024).

Moreover, the duration of the air sampling period is a critical factor in determining the total volume of air processed and the number of MNPs collected. The use of longer sampling periods may facilitate the acquisition of more comprehensive data regarding the concentrations of polymer particles. However, this approach may also result in an overloading of particles in filters, potentially leading to challenges in subsequent analysis (Lindstrom et al., 2024; Prata et al., 2020).

4.1.4.2. Physical characterization of MNPs

Microscopic images were captured and subjected to analysis in conjunction with varying flow rates and time intervals. Table B. 2 illustrates the distribution of particles on the surface filter across five stages, as detailed in the supplementary material. To assess the sampling parameters, it is necessary to employ a more comprehensive approach than that offered by the subjective nature of either optical or visual microscopy. In this context, a spectroscopic examination was conducted, wherein 20 particles were randomly selected from

a surface area of 1 cm² (Akbari Dana et al., 2024; Zhu et al., 2021), which had been cut from various slots for examination by Raman microscope. This was done with the specific intention of investigating the effects of different sampling parameters on the particles' behavior. The present study employed a 532 nm laser, which proved to be 4.7 times more efficacious than a 785 nm laser. This resulted in a superior signal-to-noise ratio (Larkin, 2017), thereby facilitating the generation of more discernible bands (Munno et al., 2020).The MPs were identified and classified into two groups based on their morphological characteristics, namely, fragments and fibers, using a spectrometric analysis. In the majority of studies on airborne MPs, fibers were the dominant component, both in rural and urban environments (Chen et al., 2023; Habibi et al., 2022). In contrast, the number of fragment particles in this study was considerably higher than the number of fiber particles. It should be noted that Kernchen et al. (2022) employed a cascade impactor to collect and analyze airborne MPs, and they did not find fibers in their samples. In this study, a total of 160 particles were examined in each stage (20 particles × 2 flow rates × 4 times), resulting in a total of 60 particles classified as MNP in the first stage. Of these particles, 66.7% were classified as fragments (with a diameter ranging from 4.3 to 38.13 µm), while the remaining 33.3% were designated as fibers (with a diameter ranging from 20.44 to 138.7 µm), with the classification determined under various sampling parameters. In stage 2, 57 MNPs were detected, with 78.9% falling within the fragment category (0.38-31.08 µm) and 21.1% within the fiber category (11.2-52.3 µm). In stage 3, 59 MNPs were identified, with 79.7% classified as fragments (0.92 - 44.8 µm) and 20.3% as fibers (16.5 - 92.5 µm). Similarly, in stage 4, 51 MNPs were identified, with 88.2% classified as fragments (0.5 - 43.35 µm) and 11.8% as fibers (20.7 - 88.5 µm). After the conclusion of the second stage, a total of 29 MNPs were identified. Of these, 83% were fragments with a diameter ranging from 1.8 to 18.7 µm, while the remaining 17% were fibers with a diameter ranging from 28.4 to 79.1 µm (Figure 4.10 and Figure B. 10). Nevertheless, the specifics of MNPs characterization at different stages and under varying conditions can be considered in Figure 4.11 and all of the details shown in Table B. 3 for the purpose of comparison and evaluation of the sampling parameters. The results of the visual analysis, based on the distribution of total particles collected in each

sampling campaign, indicated that a flow rate of 40 cfm over an 8-hour sampling duration could be a suitable choice.

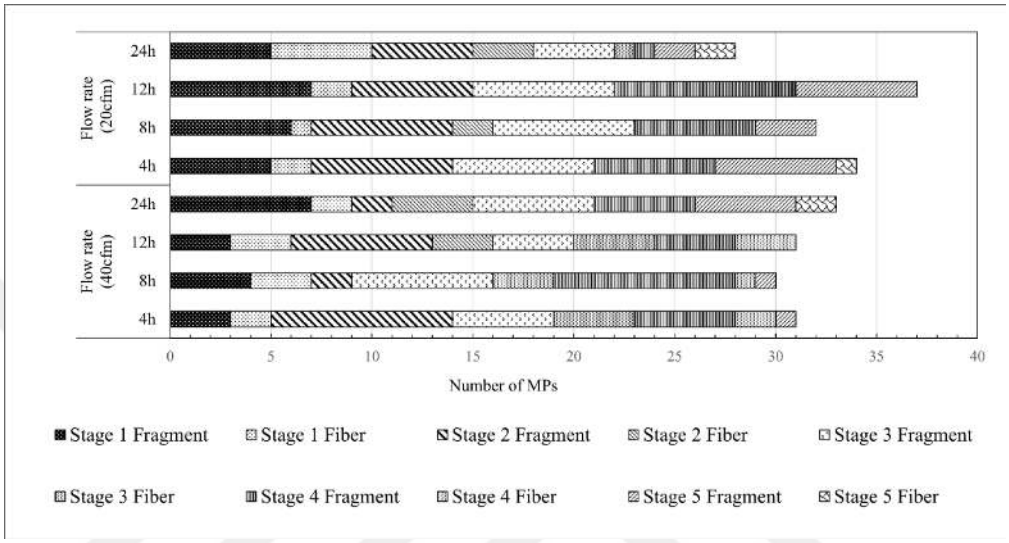

Figure 4.10. *Number of MPs in different stages based on shape.*

The rationale behind this decision was subsequently elucidated in more detail in the following sections.

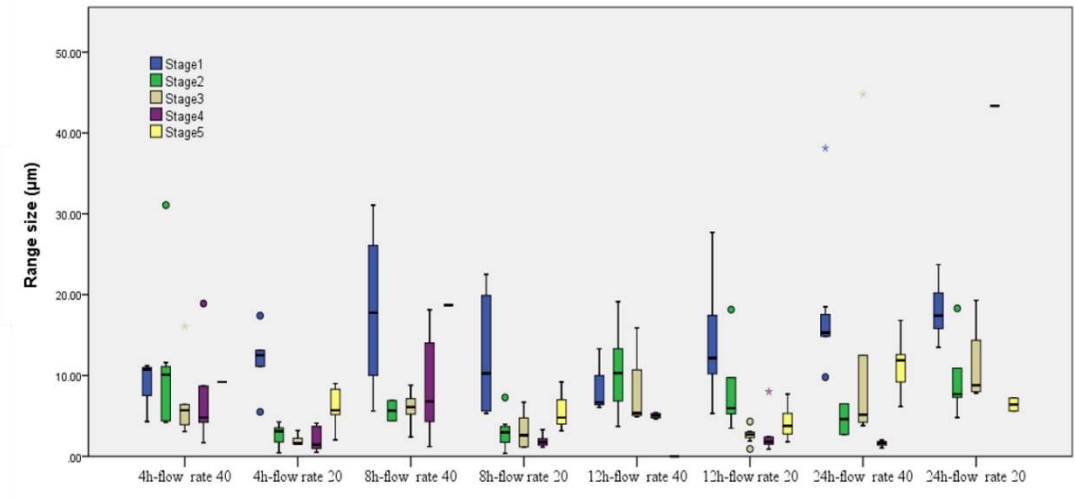

Figure 4.11. *Range size of MNPs in two groups flow rates and, the 4-, 8-, 12-, and 24-hours sampling duration, a) Stage 1, b) Stage 2, c) Stage 3, d) Stage 4, e) Stage 5.*

4.1.4.3. Sampling flow rate and time

In this phase of the study, the preliminary evaluation was focused on the flow rate (40 cfm or 20 cfm) in order to determine the most efficient and effective solution for particle-based analysis. A notable advantage of the high-volume cascade impactor is its ability to operate at a nominal flow rate of 40 scfm (1.13 m^3/min) (standard cubic feet per minute at 760 mmHg and 25°C). This enables the collection of a greater quantity of airborne particles, which is particularly advantageous for studies requiring extensive sample sizes for chemical and biological analysis (Kalisa et al., 2022). This specification is in accordance with the stipulations set forth by the United States Environmental Protection Agency (EPA). In the event that a minimum flow rate is also, required, the apparatus is capable of operating at a rate of 20 (scfm), High Volume Cascade Impactors operate at substantially lower flow rates and do not compare as well as with standard High Volume Air Samplers operating at the EPA specified rate of 40 cfm (Tisch Environmental). The utilization of a high-volume sampler equipped with a cascade impactor in five stages in this study necessitated the selection of a flow rate of 40 cfm over a rate of 20 cfm. Because the low-sample volumes indicated a restricted range of polymer types, whereas the elevated air volumes of the high-volume sampler demonstrated a more diverse polymer cluster in the air, the use of larger sample volumes is often a reliable method for the analysis of polymers with a higher limit of detection, which may result in a higher diversity of polymer clusters for high-volume samples compared to low-volume samples (Goßmann et al., 2023a).

On the other hand, the MPs data presented in Table B. 3 demonstrates that the theoretical size limit range of the cascade impactor undergoes a change in accordance with the decrease in flow rate. However, this alteration suggests that the dimensions of airborne particles are not in accordance with the theoretical values. According to the results of the literature review regarding the human respiratory system, particles with diameters equal to or greater than 10 µm tend to settle in the nasopharyngeal airway (Brown et al., 2013). When the aerodynamic diameter of a particle is 10 µm or less, it is more likely to reach and settle in the intrathoracic regions of the respiratory system. Studies indicate that the most effective particle diameter for reaching the airways is between 3 and 6 µm, while for delivery to the alveoli, it is equal to or less than 3 µm (Forbes, 2000). Consequently, the size range of the

cascade impactor in 40 cfm provided the main purposes of exposure studies and was thus determined as the optimal flow rate for the cascade impactor sampler. The selection of this time duration for sampling was motivated by the alignment of the 24-hour sampling duration at 40 cfm with the U.S. EPA Federal Reference Method guidelines and other regulatory frameworks for PM_{10} and $PM_{2.5}$ monitoring. A prevalent practice involves the segmentation of the 24-hour period into two 12-hour segments, with the objective of regulating the concentration of MNPs during diurnal and nocturnal hours. This approach facilitates the calculation of the 8-hour workday and the 8-hour period of free time for the population, as well as the 8-hour period of midnight without human activity. In environments characterized by high particle concentrations, the use of shorter durations, such as four hours, is recommended to prevent the occurrence of overloading.

Concerning the duration (4, 8, 12, and 24 hours), of the sampling, the quantity of particles that traversed the nozzle of the cascade impactor and were deposited on the Teflon filter surface in a line at the center of the slots was considerable, particularly in stages 4 and 5 after 12 and 24 hours of sampling, respectively. Therefore, the analysis of individual particles in these stages, which are nanoplastics (NPs), to detect MPs became exceedingly challenging due to the high loading and aggregation of particles. Conversely, the density of particles after four hours, particularly in stage one, was markedly inadequate, making identifying a single particle to ascertain MNP status a formidable task. It was thus determined that eight hours of sampling represented the acceptable duration for the process. However, it should be noted that these time periods are contingent upon the total particle concentration in the atmosphere. In urban environments with elevated levels of air pollution, these parameters may vary. Gaston et al, (2020) demonstrated that using the Alicat scientific mode sampler (11.7 l/min) would ensure that a sufficient particle load was attained within eight hours for the purpose of airborne MNP analysis. However, this device is not classified as a size-segregated and high-volume sampler. It is important to note that a sampling period of eight hours is insufficient for enumerating or quantifying the number or concentration of MNPs on a given day. Nevertheless, to obtain an accurate representation of the total amount of MNPs present in the atmosphere, it is necessary to conduct a series of additional samplings throughout the day.

The total air volume collected was 543 m^3 with flow rate 1.13 m^3/min in 8 hours of sampling, compared to previous studies that used particle size-segregated methods such as Kernchen et al. (2022) 0.6 m^3 air volume (flow rate 0.0034 m^3/min in 3 hours), Mizuguchi et al. (2023b) 403 m^3 air volume (flow rate 0.02 m^3/min in 2 weeks), and Morioka et al., (2024) 900 m^3 (flow rate 0.5 m^3/min in 24 hours). The high flow rate air samplers to effectively collect airborne particulate matter, including particles less than 100 micrometers in size. This is crucial for accurately measuring total suspended particulates (TSP) and specific size fractions like PM_{10}, which includes particles with aerodynamic diameters less than 10 μm (EPA, 1999; Tisch Environmental, 2004). In light of the most recent research, it is noted that a minimum of 70 m^3 of filtered air is required for the accurate quantification of airborne MPs (Azari et al., 2023; Liu et al., 2019b).

In consideration of the aforementioned evidence, it can be concluded that, sampling airborne MNPs at a flow rate of 1.13 m^3/min for a period 8 hours ensures the efficient collection of MPs, compliance with regulatory standards, and operational versatility while minimizing issues related to filter loading (EPA, 1999). The majority of studies that employed cascade impactors or analyzed MP_{10} and $MP_{2.5}$ indicated a preference for mass-based analysis, such as pyrolysis-GC/MS, over other analytical techniques (Costa-Gómez et al., 2023; Goßmann et al., 2023a; Luo et al., 2023; Mizuguchi et al., 2023a; Morioka et al., 2024). Due to the time-consuming and challenging nature of spectrometric analysis of MPs<10 μm, this method is not commonly employed.

Ultimately, the concentration of MNPs derived from Raman spectroscopy in the selected sampling parameters (flow rate of 40 cfm and an eight-hour duration) yielded the following MNP/m^3 concentrations: 434 in stage 1, 431 in stage 2, 1631 in stage 3, 1117 in stage 4, and 355 in stage 5 (Figure 4.12). While Kernchen et al (2022) analyzed two stages (larger than 4 μm were identified in both stages), they found that the mean concentration of MP was 91±47 MNP/m^3. Levermore et al. (2020) reported that 2502 particles per m^3 were derived from Raman analyses near urban roads in London (UK), with sizes of >4.7 μm, respectively. The concentration data presented in Table S3 did not yield any significant differences between the various sampling parameters. It should be noted that the operator's time was spent locating a suitable particle for analysis, rather than performing the analysis

itself. Particles could not adsorb the Raman microscope's laser light due to overlapping because of the high density of particles gathered on the filter surface throughout the 12 and 24-hour sampling period. Ultimately, the operator needed more time to locate a particle for the spectrum analysis. The issue was partially resolved by decreasing the duration of sampling to 8 hours. In the 8-hour, 40 cfm flow rate group, in stage 1, 35% (7 out of 20 particles) were identified as MNP, in stage 2, 10% (2 out of 20), in stage 3, 50% (10 out of 20 particles), in stage 5, 5% (10 out of 20 particles). The number of MNPs detected by spectrometry analysis was indicated in Table B. 3 in supplementary data.

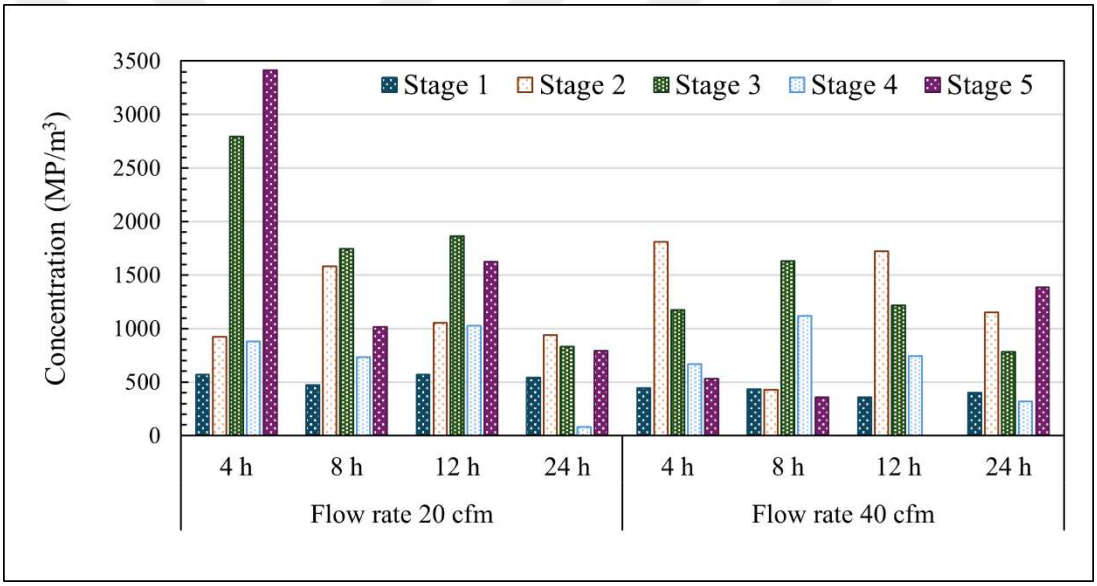

Figure 4.12. *MPs number concentration in different sampling parameters.*

4.1.4.4. Chemical characterization of MPs

The chemical characterization of individual particles through Raman spectroscopy represents a highly effective technique for enhancing the characterization of aerosols. Raman spectroscopy is a straightforward, expeditious approach that does not necessitate sample pretreatment. Following the random selection of 20 particles for analysis via spectrometry, it was determined that approximately 90% of the particles were identified as carbon black (see Figure 4.13 and, Table B.4). Other percentages include those of polytetrafluorethylene (PTFE) and polypropylene (PP), which exhibit a similarity exceeding 70%, as well as, to a lesser extent, polyethylene (PE) and polyacrylic particles (Figure B. 11). Despite the

difficulty in differentiating of carbon black from black carbon, including soot, is a challenging process (Hong et al., 2021), it is probable that these particles are tire and road wear particles for the reasons outlined here. Morphologically, the particles are black and stretchy, exhibiting characteristics similar to those observed in tire dust generated in a laboratory setting using commercially obtained vehicle tires (Munno et al., 2020).

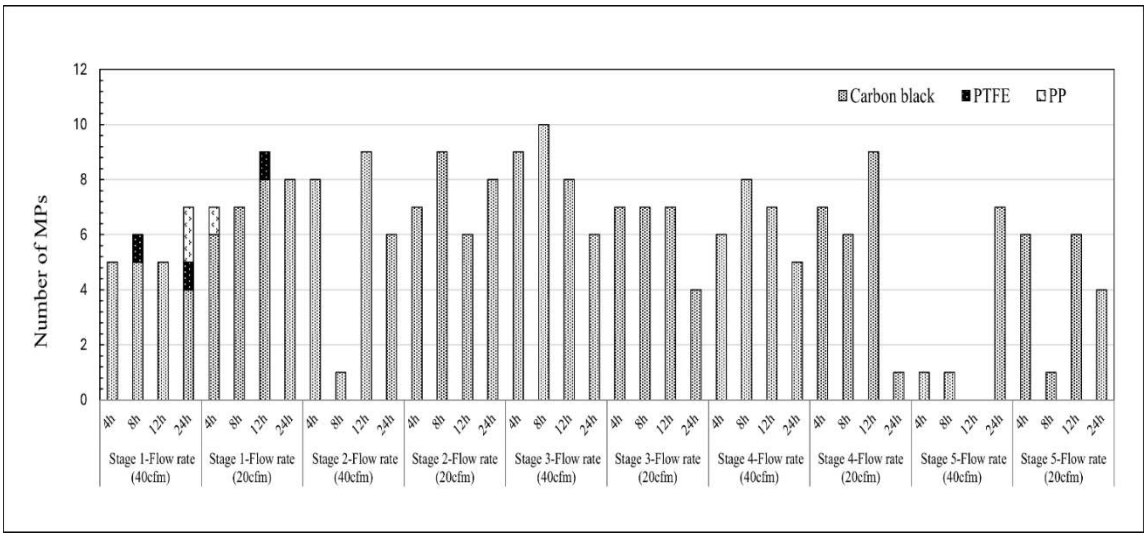

Figure 4.13. *Chemical type of MPs in the different sampling parameters (similarity score > 70%).*

The Raman spectra of the laboratory-generated tire particles and the black rubber particles from environmental samples exhibit similarities to that of carbon. It is well documented that the use of synthetic rubber in tires, such as styrene butadiene copolymers and polymers used in bitumen formulations and road marking paints, contributes to the presence of MNPs in settled road dust (Abbasi et al., 2019; Kitahara and Nakata, 2020; Yukioka et al., 2020) The bands observed in these spectra (G bands ~1585 cm^{-1} and D bond ~1360 cm^{-1}) (Marina-Montes et al., 2022) are likely to be derived from carbon fillers incorporated into black particles Figure 4.14 (Lenz et al., 2015; Marina-Montes et al., 2022)

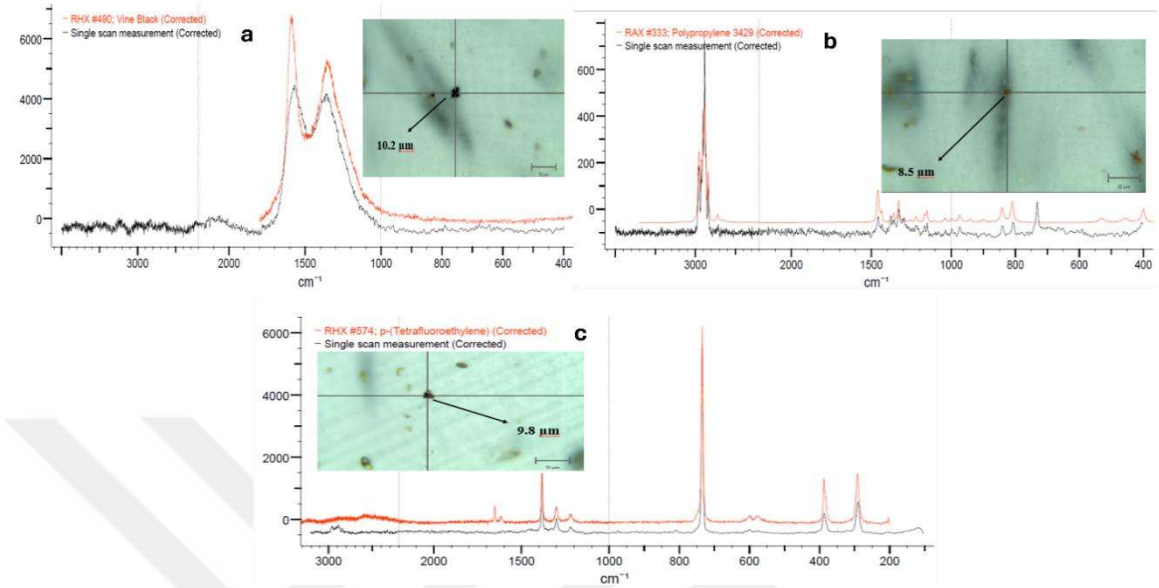

Figure 4.14. *Chemical identification of MPs in optimization sampling parameters procedure. Spectrometric peak of a) Carbon black, b) Propylene (PP), c) Polytetrafluoroethylene (PTFE) with matching ratio >70%.*

Some library and spectrum analyzer spectra such as KnowItAll include carbon-based materials such as "Diamond-like Carbon," "Ivory Black," "Lamp Black," "Carbon Black," "Vine Black," "Ketjen Carbon," and "Van Dyke Brown." Nevertheless, at this juncture, the possibility remains open to conjecture as to the origin of the exhaust combustion particles. In such cases, Munno et al (2020) recommend classifying rubber particles as anthropogenic based on feel and appearance, where size is not a limiting factor, and spectra cannot be obtained. Therefore, to confirm that the source of the carbon black is the tires, which were identified based on their spectrum fingerprint, a comparison was conducted between the carbon black particles and black carbon (soot) based on morphological characterization and their spectrum. In this study, the particles were identified as carbon black (rubber from tires) and were observed to be irregular single particles that appeared to separate from the objective (Figure B. 12). In contrast, the shape of soot particles was observed to be a cluster of agglomerated circular particles (W. Li et al., 2024a).

In a recent study, Yoo et al. (2023) found that of the 50 stained particles, 66% were identified as tire/road wear particles and 34% were classified as other types of MNPs. This proportion is consistent with the findings of a model study that roads are the primary source

of anthropogenic MNPs, representing 85% of the total (Brahney et al., 2021). In their respective studies, (Gaston et al., 2020) and Rahman et al (2021) observed that their samples exhibited considerable quantities of carbon black, originating from traffic and combustion-related sources. Kernchen et al. (2022) did not observe a higher diversity of polymer types. Of the 16 polymer plastics identified, 13 were made of PE (polyethylene). In other side, Primpke et al (2018a) found that distinguishing between PE and rubber using a spectrometric method may be challenging. The major sources of polypropylene (PP) are human activities and the use of synthetic materials, which have resulted in the release of MNPs into the atmosphere. Among these sources, the most prominent contributors are synthetic textiles and tire wear (O'Brien et al., 2023). Additionally, Kernchen et al. (2022) stated that the majority of PP particles exhibited considerably longer transport distances, reaching approximately 60 km, which was attributed to a comparatively low density in comparison to other types of MPs. Preliminary evidence of polytetrafluorethylene (PTFE) and polyethylene particles, which are hypothesized to have originated from industrial applications and paint, have been identified in deposits. Therefore, the quantification of the spray application and subsequent degradation of paint, industrial coatings, and abrasives is necessary to determine their role as a source of MNPs in the atmosphere (O'Brien et al., 2023). In conclusion, the sources of PP, PTFE, carbon black, and black carbon in the atmosphere are diverse, encompassing both consumer products and industrial processes. The degradation of synthetic materials, tire wear on roads, carbon black production, tire and rubber manufacturing, and combustion processes are of considerable consequence with respect to the presence of these materials in the atmosphere (Kim et al., 2022; Reynolds et al., 2024). Carbon black is a component added to plastics in order to achieve a specific coloration, with the objective of rendering the material opaque and black. The precise percentage of carbon black that is incorporated into plastic material varies between 2% and 5% by weight. The primary applications of this additive include the packaging, electronics, and construction materials industries (Pfaff, 2022). In addition to tires, fragments of road asphalt which contain carbon-rich materials, including carbon black have the potential to contribute black carbon particles mixed with MNPs when they are mechanically broken down and dispersed by traffic and wind (Brahney et al., 2021).

4.1.5. SEM-EDX analysis

The results of the SEM-EDX analysis, which was conducted using a 24-hour sampling duration, indicated that carbon was identified as the major element, with a mean value of 71.4±14.3% in the four spectra of stage 5 and 33.5±10.8% in the four spectra of the backup stage. The quantity of carbon observed in the particles under examination is indicative of their organic and/or polymeric composition. In consequence, the weight percentage of some elements identified in stage 5, in descending order of abundance, is as follows: Ca (11.4±8%), Al (1.66 ±1.4%), Fe (1.11±0.8%), K (0.73 ±0.2%), Na (0.45 ±0.1%), Mg (0.34 ±0.3%). In the backup stage, the relative proportions of the elements were as follows (in descending order): Si (28.5%±12%), Ca (17.3±2%), Mg (4.5±3%), Na (4.19±1%), Fe (2.97±1%), K (2.36±0.9%), Zn (1.16±1%), and Cu (0.29±0.3%) (Figure 4.15). The results of X-ray spectra obtained using SEM/EDX revealed that the particles collected in stage 5 exhibited a greater amount of organic species or polymeric nature in comparison to those collected in the backup stage. A review of SEM/EDX results from previous studies indicates that the majority of elements presented in the black particles were S, Na, Zn, Ca, K, Mg, Fe, and Al, which are the primary components of tires (Marina-Montes et al., 2023; Yoo et al., 2023). In addition, the primary constituents of the tire are rubber, which constitutes 40-45% of the total composition, and filler materials, including carbon black, silica (Si), and chalk ($CaCO_3$), which account for 30-35% of the mixture. Additionally, sulfur (S) and zinc oxide (ZnO) are utilized in small quantities, representing approximately 2-5% of the total (Giechaskiel et al., 2024; Kang et al., 2022; 2021a; Mattsson et al., 2023). In light of the aforementioned evidence, it can be concluded that these elements present within tires serve as compelling indicators of their function as a source of black particles (Figure B. 13).

As illustrated in Figure 4.16 and Figure 4.17 (Table B. 5)**,** the SEM-EDX analysis of the summer and winter backup stage samples was conducted over an eight-hour period. Utilizing optimized sampling parameters, the physical characterization of MNPs was facilitated through Raman spectrometric microscopy.

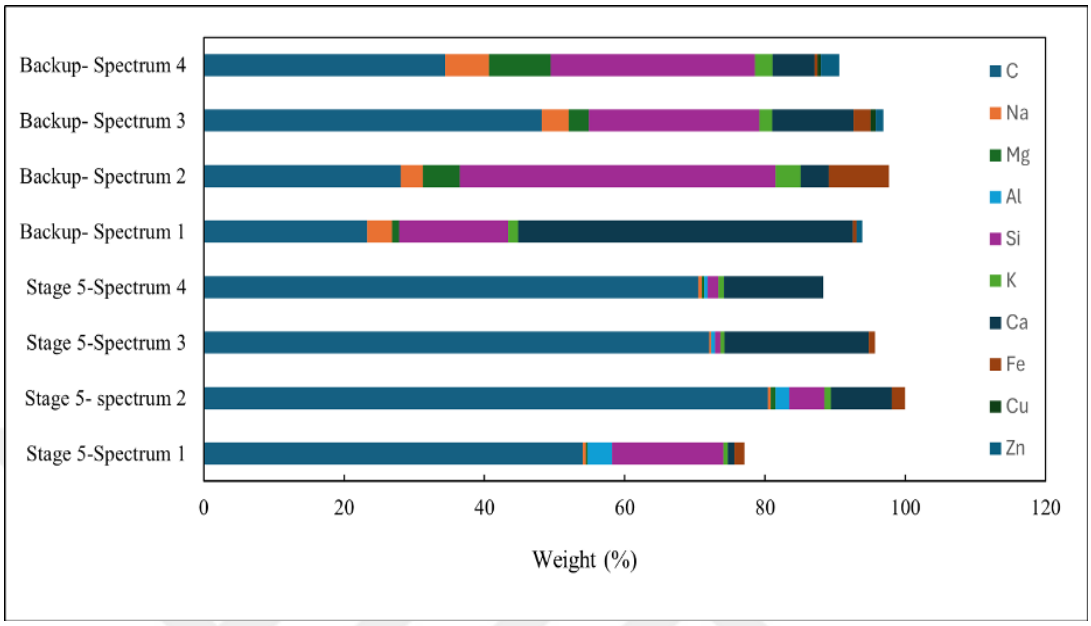

Figure 4.15. *Different elements of Stage 5 and backup stage in the three of sampling location (24 hours sampling and flow rate 40 cfm).*

Consequently, only particles that were collected on the back up stage (glass fiber filter) required physical analysis, which was subsequently performed by SEM-EDX. In the 8-hour sampling, carbon (40.8 ± 2.7%) was identified as a predominant element, suggesting the polymer source of particles. Additionally, Si (25.9 ± 4.2%) and Ca (11.6± 5.9%), and Zn (2 ±0.4%) were found to be significant elements.

Wagner et al. proposed that the elevated presence of carbon atoms, as evidenced by high carbon content, serves as an indication of the incorporation of both rubber and carbon black components in tires. Furthermore, the levels of zinc (Zn), sulfur (S), and silicon (Si) align with the conventional composition of tires, thereby substantiating the hypothesis (Wagner et al., 2018). Metals that have been identified in high concentrations include Si, S, Zn, Ca, Al, and Fe (Councell et al., 2004; Guo et al., 2023). Of these, Zn has gained a reputation as a marker for tire-wear emissions in ambient PM source apportionment studies (Grigoratos and Martini, 2014; Rødland et al., 2023). Zn and Ba are currently utilized in the manufacturing of tires. Zn is present in tires in high concentrations and plays an irreplaceable role as an activator in the vulcanization process.

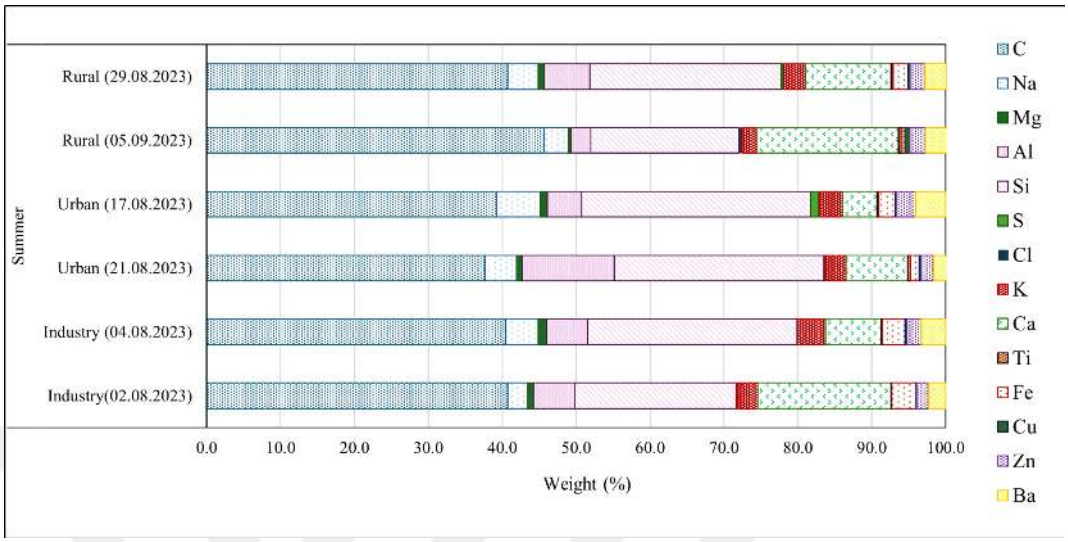

Figure 4.16. *Different elements of particles collected in the backup stage at the three of sampling location (summer).*

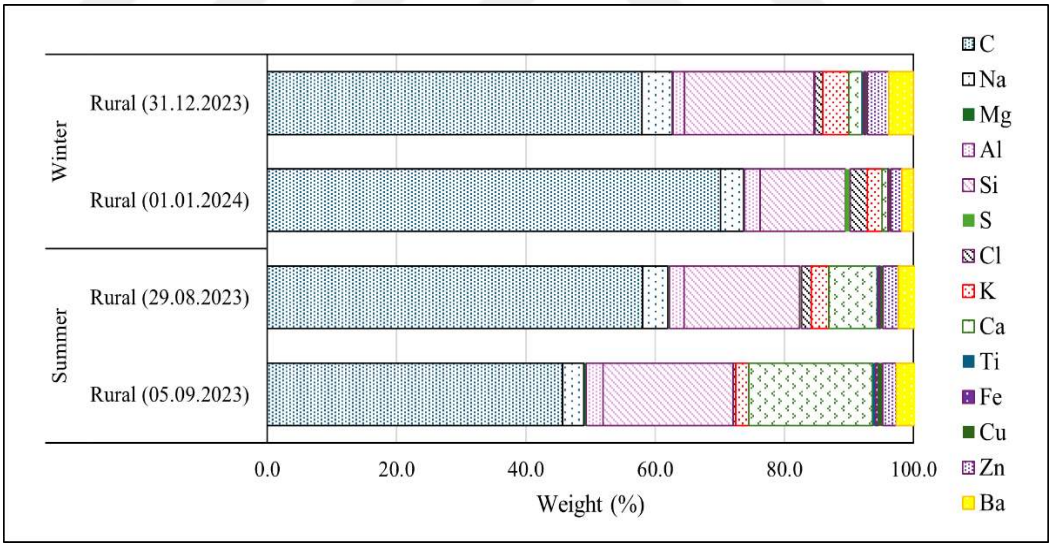

Figure 4.17. *Different elements of particles collected in the backup stage at the rural zone (summer & winter).*

Table 4.1. *The source of elements as detected by SEM-EDX analysis*

Elements	Sources	References
C	Carbon is key to the chemical structure of most plastics.	Swinnerton et al., 2024)
Na	Originate from fillers, flame retardants, or adhesives in plastic products Vehicle abrasion, fossil fuel combustion, and industrial emissions In coastal regions, airborne sea spray can deposit Na onto microplastics	(Mphaga et al., 2023), (Swinnerton et al., 2024)
Mg	Originate from fillers, flame retardants, or adhesives in plastic products Vehicle abrasion, fossil fuel combustion, and industrial emissions in pigments and additives used in paints In coastal regions, airborne sea spray can deposit Mg onto microplastics	(Mphaga et al., 2023)
Al	Used in pigments, stabilizers, or coatings to enhance plastic properties (e.g., color or UV resistance). In pigments and additives used in paints	(Swinnerton et al., 2024), (Mphaga et al., 2023)
Si	Derived from silicate minerals, including quartz, clays, and feldspars. These minerals adhere to microplastic surfaces during atmospheric transport or deposition. Construction and road dust in cities raise Si levels on microplastics. This is due to the presence of silica-rich concrete and asphalt.	(Wieland et al., 2022)
Ca	Gypsum, a common component of drywall and construction materials, releases Ca and S into the atmosphere during degradation, which subsequently adheres to microplastic surfaces. MNPs from urban areas using SEM-EDX analysis frequently reveals calcium concentrations ranging from 0.57% to 5.48%, suggesting a correlation with proximity to construction sites or unpaved roads.	(Khanum et al., 2021)
K	Agricultural regions with high fertilizer use may also contribute K-rich particulates to airborne microplastics.	(Shao et al., 2022b)
Zn	A significant proportion of tire rubber, constituting 2–3% of the total weight, is released as nano- to MNPs during the process of abrasion. Over time, Zn-coated steel structures corrode, releasing Zn-rich particulates into the atmosphere.	(van Broekhuizen, 2024), (Khan, 2012)
Cu	Cu levels in car brake linings are 5–20%, and copper particles are created when the brakes are used. Urban MNPs near traffic corridors found concentrations of Cu reaching up to 4.28%, indicating vehicular contamination.	(Neukirchen et al., 2025)
Fe	Fe-based pigments, like iron oxide red, are used to color plastics.	(Mastrotheodoros and Beltsios, 2022)
Ti	White pigment in paints and plastics is made of titanium-rich particulates. TiO_2 nanoparticles from personal care products	(Chadwick, 2015), (Oh et al., 2021)

It activates and promotes the highest number of crosslinks in the rubber chain, thereby imparting strength, stability, and other valuable properties to a finished tire. Zn transforms sticky rubber compounds into stable and durable components that enable tires to carry a vehicle's mass and stop safely. The release of trace elements such as Zn from diverse traffic-related sources, including deicing salts, road barriers, galvanized metal in automobiles, brake wear, and road markings, underscores the necessity of a comprehensive analytical approach for the identification of tire wear particles (TWPs) (Kovochich et al., 2021b; Wagner et al., 2018). This assertion underscores the inadequacy of employing single indicators for TWPs identification (Gaga et al., 2018). To this end, cross-validation was performed using alternative techniques, such as Pyr-GC/MS, to substantiate the identification of these particles.

4.1.6. Micro-Raman analysis of day and night samples

μ-Raman spectroscopy plays a pivotal role in the analysis of airborne MNPs with a diameter of less than 10 μm. This analytical technique provides critical physical and chemical insights that are pertinent to human health and environmental monitoring. In this section of the study, the visual inspection was conducted on PM collected on Teflon filter in five stages using a Leica microscope (50X and 100X magnification long-range objectives), which were placed in μ-Raman spectroscopy. The MNPs were identified and classified into two groups based on their morphological characteristics, namely fragments and fibers, through the use of a spectrometric analysis. A total of 6-night and 6-day samples were collected from three distinct zones (industrial, urban, and rural) at each stage of the study. These samples yielded a total of 552 particles that were classified as MNP (96.2% fragments [0.34-16.4 μm] and 3.8% fibers [7.6-70.4 μm]) under different stages. Furthermore, the range of MNP fragment sizes is illustrated in Figure 4.18. The comprehensive details of MNP are enumerated in Table B. 6, Table B. 7, and Table B. 8, which are categorized by stage and sampling location.

Airborne MNPs with a diameter of less than 10 microns are classified as fragments due to their irregular, angular shapes. These shapes indicate that the particles originated as broken pieces of larger plastics

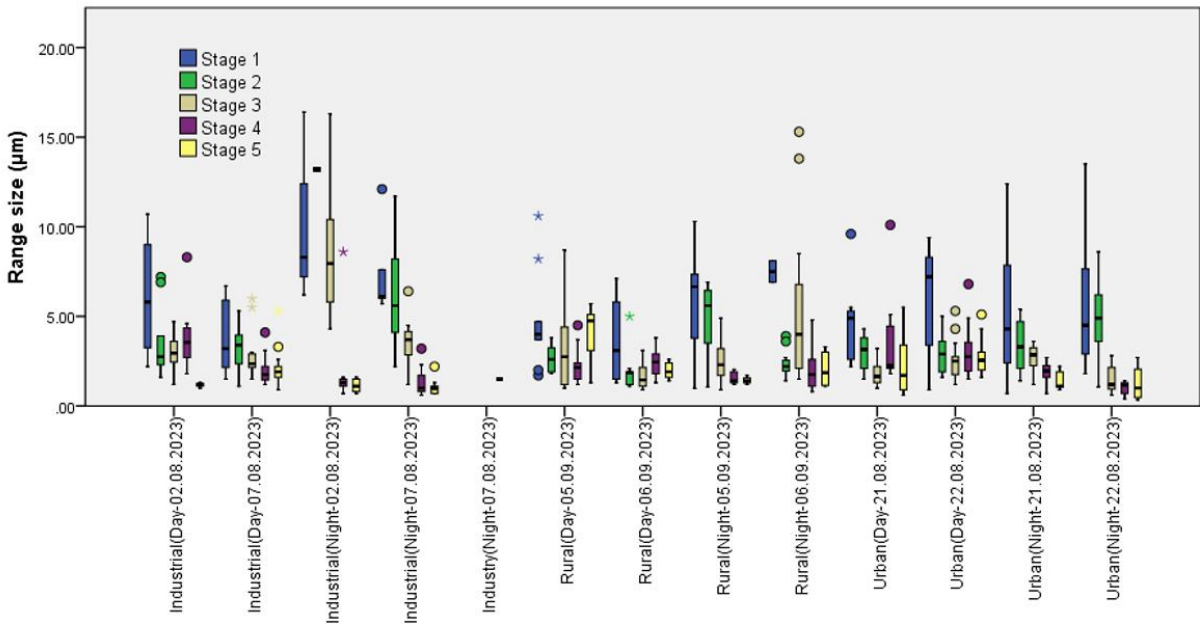

Figure 4.18. *Comparison of temporal and spatial range size of MNPs fragment in different stages.*

This classification differentiates them from fibers or beads, which possess different morphologies and formation mechanisms. Recent studies have revealed that fragments constitute the predominant MNP type in the atmosphere (Allen et al., 2021; Bergmann et al., 2019) (Trainic et al., 2020). The prevailing shape of MNPs was identified as fragments, comprising 87.0%, 82.9%, and 91.4% of the aggregate airborne MNPs in urban, rural, and wildland samples, respectively (Luo et al., 2024). However, the paucity of studies that have been carried out has employed a size-selective sampling method of airborne particulates using a cascade impactor to identify MNPs. Among them, Kernchen et al (2022) MNP particles identified in impactor samples were in the size range from 4.1 µm to 33 µm, and 67% were smaller than 10 µm (S. Kernchen et al., 2022). Furthermore, 79% of the particles exhibited irregular shapes, while 21% were found to be spherical in nature. Notably, no fibrous particles were detected in these samples. Furthermore, the maximum total MNP concentration was detected at the Bremerhaven site, while the concentrations of MPs smaller than 10 µm were comparable at the Bremerhaven (a seaport or urban area) and Solling (a rural forestry area) sites.

The present study examined the size range of MNP fragments (0.6 to 16.4 μm) and fibers (8.4 to 63.5 μm) in the industrial zone, the urban area (0.3 to 13.5 μm fragments), and fibers (9 to 21.5 μm fibers). Furthermore, the range size of MNPs (stages 1 and 2) during the nighttime period frequently exceeded that observed during the daytime. Conversely, in stages 4 and 5, during the nighttime, the range size of MNPs was diminished relative to daytime values. This phenomenon can be attributed to the higher humidity levels observed during nighttime, which resulted in the accumulation of larger MNPs. However, it should be noted that the humidity did not appear to have any significant impact on the tiniest MNPs present in the atmosphere. The size range of fragments was found to be 0.8 to 15.3 μm, and the size range of fibers was found to be 9.7 to 50.3 μm in the rural region. The size of airborne MNPs in urban regions is smaller than in industrial and rural zones. This is due to the fact that urban areas have higher population densities and intensified human activities. These factors lead to more frequent breakdown and fragmentation of larger plastic debris into smaller MNPs (Torres-Agullo et al., 2021; Yang et al., 2025). Furthermore, urban sources of MNPs, including vehicle emissions, construction activities, and waste management practices, have the potential to generate smaller MNP particles. Conversely, industrial and rural areas may contain larger plastic debris that undergoes fragmentation into larger MNPs (Rednikin et al., 2024). Urban environments are characterized by greater complexity in air circulation patterns, which is attributable to the presence of buildings and infrastructure. These elements have the capacity to facilitate the suspension of smaller particles in the air. In contrast, rural areas are subject to natural factors, such as wind and vegetation, that can trap larger particles with greater effectiveness. This phenomenon results in a relative abundance of larger MNPs.

As indicated in Table B.7, the standard deviation (SD) size of MNPs was calculated for various sampling locations; the size range of MNPs in urban areas was more closely spaced compared to other locations due to the same sources of MNPs, namely tires and traffic. Conversely, the source of MNPs can vary (such as in industrial areas), resulting in the size range of MNP fragments that exceeds that of MNPs in urban areas. As indicated by the prior research, there is a direct correlation between the reduction in MNP size and the concomitant increase in concentration (Dris et al., 2017; Kaya et al., 2018). Additionally, Levermore et al. (2020) documented that 52.5% of the confirmed MNPs measuring between

5 and 10 μm, 35% measuring between (11 - 20 μm), 2.7% (21 and 30 μm), and 0.9% measuring over 31 μm (Levermore et al., 2020).

In consideration of the correction of the estimated number of MNPs in the atmosphere in each region, it is evident that a single eight-hour sampling period is inadequate for obtaining representative results for MNPs in the air. Consequently, in order to obtain an accurate concentration of the level of airborne MNPs, two samples must be taken over the course of a 24-hour period. The number and concentration of airborne MNPs collected from three zones, identified through spectrometry, yielded Figure 4.19. A total of 400 particles were subjected to μ-Raman analysis at each of the designated sampling locations. A total of 170 particles were identified as MNPs in the industrial area, 208 MNPs were detected in urban areas, and 181 MNP particles were detected in the rural region. The higher number of airborne MNPs in urban areas compared to rural and industrial zones is primarily driven by greater human activity, higher population density, and diverse sources of plastic pollution in cities. Rural areas exhibit lower but still significant levels of MNPs due to agricultural and natural sources, while industrial areas may demonstrate lower airborne MNPs depending on the industrial type and emission controls. The distribution patterns of MNP are further influenced by environmental factors and characteristics of the urban landscape. However, it was observed that the number of MNPs was consistently higher in stage 5 compared to other stages across all regions, with a particularly pronounced difference noted during daylight hours. A comparative analysis of the number of MNPs in the three zones during both diurnal and nocturnal periods revealed that the number of MNPs observed during the day exceeded that observed at night. In the context of the industrial zone, the prevalence of MNPs at some night has been found to exceed their daytime levels. This phenomenon can be attributed to the sustained operation of the factories in the area. Furthermore, the industrial zone is situated in the eastern region of Eskişehir, and the prevailing wind direction is from west to east. This configuration suggests that the wind has the potential to transport MNPs from other regions and accumulate them in this specific area.

As reported by Zhu et al. (2021), a significant reduction in MNP concentration was observed during the morning hours compared to the concentration measured at noon, which, in turn, exhibited a higher concentration than that recorded at night (Zhu et al., 2021). The

results of this study indicate that the concentration of MNP is higher during the daytime than during the nighttime. It is noteworthy that the concentration of MNP particles in urban areas is considerably higher during the daytime than at night. This phenomenon can be attributed to the substantial volume of vehicular traffic observed during daytime hours, with the source of the collected MNPs identified as tires and rubber components. Consequently, it can be deduced that the concentration of MNPs observed during daytime hours will likely exceed that observed at night. Consequently, it can be deduced that the concentration of MNPs during daytime hours will exceed that observed at night (Zhu et al., 2021). The predominance of smaller (<100 μm) MNPs in the atmosphere of the urban-rural interface area may also reflect the longer residence time and transport distance of smaller plastic particles. This phenomenon is analogous to that observed by other atmospheric aerosol particles (Lewis and Schwartz, 2004). As illustrated in Figure 4.19, the MNP concentration in stage 5 was higher than in other stages. Consequently, a reduction in the size of MNPs, particularly in the form of smaller particles such as NPs, may result in an increase in their concentration (Limsiriwong and Winijkul, 2023). In addition, an elevated level of MNP was observed in the industrial zone on 07/08/2023, as compared to 02/08/2023. This increase can be attributed to the fact that August 7 was a Monday, and all factories commenced operations at maximum capacity. Conversely, a reduction in wind speed (see Table A.1) led to an increase in the concentration of MNP on that day. A significant decrease in wind speed was recorded in the rural area between September 5th and September 6th, 2023. This anticipated outcome is consistent with the hypothesis that such a reduction in wind speed would result in an elevated concentration of MNP in the atmosphere.

A review of the literature revealed that the documentation of diurnal variations in atmospheric MNPs was found to be inadequate. The temporal distribution patterns of atmospheric MNPs have received relatively scant research attention and have not been well developed, with no universal patterns identified in the existing literature.

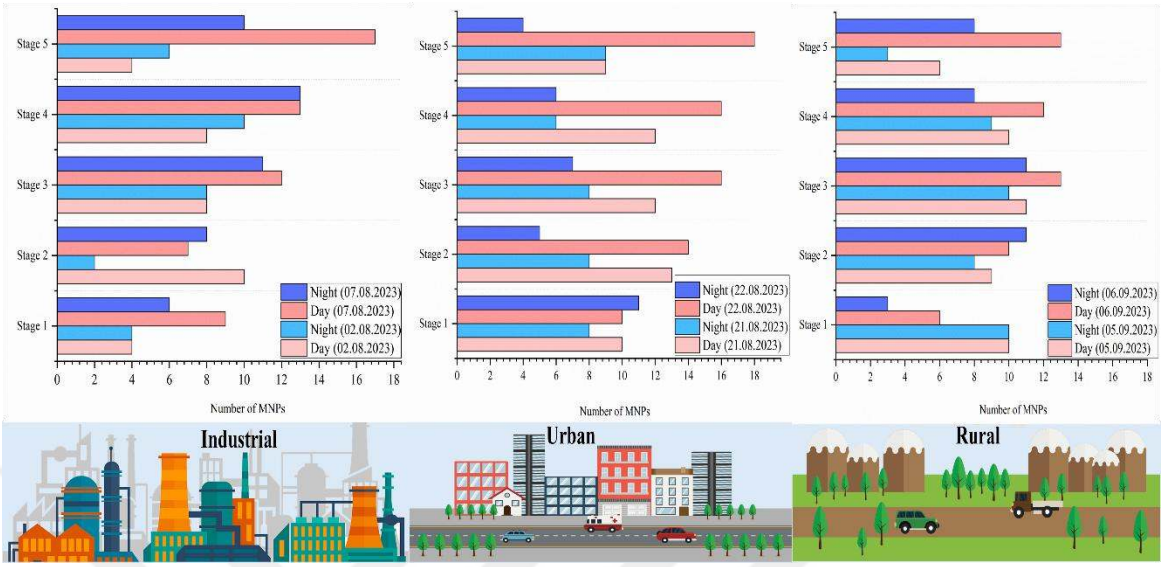

Figure 4.19. *Comparison of temporal and spatial number of MNPs in the different stages.*

A previous study conducted during the early stages of the pandemic revealed that the highest concentrations of pollutants were observed in the early hours of the day, specifically from 6:00 a.m. to 12:00 p.m., Tuesday through Thursday. In contrast, on weekends, particularly on Saturdays, the levels of pollution reached their peak during the midday hours, from 10:00 a.m. to 4:00 p.m. One hypothesis that can be postulated to explain these findings is that the reduction in vehicular and pedestrian traffic, attributable to the pandemic-induced lockdown measures, resulted in diminished levels of air pollutants (Boakes et al., 2023).

A recent investigation by Liu et al. (2019) revealed that the concentration of suspended atmospheric MNPs in the Western Pacific during diurnal hours (0.45 ± 0.46 Number MNP·m^{-3}) exceeded that measured at nighttime (0.22 ± 0.19 Number MNP·m^{-3}). However, the statistical significance of this discrepancy remains to be determined (Liu et al., 2019a). Furthermore, Liu et al. (2025) discovered that the concentration of suspended atmospheric MNPs during daytime hours in coastal cities exceeds the concentration observed at night. This phenomenon is potentially attributable to increased human activity, elevated temperatures, and ongoing ultraviolet (UV) radiation, which may facilitate the fragmentation of MNPs into smaller particles (Liu et al., 2025).

The chemical spectrometric analysis indicated that approximately 99% of the MNPs were classified as carbon black, while the remaining 1% were detected as PTFE via μ-Raman

spectroscopy (see Figure 4.20) at the matching ratio of up to 70% (Table B. 9). The particles under scrutiny are characterized by black pigmentation and a stretchy consistency, exhibiting characteristics analogous to those observed in tire dust generated in a laboratory setting using commercially obtained vehicle tires (Munno et al., 2020). A comparison of the Raman spectra of the laboratory-generated tire dust particles and the black rubber particles from environmental samples reveals a resemblance to that of carbon. The presence of MNPs in road dust has been attributed to the use of synthetic rubber in tires, including styrene-butadiene copolymers and polymers utilized in bitumen formulations and road marking paints (Abbasi et al., 2019). The bands observed in the aforementioned spectra, at 1585 cm^{-1} and 1360 cm^{-1}, are likely attributable to carbon fillers incorporated into black particles, as postulated by Lenz et al. 2015. Conversely, 54 particles were identified in another material, such as pigments, and approximately 10% of these particles were MNPs (PP, p-(Acrylic), Naylon, and PTFE) with a matching ratio of less than 70%, up to 40% Table B. 10.

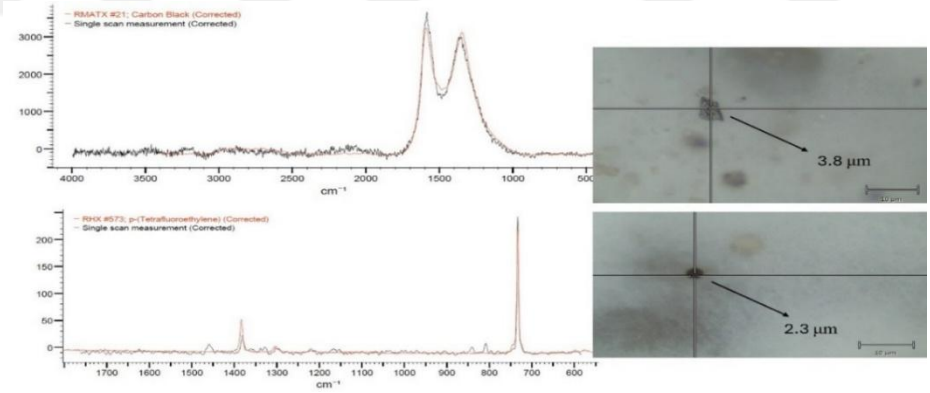

Figure 4.20. *Temporal and spatial chemical identification of MNPs with micro-Raman analysis. Carbon black and PTFE spectrometric peaks.*

It is imperative to note that when selecting 20 particles at random for spectrometric analysis, the morphological characteristics of MNPs (Luo et al., 2022) must be taken into account to prevent interference from carbon black and soot (shape of soot is a cluster of particles that are adhering together)(AkbariDana et al., 2024b). In the context of the chemical composition of airborne plastic particles, Kernchen et al (2022) research yielded the presence

of PE exclusively in the analyzed samples. However, studies involving larger-sized MPs revealed a more diverse array of polymer types. While the possibility exists to identify rubber as synthetic via FTIR in instances where sufficient dimensions are present within the microparticle, however, the capability to differentiate between PE and rubber through this method may present a challenge (Primpke et al., 2018b). This observation suggests that the form and type of MNP particles are contingent on the specific geographical location and the predominant pollution source. In a subsequent study, Levermore et al. (2020) examined a PM sample, leading to the identification of airborne MPs, these MPs included PE; (n = 220), PET; (n = 1), and PP; (n = 2). The size of these MPs ranged from 4.7 to 40.9 μm in length (Levermore et al., 2020). Likewise, Yoo et al. (2023) found that out of 50 stained particles, 66% were tire/road wear particles and 34% were other types of MPs (PS, PE, PET, ABS). These tire wear particles have been identified as a substantial source of MP pollution, with estimates suggesting that they account for a significant proportion of MP emissions to air, lakes, and oceans (Yoo et al., 2023). This proportion aligns with a model study indicating that roads are the primary source of anthropogenic MPs, representing 85% of the total (Brahney et al., 2021). According to the findings of Gaston et al. (2020) and Rahman et al.(2021), the samples exhibited substantial quantities of carbon black, with origins including traffic and combustion-related sources.

4.1.7. Micro-Raman analysis of spatial and seasonal samples

Distinct seasonal patterns in the distribution range of airborne MNPs have been demonstrated, with greater dispersion and concentration typically observed during summer months compared to winter periods. A total of 6 samples were collected: 2 nights and 2 days from summer, and 1 day and 1 night of winter. These samples were collected from rural areas, and five stages were analyzed by the spectrometric analysis method. A total of 181 particles were identified as MNPs in the summer samples, which were subsequently classified as 95% fragments (0.8 to15.3 μm) and 5% fibers (9.7 to 50.3 μm). The analysis revealed that 98% of the MNPs were classified as fragments (0.9 to 12.8 μm) while 2% of the MNPs classified as fibers (7.6 to 48.4 μm) were identified during the winter months. In addition, the mean range of MNP fragment sizes in the summer season was 3.23±1.5 μm, while the mean range

of MNP fragment sizes in the winter season was 2.86 ±1.2 μm (see Figure 4.21). The comprehensive details of MNP are enumerated in Table B6, Table B.7, and Table B .8**,** which are categorized by stage and sampling location. This seasonal variation is influenced by a multitude of environmental, meteorological, and anthropogenic factors that collectively affect the release, transportation, and distribution of MNPs in the atmosphere. It appears that temperature exerts a substantial influence on the concentration and distribution of airborne MNPs across seasonal cycles. According to a model of MNPs fragmentation (Aoki and Furue, 2021), the process of reducing particles to smaller sizes necessitates higher energy, which is less frequently available. During the summer months, an increase in wave action, wind, and other mechanical forces results in a greater supply of energy. This heightened energy supply subsequently leads to a broader size distribution, with a greater prevalence of larger particles compared to the winter months, when these forces are observed to be weaker.

The enhanced thermal uplift resulting from elevated summer temperatures give rise to more dynamic air currents, capable of transporting MNP particles to greater altitudes and distances than in cool seasons. The thermal effect is particularly pronounced in studies that observed higher MNP concentrations, as well as notably smaller sizes of MNP particles, during winter months at sites with high and low population density. This study posits that high humidity levels during summer months (see Table A.1) can lead to an augmentation in the size of airborne MNPs (magnetic nanoparticles) through a process known as aggregation and water absorption. The presence of high humidity fosters the clustering of MNP particles due to the creation of adhesive forces between them and water molecules. This aggregation process results in the suspension of larger composite particles in the air. In contrast, the findings of another study suggest that the reduction in the size of particle distribution during the summer months may indicate that MNP particles are more susceptible to fragmentation. This increased fragmentation could result in enhanced dispersal capabilities, which would expand their overall travel range (Y.-C. Chen et al., 2024).

Seasonal variations in atmospheric circulation have been demonstrated to exert a substantial influence on the range size of airborne MNPs. During summer months, the prevalence of southerly or southwesterly winds, as documented in several studies, has been observed to facilitate the transportation of MNP particles over considerable distances (Y.-C.

Chen et al., 2024; Yang et al., 2024). The stability of these summer wind patterns often enables more consistent and widespread distribution compared to the more variable wind conditions characteristic of winter months. Conversely, in winter, stronger and more turbulent currents tend to break up MNP plumes rather than facilitate their long-range transport, thereby contributing to more limited and localized distribution patterns in comparison to those observed in summer. This seasonal difference in wind behavior is a critical factor that helps explain the observed discrepancy in the distribution of MNPs between winter and summer (Wang et al., 2022).

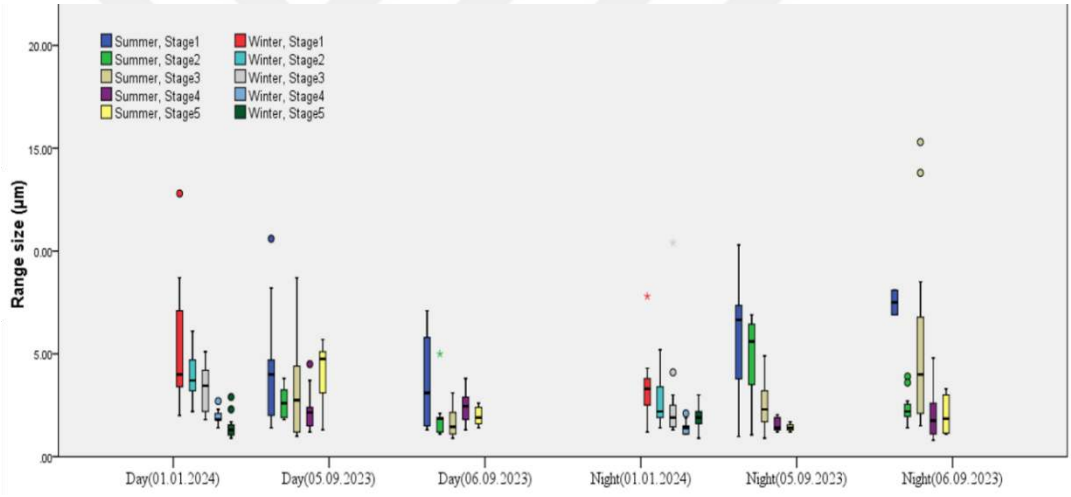

Figure 4.21. *Comparison of seasonal range size of MNPs fragment collected in stages a)1st, b) 2nd, c) 3rd, d)4th, and f) 5th, at the rural region (summer & winter).*

The mean number of MNPs during the summer period was 50±5.7, or a mean concentration equivalent of 9843.5±1857 MNPs/m³ diurnally, and 40±0.7, or a mean concentration equivalent of 7668 ± 978 MNPs/m³ nocturnally. However, a total of 56 MNPs, or a mean concentration equivalent of 10,345 MNPs/m³, were detected during the day and 57, or 11,337 MNPs/m³, at night in the winter in the rural atmosphere. The findings of this study indicate that the winter MNP concentration in the rural atmosphere was higher than that of the summer months. Sometimes, during winter inversions, the concentration of

airborne MNPs can be significantly elevated. This phenomenon occurs due to the formation of a layer of warm air that traps colder air near the surface, thereby preventing the normal vertical mixing of air. This results in the formation of a stagnant layer where pollutants, including airborne particles such as MNPs, accumulate (Nafea et al., 2025). On the other hand, winter winds have been shown to exhibit greater turbulence and vertical mixing in comparison to summer winds. This phenomenon leads to the dispersion of MNPs across a more substantial atmospheric volume, resulting in the elevation of particles to greater altitudes. Consequently, this reduces the localized concentration of MNPs in the surface layers. As demonstrated in Figure 4.22, the concentration of MNPs (stage 5) in the dry season was greater than in the wet season. This is due to the elevated temperatures characteristic of the summer months, which promotes the degradation of larger plastic debris into MNPs fragments. When exposed to intense solar radiation and heat, plastic materials undergo accelerated photodegradation and thermal breakdown, thereby increasing the release rate of MNP particles into the environment. This intensified generation process during the summer months contributes to both higher concentrations and wider distribution ranges, as a greater number of particles become available for atmospheric transport.

The findings of this study, conducted in rural regions, contrast with those of a previous study that was performed in urban areas, such as Taipei. The previous study observed a decrease in MNPs concentrations during winter, despite the presence of higher wind speeds. It can be posited that the observed decrease is attributable to the aforementioned dilution effect (Y.-C. Chen et al., 2024).

During the winter of 2023, observations were made in Eskisehir indicating a low rate of precipitation and a concomitant low relative humidity (RH%), in comparison with the summer season (weather conditions showed in Table A1). High winds have been shown to increase the efficiency of wet deposition, wherein snowflakes capture airborne MNPs and deposit them on the ground.

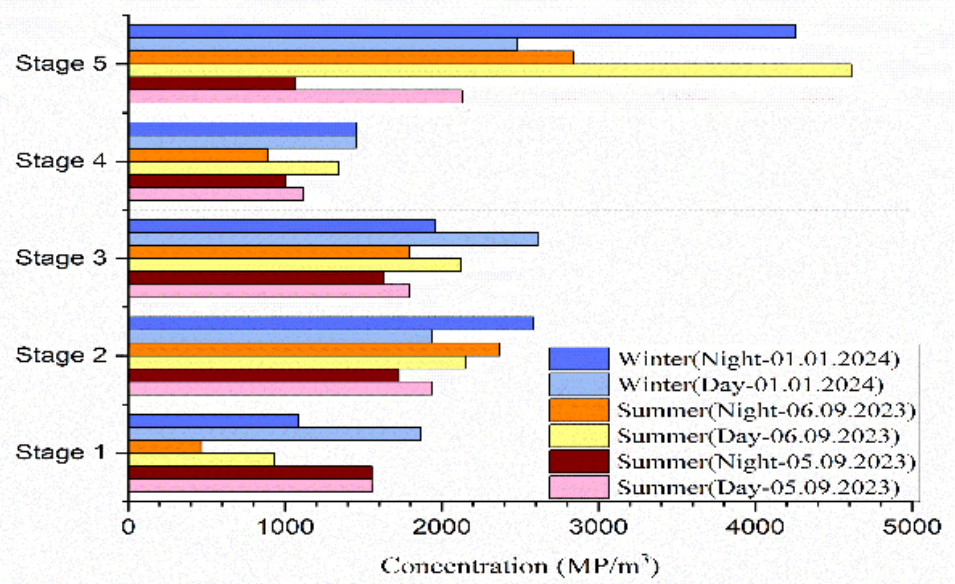

Figure 4.22. *Comparison of summer and winter number concentration of airborne MNPs in the rural region.*

The presence of MNPs in snow has been demonstrated to reduce surface albedo, thereby creating a negative feedback loop wherein darker snow surfaces melt more rapidly, further embedding particles in ice or water systems (Chubarenko, 2022; Sharma et al., 2023).

As the investigation into airborne MPs remains in its nascent phase, the correlation between airborne MPs and components of routinely monitored air pollution indices, such as atmospheric particulate matter (PM) with a diameter of less than 10 µm (PM_{10}) and 2.5 µm ($PM_{2.5}$), is yet to be elucidated. In this section, the meteorology report was consulted to select two days (the highest and lowest PM_{10} index) in each zone. Then, 20 particles were chosen at random from a surface area of 1 cm^2, which had been extracted from five stages of two diurnal. These particles were then examined by a µ-Raman microscope, with the specific intention of investigating the MNP's behavior and characterization. A total of 6-day samples based on meteorology (PM_{10}) from three zones (industrial, urban, and rural) were examined in each stage; consequently, 373 particles were classified as MNPs (96% fragments (0.8 - 10.5 µm) and 3% fibers (7.6 - 45.1 µm)) under different stages. The higher abundance of fiber MPs in urban areas compared to industrial and rural zones can be attributed to several factors. First, fiber MPs often originate from synthetic textiles (e.g., polyester, nylon) released during laundry cycles. These textiles are more concentrated in densely populated

urban areas. Second, while wastewater treatment plants (WWTPs) in urban zones filter some MNPs, they still discharge significant amounts of fibers into water systems (Y. Fan et al., 2022). As depicted in Figure 4.23, the range of MNPs fragments across the five distinct stages of the study exhibited a downward trend in fragment size distribution with decreasing cutoff size stage, (the highest PM_{10} index day is associated with a light color, while the lowest PM_{10} index day is associated with a dark color).

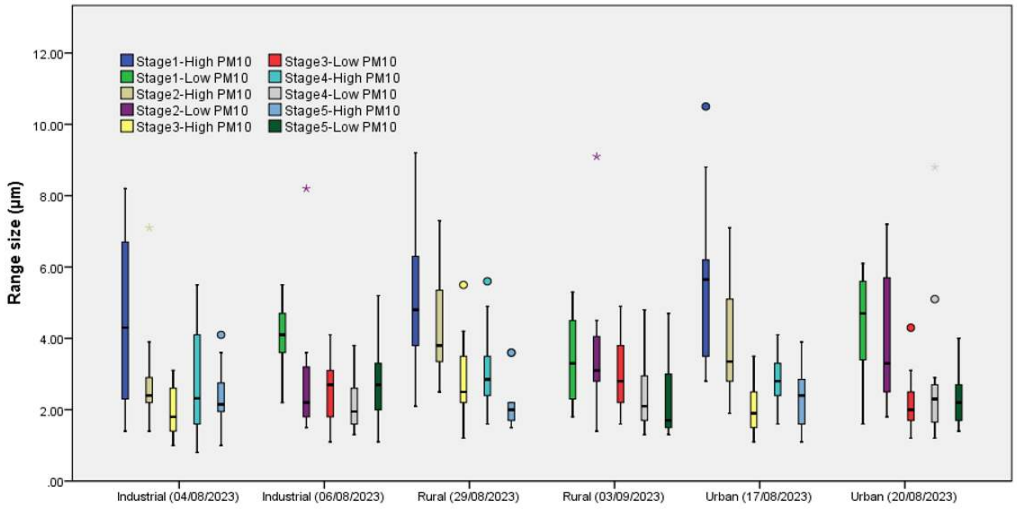

Figure 4.23. *Range size of MNPs fragment collected in stages a) 1, b) 2, c) 3, d) 4, and f) 5, based on PM_{10} index of weather condition in the three sampling locations.*

Furthermore, the observed abundance of MPs in each region appeared to be independent of PM_{10} levels reported by the meteorology center (Figure 4.24) and Figure B. 14. In the context of air quality assessments, MPs frequently comprise a subset of PM components. However, the abundance of MPs cannot be estimated solely based on their specific contribution. The present study has demonstrated a marked increase in the number concentration of MNPs in both industrial and rural atmospheres. The concentration of MNPs in the high PM_{10} category was found to be 16,043 MNPs/m³, while the concentration in the low PM_{10} category was 14,910 MNPs/m³. Similarly, the concentration of MNPs in the high PM_{10} category in rural atmospheres was found to be 12,677 MNPs/m³, while the concentration in the low PM_{10} category was 12,001 MNPs/m³. These findings are in line with

the trends observed in PM_{10} concentrations. In contrast, the concentration of MNPs in urban airborne PM_{10} was not subject to significant change. The increase in MNP concentration was not uniform across all regions. The results of urban areas in this study indicated that 10312 MNPs/m^3 in the high PM_{10} category, and 13524 MNPs/m^3 revealed in the low PM_{10} category that there is no uniform increase. The variability can be attributed to differences in sources, meteorological factors, and pollutant dispersion patterns. Industrial and rural areas often have direct sources of MNPs related to industrial emissions, agricultural activities, biomass burning, and less efficient pollutant dispersion. These sources have the potential to elevate PM_{10} and associated MNP concentrations under weather conditions conducive to accumulation, such as temperature inversions or stable atmospheric conditions. Conversely, urban areas are characterized by intricate pollutant sources and more pronounced local-scale dispersion and removal processes, which may result in the decoupling of MNP concentrations from PM_{10} trends. Urban areas frequently encounter more variable and turbulent airflows due to the built environment, which can enhance dispersion and reduce the accumulation of airborne MNPs even when PM_{10} levels rise regionally. The number of airborne MNPs on the 21st and 22nd of August in the urban area was not found to be associated with an increase in PM_{10} (Figure 4.24).

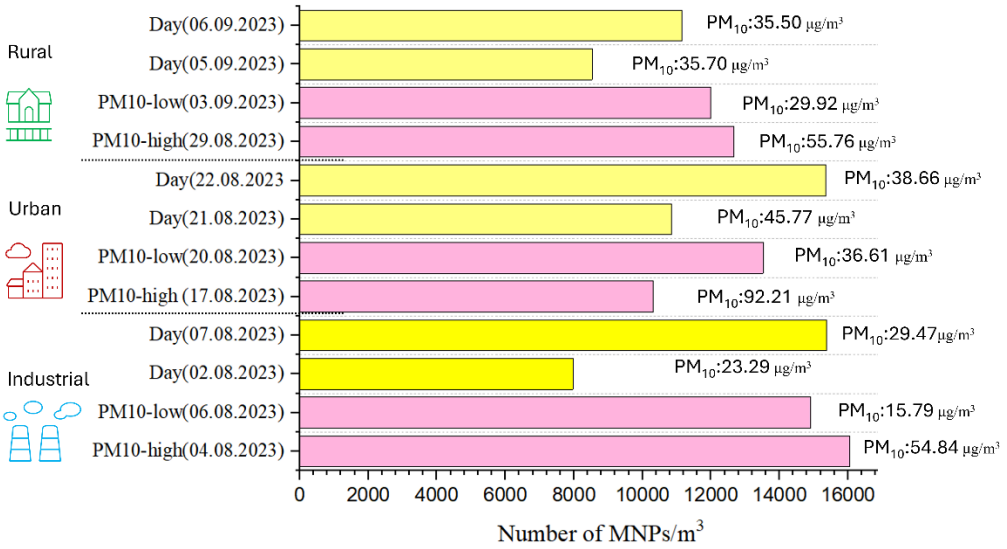

Figure 4.24. *Number of airborne MNPs based on particle-based analysis method.*

Nonetheless, research conducted in London and Beijing (urban regions) revealed the presence of thousands of MPs per cubic meter in the atmosphere. These regions are distinguished by their notably high PM_{10} levels (Amato-Lourenço et al., 2020; Sridharan et al., 2021). Furthermore, tire abrasion, which is identified as a significant source of atmospheric MNPs, contributes an estimated range of 0.8% to 8.5% of PM_{10} mass in urban areas (Amato-Lourenço et al., 2020). Notably, during periods of high traffic volume, there is a resurgence in the resuspension of road dust containing MNPs, leading to an augmentation in both PM_{10} and MNP levels (Carriera et al., 2024). Consequently, an increase in MNPs could have a direct impact on the levels of both PM_{10} and total suspended particulate matter (TSPM). These factors are influenced by the origin of the MNPs, as well as by the level of human activity within the area under consideration that was selected for monitoring of air pollutants.

μ-Raman spectrometry results for airborne MNPs frequently identify carbon black, a widely used reinforcing filler in automobile tires, rubber products, paints, and pigments. Given its pervasive presence in urban environments, it is not surprising that carbon black is frequently detected in airborne particulate matter, including MNPs (Rahman et al., 2021)(Table B. 10**).**

4.2. Mass-based Analysis of Micro(nano)plastics

4.2.1. Selection of an appropriate subsample

The findings of the Pyr-GC/MS analysis demonstrated that all of the polymers in the entire Teflon filter were identified as NR with concentrations of 0.011302, 0.015724, 0.014677, 0.01065, and 0.01529 μg/m³, respectively. However, no significant variations were observed in the polymer types and MNP concentrations across the different sections of the Teflon filter. To assess the homogeneity of the distribution of MNP s across the three sections within a single slot, as well as across different slots within the slotted Teflon filter, a chi-squared test was conducted, with a 95% confidence level ($\alpha = 0.05$). The critical chi-squared value was found to exceed the calculated chi-squared value. Consequently, the null hypothesis, which postulates the homogeneity of the distribution of MPs across the various slots of a Teflon filter, can be accepted at a 95% confidence level.

4.2.2. Pyr-GC/MS analysis of day and night samples

The analytical method of Pyr-GC-MS facilitates the identification of diverse polymer types present in MNPs through the analysis of their characteristic pyrolysis products. This method has been demonstrated to be capable of analyzing a diverse array of thermoplastic polymers and elastomers. It offers comprehensive insights into the chemical composition of MNPs, including additives and contaminants (Hermabessiere et al., 2018). In contrast to numerous spectroscopic techniques that predominantly furnish qualitative data, Pyr-GC-MS furnishes mass-quantitative information. The technique has been demonstrated to be capable of accurately quantifying the concentration of MNPs in environmental samples, which is of critical importance for the assessment of pollution levels and potential ecological impacts (Hermabessiere et al., 2018).

Pyr-GC-MS is capable of detecting MNPs at concentrations as low as picograms to micrograms, making it an effective tool for the analysis of these particles. This high sensitivity is particularly advantageous when analyzing complex samples in which MNPs may be present in trace amounts (Pipkin et al., 2021). The technique requires less extensive sample preparation than traditional methods, thereby reducing the time and resources typically required for analysis. It is often feasible to conduct analyses on samples that have undergone minimal processing directly (Seeley and Lynch, 2023). Although Pyr-GC-MS is an effective analytical technique for examining MPs, it is not without certain limitations that can potentially impact the accuracy and comprehensiveness of the analysis. Pyr-GC-MS does not provide information regarding the size distribution of MNPs particles. A comprehensive analysis necessitates an understanding of both the composition and the size distribution of the particles in question. Consequently, supplementary techniques such as Raman spectroscopy may be required to supplement the existing methodology and address this gap in knowledge (Hermabessiere et al., 2018).

The findings of the present study indicate that the maximum concentration of ∑MNPs was detected in urban areas, with a total day value of 29.86 μg/m³ and a nighttime value of 23.05 μg/m³. Rural areas demonstrated a lower maximum concentration, with a total day value of 15.42 μg/m³ and a nighttime value of 15.92 μg/m³. Industrial regions exhibited the lowest total concentration, with a total day value of 7.31 μg/m³ and a nighttime value of

23.55 µg/m³. The total findings of the mass-based analysis in this study were consistent with those of the particle-based analysis; however, only mass concentration on certain dates at night exceeded the day concentration Figure 4.25. This phenomenon could be attributed to the fact that the particle-based analysis of the five-stage, which includes larger particles, was examined by the spectrometry method, while the mass-based analysis of the backup stage was also examined. The preponderance of MNP polymer types was predominantly captured in the backup stages, as illustrated in Figure 4.26. Consequently, the number of larger MNP particles collected during the day may exceed the number collected at night; however, they began to deposit in the afternoon. Consequently, a smaller nanofraction of particles remained in the atmosphere, and the mass concentration of MNP particles captured in the backup stage at night was greater than that captured during the day. Indeed, an increased mass concentration of diverse polymer MNPs was detected during nocturnal periods, corresponding to the nanofraction stages.

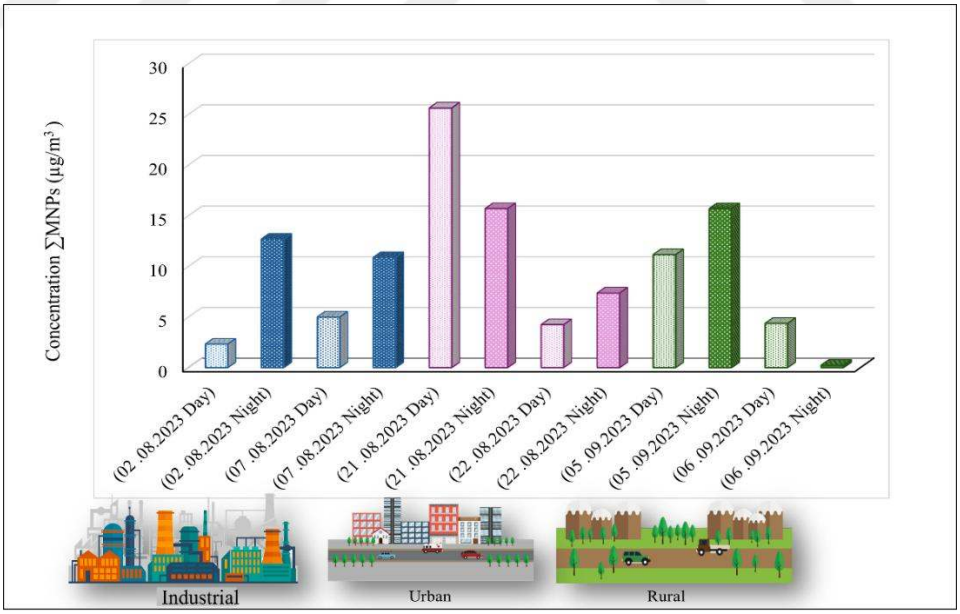

Figure 4.25. *Total mass concentrations of airborne MNPs in the three sampling locations.*

In a previous study, Chen et al. (2024) employed an active sampling method from an urban area that utilized four impactors to remove coarse particles with an aerodynamic

equivalent diameter greater than 2.5 μm, which mean concentration of fine plastic particles (FPPs) was determined to be 5.6 μg/m^3. The investigation revealed that the minimal concentrations of FPP were detected between 2:00 and 6:00 local time. This phenomenon is attributed to the reduced human activity within the city, thereby suggesting that the contributions from industrial facilities, which generally operate on a 24-hour basis, do not predominate the atmospheric concentrations of fine plastic particles within the urban environment (Y. Chen et al., 2024). In contrast, the highest FPP abundances were measured between 12:00 and 14:00, and between 18:00 and 20:00, which correspond to periods of intense traffic, shopping, and outdoor activities. These observations suggest that human activities are the primary source of FPPs in urban areas. The decline in FPPs observed from 14:00 to 16:00 can be ascribed to the reduction in traffic and decreased outdoor activities (Y. Chen et al., 2024). This finding suggests that the period of greatest exposure to FPPs coincides with human activity hours. A notable increase in the prevalence of FPPs was observed during the holiday period compared to weekdays, specifically from 4:00 to 10:00 and from 12:00 to 14:00. This increase can be attributed to the heightened engagement in outdoor activities and city trips during the holiday period (Y. Chen et al., 2024). Conversely, weekday fluctuations in FPP abundance exhibited an overall upward tendency, with significant increases observed from 4:00 to 14:00. Following a decline between 14:00 and 18:00, FPPs' concentrations increased from 18:00 to 22:00. These findings are consistent with established patterns of human behavior in metropolitan areas, where outdoor activity is typically predominant during these hours (Y. Chen et al., 2024).

The total mass concentration of the polymers in the air samples collected from all three locations was measured as follows: PET (4.36±1.2 μg/m³) < PE (2.48 ±1.6 μg/m³) < PP (1.47 ± 0.8 μg/m³) < PVC (0.96 ±0.3 μg/m³) < SBR (0.72 ±0.5 μg/m³) < NR (0.07±0.1 μg/m³). While PET (5.42±1.2 μg/m³ in industrial zone) and PE (3.83±4.5 μg/m³ in the urban zone) concentrations were identified as the highest concentrations of MNPs, they were detected in the backup stage, not in any other stage. Conversely, SBR (1.44±.09 μg/m³ in the rural region) and NR (0.1 μg/m³ in the industrial area) were identified in the lowest concentration polymers, yet they were detected in the majority of stages with larger cutoff sizes. These results were corroborated by particle-based analysis, which revealed that the majority of the

polymers identified across the five stages were classified in the carbon black group. This finding is analogous to the mass-based analysis, which indicated a similarity between SBR and NR polymers. The sequence of detection polymers in the three sampling zones exhibited similarity; however, PET was not identified in the urban area, and PS was detected in the rural area with low concentration.

A comprehensive analysis revealed that PET and PE were identified as the most prevalent polymer types in disparate geographical regions (with the exception of PET in urban areas). The utilization of PET predominantly occurs in the manufacturing of carbonated beverages and textiles. PE, on the other hand, finds application in the production of cost-effective items, including plastic bags. These polymer types (Figure 4.26a) are utilized to a considerable extent in industrial regions and are also released into the environment as a consequence of quotidian human activities. These polymers are the most commonly observed due to their extensive utilization and high production rates on a global scale (Kabir et al., 2024; Miranda-Peña et al., 2023). Specifically, PE and PP that was detected most concentration (2.35 ± 1.2 μg/m³) in the urban area in this study, account for a substantial proportion of plastic production, with estimates suggesting that they represent approximately 62% of the total plastic output on a global scale (Adetuyi et al., 2024). Furthermore, PE and PP have found applications in construction, such as in the fabrication of pipes and the production of insulation materials. Moreover, PP MNPs have the capacity to be transported over long distances by wind and other environmental factors due to their low density (Nachtnebel et al., 2017). In urban areas, the pervasive presence of PP in packaging materials, including food containers, bags, and wrappers, has led to the identification of PE and PP as the predominant polymer types (see Table B. 12). Furthermore, PVC that was detected in the urban with most mean concentration 1.12 ± 1 μg/m³ associated chemical plants, including chlor-alkali plants that produce chlorine for PVC manufacturing, have the potential to emit associated pollutants and MNP particles (Xu et al., 2024). The deterioration of synthetic textiles, rubber tires, brake pads, and vehicle components has been identified as a primary contributor to the presence of airborne MNPs in urban environments. This phenomenon includes the release of PVC fragments from these sources, which have been identified as a significant source of MNP contamination (Jahandari, 2023).

The majority of sampling locations in this study considered the NR and SBR originating from tire wear and road wear, despite the low concentration. (Figure 4.26). The term "microplastics" is generally defined as solid particles measuring between 1 and 5,000 μm in size that are insoluble in water and composed of synthetic polymers with thermoplastic or thermoset properties. Due to their chemical and physical properties, tire wear particles (TWP) are often included in the MNPs definition (Andrady, 2011; Verschoor et al., 2016). Tires are composed of a blend of styrene butadiene rubber (SBR), natural rubber, carbon black, and various additives (Sommer et al., 2018). In urban settings, the combination of traffic, construction activities, and other anthropogenic sources can enhance the dispersion of these particles into the atmosphere (Jahandari, 2023; X. Yao et al., 2022). The analysis of tire wear particle (TWP) concentration is a complex task due to the variation in rubber composition among different tire brands and the distinct manner in which tires undergo wear depending on the vehicle's type. The assumption is that 44% of styrene-butadiene rubber (SBR) is present in passenger tires and that 45% of truck tires are composed of natural rubber (NR) (Rauert et al., 2021; Unice et al., 2019). It has been estimated that, within the Nordic countries, TWP accounts for more than 50% of MNP emissions to the environment (Magnusson et al., 2016; Sundt et al., 2014). As vehicle exhaust emission limits constrict and the tendency of electric vehicles increases, TWPs are slowly overwhelming vehicular emissions, as evident in Europe (Ketzel et al., 2007), India (Nagpure et al., 2016), and the Netherlands (Timmers and Achten, 2016), where 50–85%, 66–86%, and 50% of the total PM_{10}, respectively are non-exhaust emissions. The present study proposes a viable methodology for the quantification of the SBR and NR-based TWP in road dust, employing Pyr-GC–MS across a range of tire types.

Notably, the utilization of NR is particularly prevalent in the context of radial tire treads for trucks and buses. Conversely, SBR is predominantly used in light-duty vehicles (Rattanakunuprakarn et al., 2024). Research has demonstrated that tires are a significant source of MNPs at the local level. For instance, a study of tire wear in a German city revealed that 51% of MPs were attributed to tire wear (Kovochich et al., 2021b). Similarly, a study of tire wear in Sao Paulo, Brazil, revealed a 53% contribution of MNPs (Goehler et al., 2022). In the United States, medium- and high-traffic sites reported a contribution of 38–39% (Gao

et al., 2022), and India at an urban traffic site revealed a 31% contribution of tires (Giechaskiel et al., 2024).

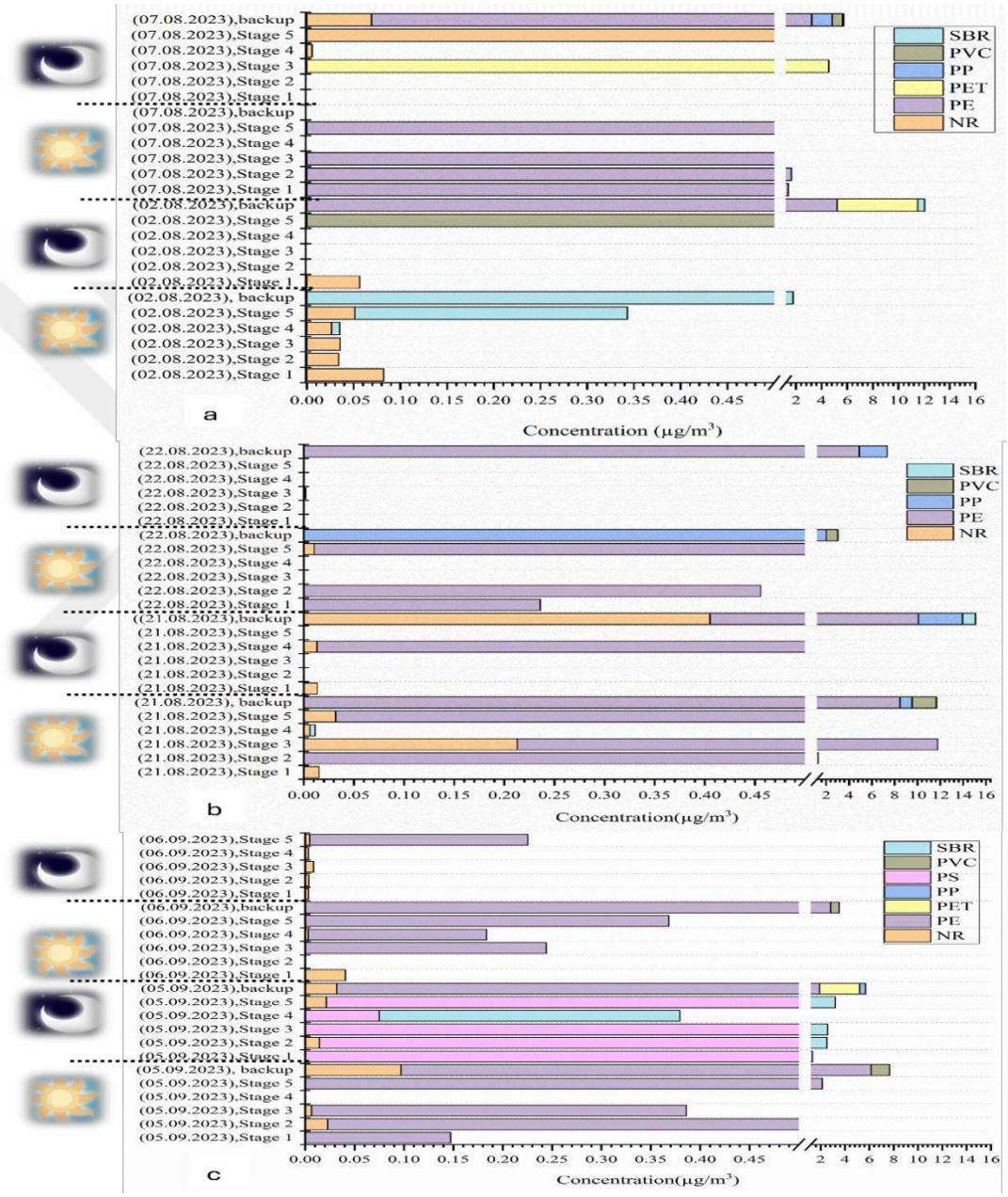

Figure 4.26. *Comparison of temporal and spatial airborne MNPs mass concentration (a) industrial, b) urban, c) rural zone).*

The findings of this study suggest a marked presence of PS (0.44±0.5 µg/m³) in the vicinity of agricultural sites, as opposed to other regions. Experimental findings have

revealed the presence of a substantial number of MNPs in the vicinity of the PS form, thereby substantiating the atmospheric emission capacity of NPs. A substantial body of research has demonstrated the potential for PS NPs to inflict considerable harm on living organisms. Consequently, the quantification of suspended PS NPs has emerged as a critical area of research (Sheng et al., 2023). Pyr-GC/MS has frequently detected the presence of PS plastic particles in atmospheric fallout (Al-Khalidy and Al-Haidarey, 2024; Goßmann et al., 2023b; Rassaei, 2024). Given its status as one of the most widely utilized plastics, the production of PS reached 20.7 metric tons in 2021. This accounts for 5.3% of the total amount of plastic produced (Sheng et al., 2023).

In a previous study reported the mean concentration of FPPs was determined to be 5.6 $\mu g/m^3$, and the mean concentrations of PE, PS, and PVC were 4.2 $\mu g/m^3$, 0.6 $\mu g/m^3$, and 0.5 $\mu g/m^3$, respectively (Y. Chen et al., 2024). While this study observed various polymer concentrations in the urban region for NR, ranging from 0.00631 to 0.4 $\mu g/m^3$ in stage 1 (greater than 7.2 μm to back up less than 0.49 μm). The SBR concentration was determined to be between 0.002 and 1.14 $\mu g/m^3$. $\mu g/m^3$ (stage 3 > 1.5 μm, backup). The results of the study indicated that urban SBR released from passenger tires was collected in stages with a smaller cutoff size than that of NR, which was created from truck tires. For PE, the concentration range was from 0.23 to 11.5 $\mu g/m^3$ (stage 1, stage 3), and for PVC, it was from 0.21 to 2.12 $\mu g/m^3$ (stage 2 > 3 μm, backup). Subsequently, the urban PE concentration was found to exceed that of the PVC, yet the PE polymer was captured in stages, exhibiting a high cutoff limit of size.

4.2.3. Pyr-GC/MS analysis of spatial and seasonal samples

The result of the Pyr-GC/MS analysis of seasonal samples indicated that, although there was no significant difference in the mean mass of MNPs in summer (15.72±15.71 $\mu g/m^3$) and winter (15.92 $\mu g/m^3$), there was a significant difference in the ∑MNPs concentration between summer samples from rural areas. The total night-time ∑MNPs concentrations from the five stages on the first day were 11.15 $\mu g/m^3$ and 15.68 $\mu g/m^3$, respectively. On the second day, the ∑MNPS concentration was 4.34 $\mu g/m^3$, and on the night, it was 0.24 $\mu g/m^3$. The elevated mass concentration of MNPs in the rural area on the first day (Tuesday), when the

relative humidity (RH) was 86.6% and the wind speed was 0.37 m/s, in comparison to the second day (Wednesday), which exhibited a higher RH (90.2%) and more robust wind speed (1.5 m/s) during the summer season, can be attributed to the synergistic impact of relative humidity and wind speed on particle formation and dispersion. The velocity of the wind plays a pivotal role in the dispersion and transport of particles. In the context of atmospheric conditions characterized by low wind speeds, with velocities as low as 0.37 m/s observed on Tuesday, the dispersion of particles is reduced. This phenomenon enables the accumulation of particles within specific areas, leading to an augmentation in the measured mass concentration of the particles in the ambient air. In contrast, elevated wind speeds (for example, 1.5 m/s on Wednesday) have been shown to enhance dispersion and dilution of particles, thereby reducing their local concentration.

The distinction between the daytime and nighttime concentrations of MNPs during the winter season was more pronounced than in the summer. The high concentration of airborne MNPs may be attributed to two primary factors: high humidity and raining during the nighttime of winter months and the phenomenon of inversion, which can result in elevated pollution levels in the morning (Figure 4.27, Table B. 13). Furthermore, an increase in the concentration of MNP deposits was identified on Stage 5 and the back-up, which included extremely small particles.

At elevated humidity levels, airborne MNPs may undergo hygroscopic growth, which can result in an increase in their effective size. This phenomenon can result in enhanced coagulation and aggregation of smaller particles, which may lead to an increase in their mass concentration in the air. For example, research has demonstrated that at 85% relative humidity (RH), concentrations of specific particle sizes are elevated in comparison to lower RH levels (30%), due to the hygroscopic effect (Qiu et al., 2024). However, the humidity level in the winter (76%) was lower than in the summer (90%), and the wind speed in the winter (5.3 m/s) was greater than in the summer (1.5 m/s). These phenomena resulted in the transportation of MNPs to remote regions and a decrease in MNP concentration (Table A.1).

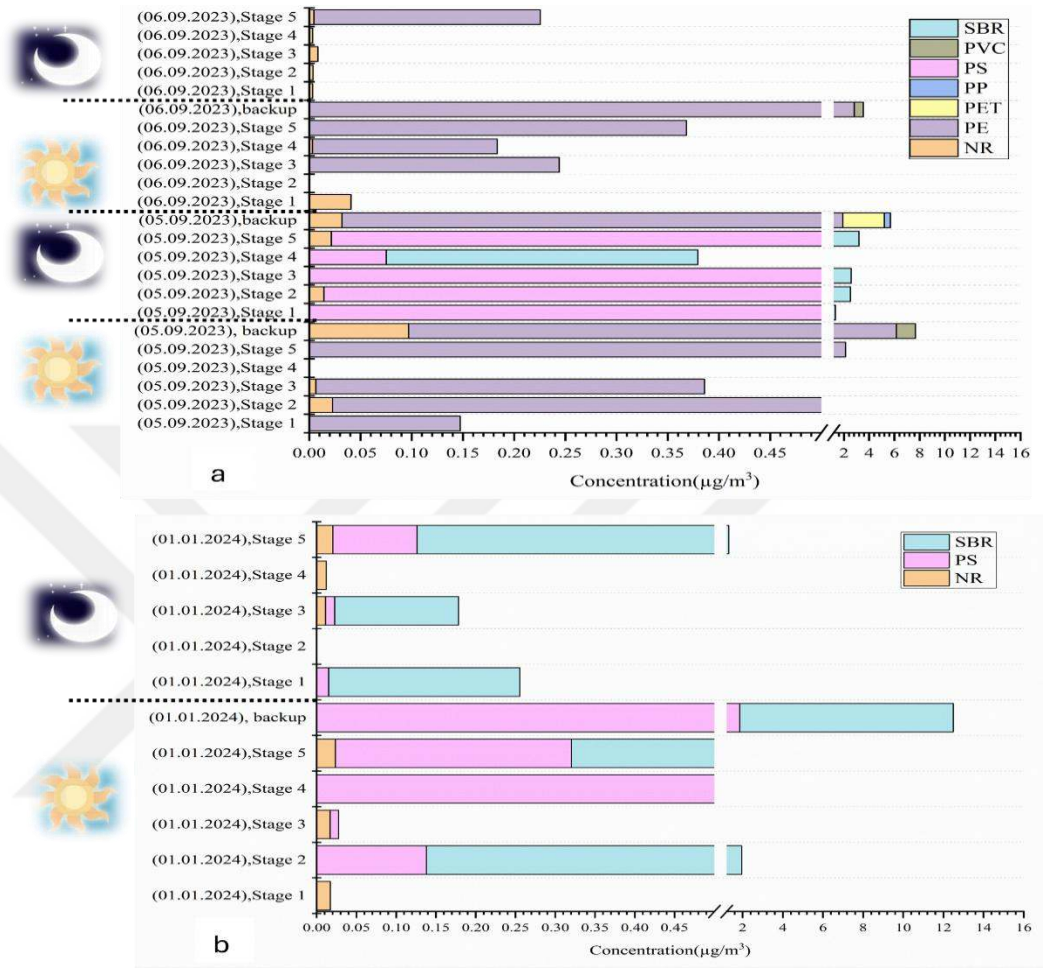

Figure 4.27. *Seasonal airborne MNPs mass concentration in Rural zone (a, summer; b, winter).*

Additionally, the type of polymers that were identified in the winter season (NR: 0.0097 μg/m³; PS: 2.95 μg/m³; and SBR: 14.71 μg/m³) were lower than those identified in the summer season: PET: 3.3 μg/m³; SBR: 1.44 ± 0.9 μg/m³; and PE: 1.18 ± 1.8 μg/m³. The concentration of PVC was measured at 1.1 ± 0.6 μg/m³, while the concentration of PP was determined to be 0.5 μg/m³. The concentration of PE was found to be 0.44 ± 0.5 μg/m³, and the concentration of NR was recorded at 0.02 ± 0.01 μg/m³. The greater variety of polymer types of airborne micro and nanoplastics (MNPs) detected in rural areas during summer (including PET, SBR, PE, PVC, PP, PS, and NR) compared to winter (mainly SBR, PS, and NR) can be explained by several seasonal and environmental factors. Higher human and agricultural activities in summer lead to increased emissions of various plastic types. Some

polymers, such as PET and PVC, are more prone to photodegradation and chemical weathering, which are intensified during summer months due to higher UV radiation. This process can result in the fragmentation of these polymers into smaller airborne particles, which are more readily identifiable during summer months but are less evident in winter.

In this section of the study, two days were selected based on the highest and lowest PM_{10} levels, as indicated by weather condition reports, which were detailed in Table A1. The mass-based analysis of the results did not confirm an increase in the mass concentration of MNPs following an increase in PM_{10} concentration, especially in urban areas. On August 17, the mass concentration of MNPs in the urban area was recorded at 4.58 μg/m³, while the concentration of PM_{10} was 92.2 μg/m³. These concentrations were significantly lower than those observed on August 21, with MNP mass concentrations measuring 25.6 μg/m³ and PM_{10} concentrations reaching 45.7 μg/m³ (Figure 4.28). Meteorological factors, such as wind speed and humidity, exert a more direct and significant influence on the airborne mass concentration of MNPs. This is due to their impact on factors such as particle dispersion, size distribution, and hygroscopic growth. By contrast, the PM_{10} index primarily reflects coarser particle mass and, as a result, exerts a lesser effect on MNP concentrations in urban air.

As demonstrated in Figure 4.28, the mass concentration of airborne MNP on dates with elevated PM_{10} index in the industrial zone exhibited a marginal increase compared to dates with reduced PM_{10} index (PM_{10} concentrations are documented in Table A.1, contingent on prevailing weather conditions). Notably, the aforementioned regulatory framework overlooked the significance of the alternative sampling location. Consequently, it was hypothesized that the PM index enumerated in the meteorological report may not accurately reflect the presence of MNPs in the atmosphere. The meteorology station responsible for monitoring the air quality index was situated a considerable distance from the sampling locations, which hindered its capacity to accurately record the PM_{10} index.

A previous study measured the daily concentration of PM_{10} in the northeast of Spain using a low-volume sampler for 24 hours. The range of concentrations during the winter period was from 4.71 to 43.39 μg/m³ (mean: 25.56 μg/m³), and the range during the spring period was from 11.68 to 30.79 μg/m³ (mean: 22.23 μg/m³) (Marina-Montes et al., 2023). During the winter period, samples registered concentrations that exceeded the mean PM_{10}

concentration (25.56 μg/m^3). These episodes of elevated PM_{10} concentrations were primarily attributable to specific meteorological conditions that prevailed in those days, characterized by low wind speeds (less than 3.3 km/h) and low temperatures. It is important to note that high wind speeds contribute to the renewal of PM_{10} suspended in the air, thereby helping to purify the atmosphere and dispersing the PM_{10} over greater distances (Marina-Montes et al., 2023). During the winter period, a strong correlation was observed between PM_{10} concentration and wind speed. Additionally, a positive relationship was identified between minimum daily temperatures and PM_{10} concentration (r^2 = 0.69; p-value <0.05). This suggests that as wind speed decreases, PM_{10} concentration increases (Marina-Montes et al., 2023). A temperature inversion is a meteorological phenomenon that produces a stratification in the air layers, thereby trapping PM_{10} in the lower atmospheric layers. This phenomenon plays a major role in air quality, especially during winter and in valleys. Consequently, the presence of this meteorological thermal inversion was favored by low temperatures (cool air) recorded during specific days of the study. The annual mean $TWP_{2.5}$ concentration was 1.28 μg/m³, and the order of the $TWP_{2.5}$ concentration was winter > fall > spring > summer (Chae et al., 2024). The $TWP_{2.5}$ concentration in the winter season exhibited a 1.7-fold increase compared to the summer season. The elevated concentrations of $PM_{2.5}$ and $TWP_{2.5}$ during the winter months may be attributable to the increased rigidity of the road surface in comparison to the summer and fall seasons. Tire wear is known to be more pronounced on rigid surfaces compared to soft surfaces. The presence of a significant number of wear particles originating from asphalt pavement and tire tread contributes to the accumulation of particulate matter (PM) on the road. These particles undergo a transformation during the winter months, becoming more rigid and susceptible to fragmentation during vehicular traffic (Chae et al., 2024).

A recent study estimated that, in 2022, 2.2 billion tires were produced around the world, of which 0.42 billion were manufactured in Europe (Giechaskiel et al., 2024). Other sources reported that approximately 1.8 billion tires have been produced on an annual basis since 2017 in an effort to meet global demand (Luo et al., 2021), while approximately 0.324 billion new tires were sold in the EU in 2020. This figure corresponds to approximately 90% of the annual new tire sales average between 2015 and 2019. The reduction in new tire sales in

2020 can be attributed to the impact of the novel Coronavirus COVID-19 on society, which resulted in a decline in the number of kilometers traveled (Giechaskiel et al., 2024). It has been established that TRWPs present on the road surface are subject to compression, resulting in their fragmentation into smaller particulate forms. This transformation occurs in response to mechanical stress exerted upon the primary TRWPs upon their initial contact with tires during vehicular transit. The presence of numerous mineral particles within the TRWP has been shown to expedite the crushing process. This process can lead to the secondary generation of $TRWP_{2.5}$, which is more likely to occur during the colder months due to the increased rigidity of TRWPs on the road surface as the temperature drops (Chae et al., 2024).

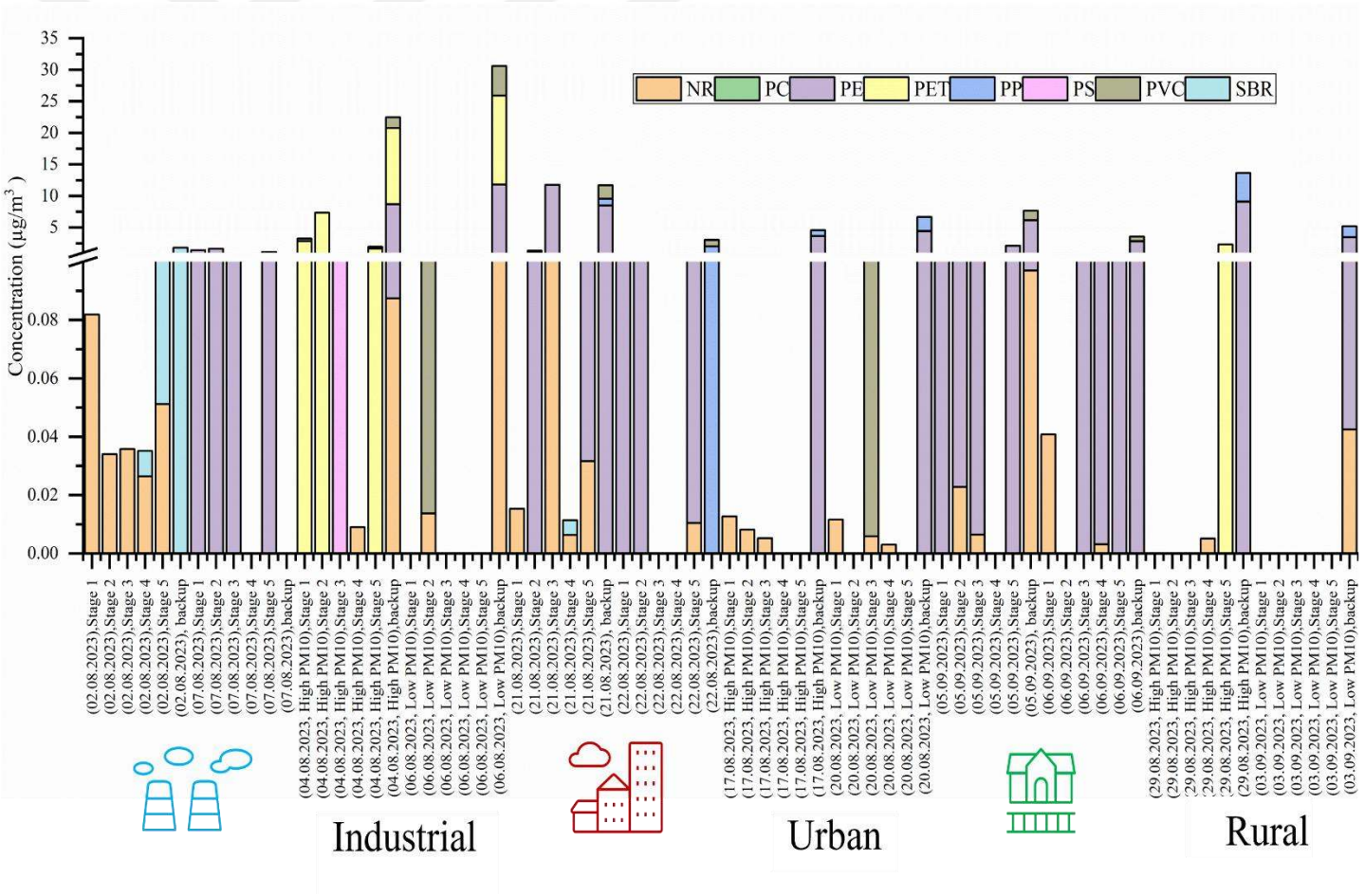

Figure 4.28. *Airborne MNPs mass concentration in three locations based on weather conditions (PM $_{10}$).*

4.2.4. Pyr-GC/MS analysis of nano(micro)plastics

The presence of NPs, defined as nanoscale fragments of plastic, in the atmosphere has been attributed to various sources, including the degradation of larger plastics, industrial activities, and widespread urban practices such as pipe repair techniques. The small size of these particles allows for their inhalation, which raises concerns about potential health risks that are still being elucidated. The concentration and distribution of airborne MNPs in the various sampling locations yielded a range in the industrial area (0.62 to 33.25 μg/m³ with a mean of 12.9±10.6 μg/m³) that was fairly higher than the urban area (0.22 to 18.4 μg/m³ with a mean of 7.6±5.1 μg/m³) and the rural area (0.05 to 28.8 with a mean of 7.4±7.3 μg/m³). The mean MNP levels in both urban and rural regions exhibited a comparable trend; however, a notable disparity was observed in the rural area variation, which manifested as a higher degree of variability. Such variation suggests significant spatial or temporal variability. While rural areas are often perceived as being less polluted than urban areas, they can nevertheless experience localized sources of MNP release. These localized sources include agricultural activities, waste burning, and dispersed settlements which intermittently release MNPs into the atmosphere. Rural environments are more exposed to the influence of long-range atmospheric transport, which can sporadically deliver MNPs from distant urban or industrial sources, leading to fluctuations in measured concentrations. Seasonal changes, such as agricultural activities or varying wind patterns, can cause episodic increases in airborne particulate matter, including MNPs, thereby increasing variability. As indicated in Figure 4.29 and Table B.15, the observed pattern of maximum MNP concentrations was evident on Tuesday in industrial areas, on Monday in urban areas, and on Thursday in rural areas. It is a common occurrence in industrial operations that emissions reach their maximum levels after the weekend. However, these levels may not be attained immediately on Monday. Conversely, the period of maximum activity and associated emissions frequently exhibits a build-up effect, reaching its zenith on Tuesday as factories attain their maximum operational capacity. This delay can be attributed to the time required for machinery to reach a state of steady-state operation and for accumulated emissions to disperse into the atmosphere. Urban environments experience a surge in human activities, traffic, and waste generation at the start of the workweek, leading to an immediate increase in airborne MNP emissions on Monday.

The elevated population density and concentration of sources such as vehicles, construction, and commercial activities contribute to this early-week peak. In rural locations, the maximum in airborne MNP concentrations observed later in the week (Thursday) is likely attributable to atmospheric transport. The presence of MNPs in urban and industrial areas has been demonstrated to be transported by wind over the course of several days, ultimately reaching rural regions. This delay in the arrival of the particles results in the presence of the highest concentrations of particles in rural sites mid- to late-week, as the particles accumulate after being transported from upwind sources. Furthermore, local agricultural activities or sporadic rural sources have the potential to contribute to this timing; however, the predominant factor is generally long-range atmospheric movement and deposition.

Likewise, it was observed that there was an elevated concentration of airborne MNPs in the nanofractions in urban areas on weekends (i.e., Saturday, 12.08.2023, and 19.08.2023). This phenomenon can be attributed to two factors. Firstly, there was a prevalence of leisure activities outside the home during the holiday period. Secondly, there was a typical increase in human activity and traffic in urban regions. In addition, a correlation coefficient of R^2 = 0.64 indicated a moderately strong positive relationship between airborne PM and MNP concentrations. This correlation is indicative of the fact that MNPs frequently coexist with general particulate matter in the atmosphere due to overlapping sources and analogous atmospheric behaviors to the mass concentration of MNPs in the industrial zone and rural region of the atmosphere, which were observed on Tuesday and Wednesday, indications of peak work and production in those regions were also noted. Consequently, a moderate correlation (R^2=0.64) may be postulated between MNPs collected in backup stages and the PM_{10} concentration, (see Table B.15). In this study, of the total 45 nano-fraction samples, MNPs were contributed within 10 days in less than 10% of the PM separately. While MNPs on 11 and 14 of the sampling days contributed 25-50% and finally a mean of 60% of the total PM collected in the backup. A review of the scientific literature indicates significant variability in PM_{10} composition across diverse environmental settings, seasonal variations, and varying sampling methodologies. Research has repeatedly demonstrated that the composition of PM_{10} is contingent on geographical location, prevailing meteorological conditions, and the measurement techniques employed. Research has indicated that organic

carbon comprises between 8% and 50% of PM_{10} mass (Edgerton et al., 2009; Gianini et al., 2013; Gu et al., 2010). In the southeastern United States, the total carbon (OC + EC) composition of PM_{10} was found to be approximately 30% of the total mass (Edgerton et al., 2009). European studies demonstrate that total carbonaceous material constitutes 30 ±9% of PM_{10} at rural background sites (Yttri et al., 2007). Research conducted in China has determined that organic matter contributes 28% of PM_{10} in rural Mediterranean regions (Gómez-Sánchez et al., 2024). This section focuses specifically on the nano-fraction of PM, which differs fundamentally from the composition of bulk PM_{10} (Fang et al., 2005). The extant literature indicates that nanoparticles exhibit distinct compositional profiles in comparison to larger particles. As the size of particles decreases to the nanoscale, the concentration of metallic elements exhibits a decline (Furuuchi et al., 2010). According to the findings of a preceding report, the contribution of tire wear to PM_{10} emissions is estimated to range from 5 to 30% by mass of total non-exhaust traffic-related PM_{10} emissions in urban environments. Furthermore, the phenomenon of brake wear has been demonstrated to contribute a higher percentage, with estimates ranging from 16 to 55% by mass, to total non-exhaust traffic-related PM_{10} emissions in urban environments (Grigoratos and Martini, 2014).

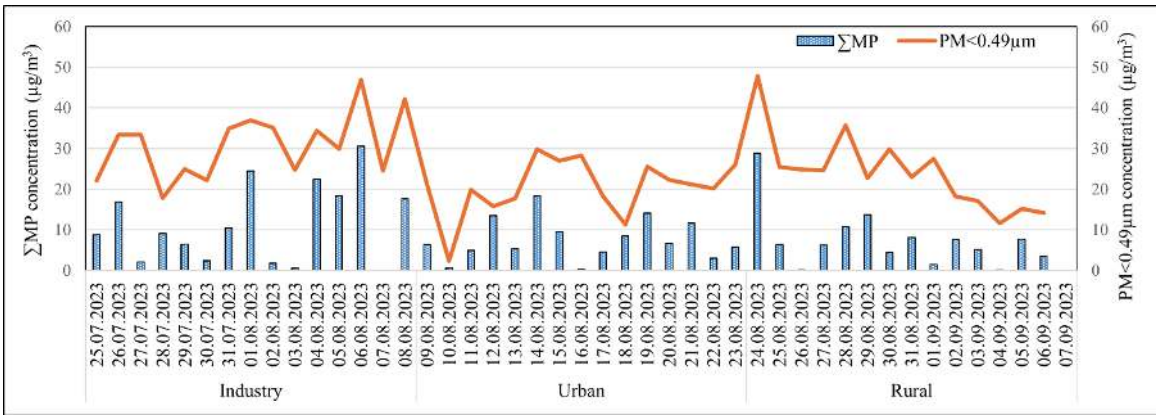

Figure 4.29. *MNPs mass concentration collected in backup stage (nano range particles) at the three locations.*

Furthermore, in the context of mass-based analysis, a random sample of less than 20 µg was cut and analyzed from the backup filter (20 × 25 cm²). This could be attributed to the relatively low concentration of OC in the specific section of the filter. Furthermore, the

discrepancy between MNPs and PM is minimal, frequently resulting in the identification of PET or PC. Given their P2/P1 calibration ratio, it is likely that interference has occurred.

A prior modeling investigation revealed that the mean lifetime of PM_{10} MNPs in the atmosphere was 8.3 days, while that of $PM_{2.5}$ MNPs was as long as 28 days (Evangeliou et al., 2020). This finding indicates a potential correlation between the atmospheric lifetime of MNPs and their physical dimensions. Consequently, it can be hypothesized that the atmospheric longevity (lifetime) of NPs may exceed that of $PM_{2.5}$ MNPs, resulting in continuous inhalation into the human respiratory system through breathing and subsequent translocation to other organs or the blood circulation systems (Leslie et al., 2022). In comparison with the aforementioned findings, our results indicated the presence of comparable or even elevated concentrations of MNPs. This observation is consistent with the prevailing hypothesis that atmospheric concentrations of plastics less than 10 μm in size are increasing, while those exceeding 10 μm are relatively stable. Furthermore, a substantial number of plastics were observed to be less than 1 μm in size in backup stages. Consequently, a more precise evaluation of the prevalence and impact of atmospheric plastics necessitates the quantification of particles below 10 μm in size. Incorporating particles below 10 μm into thermal and spectroscopic analyses is imperative to further refine our understanding of this phenomenon.

Moreover, the distribution of airborne MNPs in rural areas ($p = 0.004 < 0.05$) may not be normal according to the Shapiro-Wilk test, while distributions in industrial ($p = 0.07 > 0.05$), and urban regions ($p = 0.77 > 0.05$) are normal. Urban and industrial regions are characterized by a greater prevalence of consistent and numerous sources of airborne MNPs, including traffic, industrial emissions, and dense human activity. This results in a more homogeneous and continuous input of MNPs, which tends to produce a distribution that approaches normality, particularly when numerous independent sources contribute. Conversely, rural areas are characterized by a paucity of MNPs, with these sources being less frequent and more sporadic in nature. Inputs may be dominated by episodic events, such as wind-blown particles from distant sources or agricultural activities. These events can result in greater variability, skewness, or even the presence of outliers. While the distribution of airborne MNPs in rural areas ($p = 0.004 < 0.05$) is log normal, the distributions in industrial

($p = 0.07 > 0.05$), and urban areas ($p = 0.77 > 0.05$) are normal. Moreover, given the value of p, which was 0.158, this value was greater than 0.05. As a result, it was evident that the independent t-test likely did not identify a significant difference between the mean of MNPs concentration in the industrial and urban regions. This outcome was attributed to the fact that the mean concentrations of airborne MNPs in industrial and urban areas were statistically similar, thereby reflecting the presence of overlapping sources and environmental factors.

A more rigorous evaluation of such results can be achieved by interpreting the data of specific polymers of concern over the sampling points. PE was identified as the most prevalent polymer type in urban (4.99±2.8 μg/m³) and rural (5.97±2.2 μg/m³) environments during 80% and 66% of the sampling days, respectively. The presence of PE in the industrial zone was detected at a rate of 7.89±1.9 μg/m³ in 53% of the samples collected on the day in question. This finding places the concentration and frequency of PE at the third level among other polymers. PE is utilized in the fabrication of cost-effective items, such as plastic bags. Polymer types such as PE are utilized extensively within industrial contexts and, concomitantly, are released into the environment due to the scope of everyday human activities. PP was the second most commonly detected type of MNPs in both urban (3.72±2.8 μg/m³ on 60% of days) and rural (4.66±5.9 μg/m³ on 53% of days) environments. The prevalence of PP was identified in 33% of the sampling days from industrial areas, with a mean concentration of 8.15±4.8 μg/m³ (see Figure 4.30). PP are among the highest-produced plastics, with various applications in diverse industries, encompassing packaging, textiles, and consumer goods. Their pervasive presence in industrial contexts is closely associated with their extensive utilization in manufacturing processes rates. Furthermore, PP finds application in the field of construction, encompassing the fabrication of pipes and the production of insulation materials (Wright et al., 2020). However, PVC was detected on 73% of the sampling days in the industrial zone, with a concentration of 2.41±1.4 μg/m³, while the PVC concentration in the urban area was 1.13±0.6 μg/m³ on 40% of the days and 1.2±0.3 μg/m³ on 33% of the days in the rural area. Products manufactured from PVC, including pipes, flooring, and coatings, are susceptible to degradation when exposed to the environment over time. This degradation process gives rise to the formation of smaller plastic particles, including NPs. The mechanical wear from these products contributes significantly to the

presence of NPs in industrial areas (Joksimovic et al., 2022; Khanna et al., 2024). It seems that, in this context, there was a possibility that NR and SBR, which have a relatively high frequency but low concentration in the three sampling locations, could be indicative of chronic exposure (see Figure 4.30). This phenomenon is predominantly attributable to the following factors: tire wear, road dust accumulation, stormwater runoff, wastewater treatment processes, and improper waste management practices (Rosso et al., 2023b). PET were detected with high concentration (9.8±4.7 μg/m³ and 4.2±1.5 μg/m³) but low frequency (33% and 13%) in industrial and urban atmospheres, respectively, because their higher density and reactivity cause them to settle or degrade faster, leading to sporadic atmospheric presence (Wright et al., 2020). Additionally, it was found in textile manufacturing, plastic production, packaging, and other plastic-processing factories (Lee et al., 2024). PS was detected in only one day in three areas with low concentration (industrial: 0.19 μg/m³, urban: 0.02 μg/m³, rural: 0.002 μg/m³), and sources include degradation of plastic debris in rural waste or agricultural plastic films, though PS is less commonly used in agriculture compared to other polymers (O'Brien et al., 2023). Totally, PC was found in a single day of sampling in the industrial zone, with a concentration recorded at 0.05 μg/m³. PC is a popular material for its benefits, including shatter resistance, making it great for safety glasses, sunglasses, and face shields(Kausar, 2018).

As illustrate in Table 4.2, the frequency and mean concentration of a given polymer detected at each sampling location were documented. The distribution of polymers was conducted with consideration for their respective concentrations, with PET>PE>PP>PVC>SBR>NR>PS>PC. The distribution was further categorized based on frequency, with PE>NR>PP>PVC>SBR>PET>PS>PC. In comparison to the general trend, the frequency and distribution exhibited variation according to polymer types, with a leading polymer of PVC, SBR, and NR, and almost similar order in the industrial zone, respectively. In addition, the sequence of urban and rural trends aligns with that of general trends, with the exception of the frequency of NR in both rural and urban contexts

Table 4.2. *Number of days and means mass concentration of different chemical types of polymers during 15 days in each sampling location.*

Location	Value	Type of polymer (number of day) & (mean concentration (μg/m³))							
		NR	PC	PE	PET	PP	PS	PVC	SBR
Industrial	Frequency (%)	53	6	53	33	33	6	73	60
	Mean	0.15	0.05	7.89	9.87	8.15	0.19	2.49	0.54
	SD	0.07	-	1.92	4.78	4.23	-	1.41	0.58
Urban	Frequency (%)	46.7	-	80	13	60	6	40	33
	Mean	0.07	-	4.99	4.21	3.72	0.02	1.13	0.23
	SD	0.06	-	2.85	1.48	2.89	-	0.64	0.22
Rural	Frequency (%)	60	-	66	-	53	6	33	20
	Mean	0.08	-	5.97	-	4.66	0.002	1.20	0.14
	SD	0.03	-	2.20	-	5.94	-	0.37	0.10

A review of the extant literature indicates that Morioka et al. and Sheng et al. employed low-volume, size-segregated samplers and found 70 ng/m³ in a size range of 0.43–11 μm and 57 to 59 pg/m³ for MP < 1 μm, respectively, using mass-based analysis (Morioka et al., 2024; Sheng et al., 2023). It should be noted that a single study by Ma et al.(Ma et al., 2025) is notable for its use of a high-volume, single-stage sampler to collect urban PM <2.5 μm, which was obtained at a concentration around 960 ng/m³. Furthermore, PE, PET, and PS were identified as the predominant polymer types in the atmosphere of urban areas in three of studies. Guangzhou, China (Ma et al., 2025), with concentrations of 480±17 ng/m³ for PE and 240±25 ng/m³ for PET. In contrast, the most prevalent polymer in Beijing, China (Sheng et al., 2023), was PS at 53 pg/m³. Concurrently, in Kyoto, Japan(Morioka et al., 2024), the principal polymers were identified as PE at 47 ng/m³, PET at 14 ng/m³, and PS at 10 ng/m³. In contrast, the present study employed high-volume size-fractionated samplers with disparate cascade stages, analogous to the human respiratory system, to evaluate the health risk posed by NPs. Therefore, it is imperative to implement a more representative sampling strategy across diverse environmental settings, including industrial, urban, and rural regions. This approach is crucial for mitigating variability and enhancing the statistical reliability of data.

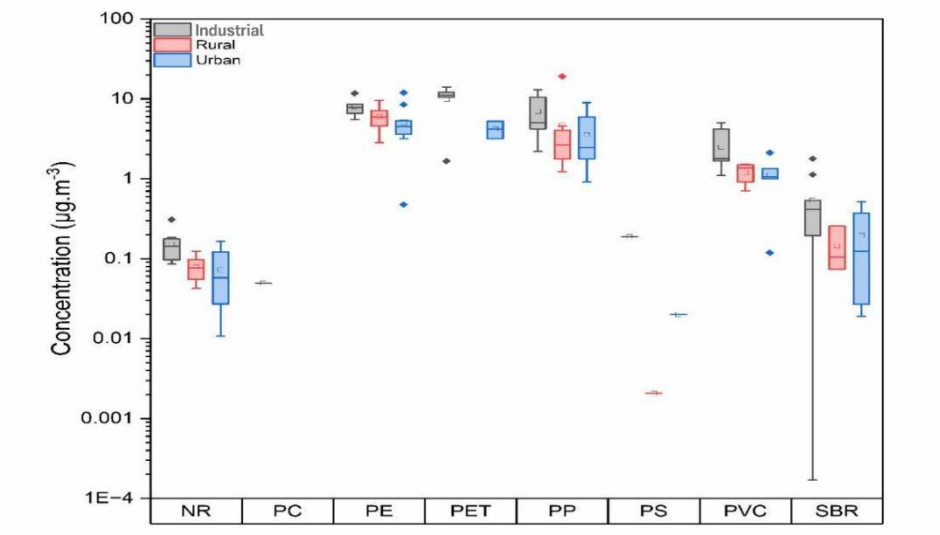

Figure 4.30. *The distribution mass concentration of MNP polymers in three locations. In the box plots, whiskers (error bars) above and below the box indicate the 90th and 10th percentiles, respectively. Outliers are graphed by large dots.*

Evidence suggests that the frequency of polymer use is a more significant factor than the concentration of a given polymer. The high concentration of a particular polymer can be attributable to temporary sources, such as the incineration of tires in urban areas. However, prolonged exposure can lead to chronic adverse effects. A review of the literature indicates that Morioka et al.(Morioka et al., 2024) and Sheng et al.(Sheng et al., 2023) employed low-volume, size-segregated samplers and found 70 ng/m³ in a size range of 0.43–11 µm and 57 to 59 pg/m³ for MP < 1 µm, respectively, using mass-based analysis. It should be noted that a single study by Ma et al.(Ma et al., 2025) is notable for its use of a high-volume, single-stage sampler to collect urban PM <2.5 µm, which was obtained at a concentration around 960 ng/m³. Furthermore, PE, PET, and PS were identified as the predominant polymer types in the atmosphere of urban areas in three of studies. Guangzhou, China(Ma et al., 2025), with concentrations of 480±17 ng/m³ for PE and 240±25 ng/m³ for PET. In contrast, the most prevalent polymer in Beijing, China (Sheng et al., 2023), was PS at 53 pg/m³. Concurrently, in Kyoto, Japan(Morioka et al., 2024), the principal polymers were identified as PE at 47 ng/m³, PET at 14 ng/m³, and PS at 10 ng/m³.

4.3. Exposure Assessment of the Respirable Micro(nano)plastics

4.3.1. Particle-based assessment

The present study employs a multifaceted approach, integrating a range of analytical tools and techniques, to assess the health impact on the exposed population. The study elucidates the fractional deposition of inhaled MPs released during both diurnal and nocturnal periods and its inevitable impact on human health. The present study employs a novel approach to utilize the ICRP model for the calculation of the deposition fraction resulting from prolonged exposure to airborne MPs. Initially, the mean MP diameter for each stage in the day was calculated. Subsequently, the estimated inhalable fraction (IF) and deposition fraction of the head airway (DFHA), tracheobronchial region (DFTB), and alveolar region (DFAR) were determined. Two series tables calculated the deposition fraction of MPs based on the ICRP model in different locations. One series estimated the deposition rate in each day, while two groups of tables showed results in each stage from a day. As demonstrated in all of the tables, particles with the largest diameter had a low inhalable fraction, and most of this group of particles deposited in the head of the human respiratory system and were placed in the low-risk group. Conversely, MNPs with the smallest diameter that had a greater inhalable fraction can penetrate into the deeper respiratory system and may cross vessels and enter the blood system. Despite the finding of the smallest MNPs in the rural area (Table 4.3), the range size of MNPs in the urban area was smaller than in other locations, where a high fraction of deposition in the alveoli was observed. As indicated by the findings presented in Table 4.4, and Table 4.5, the maximum observed diameter of MPs (13.2 μm) was recorded on night (02/08/2023) in the industrial area. Consequently, the deposition fraction in the head airway was determined to be the most significant. Conversely, the smallest diameter MNPs (1 μm) were identified on 22/08/2023 (night) in the urban area, indicating the highest deposition fraction in the alveolar region and the lowest deposition fraction in the head airway. The analysis demonstrated that the deposition of coarser particles occurred in the upper region of the respiratory tract, while finer fractions were inhaled deep into the pulmonary/alveolar region. The head airways were identified as the site for maximum deposition. Of particular interest was the finding that finer particles reached the alveolar region and deposited there.

The presence of airborne MNPs in urban areas poses a heightened inhalation risk in comparison to suburban and industrial regions (Figure 4.31). This elevated risk is attributable to the smaller particle sizes resulting from unique urban emission sources and environmental dynamics. Urban MNPs are predominantly smaller in size (often <10 μm) due to mechanical abrasion from traffic (tire/brake wear), construction activities, and synthetic textile erosion, which generate MNPs (Cao and Cai, 2023; Han et al., 2024; Rednikin et al., 2024). Atmospheric aging was caused by UV radiation and oxidative processes that further break down particles (Cao and Cai, 2023). Furthermore, the presence of hydrophobic surfaces in urban areas has been observed to adsorb air pollutants, such as heavy metals and polycyclic aromatic hydrocarbons (PAHs), which can generate a "toxic cocktail" that contributes to the exacerbation of lung inflammation and oxidative stress (Hossain, 2024).

While exposure to MNPs, for instance, via food intake, can also exert deleterious effects on health, the focal point of this analysis is the role of MNPs as an inhaled toxicant and/or airborne vector for toxicants and pathogens. Although they are significant, existing data regarding the distribution, shape, and size of MNPs in the atmosphere remain disorganized (Gasperi et al., 2018). A multitude of factors have been identified as contributors to the dispersion of MNPs into the atmosphere. These include, but are not limited to, synthetic fabrics from clothing, the deterioration of tires (particularly from automobiles and trucks), household objects, the incineration of waste, building materials, sewage sludge, landfills, abrasive powders, 3D printing, and the resuspension of polymer fragments in urban dust (Amato-Lourenço et al., 2020; Catarino et al., 2018). In urban areas, MNPs such as soil and road dust can accumulate. The presence of polymeric materials with low density in the atmosphere may be attributable to wind and vehicular traffic effects (Abbasi et al., 2019). The presence of MNPs in the atmosphere has been attributed, in part, to automotive wear and tears from car tires, which releases mechanical abrasion-generated particles into the environment (Kole et al., 2017). Synthetic rubber, a hydrocarbon-based polymer, is a constituent of many products, including styrene-1,3-butadiene rubber (SBR). Studies of air pollution frequently report material generated by automotive tire abrasion as a PM constituent (Wright and Kelly, 2017). Tire wear particles mass fraction ranging from 0.8% to 8.5% for PM_{10} and from 1% to 10% for $PM_{2.5}$ (Panko et al., 2019). In the Netherlands, the

estimated annual release of rubber tire wear into the environment is 17,000 tons (Verschoor et al., 2014). In Germany, this emission has been calculated to reach up to 92,594 tons per year. On a global scale, the estimated average per capita emission of tire wear particles is 0.81 kilograms per year (Kole et al., 2017).

The concentration of atmospheric MNP in urban regions has been reported to reach 175 particles/m^3, while indoor concentrations can reach up to 60 particles/m^3 (Y. Zhang et al., 2020) Accordingly, Zhang et al. indicated that inhalation is a significant pathway for human exposure to MNPs, with an estimated burden of (0−3.0) × 107 items per year per person (Q. Zhang et al., 2020). This review explores the role of MNPs as an emerging airborne pollutant, emphasizing the potential consequences of inhaled MNPs on human health. As humans typically take between ten and twenty breaths per minute while at rest, airborne MP particles are readily inhaled and enter the body via the respiratory system (Akhbarizadeh et al., 2021). Once inhaled, MNPs can trigger a series of detrimental reactions within the respiratory system that can lead to various health complications. These toxic effects manifest primarily as an increase in oxidative stress levels, as well as apoptosis, the process through which cells die, and the subsequent development of pulmonary fibrosis, or the formation of scar tissue in the lungs (Liu and You, 2023). The extent of the impact that MNPs have on bodily functions is influenced by a multitude of factors, including the size, burden, density, and charge of the particles, as well as the specific type of MNP and characteristics of the individual.

The first to characterize the presence of MNPs in human lung tissues procured during autopsies, as documented by Amato-Lourenço et al (2021). Of the 20 tissue samples examined, 13 contained synthetic polymer particles measuring between 1.60 and 5.56 micrometers in diameter, along with fibers ranging from 8.12 to 16.8 micrometers. The most prevalent particles identified were PP and PE. It must be acknowledged that the number of sample cases studied is limited, precluding the identification of reliable associations or the elucidation of potential adverse health effects associated with these compounds (Amato-Lourenço et al., 2021). In contrast, Baeza-Martinez et al. (2022) examined the presence of MPs in the lower human airways using bronchoalveolar lavage fluid (i.e., BALF). The study's findings suggest that the BALF samples were contaminated with an average microfiber

concentration of 9.18 ± 2.45 items 100 mL^{-1} BALF and with an average size of 1.73 ± 0.15 mm.

Table 4.3 *Deposition fraction of MNPs in different human respiratory system regions, based on the ICRP Model in the three sampling locations and two seasons.*

	Date	Dpi (mean) (µm)	IF	DFHA	DFTB	DFAR
Industrial	Day (02.08.2023)	3.56	0.987045	0.8027	0.0575	0.0829
	Night (02.08.2023)	**6.92**	**0.926969**	**0.8699**	**0.0298**	**0.0366**
	Day (07.08.2023)	2.82	0.993169	0.7322	**0.0610**	**0.0998**
	Night (07.08.2023)	3.94	0.982936	0.8262	0.0545	0.0752
	Day (04.08.2023)	2.86	0.992898	0.7371	0.0609	0.0989
	Day (06.08.2023)	2.82	0.993169	0.7322	0.0575	**0.0998**
Urban	Day (21.08.2023)	3.22	0.990115	0.7755	0.0596	0.0903
	Night (21.08.2023	3.02	0.991748	0.7552	0.0605	0.0950
	Day (22.08.2023)	3.4	0.988574	0.7906	0.0586	0.0863
	Night (22.08.2023	2.9	0.99262	0.7418	0.0608	0.0979
	Day (17.08.2023)	3.32	0.989295	0.7839	0.0590	0.0881
	Day (20.08.2023)	3.14	0.990814	0.7675	0.0600	0.0922
Rural (summer)	Day (05.09.2023)	3.4	0.988574	0.7906	0.0586	0.0863
	Night (05.09.2023)	3.26	0.989817	0.7787	0.0594	0.0895
	Day (06.09.2023)	**2.34**	**0.995926**	**0.6611**	0.0599	0.1116
	Night (06.09.2023)	3.92	0.983169	0.8251	0.0547	0.0756
	Day (29.08.2023)	3.56	0.987045	0.8027	0.0575	0.0829
	Day (03.09.2023)	2.94	0.992336	0.7464	0.0607	0.0969
Rural (winter)	Day (01.01.2024)	3.32	0.989295	0.7839	0.0590	0.0881
	Night (01.01.2024)	2.4	0.995629	0.6714	0.0603	0.1101

* **Bold red** indicates the highest deposition fraction among the three sampling locations, while **bold blue** indicates the lowest deposition fraction. Red and blue normal font show low and high the deposition fraction for each sampling location individually.

In health risk assessment, both the concentration and size of MNP particles are critical parameters. However, evidence suggests that particle size may be the more critical factor in determining potential health impacts. This is primarily due to the direct influence of particle

size on respiratory penetration depth, deposition patterns, clearance mechanisms, and ultimately, the biological interactions that determine toxicity. The deposition patterns of MNPs in the respiratory system exhibit significant variation based on the size of the particles. Different physical mechanisms predominate at varying size ranges. In a particular study, Islam et al. demonstrated that cylindrical MNPs with diameters of 2.56 and 5.56 µm exhibit higher deposition rates in lung airways than smaller particles of 1.6 µm at lower flow rates (Islam et al., 2023). The present study posited that the MNPs in the range of 2.7 to 5.9 were a potential indicator of deposition in the head and airway of the human respiratory system (Table 4.5). The physical mechanisms governing particle deposition, which include inertial impaction, gravitational sedimentation, and Brownian diffusion, are all size-dependent. At lower flow rates, Brownian diffusion becomes more pronounced for particles of a smaller magnitude. Conversely, as flow rates increase, this diffusion diminishes. These complex interactions between particle size and respiratory physiology give rise to size-specific deposition profiles. These profiles are more deterministic of health risk than concentration alone (Saha and Saha, 2024).

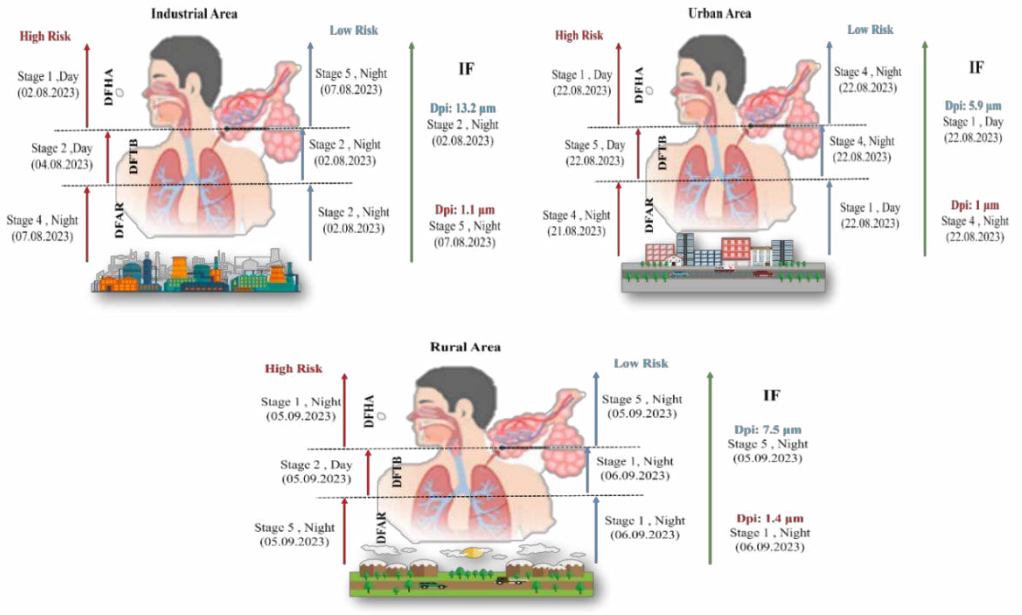

Figure 4.31. *Exposure assessment of MNPs according to particle-based analysis method in different sampling locations.*

It has been demonstrated that MNP particles, despite their minute size, demonstrate the capacity to traverse biological barriers and infiltrate the circulatory system, with the potential to disseminate to other organs. This capacity to translocate is predominantly governed by the physical dimensions of the particles rather than by their concentration. Once incorporated into the circulatory system, these MNPs can potentially trigger a range of health concerns, including cardiovascular and cerebrovascular diseases, cancer, and immune system dysfunction (Marfella et al., 2024). In comparison to larger particles, which are predominantly constrained within the respiratory system irrespective of their concentration, the systemic spread of MNPs signifies a markedly divergent risk profile. Recent advances in computational modeling have enhanced our understanding of how MNP size influences deposition patterns and potential health implications. These models were collected and discussed by (Saha and Saha, 2024), allow for the exploration of particle dynamics, deposition patterns, and interaction mechanisms at various levels of complexity. They can simulate the movement of particles of different sizes through the complex branching structure of human airways under various breathing conditions. However, there are significant challenges associated with the accuracy of computational modeling of MNP effects related to the representation of size distributions. The intricacy of the respiratory system's anatomy and the variability in physiological processes demand precise modeling. Additionally, the heterogeneity of MNPs, encompassing variations in size, shape, and chemical composition, poses challenges in capturing their comprehensive behaviors. Consequently, size parameters often prove to be more deterministic indicators of health risks than simple concentration measurements in risk assessments. Likewise, the dimensions of airborne MNPs are typically diminished during nocturnal hours, particularly during winter months, in comparison to the diurnal period. This phenomenon can be attributed to the reduced human activity and diminished environmental turbulence that characterize these periods. Consequently, the deposition rate within the alveolar respiratory system during nocturnal sampling was found to be higher than that observed in daytime samples. This observation carries significant implications for the potential harmfulness of these particles (Figure 4.31).

Table 4.4. *Deposition fraction of industrial MNPs in different human respiratory system regions, based on the ICRP Model.*

Date	Stage	Dpi (mean) (um)	IF	DFHA	DFTB	DFAR	MNPs Concentration (MP/m^3)	Date	Stage	Dpi (mean) (µm)	IF	DFHA	DFTB	DFAR	MNPs Concentration (MP/m^3)
Day (02.08.2023)	1	**6.1**	0.946367	0.8737	0.0357	0.0441	773	Night (07.08.2023)	1	**7.5**	0.911766	0.8631	0.0262	0.0322	1160
	2	**3.6**	0.986644	0.8055	0.0572	0.0820	2685		2	**6.2**	0.944148	0.8736	0.0349	0.0431	2148
	3	**3**	0.991897	0.7531	0.0605	0.0955	1627		3	**3.6**	0.986644	0.8055	0.0572	0.0820	2236
	4	**3.9**	0.9834	0.8240	0.0548	0.0760	1114		4	**1.3**	0.999209	0.3947	0.0392	0.1274	1810
	5	**1.2**	0.999368	0.3595	0.0355	0.1265	1768		5	1.1	0.999504	0.3229	0.0314	0.1247	4420
Night (02.08.2023)	1	**9.8**	0.844079	0.8163	0.0158	0.0201	773	Day (04.08.2023)	1	**4.5**	0.975618	0.8501	0.0495	0.0652	2514
	2	**13.2**	**0.744699**	0.7305	0.0079	0.0110	537		2	**2.8**	0.993302	0.7298	0.0610	0.1003	3491
	3	**8.6**	0.880417	0.8437	0.0206	0.0255	1627		3	**2**	0.997367	0.5934	0.0565	0.1194	1017
	4	**1.9**	0.997718	0.5702	0.0550	0.1215	1392		4	**2.7**	0.993942	0.7167	0.0610	0.1028	1949
	5	1.1	0.999504	0.3229	0.0314	0.1247	2652		5	**2.3**	0.996116	0.6540	0.0597	0.1126	7072
Day (07.08.2023)	1	**3.9**	0.9834	0.8240	0.0548	0.0760	1740	Day (06.08.2023)	1	**3.9**	0.9834	0.8240	0.0548	0.0760	1740
	2	**3.2**	0.990324	0.7732	0.0597	0.0908	1880		2	**2.9**	0.99262	0.7418	0.0608	0.0979	2685
	3	**2.9**	0.99262	0.7418	0.0608	0.0979	2440		3	**2.5**	0.995105	0.6876	0.0607	0.1077	1627
	4	**2**	0.997367	0.5934	0.0565	0.1194	1810		4	**2.1**	0.996984	0.6150	0.0578	0.1172	2228
	5	**2.1**	0.996984	0.6150	0.0578	0.1172	7514		5	**2.7**	0.993942	0.7167	0.0610	0.1028	6630

* **Bold red** indicates the highest deposition fraction among the three sampling locations, while **bold blue** indicates the lowest deposition fraction. Red and blue normal font show low and high the deposition fraction for each sampling location individually.

Table 4.5. *Deposition fraction of urban MNPs in different human respiratory system regions, based on the ICRP Model.*

Date	Stage	Dp(mean) (µm)	IF	DFHA	DFTB	DFAR	MNPs Concentration (MP/m³)	Date	Stage	Dp(mean) (µm)	IF	DFHA	DFTB	DFAR	MNPs Concentration (MP/m³)
Day (21.08.2023)	1	**4.6**	0.974151	0.8533	0.0486	0.0636	1552	Night (22.08.2023)	1	**5.8**	0.952763	0.8729	0.0381	0.0474	1707
	2	**3**	0.991897	0.7531	0.0605	0.0955	2801		2	**4.9**	0.969454	0.8612	0.0459	0.0590	1077
	3	**1.8**	0.998037	0.5453	0.0531	0.1233	1958		3	**1.5**	0.99882	0.4603	0.0458	0.1272	1142
	4	**3.5**	0.987632	0.7983	0.0579	0.0841	1341		4	**1**	**0.99962**	0.2851	0.0272	0.1217	670
	5	**2.3**	0.996116	0.6540	0.0597	0.1126	3192		5	**1.3**	0.999209	0.3947	0.0392	0.1274	1419
Night (21.08.2023)	1	**5.3**	0.962511	0.8683	0.0423	0.0534	1241	Day (17.08.2023)	1	**5.5**	0.958752	0.8707	0.0406	0.0509	2327
	2	**3.4**	0.988574	0.7906	0.0586	0.0863	1724		2	**3.9**	0.9834	0.8240	0.0548	0.0760	1939
	3	**2.7**	0.993942	0.7167	0.0610	0.1028	1305		3	**2.1**	0.996984	0.6150	0.0578	0.1172	2427
	4	**1.4**	0.999027	0.4284	0.0427	0.1276	894		4	**2.8**	0.993302	0.7298	0.0610	0.1003	782
	5	**2.3**	0.996116	0.6540	0.0597	0.1126	2128		5	**2.3**	0.996116	0.6540	0.0597	0.1126	2837
Day (22.08.2023)	1	**5.9**	0.950675	0.8733	0.0373	0.0462	1552	Day (20.08.2023)	1	**4.4**	0.977037	0.8466	0.0504	0.0669	1552
	2	**2.9**	0.99262	0.7418	0.0608	0.0979	3016		2	**4**	0.982224	0.8293	0.0540	0.0740	3016
	3	**2.5**	0.995105	0.6876	0.0607	0.1077	2610		3	**2.2**	0.996568	0.6352	0.0589	0.1149	2447
	4	**3**	0.991897	0.7531	0.0605	0.0955	1787		4	**2.7**	0.993942	0.7167	0.0610	0.1028	1899
	5	**2.7**	0.993942	0.7167	0.0610	0.1028	6384		5	**2.4**	0.995629	0.6714	0.0603	0.1101	4610

***Bold red** indicates the highest deposition fraction among the three sampling locations, while **bold blue** indicates the lowest deposition fraction. Red and blue normal font show low and high the deposition fraction for each sampling location individually.

Table 4.6. *Deposition fraction of rural MNPs in different human respiratory system regions, based on the ICRP Model (summer and winter).*

Date	Stage	Dp(mean) (µm)	IF	DFHA	DFTB	DFAR	MNPs Concentration (MP/m³)	Date	Stage	Dp(mean) (µm)	IF	DFHA	DFTB	DFAR	MNPs Concentration (MP/m³)
Day (05.09.2023)	1	**4.8**	0.971068	0.8588	0.0468	0.0605	1552	Night (06.09.2023)	1	**7.5**	0.911766	0.8631	0.0262	0.0322	465
	2	**2.6**	0.994543	0.7027	0.0609	0.1052	1939		2	**2.4**	0.995629	0.6714	0.0603	0.1101	2370
	3	**3.2**	0.990324	0.7732	0.0597	0.0908	1794		3	**5.5**	0.958752	0.8707	0.0406	0.0509	1794
	4	**2.3**	0.996116	0.6540	0.0597	0.1126	1117		4	**2.1**	0.996984	0.6150	0.0578	0.1172	894
	5	**4.1**	0.981	0.8342	0.0531	0.0722	2128		5	**2.1**	0.996984	0.6150	0.0578	0.1172	2837
Night (05.09.2023)	1	**5.9**	0.950675	0.8733	0.0373	0.0462	1552	Day (29.08.2023)	1	**5.3**	0.962511	0.8683	0.0423	0.0534	1552
	2	**4.9**	0.969454	0.8612	0.0459	0.0590	1724		2	**4.3**	0.978407	0.8428	0.0513	0.0686	3447
	3	**2.5**	0.995105	0.6876	0.0607	0.1077	1631		3	**2.9**	0.99262	0.7418	0.0608	0.0979	2121
	4	**1.6**	0.998587	0.4904	0.0486	0.1263	1005		4	**3.1**	0.991132	0.7635	0.0602	0.0931	2011
	5	**1.4**	0.999027	0.4284	0.0427	0.1276	1064		5	**2.2**	0.996568	0.6352	0.0589	0.1149	3546
Day (06.09.2023)	1	**3.7**	0.98561	0.8122	0.0564	0.0799	931	Day (03.09.2023)	1	**3.4**	0.988574	0.7906	0.0586	0.0863	931
	2	**2**	0.997367	0.5934	0.0565	0.1194	2154		2	**3.6**	0.986644	0.8055	0.0572	0.0820	2801
	3	**1.7**	0.998327	0.5188	0.0510	0.1250	2121		3	**3**	0.991897	0.7531	0.0605	0.0955	2936
	4	**2.4**	0.995629	0.6714	0.0603	0.1101	1341		4	**2.4**	0.995629	0.6714	0.0603	0.1101	1787
	5	**1.9**	0.997718	0.5702	0.0550	0.1215	4610		5	**2.3**	0.996116	0.6540	0.0597	0.1126	3546
Day-winter (01.01.2024)	1	**6.1**	0.946367	0.8737	0.0357	0.0441	1862	Night-winter (01.01.2024)	1	3.4	0.988574	0.7906	0.0586	0.0863	1086
	2	3.8	0.984529	0.8183	0.0556	0.0779	1939		2	2.7	0.993942	0.7167	0.0610	0.1028	2585
	3	3.3	0.989471	0.7822	0.0592	0.0886	2610		3	2.6	0.994543	0.7027	0.0609	0.1052	1958
	4	1.9	0.997718	0.5702	0.0550	0.1215	1452		4	**1.4**	0.999027	0.4284	0.0427	0.1276	1452
	5	1.5	0.99882	0.4603	0.0458	0.1272	2482		5	1.9	0.997718	0.5702	0.0550	0.1215	4256

***Bold red** indicates the highest deposition fraction among the three sampling locations, while **bold blue** indicates the lowest deposition fraction. Red and blue normal font show low and high the deposition fraction for each sampling location individually.

4.3.2. Mass-based assessment

4.3.2.1. Risk level of micro(nano)plastics

The assessment of airborne MNPs necessitates the implementation of sophisticated sampling and analytical methodologies. The employment of techniques such as Pyr-GC/MS is imperative for the quantification of mass concentrations, while microscopic methods assume significant importance in the characterization of particle morphology, particularly the size of MNPs. Nevertheless, the standardization of these methodologies remains deficient, impeding the comparability of risk assessments across disparate studies. The incorporation of mass concentration methods can serve as a valuable adjunct to risk assessment of airborne MNPs, informed by particle-based analysis. However, risk assessment frameworks that prioritize concentration metrics (whether mass-based or count-based) exhibit several inherent limitations when applied to MNPs. To date, there is an absence of a risk assessment framework that incorporates the multidimensionality of MNP particles within the context of the broader spectrum of naturally occurring particles. This lacuna poses a substantial challenge for regulatory bodies seeking to establish safety standards (Koelmans et al., 2022).

According to the Chemical Abstracts Service Registry Number 1333-86-4-Environment Notwithstanding the results of the mass concentration analysis, which demonstrated the presence of different types of polymers, it is important to note that there is currently no reference concentration (RfC) available for various polymers. The spectrometric analysis revealed the presence of carbon black particles in the majority of MNP particles, and rubber and tires were identified as their source. According to Kreider et al. (2019), TRWP demonstrated a minimal risk to human health, substantiated by the absence of an observed adverse effect concentration (NOAEC) for respirable TRWP at a concentration of 55 $\mu g/m^3$ and the estimated daily exposure range to TRWP ranging from 0.079 $\mu g/m^3$ to 0.147 $\mu g/m^3$ (Kreider et al., 2020). Furthermore, the mass concentration methods SBR and NR corroborated that MP particles generated from rubber and tire sources were selected polymers in MNPs risk assessment based on the mass analysis method, and carbon black was found by particle-based analysis, indicating the amount of tire in the atmosphere. Regarding the amount of carbon black, SBR and NR were found from different methods that demonstrated tire wear concentration in the atmosphere. Consequently, SBR and NR can be considered representative

of carbon black in microscopic analysis. By using SBR and NR concentration and carbon black RfC, the risk level of airborne MNPs can be calculated. A review of the available literature indicates that the search results do not provide specific data on SBR and NR airborne MNP concentrations or their specific respiratory effects. However, tire wear is explicitly mentioned as a significant source of airborne MNPs, suggesting that SBR from tires may contribute substantially to environmental and respiratory exposure. Given the pervasive utilization of SBR in tires and associated products, coupled with the inherent presence of NR in numerous applications, there is a compelling rationale for targeted research endeavors to elucidate their distinct respiratory implications (Saha and Saha, 2024). The research community has acknowledged this subject as a matter of paramount importance, underscoring the urgency and the dynamic nature of this research domain.

Consequently, the level of risk was estimated on different days of sampling and locations. If the results of HQ placed between 0 and 0.1 are negligible (green), if risk between 0.1 and 1 is low risk (yellow), if risk results placed between 1 and 10 are moderate (orange), and if larger than 10 is high risk (red), then the level of risk can be determined (Table 4.7).

It is imperative to acknowledge the limitations of this risk assessment, which pertains exclusively to SBR and NR concentrations in MNPs derived from tire and traffic-related sources. This assessment excludes other polymer types for which no reference concentrations have been established to date. Consequently, the identified risk level is confined to MNPs originating from tires and traffic. On Monday, Thursday, and Wednesday, moderate risk levels were identified in the three sampling locations, coinciding with periods of increased traffic activity. Furthermore, the presence of moderate risk in the industrial zone during daytime hours can potentially be caused by a surge in production during work hours. Conversely, a moderate risk of MNPs was observed in urban and rural locations during nighttime hours, which corresponds with the period of peak traffic activity and accumulation of MNPs at night.

Table 4.7. *Assessment exposure risk of MNPs according to mass-based analysis method in different sampling locations.*

Location	Date	Stages	Type of polymer (µg/m^3)		Total (NR+SBR) (µg/m^3)	HQ Level	Date	Stages	Type of polymer (µg/m^3)		Total (NR+SBR) (µg/m^3)	HQ level
			NR	SBR					NR	SBR		
Industrial	02.08.2023 (Day)	Stage 1	0.08189		0.08189	0.15	07.08.2023 (Day)	Stage 1	-	-	-	-
		Stage 2	0.03398		0.03398	0.06		Stage 2	-	-	-	-
		Stage 3	0.03574		0.03574	0.06		Stage 3	-	-	-	-
		Stage 4	0.02640	0.00868	0.03508	0.06		Stage 4	-	-	-	-
		Stage 5	0.05118	0.29167	0.34284	0.62		Stage 5	-	-	-	-
		Backup		1.78887	1.78887	3.25		Backup	-	-	-	-
	02.08.2023 (Night)	Stage 1	0.05651		0.05651	0.11	07.08.2023 (Night)	Stage 1	-	-	-	
		Stage 2	-	-	-			Stage 2	-	-	-	
		Stage 3	-	-	-			Stage 3	-	-	-	
		Stage 4	-	-	-			Stage 4	0.00592		0.00592	0.01
		Stage 5		0.04001	0.04001	0.07		Stage 5	0.56745		0.56745	1.03
		Backup		0.53801	0.53801	0.98		Backup	0.06928	0.09801	0.16728	0.30
	04.08.2023 (Day)	Stage 1		0.00004	0.00004	0.001	06.08.2023 (Day)	Stage 1	-	-	-	
		Stage 2	-	-	-			Stage 2	0.0137		0.01366	0.02
		Stage 3		0.00010	0.00010	0.001		Stage 3	-	-	-	
		Stage 4	0.0090		0.00904	0.02		Stage 4	-	-	-	
		Stage 5	-	-	-			Stage 5		0.00003	0.00003	0.00005
		Backup	0.0875	0.00017	0.08765	0.16		Backup	0.1055		0.10545	0.19
Urban	21.08.2023 (Day)	Stage 1	0.01531		0.01531	0.03	22.08.2023 (Day)	Stage 1	-	-	-	-
		Stage 2	-	-	-	-		Stage 2	-	-	-	-
		Stage 3	0.21303		0.21303	0.39		Stage 3	-	-	-	-
		Stage 4	0.00631	0.00507	0.01138	0.02		Stage 4	-	-	-	-
		Stage 5	0.03165		0.03165	0.06		Stage 5	0.01049		0.01049	0.02
		Backup		0.02842	0.02842	0.05		Backup		0.02694	0.02694	0.05
	21.08.2023 (Night)	Stage 1	0.01362		0.01362	0.02	22.08.2023 (Night)	Stage 1				
		Stage 2	-	-	-			Stage 2				
		Stage 3	-	-	-			Stage 3		0.00180	0.00180	0.003
		Stage 4	0.01335		0.01335	0.02		Stage 4	-	-	-	-
		Stage 5	-	-	-			Stage 5	-	-	-	-
		Backup	0.40510	1.13849	1.54359	2.81		Backup	-	-	-	-

Table 4.7. (Continued) *Assessment exposure risk of MNPs according to mass-based analysis method in different sampling locations.*

Location	Date	Stages	Type of polymer (µg/m^3)		Total (NR+SBR) (µg/m^3)	HQ Level	Date	Stages	Type of polymer (µg/m^3)		Total (NR+SBR) (µg/m^3)	HQ Level
			NR	SBR					NR	SBR		
Urban	17.08.2023 (Day)	Stage 1	0.0127		0.01266	0.02	20.08.2023 (Day)	Stage 1	0.0116		0.01156	0.02
		Stage 2	0.0081		0.00812	0.01		Stage 2				
		Stage 3	0.0052		0.00517	0.01		Stage 3	0.0059		0.00593	0.01
		Stage 4	-	-	-	-		Stage 4	0.0030		0.00297	0.01
		Stage 5	-	-	-	-		Stage 5	-	-	-	-
		Backup	-	-	-	-		Backup	-	-	-	-
Rurak (summer)	05.09.2023 (Day)	Stage 1	-	-	-	-	06.09.2023 (Day)	Stage 1	0.04077		0.04077	0.07
		Stage 2	0.02287		0.02287	0.04		Stage 2				
		Stage 3	0.00650		0.00650	0.01		Stage 3				
		Stage 4	-	-	-	-		Stage 4	0.00314		0.00314	0.01
		Stage 5	-	-	-	-		Stage 5	-	-	-	-
		Backup	0.09696		0.09696	0.18		Backup	-	-	-	-
	05.09.2023 (Night)	Stage 1		0.67178	0.67178	1.22	06.09.2023 (Night)	Stage 1	0.00376		0.00376	0.01
		Stage 2	0.01448	1.97794	1.99242	3.62		Stage 2	0.00848		0.00848	0.01
		Stage 3		1.71340	1.71340	3.12		Stage 3	0.00332		0.00332	0.02
		Stage 4		0.30415	0.30415	0.55		Stage 4	0.00457		0.00457	0.01
		Stage 5	0.02146	2.55306	2.57452	4.68		Stage 5	0.00340		0.00340	0.01
		Backup	0.03198		0.03198	0.06		Backup	0.00376		0.00376	0.0001
	29.08.2023 (Day)	Stage 1	-	-	-	-	03.09.2023 (Day)	Stage 1	0.00001		0.00001	0.000003
		Stage 2	-	-	-	-		Stage 2	-	-	-	-
		Stage 3	-	-	-	-		Stage 3	-	-	-	-
		Stage 4	0.0051		0.00509	0.002		Stage 4	-	-	-	-
		Stage 5	-	-	-	-		Stage 5	-	-	-	-
		Backup	-	-	-	-		Backup	0.0426		0.04259	0.01

Table 4.7. (Continued) *Assessment exposure risk of MNPs according to mass-based analysis method in different sampling locations.*

Location	Date	Stages	Type of polymer (µg/m^3)		Total (NR+SBR) (µg/m^3)	HQ Level	Date	Stages	Type of polymer (µg/m^3)		Total (NR+SBR) (µg/m^3)	HQ Level
			NR	SBR					NR	SBR		
Rural (winter)	01.01.2024 (Day)	Stage 1	0.01721		0.01721	0.03	01.01.2024 (Night)	Stage 1		0.24001	0.24001	0.44
		Stage 2		1.81159	1.81159	3.29		Stage 2	-	-	-	-
		Stage 3	0.01671		0.01671	0.03		Stage 3	0.01105	0.15571	0.16675	0.30
		Stage 4	-	-	-	-		Stage 4	0.01209		0.01209	0.02
		Stage 5	0.02355	0.68595	0.70951	1.29		Stage 5	0.02036	1.17459	1.19495	2.17
		Backup		10.64041	10.64041	19.35		Backup	-	-	-	-

Another important limitation of concentration-based assessments is the potential mismatch between exposure and effect metrics. This mismatch is further exacerbated by variability in the mechanisms of damage caused by MNPs depending on their size characteristics. The effects observed may be influenced by factors other than the particle count, such as mass concentration, surface area, or volume. Consequently, without considering these metrics and their relationship to particle size, risk assessments may fail to capture the full exposure-effect relationship. Research findings demonstrate an inherent discordance between mass and count concentrations, where a sample with high mass concentration might exhibit relatively low particle counts due to the predominance of larger particles. This incongruity emphasizes the limitations of relying on a solitary concentration metric devoid of size characterization (Koelmans et al., 2022). Although size is a critical factor, a comprehensive risk assessment must also consider other characteristics of particles, such as polymer type and shape. It is well established that different polymers may have different toxicity profiles, and the shape of particles can influence both environmental fate and biological interactions.

In the context of risk assessment, SBR and NR mass-based analysis has revealed that the majority of moderate and high-risk levels are observed in rural regions during nighttime hours, particularly during winter months (Figure 4.32 , Table 4.7). This phenomenon can be attributed to the occurrence of temperature inversions in these areas. Temperature inversions occur when a layer of cooler air is trapped near the ground by a warmer layer situated above. This stable atmospheric condition impedes vertical mixing, leading to the accumulation of airborne particles, including MNPs, near the surface. Additionally, canopy effects must be considered. In forested or vegetated rural areas, the canopy can trap airborne particles through a "comb-out effect," thereby further concentrating MNPs near the ground (Klein et al., 2023).

Additionally, truck traffic at night in rural areas and the use of icebreaker rubber in winter contribute to the accumulation of MNPs (SBR and NR). Overall, icebreaker operations not only generate MNPs through direct mechanical processes but also facilitate their release from seasonal ice, thereby amplifying their presence in the atmosphere. It is well-documented that both SBR and NR particles have the capacity to leach chemicals, thereby potentially resulting in deleterious effects across a broad array of habitats and species. Their

environmental ramifications, while not yet fully elucidated, have been posited to potentially pose significant health risks, particularly to humans; however, there is a paucity of empirical studies that specifically investigate this matter (Halsband et al., 2024). Previous epidemiological investigations have underscored the potential health implications associated with occupational exposure to SBR, particularly in regard to an elevated risk of leukemia and other hematopoietic malignancies among professionals within the SBR industrial (Meinhardt et al., 1978).

Eventually, the inhalation of high concentrations of each chemical type of MNPs has the potential to induce acute physiological effects in human subjects. Currently, there is an absence of standard criteria for defining exposure concentration levels and time-integrated exposure thresholds for polymer particles present within the atmosphere. Nonetheless, it has been demonstrated that the inhalation of these particles over a prolonged timeframe can result in the onset of chronic diseases.

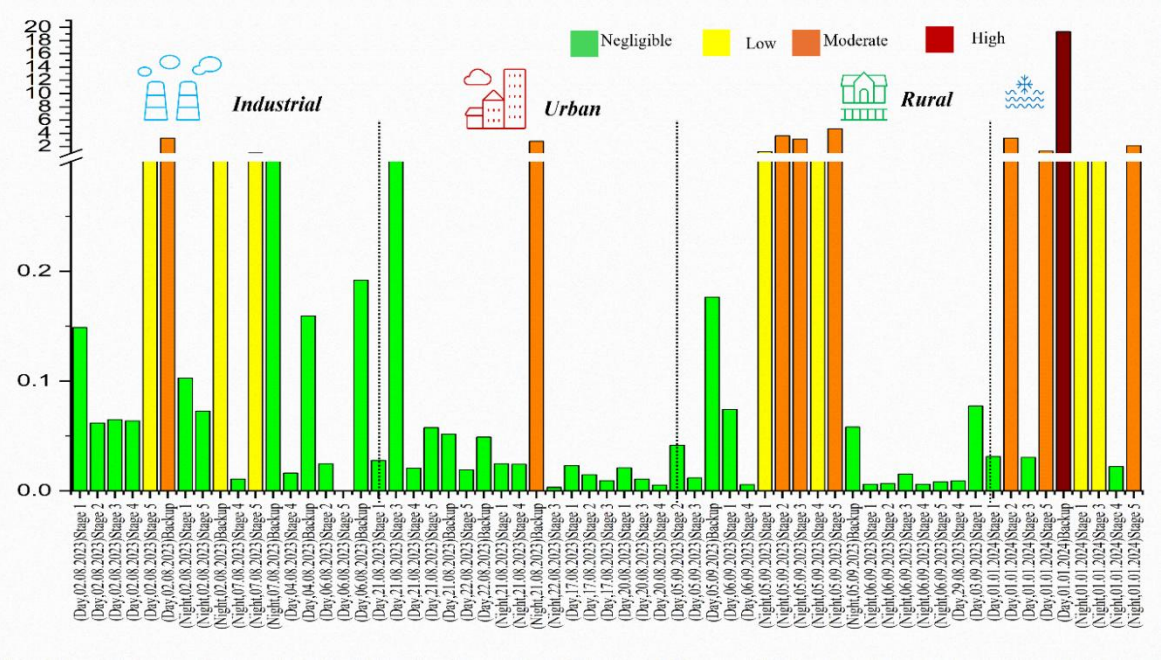

Figure 4.32. *Assessment of temporal and spatial exposure risk of MNPs (SBR and NR) according to mass-based analysis method.*

4.3.2.2. Risk level of nano(micro)plastics

As illustrated in Figure 4.33, SBR and NR have been observed to be present in substantial concentrations across all locations, attributable to their pervasive sources and enduring release mechanisms. However, airborne MNPs derived from SBR and NR pose significantly higher risks in industrial areas compared to urban and rural regions (Figure 4.33, Table S11). This discrepancy can be attributed to three factors: concentrated emission sources, unique physicochemical properties of rubber particles, and heightened exposure pathways in industrial settings. Industrial zones have been shown to have 2.5 times higher concentrations of tire and road wear particles (Youn et al., 2021) in road dust compared to residential areas. This is due to the enhanced mobility and toxicity of airborne NR and SBR-MNPs resulting from additive leaching. NR is an integral component of tires, contributing to their structural integrity and functionality. Tire wear, particularly in areas with high traffic density, characteristic of industrial zones, and during the week (especially Monday and Tuesday, Figure 4.33), results in the release of tire wear particles into the environment that contain the aforementioned polymers. Moreover, the industrial region was situated in the eastern part of Eskişehir, where predominant winds blew from west to east, thereby facilitating the transportation of NPs and their subsequent accumulation within the industrial area. In addition, the closure of the industrial area with landfills and the storage of old tires, as well as the establishment of tire recycling centers, has the potential to increase exposure to SBR and NR polymers in this region. This is due to the fact that tire wear is a ubiquitous and persistent source of these polymers, largely independent of specific local activities (Mutshekwa et al., 2025).

The level risk of MNPs was observed in the backup stage, which collected nanofraction particles with an aerodynamic diameter less than 0.49 μm. These particles are classified as NPs and have the potential to be deposited in the human respiratory system, penetrate the blood cycle, and reach other organs. Therefore, the potential of Pyr-GC/MS to analyze NP particles captured in the backup stages was demonstrated. However, the examination of particles collected in this stage by Raman spectrometry was precluded due to their size being less than 1 μm (Mayorga et al., 2025).

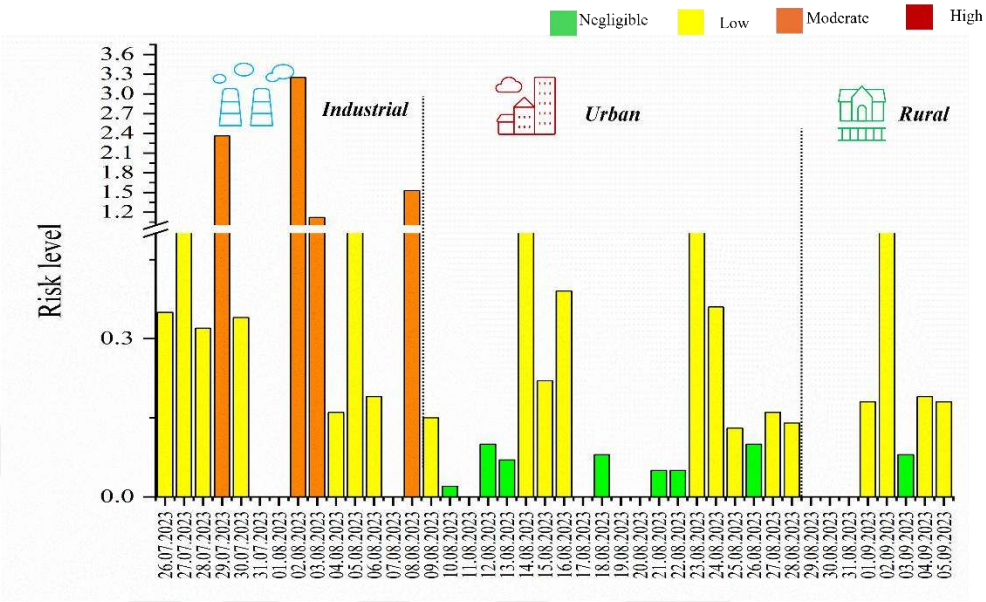

Figure 4.33. *Risk level of MNPs (SBR and NR) in nanofraction stage in the three sampling locations.*

The precise mass concentration thresholds that would lead to an elevated risk of developing chronic or acute exposure from airborne NPs are not yet well-defined. However, given the ability of NPs to penetrate deep into the lungs and potentially enter the bloodstream, high concentrations are likely to exacerbate respiratory and systemic health issues. SBR have been observed to generate reactive oxygen species (ROS) through surface redox reactions and leaching of styrene derivatives. In BEAS-2B human lung cells, 40-nm polystyrene nanoparticles (analogous to SBR) induced 2.3-fold increases in ROS, depleting glutathione reserves and depolarizing mitochondrial membranes(T. Zhang et al., 2022). It can be posited that analogous mechanisms are likely to be applicable to SBR, given styrene's capacity to uncouple oxidative phosphorylation. While the subject of NPs has been the focus of relatively fewer scholarly publications, there is a growing body of research that suggests a link between NR and oxidative stress. This link is believed to result from the presence of zinc oxide additives in the NPs, which have been shown to generate hydroxyl radicals in alveolar macrophages. Consequently, further research is necessary to establish precise exposure limits and to understand the long-term health effects (Mutshekwa et al., 2025). Moreover, exposure to airborne NPs promotes expression of pro-fibrotic genes and pathways (e.g., epithelial-mesenchymal transition, Wnt/β-catenin signaling), leading to

extracellular matrix deposition and fibrosis. NR may contribute to fibrosis through zinc oxide-induced effects, while SBR components may worsen protease-antiprotease imbalances, further damaging lung architecture (Gou et al., 2024).

4.3.3. Comparison of particles and mass-based assessment

In the evaluation of the risks posed by airborne MNPs, a myopic focus on either size or concentration is inadequate. A comprehensive understanding of the associated risks necessitates a synergistic evaluation of both parameters. The size of MNPs influences their surface area-to-volume ratio, which affects their chemical interactions and toxicity. It has been demonstrated that smaller particles possess a greater surface area in relation to their mass. This increased surface area is associated with enhanced adsorption efficiency for toxic elements and the potential for augmented biological reactivity. However, size alone does not provide information on the number of particles present or their total mass, which is critical for assessing exposure levels and dose-response relationships. Concentration is indicative of the number of particles present in the air; however, it does not provide information regarding the size distribution of these particles. The behavior of particles of different sizes in the environment and biological systems is distinct. For example, particles of different sizes have different behaviors, such as deposition in the respiratory tract or cellular uptake. It has been demonstrated that larger particles may carry more adsorbed toxic elements per unit surface area, but fewer in number. Conversely, smaller particles may be more numerous but carry less per particle. Absent size-specific data, the risk posed by these divergent behaviors cannot be accurately assessed. The integration of size and concentration data facilitates a more precise estimation of exposure and toxicological impact. Risk assessments that integrate both factors have been shown to improve predictions of environmental fate, transport, and biological effects, thereby facilitating more accurate and reliable health risk evaluations. A risk assessment was conducted based on the particles collected from the industrial area, where the highest deposition was found in the human respiratory system on the 7th of August at stage 5. Furthermore, the majority of MNPs had the capacity to penetrate the alveoli on the 7th of August at stage 4. While the risk level based on the mass concentration of MNPs in the industrial samples indicated a backup stage on the 2nd of August, with a moderate risk level.

In the urban area, the maximum penetration of alveoli was observed on the night of August 21st in stage 4, and a significant accumulation of deposits in the airway was noted on the night of August 22nd in stage 4. Conversely, the highest concentration of MNPs was observed on the 21st of night August at the backup stage. The highest deposition in the alveoli and airway in the rural area was detected in stage 5 on the 5th night of September. Furthermore, the majority of airborne MNP concentrations were observed on the fifth night of September, across all stages. Indeed, the concentration of airborne MNPs has been demonstrated to serve as an indicator of the extent of chronic or acute exposure. While air contains a substantial quantity of MNPs, its substantial aerodynamic size precludes the penetration of the human respiratory system by air alone. Consequently, when evaluating the threshold for the presence of airborne MNPs, it is imperative to consider two factors: the concentration of MNPs in the atmosphere and their size.

4.4. Limitations

Although the study offers valuable insights into the sampling parameters and corresponding characterization artifacts of airborne MNPs, addressing its limitations and pursuing the suggested future research directions will enhance the understanding of the behavior of polymeric particles. In this study, only a high-volume cascade impactor sampler was available, therefore, the second set of samplings (20 and 40 cfm) was conducted on two separate days. It would have been preferable to conduct two of the samplings on the same day under identical weather conditions and with the same suspended particles, but the lack of an additional sampler precluded this possibility.

The use of micro-Raman spectroscopy for the analysis of airborne MNP samples presents challenges due to several important limitations, primarily cost and accessibility. Although micro-Raman spectroscopy is capable of detecting particles as small as approximately 1 micrometer, the analysis of nano-sized plastics can pose a significant challenge due to the complexity and cost associated with more sophisticated or complementary techniques. Consequently, micro-Raman spectroscopy is not a viable method for examining the backup stage. Due to the time-consuming nature of the spectrometric method and the presence of airborne MNPs, analysis of many particles per sample was necessary. For instance, a minimum of 20 particles per square centimeter of filter area was reported. This process was labor-intensive, and the analysis of all samples was not feasible.

One of the study's limitations was the impracticality of calibrating the Pyr-GC/MS to replicate actual conditions. This challenge stemmed from the inherent constraints of the standard cup-shaped pyrolyzer, which precluded the utilization of spiked polymer matrix samples. The capacity of the Eco-Cup One Shot Pyrolyzer was found to be limited to 6 microliters (i.e., <20 μg), a limitation that precluded the preparation and analysis of the airborne matrix samples. Consequently, matrix spiking and/or matrix-based calibration have been identified as limitations that necessitate further research to evaluate the performance of analytical procedures in testing size-fractionated air samples.

The absence of an observed adverse effect concentration (NOAEC) or reference concentration (RfC) for polymers other than styrene-butadiene rubber SBR and NR significantly limits the ability to determine risk levels of other polymer types based solely on

the mass concentration of airborne micro- and nanoplastics (MNPs). This is due to the fact that, in the absence of established dose-response relationships and toxicity thresholds specific to each polymer type, it is not possible to accurately quantify potential health impacts from exposure to those polymers. The development of future studies that focus on dose-response curves and the determination of NOAEC or RfC values for a broader range of polymer types is imperative. Conducting such research would provide the necessary toxicological benchmarks to facilitate more reliable and polymer-specific risk assessments of airborne MNPs. This approach acknowledges the fact that different polymers have distinct chemical structures, physical properties, and potential toxicities, which influence their environmental behavior and biological effects. In the absence of polymer-specific toxicity data, risk assessments based solely on mass concentration may be considered incomplete and potentially misleading.

5. CONCLUSION

Airborne microplastics (MPs) and nanoplastics (NPs) are diminutive plastic particles suspended in the atmosphere, originating from the breakdown of larger plastic materials or direct emissions. The classification of these particles is based on their size: microplastics MPs range from 1 μm to 5 mm, while NPs are smaller than 1 μm. Due to their small size and lightweight nature, MPs and NPs are capable of traveling long distances through atmospheric transport mechanisms, such as wind and turbulence, resulting in their pervasive presence across diverse geographical regions, including urban, rural, and remote areas. The necessity of monitoring airborne MNPs is threefold: first, due to their ubiquitous presence; second, due to the potential health risks they pose; and third, due to their environmental impacts. These particles, once inhaled, can penetrate deep into the respiratory system, potentially causing oxidative stress, inflammation, and immune responses. Of particular concern are NPs, given their ability to traverse biological barriers and enter the bloodstream. These particles have the potential to carry harmful chemicals or adsorb pollutants, thereby amplifying their toxic effects when inhaled. However, the efficacy of current monitoring efforts is impeded by the lack of uniform sampling and detection methodologies. Standardization is imperative to accurately assess exposure risks, compare data across studies, and develop mitigation strategies. Active sampling has been demonstrated to be superior to passive sampling for the collection of airborne MPs with a diameter smaller than 10 microns. This superiority can be attributed to several advantages that enhance precision, reproducibility, and efficiency. The monitoring or sampling of airborne MNPs using a high-volume cascade impactor is regarded as one of the most effective methods due to its capacity to efficiently collect size-fractionated particles, minimize contamination, and facilitate detailed analysis. These impactors are capable of separating particles into discrete size ranges, such as PM_{10}, $PM_{2.5}$, and PM_{1}, thereby enabling targeted analysis of MNPs based on their aerodynamic diameters. These impactors operate at elevated flow rates (e.g., 40 cfm or higher), enabling the collection of sufficient particulate matter in shorter sampling durations. This enhanced efficiency is particularly advantageous for the detection of low concentrations of MNPs in ambient air, where prolonged sampling periods might otherwise be necessary.

The selection of filters is of paramount importance in the collection of airborne MNPs due to the heterogeneity in size, shape, and physical-chemical properties that is characteristic of these particles. The utilization of filters is indispensable for the efficient execution of sampling, the mitigation of contamination, and the facilitation of accurate downstream analysis. Among slotted filters, Teflon filters have been shown to be more useful than glass fiber filters for analyzing airborne MNPs, especially with spectrometric methods, due to their superior properties for particle collection and compatibility with analytical techniques. In addition, in many instances, airborne MNPs are present in low concentrations within complex matrices. Pretreatment methods, such as those employing functionalized MNPs, facilitate the separation and concentration of target particles from impurities. The isolation of MNPs from inorganic and organic materials necessitates two distinct procedures: density separation and chemical digestion. The efficacy of density separation as a standalone technique is hindered by the high similarity in density between airborne MNPs and other particles, rendering it an ineffective method for isolating MNPs from inorganic materials. The process of chemical digestion has the potential to impact the color and size of the MNPs, thereby hindering the analysis of their size distribution and morphological properties. On the other hand, the parameters utilized for sampling play a pivotal role in the capture of airborne particles for the purpose of studying MNPs. At times, the presence of excess PM on the surface filter hinders the examination of microscopic MNP analysis. Consequently, the optimization of sampling parameters based on airborne PM concentration necessitated the study of microscopic spectrometry techniques. In this study, a detection of 40 cfm in the 8-hour sampling was identified as adequate. However, to accurately monitor the concentration of MNPs over the course of a day, it was necessary to collect two sets of sampling data: one during the day and one at night. Following the determination of the sampling conditions and preparation steps for the experiment, the sampling was conducted in three distinct areas (industrial, urban, and rural) for a period of 15 days in each location. Two dates of area night sampling were performed in the summer, and sampling in the rural region was conducted in the winter to evaluate the concentration of MNPs in the cooled seasons. A comprehensive analysis of the samples was conducted to differentiate between two distinct groups. The particle-based analysis was performed using a micro-Raman microscope, while the mass-based analysis was

conducted by means of Pyr-GC/MS. A two-day and two-night sampling was conducted at each location, with two days of sampling at each area selected based on meteorological conditions, specifically the highest and lowest PM_{10} indexes. These samples were examined using particles and mass analysis method. Additionally, all of the backup filters were studied using the mass analysis method, and the visual aspect of this stage was examined using a SEM-EDX microscope. The findings of the particle and mass-based analysis demonstrated that the concentration of airborne MNPs was higher during the daytime than at night. The underlying reasons for this phenomenon were thoroughly expounded in a designated section.

The size range of MNPs was more dependent on the humidity of the date of sampling, which led to the accumulation of smaller particles and the creation of larger particles. Furthermore, the chemical identification of MNPs indicates that a higher percentage of them are identified as carbon black, with a matching ratio of up to 70%, as well as PTFE. However, other polymers, including PP, p-(acrylic acid), and nylon, were identified in the samples, with a maximum matching ratio of up to 40%, as determined by particle-based analysis methods. The detection of SBR and NR in the results of Pyr-GC/MS verifies the presence of carbon black in the spectroscopic findings. Consequently, rubber originating from tires and brake pads, in conjunction with overall tire road wear, can be identified as the predominant sources of MNPs in ambient air, especially within urban environments. In addition, a variety of polymers were identified through the use of Pyr-GC/MS (PE, PP, PET, PC, PS), contingent on the geographical location of sampling. For instance, polystyrene (PS) was identified in rural areas where agricultural activities are particularly prevalent. Additionally, the concentration of mass and particle MNPs was observed to be higher during the winter season compared to the summer season. This variation was attributed to the presence of inversion and stable airflow, which are phenomena known to influence the distribution of MNPs in the atmosphere. A comparison of the lowest and highest PM_{10} indexes revealed that the concentration of PM does not affect the presence of MNPs in the atmosphere. This indicated that a day with low PM concentration can still contain high MNP levels. Concerning the nanoparticles that were collected on the glass fiber filter's backup stages, a visual analysis was conducted using an SEM-EDX. This analysis revealed the presence of carbon, indicating the polymer structure. Additionally, the presence of elements such as Si, Zn, S, Cu, Al, and Fe

was observed, suggesting the presence of carbon black and confirming tire road wear as the major sources. Furthermore, the analysis revealed the presence of a wide array of MNP types detected in the industrial zone, attributable to the established factories and geographical conditions that facilitate wind transport of MNPs to this region, thereby leading to their accumulation.

The final section of the study entailed a risk assessment and an examination of the adverse effects of airborne MNPs on the human respiratory system. The risk assessment, as determined by the particle-based analysis method, concentrated on the dimensions of MNPs and the deposition rate of MNPs in various regions of the human respiratory system. It was determined that if the size of MNPs were reduced, they would be able to penetrate deeper into the respiratory system, thereby increasing the probability of crossing into the blood system. However, the predominant proportion of night sampling, particularly in urban areas, comprised smaller MNPs capable of being inhaled. Conversely, risk assessment based on mass-based analysis was conducted using MNPs (SBR and NR) concentration in the atmosphere. The winter season in rural areas was found to be particularly hazardous, with a high-risk level being identified. Conversely, a moderate risk level was observed during summer nights in rural areas. While the concentration of SBR and NR MNPs is a contributing factor, the presence of larger-sized MNPs in high concentrations can lead to a decrease in inhalable exposure probability and, consequently, a reduction in risk level. Conversely, low concentrations of MNPs, particularly those smaller in size, can result in an increase in human exposure levels. The frequency of MNP presence, along with their concentration and size, emerges as a pivotal factor in the onset of chronic and acute diseases.

It is imperative to acknowledge that this study, which encompasses this extension of information, is pioneering in literature. The study endeavored to utilize high-volume, size-segregated samplers to collect PM with a diameter less than 10 micrometers from multiple locations, encompassing six distinct size levels. Consequently, the findings can enhance temporal and spatial comparisons concerning airborne inhalable MNPs. Furthermore, the selection of examination instruments, devices, and analysis methods was made with consideration for size distribution properties. This included the implementation of a visual analysis of nano-fraction particles using SEM-EDX and the utilization of an Axioscope for

other size ranges. The selection of each step was guided by the outcomes of the experiment, encompassing the selection of a filter, the determination of sampling parameters, and pretreatment procedures for spectrometric and thermal methods. This study proposes a range of suitable analytical methodologies, selected based on the objective of the research and the quantity of PM in the samples. Additionally, the study aims to refine these methods in accordance with the experimental conditions. This study demonstrates considerable promise in advancing literature pertaining to MNPs with a diameter of less than 10 microns.

6. FUTURE RECOMMENDATIONS

The selection of a substrate filter is contingent upon the analytical methodology and the selected analysis instrument. Glass fiber filters are highly recommended for Pyr-GC/MS analysis. These filters enable direct measurement with minimal sample preparation, such as cryomilling, which ensures homogeneity and efficient transfer of pyrolyzates to the GC/MS system. This method provides high sensitivity, enabling nanogram-level detection of MNPs in air samples. Consequently, for studies focused on mass monitoring, optimization of the sampling parameter is not necessary. On the other hand, Teflon filters (e.g., polytetrafluoroethylene, PTFE) are well-suited for Raman spectroscopy due to their compatibility with hyperspectral imaging and their capacity to detect particles down to sub micrometer sizes without requiring any pretreatment. The application of Raman micro-spectrometry has yielded successful results in the analysis of the distribution and chemical composition of MNPs collected on Teflon filters. This approach has enabled the precise identification of polymer types, including carbon black and polypropylene.

In the context of meteorological conditions, the direction of wind plays a pivotal role in the interpretation of findings and the spatial analysis of MNPs. The record of wind direction plays a crucial role in studying airborne MNP concentrations across industrial, urban, and rural regions. The direction of wind plays a pivotal role in the transportation, dispersion, and deposition of airborne particles, including MNPs. This is due to the fact that it is associated with specific source areas and atmospheric conditions. Consequently, the documentation of wind direction is imperative for a comprehensive understanding of airborne MNP concentrations.

In the context of future studies, it is recommended that the double-shot pyrolysis approach offers significant advantages for the analysis of airborne MNP. This recommendation was made by virtue of the approach's ability to effectively separate volatile compounds from polymer degradation products. In addition, a concentration on polycyclic aromatic hydrocarbons (PAHs), benzenes, and benzonitrile as characteristic pyrolysis products is warranted. Furthermore, a combination of Py-GC-MS with complementary techniques is necessary for comprehensive characterization. One such technique is the integration of thermal desorption-PTR-MS for real-time detection of nanoplastics in the sub-

nanogram range. Thermal desorption-proton-transfer reaction-mass spectrometry (thermal desorption-PTR-MS) is an advanced analytical technique designed for the real-time, highly sensitive detection of volatile and semi-volatile organic compounds. When applied to airborne MNPs, this technique allows researchers to detect trace amounts of characteristic pyrolysis products or volatile compounds released from plastics upon heating. It is recommended as a complementary technique alongside Py-GC-MS double-shot pyrolysis methods to enhance analytical capabilities in airborne MNP research. It is imperative that priority be given to the development of standardized protocols, the improvement of detection limits, and the conducting of long-term monitoring studies to assess the global impact of airborne MNPs on human health and environmental systems.

REFERENCES

Abbasi, S., Keshavarzi, B., Moore, F., Turner, A., Kelly, F. J., Dominguez, A. O., and Jaafarzadeh, N. (2019). Distribution and potential health impacts of microplastics and microrubbers in air and street dusts from Asaluyeh County, Iran. *Environmental pollution*, 244, 153-164.

Adetuyi, B. O., Mathew, J. T., Inobeme, A., Falana, Y. O., Adetunji, C. O., Shahnawaz, M., Oyewole, O. A., Eniola, K., Yerima, M. B., and Popoola, O. A. (2024). Tyres, Bitumen Wear and Plastic Bottles, Other Single Used Plastic as Major Sources of Microplastic. In Microplastic Pollution (pp. 141-160). *Springer*.

Aeschlimann, M., Li, G., Kanji, Z. A., and Mitrano, D. M. (2022). Potential impacts of atmospheric microplastics and nanoplastics on cloud formation processes. *Nature Geoscience*, 15(12), 967-975.

Akbari Dana, P., Gaga, E. O., and Gedik, K. (2024). Analytical challenges and strategies for particle-based analysis of airborne microplastics in size-fractionated samples using microscopy, SEM/EDX, and Raman spectroscopy. *Anal. Chem*, 96, 20622−20634. https://doi.org/https://doi.org/10.1021/acs.analchem.4c05335

AkbariDana, P., GACHAYZADE, Z., and GEDİK, K. (2024a). The Fixtures of Life: Polymers, Plastics, Microplastics, Nanoplastics. *Turkiye Klinikleri Periodontology-Special Topics*, 10(1), 1-11.

AkbariDana, P., Gaga, E. O., and Gedik, K. (2024b). Analytical challenges and strategies for particle-based analysis of airborne microplastics in size-fractionated samples using microscopy, SEM/EDX, and Raman spectroscopy. *Anal. Chem*, 96, 20622−20634. https://doi.org/https://doi.org/10.1021/acs.analchem.4c05335

Akhbarizadeh, R., Dobaradaran, S., Torkmahalleh, M. A., Saeedi, R., Aibaghi, R., and Ghasemi, F. F. (2021). Suspended fine particulate matter (PM2. 5), microplastics (MPs), and polycyclic aromatic hydrocarbons (PAHs) in air: their possible relationships and health implications. *Environmental Research*, 192, 110339.

Akoueson, F., Chbib, C., Monchy, S., Paul-Pont, I., Doyen, P., Dehaut, A., and Duflos, G. (2021). Identification and quantification of plastic additives using pyrolysis-GC/MS: A review. *Science of the Total Environment*, 773, 145073.

Al-Azzawi, M. S., Knoop, O., and Drewes, J. E. (2022). Validation of sample preparation methods for small microplastics (≤ 10 μm) in wastewater effluents. *Chemical Engineering Journal*, 446, 137082. https://doi.org/10.1016/j.cej.2022.137082

Al-Khalidy, H. I., and Al-Haidarey, M. J. S. (2024). *Determination of polystyrene concentrations in Kufa River/Iraq*. BIO Web of Conferences,

Albignac, M., de Oliveira, T., Landebrit, L., Miquel, S., Auguin, B., Leroy, E., Maria, E., Mingotaud, A. F., and ter Halle, A. (2023). Tandem mass spectrometry enhances the performances of pyrolysis-gas chromatography-mass spectrometry for microplastic quantification. *Journal of Analytical and Applied Pyrolysis*, 172, 105993.

Aliff, M. N., Reavie, E. D., Post, S. P., and Zanko, L. M. (2020). Anthropocene geochemistry of metals in sediment cores from the Laurentian Great Lakes. *PeerJ*, 8, e9034.

Allen, S., Allen, D., Baladima, F., Phoenix, V., Thomas, J., Le Roux, G., and Sonke, J. (2021). Evidence of free tropospheric and long-range transport of microplastic at Pic du Midi Observatory. *Nature communications*, 12(1), 7242.

Allen, S., Allen, D., Karbalaei, S., Maselli, V., and Walker, T. R. (2022). Micro (nano) plastics sources, fate, and effects: What we know after ten years of research. *Journal of Hazardous Materials Advances*, 6, 100057.

Allen, S., Allen, D., Moss, K., Le Roux, G., Phoenix, V. R., and Sonke, J. E. (2020). Examination of the ocean as a source for atmospheric microplastics. *PloS one*, 15(5), e0232746.

Allen, S., Allen, D., Phoenix, V. R., Le Roux, G., Durántez Jiménez, P., Simonneau, A., Binet, S., and Galop, D. (2019). Atmospheric transport and deposition of microplastics in a remote mountain catchment. *Nature Geoscience*, 12(5), 339-344.

Amato-Lourenço, L. F., Carvalho-Oliveira, R., Júnior, G. R., dos Santos Galvão, L., Ando, R. A., and Mauad, T. (2021). Presence of airborne microplastics in human lung tissue. *Journal of Hazardous Materials*, 416, 126124. https://doi.org/https://doi.org/10.1016/j.jhazmat.2021.126124.

Amato-Lourenço, L. F., dos Santos Galvão, L., de Weger, L. A., Hiemstra, P. S., Vijver, M. G., and Mauad, T. (2020). An emerging class of air pollutants: potential effects of microplastics to respiratory human health? *Science of the total environment*, 749, 141676.

Amato-Lourenço, L. F., dos Santos Galvão, L., Wiebeck, H., Carvalho-Oliveira, R., and Mauad, T. (2022). Atmospheric microplastic fallout in outdoor and indoor environments in São Paulo megacity. *Science of The Total Environment*, 821, 153450.

Amobonye, A., Bhagwat, P., Raveendran, S., Singh, S., and Pillai, S. (2021). Environmental impacts of microplastics and nanoplastics: A current overview. *Frontiers in Microbiology*, 12, 768297.

Andrady, A. L. (2011). Microplastics in the marine environment. *Marine pollution bulletin*, 62(8), 1596-1605.

Aoki, K., and Furue, R. (2021). A model for the size distribution of marine microplastics: A statistical mechanics approach. *PLoS One*, 16(11), e0259781.

Arı, A., Arı, P. E., and Gaga, E. O. (2020). Chemical characterization of size-segregated particulate matter (PM) by inductively coupled plasma–Tandem mass spectrometry (ICP-MS/MS). *Talanta*, 208, 120350. https://doi.org/https://doi.org/10.1016/j.talanta.2019.120350

Azari, A., Vanoirbeek, J. A., Van Belleghem, F., Vleeschouwers, B., Hoet, P. H., and Ghosh, M. (2023). Sampling strategies and analytical techniques for assessment of airborne micro and nano plastics. *Environ. Int*, 174, 107885. https://doi.org/https://doi.org/10.1016/j.envint.2023.107885

Baensch-Baltruschat, B., Kocher, B., Stock, F., and Reifferscheid, G. (2020). Tyre and road wear particles (TRWP)-A review of generation, properties, emissions, human health risk, ecotoxicity, and fate in the environment. *Science of the total Environment*, 733, 137823.

Barceló, D., Picó, Y., and Alfarhan, A. H. (2023). Microplastics: Detection in human samples, cell line studies, and health impacts. *Environmental toxicology and pharmacology*, 104204.

Bergmann, M., Gutow, L., and Klages, M. (2015). *Marine anthropogenic litter*. Springer Nature. https://doi.org/https://pubs.acs.org/doi/10.1007/978-3-319-16510-3

Bergmann, M., Mützel, S., Primpke, S., Tekman, M. B., Trachsel, J., and Gerdts, G. (2019). White and wonderful? Microplastics prevail in snow from the Alps to the Arctic. *Science advances*, 5(8), eaax1157.

Bergmann, M., Wirzberger, V., Krumpen, T., Lorenz, C., Primpke, S., Tekman, M. B., and Gerdts, G. (2017). High quantities of microplastic in Arctic deep-sea sediments from the HAUSGARTEN observatory. *Environmental science & technology*, 51(19), 11000-11010. https://doi.org/10.1021/acs.est.7b03331

Besseling, E., Quik, J. T., Sun, M., and Koelmans, A. A. (2017). Fate of nano-and microplastic in freshwater systems: A modeling study. *Environmental Pollution*, 220, 540-548.

Blair, R. M., Waldron, S., Phoenix, V. R., and Gauchotte-Lindsay, C. (2019). Microscopy and elemental analysis characterisation of microplastics in sediment of a freshwater urban river in Scotland, UK. *Environmental Science and Pollution Research*, 26, 12491-12504.

Boakes, L. C., Patmore, I. R., Bancone, C. E., and Rose, N. L. (2023). High temporal resolution records of outdoor and indoor airborne microplastics. *Environmental Science and Pollution Research*, 30(13), 39246-39257. https://doi.org/https://doi.org/10.1007/s11356-022-24935-0.

Boisseaux, P., Rauert, C., Dewapriya, P., Delignette-Muller, M.-L., Barrett, R., Durndell, L., Pohl, F., Thompson, R., Thomas, K. V., and Galloway, T. (2024). Deep dive into the chronic toxicity of tyre particle mixtures and their leachates. *Journal of Hazardous Materials*, 466, 133580.

Borase, S. J. (2023). Facts and Effects of Plastic Wastes Disposal. *Advances in Geographical Research*.

Bourzac, K. (2022). Scientists race to study microplastic pollution in the atmosphere. *Chemical and Engineering News*, 100(7).

Brahney, J., Hallerud, M., Heim, E., Hahnenberger, M., and Sukumaran, S. (2020). Plastic rain in protected areas of the United States. *Science*, 368(6496), 1257-1260.

Brahney, J., Mahowald, N., Prank, M., Cornwell, G., Klimont, Z., Matsui, H., and Prather, K. A. (2021). Constraining the atmospheric limb of the plastic cycle. *Proceedings of the National Academy of Sciences*, 118(16), e2020719118.

Brown, J. S., Gordon, T., Price, O., and Asgharian, B. (2013). Thoracic and respirable particle definitions for human health risk assessment. *Part fibre toxicol*, 10, 1-12.

Burton, N. C., Grinshpun, S. A., and Reponen, T. (2007). Physical collection efficiency of filter materials for bacteria and viruses. *Ann. Occup. Hyg*, 51(2), 143-151. https://doi.org/https://doi.org/10.1093/annhyg/mel073

Cabernard, L., Roscher, L., Lorenz, C., Gerdts, G., and Primpke, S. (2018). Comparison of Raman and Fourier transform infrared spectroscopy for the quantification of microplastics in the aquatic environment. *Environmental science & technology*, 52(22), 13279-13288.

Cai, L., Wang, J., Peng, J., Tan, Z., Zhan, Z., Tan, X., and Chen, Q. (2017). Characteristic of microplastics in the atmospheric fallout from Dongguan city, China: preliminary research and first evidence. *Environmental Science and Pollution Research*, 24, 24928-24935.

Cao, G., and Cai, Z. (2023). Getting health hazards of inhaled nano/microplastics into focus: Expectations and challenges. *Environmental Science & Technology*, 57(9), 3461-3463.

Carriera, F., Di Fiore, C., and Avino, P. (2024). Occurrence of Microplastics in the Atmosphere: An Overview on Sources, Analytical Challenges, and Human Health Effects. *Atmosphere*, 15(7), 863.

Catarino, A. I., Macchia, V., Sanderson, W. G., Thompson, R. C., and Henry, T. B. (2018). Low levels of microplastics (MP) in wild mussels indicate that MP ingestion by humans is minimal compared to exposure via household fibres fallout during a meal. *Environmental pollution*, 237, 675-684. https://doi.org/10.1016/j.envpol.2018.02.069

Cau, A., Avio, C. G., Dessì, C., Moccia, D., Pusceddu, A., Regoli, F., Cannas, R., and Follesa, M. C. (2020). Benthic crustacean digestion can modulate the environmental fate of microplastics in the deep sea. *Environmental Science & Technology*, 54(8), 4886-4892.

Chadwick, N. P. (2015). *Aerosol Assisted Chemical Vapour Deposition of Photo-catalytic Composite and Doped TiO2 Thin Films.* UCL (University College London)].

Chae, E., Jung, U., and Choi, S.-S. (2024). Seasonal variations in concentrations of PM2. 5 and tire wear particle of< 2.5 μm (TWP2. 5) and polymeric components of PM2. 5 at a bus stop. *Atmospheric Environment*, 318, 120243.

Chen, Q., Shi, G., Revell, L. E., Zhang, J., Zuo, C., Wang, D., Le Ru, E. C., Wu, G., and Mitrano, D. M. (2023). Long-range atmospheric transport of microplastics across the southern hemisphere. *Nature Communications*, 14(1), 7898. https://doi.org/https://doi.org/10.1038/s41467-023-43695-0

Chen, Y.-C., Wei, C.-H., Hsu, W.-T., Proborini, W. D., Hsiao, T.-C., Liu, Z.-S., Chou, H.-C., Soo, J.-C., Dong, G.-C., and Chen, J.-K. (2024). Impact of seasonal changes and environmental conditions on suspended and inhalable microplastics in urban air. *Environmental Pollution*, 362, 124994.

Chen, Y., Jing, S., Wang, Y., Song, Z., Xie, L., Shang, X., Fu, H., Yang, X., Wang, H., and Wu, M. (2024). Quantification and characterization of fine plastic particles as considerable components in atmospheric fine particles. *Environmental Science & Technology*, 58(10), 4691-4703.

Chow, J. C., Watson, J. G., Wang, X., Abbasi, B., Reed, W. R., and Parks, D. (2022). Review of filters for air sampling and chemical analysis in mining workplaces. *Minerals*, 12(10), 1314. https://doi.org/https://doi.org/10.3390/min12101314

Chubarenko, I. (2022). Physical processes behind interactions of microplastic particles with natural ice. *Environmental Research Communications*, 4(1), 012001.

Copley, M., and Scientific, C. (2008). *Cascade Impactors. Theory, Design, and Practical Information for Optimal Testing.* Inhalation.

Costa-Gómez, I., Suarez-Suarez, M., Moreno, J. M., Moreno-Grau, S., Negral, L., Arroyo-Manzanares, N., López-García, I., and Peñalver, R. (2023). A novel application of thermogravimetry-mass spectrometry for polystyrene quantification in the PM10 and PM2. 5 fractions of airborne microplastics. *Sci. Total Environ*, 856, 159041. https://doi.org/https://doi.org/10.1016/j.scitotenv.2022.159041

Councell, T. B., Duckenfield, K. U., Landa, E. R., and Callender, E. (2004). Tire-wear particles as a source of zinc to the environment. *Environmental science & technology*, 38(15), 4206-4214.

Crawford, C. B., and Quinn, B. (2016). *Microplastic pollutants.* Elsevier Limited.

Cunningham, E. M., Rico Seijo, N., Altieri, K. E., Audh, R. R., Burger, J. M., Bornman, T. G., Fawcett, S., Gwinnett, C., Osborne, A. O., and Woodall, L. C. (2022). The transport and fate of microplastic fibres in the Antarctic: The role of multiple global processes. *Frontiers in Marine Science*, 9, 2353. https://doi.org/10.3389/fmars.2022.1056081

Dahl, A., Gharibi, A., Swietlicki, E., Gudmundsson, A., Bohgard, M., Ljungman, A., Blomqvist, G., and Gustafsson, M. (2006). Traffic-generated emissions of ultrafine particles from pavement–tire interface. *Atmospheric Environment*, 40(7), 1314-1323.

De Frond, H., O'Brien, A. M., and Rochman, C. M. (2023). Representative subsampling methods for the chemical identification of microplastic particles in environmental samples. *Chemosphere*, 310, 136772.

Debroas, D., Mone, A., and Ter Halle, A. (2017). Plastics in the North Atlantic garbage patch: a boat-microbe for hitchhikers and plastic degraders. *Science of the total environment*, 599, 1222-1232.

Dehghani, S., Moore, F., and Akhbarizadeh, R. (2017). Microplastic pollution in deposited urban dust, Tehran metropolis, Iran. *Environmental Science and Pollution Research*, 24, 20360-20371.

Din, K. S., Khokhar, M. F., Parvez, S., and Niazi, M. B. K. (2024). Emerging environmental challenge: a critical review of airborne microplastics. *Environmental Research Communications*.

Dong, H., Wang, L., Wang, X., Xu, L., Chen, M., Gong, P., and Wang, C. (2021). Microplastics in a remote lake basin of the Tibetan Plateau: Impacts of atmospheric transport and glacial melting. *Environmental science & technology*, 55(19), 12951-12960.

Dris, R., Gasperi, J., Mirande, C., Mandin, C., Guerrouache, M., Langlois, V., and Tassin, B. (2017). A first overview of textile fibers, including microplastics, in indoor and outdoor environments. *Environmental Pollution*, 221, 453-458. https://doi.org/https://doi.org/10.1016/j.envpol.2016.12.013.

Dris, R., Gasperi, J., Rocher, V., Saad, M., Renault, N., and Tassin, B. (2015). Microplastic contamination in an urban area: a case study in Greater Paris. *Environmental Chemistry*, 12(5), 592-599.

Dris, R., Gasperi, J., Saad, M., Mirande, C., and Tassin, B. (2016). Synthetic fibers in atmospheric fallout: a source of microplastics in the environment? *Marine pollution bulletin*, 104(1-2), 290-293.

Dümichen, E., Eisentraut, P., Celina, M., and Braun, U. (2019). Automated thermal extraction-desorption gas chromatography mass spectrometry: A multifunctional tool for comprehensive characterization of polymers and their degradation products. *Journal of Chromatography A*, 1592, 133-142.

Ebert, M., Weinbruch, S., Hoffmann, P., and Ortner, H. M. (2004). The chemical composition and complex refractive index of rural and urban influenced aerosols determined by individual particle analysis. *Atmos. Environ*, 38(38), 6531-6545. https://doi.org/https://doi.org/10.1016/j.atmosenv.2004.08.048

Edgerton, E. S., Casuccio, G. S., Saylor, R. D., Lersch, T. L., Hartsell, B. E., Jansen, J. J., and Hansen, D. A. (2009). Measurements of OC and EC in coarse particulate matter in the southeastern United States. *Journal of the Air & Waste Management Association*, 59(1), 78-90.

Elmes, M., and Gasparon, M. (2017). Sampling and single particle analysis for the chemical characterisation of fine atmospheric particulates: A review. *Journal of Environmental management*, 202, 137-150. https://doi.org/10.1016/j.jenvman.2017.06.067

Enyoh, C. E., Verla, A. W., Verla, E. N., Ibe, F. C., and Amaobi, C. E. (2019). Airborne microplastics: a review study on method for analysis, occurrence, movement and risks. *Environmental monitoring and assessment*, 191, 1-17.

EPA. (1989). *Risk assessment guidance for superfund.* Volume I: human health evaluation manual (part a), Center for Environmental Research Information Office of Research and Development: EPA, U.S. Environmental Protection Agency.

EPA, U. S. E. P. A. (1999). *Sampling of Ambient Air for Total Suspended Particulate Matter (Spm) and PM10 Using High Volume (HV) Sampler*. In (Vol. EPA/625/R-96/010a). Center for Environmental Research Information Office of Research and Development: EPA, U.S. Environmental Protection Agency.

EPA, U. S. E. P. A. (2001). *Risk Assessment Guidance for Superfund (RAGS)*. In Human Health Evaluation Manua (Vol. Volume I). Washington, DC 20460: U.S. Environmental Protection Agency.

Evangeliou, N., Grythe, H., Klimont, Z., Heyes, C., Eckhardt, S., Lopez-Aparicio, S., and Stohl, A. (2020). Atmospheric transport is a major pathway of microplastics to remote regions. *Nature communications*, 11(1), 3381.

Fan, W., Salmond, J. A., Dirks, K. N., Cabedo Sanz, P., Miskelly, G. M., and Rindelaub, J. D. (2022). Evidence and mass quantification of atmospheric microplastics in a coastal New Zealand city. *Environmental Science & Technology*, 56(24), 17556-17568.

Fan, Y., Zheng, J., Deng, L., Rao, W., Zhang, Q., Liu, T., and Qian, X. (2022). Spatiotemporal dynamics of microplastics in an urban river network area. *Water Research*, 212, 118116.

Fang, G.-C., Wu, Y.-S., Wen, C.-C., Lin, C.-K., Huang, S.-H., Rau, J.-Y., and Lin, C.-P. (2005). Concentrations of nano and related ambient air pollutants at a traffic sampling site. *Toxicology and Industrial Health*, 21(9), 259-271.

Feng, Y., Tu, C., Li, R., Wu, D., Yang, J., Xia, Y., Peijnenburg, W. J., and Luo, Y. (2023). A systematic review of the impacts of exposure to micro-and nano-plastics on human tissue accumulation and health. *Eco-Environment & Health*.

Ferrero, L., Scibetta, L., Markuszewski, P., Mazurkiewicz, M., Drozdowska, V., Makuch, P., Jutrzenka-Trzebiatowska, P., Zaleska-Medynska, A., Andò, S., and Saliu, F. (2022). Airborne and marine microplastics from an oceanographic survey at the Baltic Sea: an emerging role of air-sea interaction? *Science of the Total Environment*, 824, 153709.

Forbes, B. (2000). Human airway epithelial cell lines for in vitro drug transport and metabolism studies. *J PHARM SCI. Tech*, 3(1), 18-27. https://doi.org/https://doi.org/10.1016/S1461-5347(99)00231-X

Furuuchi, M., Eryu, K., Nagura, M., Hata, M., Kato, T., Tajima, N., Sekiguchi, K., Ehara, K., Seto, T., and Otani, Y. (2010). Development and performance evaluation of air sampler with inertial filter for nanoparticle sampling. *Aerosol and Air Quality Research*, 10(2), 185-192.

Gaga, E. O., Arı, A., Akyol, N., Üzmez, Ö. Ö., Kara, M., Chow, J. C., Watson, J. G., Özel, E., Döğeroğlu, T., and Odabasi, M. (2018). Determination of real-world emission factors of trace metals, EC, OC, BTEX, and semivolatile organic compounds (PAHs, PCBs and PCNs) in a rural tunnel in Bilecik, Turkey. *Science of the Total Environment*, 643, 1285-1296.

Gao, Z., Cizdziel, J. V., Wontor, K., Clisham, C., Focia, K., Rausch, J., and Jaramillo-Vogel, D. (2022). On airborne tire wear particles along roads with different traffic characteristics using passive sampling and optical microscopy, single particle SEM/EDX, and μ-ATR-FTIR analyses. *Frontiers in Environmental Science*, 10, 1022697.

Gasperi, J., Wright, S. L., Dris, R., Collard, F., Mandin, C., Guerrouache, M., Langlois, V., Kelly, F. J., and Tassin, B. (2018). Microplastics in air: are we breathing it in? *Current Opinion in Environmental Science & Health*, 1, 1-5.

Gaston, E., Woo, M., Steele, C., Sukumaran, S., and Anderson, S. (2020). Microplastics differ between indoor and outdoor air masses: insights from multiple microscopy methodologies. *Applied spectroscopy*, 74(9), 1079-1098. https://doi.org/10.1177/0003702820920652

Gianini, M., Piot, C., Herich, H., Besombes, J.-L., Jaffrezo, J.-L., and Hueglin, C. (2013). Source apportionment of PM10, organic carbon and elemental carbon at Swiss sites: An intercomparison of different approaches. *Science of the total environment*, 454, 99-108.

Giechaskiel, B., Grigoratos, T., Mathissen, M., Quik, J., Tromp, P., Gustafsson, M., Franco, V., and Dilara, P. (2024). Contribution of Road Vehicle Tyre Wear to Microplastics and Ambient Air Pollution. *Sustainability*, 16(2), 522.

Gillibert, R., Balakrishnan, G., Deshoules, Q., Tardivel, M., Magazzù, A., Donato, M. G., Maragò, O. M., Lamy de La Chapelle, M., Colas, F., and Lagarde, F. (2019). Raman tweezers for small microplastics and nanoplastics identification in seawater. *Environmental science & technology*, 53(15), 9003-9013. https://doi.org/10.1021/acs.est.9b03105

Girão, A. V. (2022). *SEM/EDS and optical microscopy analysis of microplastics.* In Handbook of Microplastics in the Environment (pp. 57-78). Springer.

Gnoffo, C., and Frache, A. (2023). Identification of plastics in mixtures and blends through pyrolysis-gas chromatography/mass spectrometry. *Polymers*, 16(1), 71.

Goedecke, C., Dittmann, D., Eisentraut, P., Wiesner, Y., Schartel, B., Klack, P., and Braun, U. (2020). Evaluation of thermoanalytical methods equipped with evolved gas analysis for the detection of microplastic in environmental samples. *Journal of Analytical and Applied Pyrolysis*, 152, 104961.

Goehler, L. O., Moruzzi, R. B., da Conceição, F. T., Júnior, A. A. C., Speranza, L. G., Busquets, R., and Campos, L. C. (2022). Relevance of tyre wear particles to the total content of microplastics transported by runoff in a high-imperviousness and intense vehicle traffic urban area. *Environmental Pollution*, 314, 120200.

Gómez-Sánchez, N., Galindo, N., Alfosea-Simón, M., Nicolás, J. F., Crespo, J., and Yubero, E. (2024). Chemical composition of PM10 at a rural site in the western Mediterranean and its relationship with the oxidative potential. *Chemosphere*, 363, 142880.

González-Pleiter, M., Edo, C., Aguilera, Á., Viúdez-Moreiras, D., Pulido-Reyes, G., González-Toril, E., Osuna, S., de Diego-Castilla, G., Leganés, F., and Fernández-Piñas, F. (2021). Occurrence and transport of microplastics sampled within and above the planetary boundary layer. *Science of The Total Environment*, 761, 143213. https://doi.org/10.1016/j.scitotenv.2020.143213

Goßmann, I., Herzke, D., Held, A., Schulz, J., Nikiforov, V., Georgi, C., Evangeliou, N., Eckhardt, S., Gerdts, G., and Wurl, O. (2023a). Occurrence and backtracking of microplastic mass loads including tire wear particles in northern Atlantic air. *Nat. Commun*, 14(1), 3707.

Goßmann, I., Mattsson, K., Hassellöv, M., Crazzolara, C., Held, A., Robinson, T.-B., Wurl, O., and Scholz-Böttcher, B. M. (2023b). Unraveling the marine microplastic cycle: the first simultaneous data set for air, sea surface microlayer, and underlying water. *Environmental Science & Technology*, 57(43), 16541-16551.

Gou, Z., Wu, H., Li, S., Liu, Z., and Zhang, Y. (2024). Airborne micro-and nanoplastics: emerging causes of respiratory diseases. *Particle and Fibre Toxicology*, 21(1), 1-22.

Gouin, T. (2021). Addressing the importance of microplastic particles as vectors for long-range transport of chemical contaminants: perspective in relation to prioritizing research and regulatory actions. *Microplastics and Nanoplastics*, 1(1), 14.

Grigoratos, T., and Martini, G. (2014). *Non-exhaust traffic related emissions. Brake and tyre wear PM*. Report EUR, 26648.

Grigoratos, T., and Martini, G. (2015). Brake wear particle emissions: a review. *Environmental science and pollution research*, 22, 2491-2504.

Gu, J., Bai, Z., Liu, A., Wu, L., Xie, Y., Li, W., Dong, H., and Zhang, X. (2010). Characterization of atmospheric organic carbon and element carbon of PM2. 5 and PM10 at Tianjin, China. *Aerosol Air Qual Res* 10: 167–176. In.

Guha, S., Hariharan, P., and Myers, M. R. (2014). Enhancement of ICRP's lung deposition model for pathogenic bioaerosols. *Aerosol Sci Technol*, 48(12), 1226-1235.

Guo, Q., Men, Z., Liu, Z., Niu, Z., Fang, T., Liu, F., Wu, L., Peng, J., and Mao, H. (2023). Chemical characteristics of fine tire wear particles generated on a tire simulator. *Environmental Pollution*, 336, 122399.

Habibi, N., Uddin, S., Fowler, S. W., and Behbehani, M. (2022). Microplastics in the atmosphere: A review. *J. Environ. Expo. Assess*, 1(6), 10.20517.

Hale, R. C., Seeley, M. E., La Guardia, M. J., Mai, L., and Zeng, E. Y. (2020). A global perspective on microplastics. *Journal of Geophysical Research: Oceans*, 125(1), e2018JC014719.

Haller, T., Rentenberger, C., Meyer, J. C., Felgitsch, L., Grothe, H., and Hitzenberger, R. (2019). Structural changes of CAST soot during a thermal–optical measurement protocol. *Atmospheric Measurement Techniques*, 12(7), 3503-3519.

Halsband, C., Sørensen, L., Khan, F. R., Herzke, D., and Wagner, S. (2024). Environmental impacts and risks of car tire and styrene-butadiene rubber: microplastic pollution and contaminant transport. In (Vol. 11, pp. 1355263)*: Frontiers Media SA*.

Han, I., Lee, C., Belchez, C., Shipper, A. G., and Wiens, K. E. (2024). Microplastics in Urban Ambient Air: A Rapid Review of Active Sampling and Analytical Methods for Human Risk Assessment. *Environments*, 11(11), 256.

Haque, F., and Fan, C. (2023). Fate and impacts of microplastics in the environment: hydrosphere, pedosphere, and atmosphere. *Environments*, 10(5), 70.

Haram, L. E., Carlton, J. T., Ruiz, G. M., and Maximenko, N. A. (2020). A plasticene lexicon. *Marine Pollution Bulletin*, 150, 110714.

Hartmann, N. B., Huffer, T., Thompson, R. C., Hassellov, M., Verschoor, A., Daugaard, A. E., Rist, S., Karlsson, T., Brennholt, N., and Cole, M. (2019). Are we speaking the same language? Recommendations for a definition and categorization framework for plastic debris. In*: ACS Publications*.

Hatinoğlu, M. D., and Sanin, F. D. (2021). Sewage sludge as a source of microplastics in the environment: a review of occurrence and fate during sludge treatment. *Journal of environmental management*, 295, 113028.

Hermabessiere, L., Himber, C., Boricaud, B., Kazour, M., Amara, R., Cassone, A.-L., Laurentie, M., Paul-Pont, I., Soudant, P., and Dehaut, A. (2018). Optimization, performance, and application of a pyrolysis-GC/MS method for the identification of microplastics. *Analytical and bioanalytical chemistry*, 410, 6663-6676.

Hofmann, W. (2011). Modelling inhaled particle deposition in the human lung—A review. *Journal of Aerosol Science*, 42(10), 693-724.

Hong, J., Moon, H., Kim, J., Lee, B.-c., Kim, G.-B., Lee, H., and Kim, Y. (2021). Differentiation of carbon black from black carbon using a ternary plot based on elemental analysis. *Chemosphere*, 264, 128511. https://doi.org/https://doi.org/10.1016/j.chemosphere.2020.128511

Horvath, H. (1998). *Influence of atmospheric aerosols upon the global radiation balance. In Atmospheric particles* (Vol. 5, pp. 62-63). Wiley.

Hossain, M. (2024). Trending Physico-Chemical Characteristics of Microplastics (MPs) and Nano-plastics (NPs) in Different Physical Environments and Their Role in Various Emerging Environmental Issues: A Review. *Available at SSRN 5095223*.

Hu, W., Tang, R., Yuan, S., Gong, M., Shi, P., Wang, W., and Hu, Z.-H. (2023). Modification of fluorescence staining method for small-sized microplastic quantification: Focus on the interference exclusion and exposure time optimization. *Environmental Science and Pollution Research*, 1-13.

Huang, Z., Hu, B., and Wang, H. (2023). Analytical methods for microplastics in the environment: a review. *Environmental chemistry letters*, 21(1), 383-401.

Hurley, R. R., Lusher, A. L., Olsen, M., and Nizzetto, L. (2018). Validation of a method for extracting microplastics from complex, organic-rich, environmental matrices. *Environmental science & technology*, 52(13), 7409-7417. https://doi.org/10.1021/acs.est.8b01517

Ilyas, S., Mehnaz, S., and Machado, S. (2024). Silent threats of 21st century: microplastic contamination of agroecosystems and its implications for the food chain toxicity. *Environmental Sustainability*, 1-4.

Islam, M. S., Rahman, M. M., Larpruenrudee, P., Arsalanloo, A., Beni, H. M., Islam, M. A., Gu, Y., and Sauret, E. (2023). How microplastics are transported and deposited in realistic upper airways? *Physics of Fluids*, 35(6).

Ivleva, N. P., Wiesheu, A. C., and Niessner, R. (2017). Microplastic in aquatic ecosystems. *Angewandte Chemie International Edition*, 56(7), 1720-1739.

Jahandari, A. (2023). Microplastics in the urban atmosphere: Sources, occurrences, distribution, and potential health implications. *Journal of Hazardous Materials Advances*, 12, 100346.

Jannah, B. R., Maharani, H. A., Rahmawati, S., Nugroho, A. R., and Abdull, N. B. (2024). Occurrence and characteristic of microplastics in suspended particulate, a case study in street of Yogyakarta. *E3S Web of Conferences,*

Järlskog, I., Strömvall, A.-M., Magnusson, K., Gustafsson, M., Polukarova, M., Galfi, H., Aronsson, M., and Andersson-Sköld, Y. (2020). Occurrence of tire and bitumen wear microplastics on urban streets and in sweepsand and washwater. *Science of the Total Environment*, 729, 138950.

Joksimovic, N., Selakovic, D., Jovicic, N., Jankovic, N., Pradeepkumar, P., Eftekhari, A., and Rosic, G. (2022). Nanoplastics as an Invisible Threat to Humans and the Environment. *Journal of Nanomaterials*, 2022(1), 6707819.

Ju, S., Yi, J., Lee, J., Kim, J., Lim, C., Lee, J., Kim, K., and Yoon, Y. (2023). High-efficiency microplastic sampling device improved using CFD analysis. *Sustainability*, 15(5), 3907. https://doi.org/https://doi.org/10.3390/su15053907

Kaal, J., Goñi-Urtiaga, A., Wenig, P., Veliu, M., Moreno-Jiménez, E., Plaza, C., and Panettieri, M. (2023). Simultaneous molecular fingerprinting of natural organic matter and synthetic polymers (PE, PET, PP, PS and PVC) using analytical pyrolysis. *Journal of Analytical and Applied Pyrolysis*, 175, 106159.

Kabir, S. A., Bhuiyan, M. A., Zhang, G., and Pramanik, B. K. (2024). Microplastic distribution and ecological risks: investigating road dust and stormwater runoff across land uses. *Environmental Science: Advances*, 3(1), 62-75.

Kalisa, E., Kuuire, V., and Adams, M. (2022). A preliminary investigation comparing high-volume and low-volume air samplers for measurement of PAHs, NPAHs and airborne bacterial communities in atmospheric particulate matter. *Environ. Sci.: Atmos*, 2(5), 1120-1131. https://doi.org/https://doi.org/10.1039/D2EA00078D

Kang, H., Park, S., Lee, B., Kim, I., and Kim, S. (2022). Concentration of microplastics in road dust as a function of the drying period—a case study in G City, Korea. *Sustainability*, 14(5), 3006.

Käppler, A., Windrich, F., Löder, M. G., Malanin, M., Fischer, D., Labrenz, M., Eichhorn, K.-J., and Voit, B. (2015). Identification of microplastics by FTIR and Raman microscopy: a novel silicon filter substrate opens the important spectral range below 1300 cm− 1 for FTIR transmission measurements. *Analytical and bioanalytical*

chemistry, 407, 6791-6801. https://doi.org/https://doi.org/10.1007/s00216-015-8850-8

Kaul, D., and Sharma, M. (2009). Traffic generated non-exhaust particulate emissions from concrete pavement: a mass and particle size study for two-wheelers and small cars. *Atmospheric Environment*, 43(35), 5691-5697.

Kausar, A. (2018). A review of filled and pristine polycarbonate blends and their applications. *Journal of Plastic Film & Sheeting*, 34(1), 60-97.

Kaya, A. T., Yurtsever, M., and Bayraktar, S. C. (2018). Ubiquitous exposure to microfiber pollution in the air. *The European Physical Journal Plus*, 133(11), 488.

Kelly, F. J., and Fussell, J. C. (2012). Size, source and chemical composition as determinants of toxicity attributable to ambient particulate matter. *Atmospheric environment*, 60, 504-526.

Kernchen, S., Löder, M. G., Fischer, F., Fischer, D., Moses, S. R., Georgi, C., Nölscher, A. C., Held, A., and Laforsch, C. (2022). Airborne microplastic concentrations and deposition across the Weser River catchment. *Science of the Total Environment*, 818, 151812.

Kernchen, S., Loder, M. G. J., Fischer, F., Fischer, D., Moses, S. R., Georgi, C., Nolscher, A. C., Held, A., and Laforsch, C. (2022). Airborne microplastic concentrations and deposition across the Weser River catchment. *Sci Total Environ*, 818, 151812. https://doi.org/10.1016/j.scitotenv.2021.151812

Kernchen, S., Schmalz, H., Löder, M. G., Georgi, C., Einhorn, A., Greiner, A., Nölscher, A. C., Laforsch, C., and Held, A. (2024). Atmospheric deposition studies of microplastics in Central Germany. *Air Quality, Atmosphere & Health*, 1-15.

Ketzel, M., Omstedt, G., Johansson, C., Düring, I., Pohjola, M., Oettl, D., Gidhagen, L., Wåhlin, P., Lohmeyer, A., and Haakana, M. (2007). Estimation and validation of PM2. 5/PM10 exhaust and non-exhaust emission factors for practical street pollution modelling. *Atmospheric Environment*, 41(40), 9370-9385.

Khan, K. (2012). *Investigation into the role of primer, pre-treatments and coating microstructure in preventing cut edge corrosion of organically coated steels*. Swansea University (United Kingdom).

Khanna, R., Chandra, A., Sen, S., Konyukhov, Y., Fuentes, E., Burmistrov, I., and Kravchenko, M. (2024). Microplastics and Nanoplastics as Environmental Contaminants of Emerging Concern: Potential Hazards for Human Health. *Sustainability*, 16(19), 8704.

Khanum, F., Chaudhry, M. N., Skouteris, G., Saroj, D., and Kumar, P. (2021). Chemical composition and source characterization of PM10 in urban areas of Lahore, Pakistan. *Indoor and Built Environment*, 30(7), 924-937.

Kibria, M. G., Masuk, N. I., Safayet, R., Nguyen, H. Q., and Mourshed, M. (2023). Plastic waste: challenges and opportunities to mitigate pollution and effective management. *International Journal of Environmental Research*, 17(1), 20.

Kim, J., Park, E., Moon, H., Son, H., Hong, J., Wi, E., Kwon, J.-T., Seo, D. Y., Lee, H., and Kim, Y. (2022). Estimation of the concentration of nano-carbon black in tire-wear particles using emission factors of PM10, PM2. 5, and black carbon. *Chemosphere*, 303, 134976.

Kitahara, K.-I., and Nakata, H. (2020). Plastic additives as tracers of microplastic sources in Japanese road dusts. *Science of the Total Environment*, 736, 139694.

Klein, M., Bechtel, B., Brecht, T., and Fischer, E. K. (2023). Spatial distribution of atmospheric microplastics in bulk-deposition of urban and rural environments–A one-year follow-up study in northern Germany. *Science of The Total Environment*, 901, 165923.

Klein, M., and Fischer, E. K. (2019). Microplastic abundance in atmospheric deposition within the Metropolitan area of Hamburg, Germany. *Science of the Total Environment*, 685, 96-103.

Knight, L. J., Parker-Jurd, F. N., Al-Sid-Cheikh, M., and Thompson, R. C. (2020). Tyre wear particles: an abundant yet widely unreported microplastic? *Environmental Science and Pollution Research*, 27, 18345-18354.

Knobloch, E., Ruffell, H., Aves, A., Pantos, O., Gaw, S., and Revell, L. E. (2021). Comparison of deposition sampling methods to collect airborne microplastics in Christchurch, New Zealand. *Water, Air, & Soil Pollution*, 232(4), 133.

Koelmans, A. A., Redondo-Hasselerharm, P. E., Nor, N. H. M., de Ruijter, V. N., Mintenig, S. M., and Kooi, M. (2022). Risk assessment of microplastic particles. *Nature Reviews Materials*, 7(2), 138-152. https://doi.org/10.1038/s41578-021-0411-y

Kole, P. J., Löhr, A. J., Van Belleghem, F. G., and Ragas, A. M. (2017). Wear and tear of tyres: a stealthy source of microplastics in the environment. *International journal of environmental research and public health*, 14(10), 1265.

Kovochich, M., Liong, M., Parker, J. A., Oh, S. C., Lee, J. P., Xi, L., Kreider, M. L., and Unice, K. M. (2021a). Chemical mapping of tire and road wear particles for single particle analysis. *Science of the Total Environment*, 757, 144085.

Kovochich, M., Parker, J. A., Oh, S. C., Lee, J. P., Wagner, S., Reemtsma, T., and Unice, K. M. (2021b). Characterization of individual tire and road wear particles in environmental road dust, tunnel dust, and sediment. *Environmental Science & Technology Letters*, 8(12), 1057-1064.

Kreider, M. L., Panko, J. M., McAtee, B. L., Sweet, L. I., and Finley, B. L. (2010). Physical and chemical characterization of tire-related particles: Comparison of particles generated using different methodologies. *Science of the Total Environment*, 408(3), 652-659.

Kreider, M. L., Unice, K. M., and Panko, J. M. (2020). Human health risk assessment of Tire and Road Wear Particles (TRWP) in air. *Human and Ecological Risk Assessment: An International Journal*, 26(10), 2567-2585.

Kumar, R., Sharma, P., Verma, A., Jha, P. K., Singh, P., Gupta, P. K., Chandra, R., and Prasad, P. V. (2021). Effect of physical characteristics and hydrodynamic conditions on transport and deposition of microplastics in riverine ecosystem. *Water*, 13(19), 2710.

Kwon, S., Lim, K., Jung, J., Bae, G., and Lee, K. (2003). Design and calibration of a 5-stage cascade impactor (K-JIST cascade impactor). *Journal of aerosol science*, 34(3), 289-300.

Lai, F. Y., Rauert, C., Gobelius, L., and Ahrens, L. (2019). A critical review on passive sampling in air and water for per-and polyfluoroalkyl substances (PFASs). *TrAC Trends in Analytical Chemistry*, 121, 115311.

Lai, H., Liu, X., and Qu, M. (2022). Nanoplastics and human health: hazard identification and biointerface. *Nanomaterials*, 12(8), 1298.

Larkin, P. (2017). *Infrared and Raman spectroscopy: principles and spectral interpretation.*Elsevier.

Laube, B. L., Afshar-Mohajer, N., Koehler, K., Chen, G., Lazarus, P., Collaco, J. M., and McGrath-Morrow, S. A. (2017). Acute and chronic in vivo effects of exposure to nicotine and propylene glycol from an E-cigarette on mucociliary clearance in a murine model. *Inhalation Toxicology*, 29(5), 197-205.

Lee, J.-Y., Chia, R. W., Veerasingam, S., Uddin, S., Jeon, W.-H., Moon, H. S., Cha, J., and Lee, J. (2024). A comprehensive review of urban microplastic pollution sources, environment and human health impacts, and regulatory efforts. *Science of the Total Environment*, 174297.

Lehner, R., Weder, C., Petri-Fink, A., and Rothen-Rutishauser, B. (2019). Emergence of nanoplastic in the environment and possible impact on human health. *Environmental science & technology*, 53(4), 1748-1765.

Lenz, R., Enders, K., Stedmon, C. A., Mackenzie, D. M., and Nielsen, T. G. (2015). A critical assessment of visual identification of marine microplastic using Raman spectroscopy for analysis improvement. *Marine pollution bulletin*, 100(1), 82-91.

Leslie, H. A., Van Velzen, M. J., Brandsma, S. H., Vethaak, A. D., Garcia-Vallejo, J. J., and Lamoree, M. H. (2022). Discovery and quantification of plastic particle pollution in human blood. *Environment international*, 163, 107199.

Levermore, J. M., Smith, T. E., Kelly, F. J., and Wright, S. L. (2020). Detection of microplastics in ambient particulate matter using Raman spectral imaging and chemometric analysis. *Analytical Chemistry*, 92(13), 8732-8740.

Lewis, E. R., and Schwartz, S. E. (2004). *Sea salt aerosol production: mechanisms, methods, measurements, and models (*Vol. 152). American geophysical union.

Li, K., Du, L., Qin, C., Bolan, N., Wang, H., and Wang, H. (2024). Microplastic pollution as an environmental risk exacerbating the greenhouse effect and climate change: a review. *Carbon Research*, 3(1), 9.

Li, W., Riemer, N., Xu, L., Wang, Y., Adachi, K., Shi, Z., Zhang, D., Zheng, Z., and Laskin, A. (2024a). Microphysical properties of atmospheric soot and organic particles: measurements, modeling, and impacts. *npj clim. atmos. sci*, 7(1), 65. https://doi.org/https://doi.org/10.1038/s41612-024-00610-8

Li, W., Riemer, N., Xu, L., Wang, Y., Adachi, K., Shi, Z., Zhang, D., Zheng, Z., and Laskin, A. (2024b). Microphysical properties of atmospheric soot and organic particles: measurements, modeling, and impacts. *npj Climate and Atmospheric Science*, 7(1), 65.

Li, Y., Lu, Z., Zheng, H., Wang, J., and Chen, C. (2020). Microplastics in surface water and sediments of Chongming Island in the Yangtze Estuary, China. *Environmental Sciences Europe*, 32, 1-12.

Li, Y., Shao, L., Wang, W., Zhang, M., Feng, X., Li, W., and Zhang, D. (2020). Airborne fiber particles: Types, size and concentration observed in Beijing. *Science of the Total Environment*, 705, 135967.

Li, Y., Shi, T., Li, X., Sun, H., Xia, X., Ji, X., Zhang, J., Liu, M., Lin, Y., and Zhang, R. (2022). Inhaled tire-wear microplastic particles induced pulmonary fibrotic injury via epithelial cytoskeleton rearrangement. *Environment International*, 164, 107257.

Limsiriwong, K., and Winijkul, E. (2023). Exploring Personal Exposure to Airborne Microplastics across Various Work Environments in Pathum Thani Province, Thailand. *International Journal of Environmental Research and Public Health*, 20(24), 7162.

Lindstrom, A. P., Conny, J. M., and Ortiz-Montalvo, D. L. (2024). Sampling of microplastics at a materials recovery facility. *Anal. Bioanal. Chem*, 416(12), 2885-2891. https://doi.org/https://doi.org/10.1007/s00216-024-05231-x

Liu, D., Song, Y., Li, F., and Chen, L. (2020). A detection method of small-sized microplastics based on micro-Raman mapping. *China Environmental Science*, 40(10), 4429-4438.

Liu, H., Liu, K., Fu, H., Ji, R., and Qu, X. (2020). Sunlight mediated cadmium release from colored microplastics containing cadmium pigment in aqueous phase. *Environmental Pollution*, 263, 114484.

Liu, K., Wang, X., Fang, T., Xu, P., Zhu, L., and Li, D. (2019a). Source and potential risk assessment of suspended atmospheric microplastics in Shanghai. *Science of the total environment*, 675, 462-471.

Liu, K., Wang, X., Wei, N., Song, Z., and Li, D. (2019b). Accurate quantification and transport estimation of suspended atmospheric microplastics in megacities: Implications for human health. *Environ. Int*, 132, 105127. https://doi.org/https://doi.org/10.1016/j.envint.2019.105127

Liu, P., Shao, L., Guo, Z., Zhang, Y., Cao, Y., Ma, X., and Morawska, L. (2025). Physicochemical characteristics of airborne microplastics of a typical coastal city in the Yangtze River Delta Region, China. *Journal of Environmental Sciences*, 148, 602-613.

Liu, X., Lu, J., He, S., Tong, Y., Liu, Z., Li, W., and Xiayihazi, N. (2022). Evaluation of microplastic pollution in Shihezi city, China, using pine needles as a biological passive sampler. *Science of The Total Environment*, 821, 153181. https://doi.org/10.1016/j.scitotenv.2022.153181

Liu, Y., Hu, J., Lin, L., Yang, B., Huang, M., Chang, M., Huang, X., Dai, Z., Sun, S., and Ren, L. (2023). Overcoming the fluorescent interference during Raman spectroscopy detection of microplastics. *Science of The Total Environment*, 897, 165333.

Liu, Z., and You, X.-y. (2023). Recent progress of microplastic toxicity on human exposure base on in vitro and in vivo studies. *Science of The Total Environment*, 166766.

Löber, M., Bondorf, L., Grein, T., Reiland, S., Wieser, S., Epple, F., Philipps, F., and Schripp, T. (2024). Investigations of airborne tire and brake wear particles using a novel vehicle design. *Environmental Science and Pollution Research*, 1-11.

Löder, M. G., and Gerdts, G. (2015). Methodology used for the detection and identification of microplastics—a critical appraisal. *Marine anthropogenic litter*, 201-227.

Löder, M. G., Imhof, H. K., Ladehoff, M., Löschel, L. A., Lorenz, C., Mintenig, S., Piehl, S., Primpke, S., Schrank, I., and Laforsch, C. (2017). Enzymatic purification of microplastics in environmental samples. *Environmental science & technology*, 51(24), 14283-14292.

Logvina, Y., Matas, I. M., Ribeiro, H., Pinto da Silva, L., Rodrigues, P., Leitão, J., and da Silva, J. E. (2024). Micro-and Nanoplastics in the Atmosphere: Methodology for Microplastics Size-Fractionation Sampling. *Microplastics*, 3(1), 82-97.

Long, C. M., Nascarella, M. A., and Valberg, P. A. (2013). Carbon black vs. black carbon and other airborne materials containing elemental carbon: Physical and chemical distinctions. *Environmental pollution*, 181, 271-286.

Lou, F., Wang, J., Sun, C., Song, J., Wang, W., Pan, Y., Huang, Q., and Yan, J. (2022). Influence of interaction on accuracy of quantification of mixed microplastics using Py-GC/MS. *Journal of Environmental Chemical Engineering*, 10(3), 108012.

Lowenthal, D. H., Watson, J. G., and Saxena, P. (2000). Contributions to light extinction during project MOHAVE. *Atmospheric Environment*, 34(15), 2351-2359. https://doi.org/10.1016/S1352-2310(99)00449-5

Luo, D., Wang, Z., Liao, Z., Chen, G., Ji, X., Sang, Y., Qu, L., Chen, Z., Wang, Z., and Dahlgren, R. A. (2024). Airborne microplastics in urban, rural and wildland environments on the Tibetan Plateau. *Journal of Hazardous Materials*, 465, 133177.

Luo, P., Bai, M., He, Q., Peng, Z., Wang, L., Dong, C., Qi, Z., Zhang, W., Zhang, Y., and Cai, Z. (2023). A novel strategy to directly quantify polyethylene microplastics in PM2. 5 based on pyrolysis-gas chromatography–tandem mass spectrometry. *Anal. Chem*, 95(7), 3556-3562. https://doi.org/https://doi.org/10.1021/acs.analchem.2c05477

Luo, X., Wang, Z., Yang, L., Gao, T., and Zhang, Y. (2022). A review of analytical methods and models used in atmospheric microplastic research. *Science of The Total Environment*, 828, 154487.

Luo, Z., Zhou, X., Su, Y., Wang, H., Yu, R., Zhou, S., Xu, E. G., and Xing, B. (2021). Environmental occurrence, fate, impact, and potential solution of tire microplastics: Similarities and differences with tire wear particles. *Science of the Total Environment*, 795, 148902.

Lv, L., Yan, X., Feng, L., Jiang, S., Lu, Z., Xie, H., Sun, S., Chen, J., and Li, C. (2021). Challenge for the detection of microplastics in the environment. *Water Environment Research*, 93(1), 5-15.

Lwanga, E. H., Beriot, N., Corradini, F., Silva, V., Yang, X., Baartman, J., Rezaei, M., van Schaik, L., Riksen, M., and Geissen, V. (2022). Review of microplastic sources, transport pathways and correlations with other soil stressors: a journey from agricultural sites into the environment. *Chemical and Biological Technologies in Agriculture*, 9(1), 20.

Ma, J., Zhao, S., He, K., Tian, L., Zhong, G., Jones, K. C., Sweetman, A. J., Li, J., Zhou, Q., and Chen, D. (2025). Quantification of Micro-and Nano-plastics in Atmospheric Fine Particles by Pyrolysis-Gas Chromatography-Mass Spectrometry with Chromatographic Peak Reconstruction. *Journal of Hazardous Materials*, 137292.

Magnusson, K., Eliaeson, K., Fråne, A., Haikonen, K., Olshammar, M., Stadmark, J., and Hultén, J. (2016). *Swedish sources and pathways for microplastics to the marine environment.* In: IVL Svenska Miljöinstitutet.

Manoli, E., Voutsa, D., and Samara, C. (2002). Chemical characterization and source identification/apportionment of fine and coarse air particles in Thessaloniki, Greece. *Atmospheric Environment*, 36(6), 949-961.

Marathe, D., Balbudhe, S., and Kumari, K. (2021). *Persistent organic pollutants: A global issue, a global response. In Persistent Organic Pollutants* (pp. 1-32). CRC Press.

Marfella, R., Prattichizzo, F., Sardu, C., Fulgenzi, G., Graciotti, L., Spadoni, T., D'Onofrio, N., Scisciola, L., La Grotta, R., and Frigé, C. (2024). Microplastics and nanoplastics in atheromas and cardiovascular events. *New England Journal of Medicine*, 390(10), 900-910.

Marina-Montes, C., Abás, E., Buil-García, J., and Anzano, J. (2023). From multi to single-particle analysis: A seasonal spectroscopic study of airborne particulate matter in Zaragoza, Spain. *Talanta*, 259, 124550.

Marina-Montes, C., Pérez-Arribas, L. V., Anzano, J., de Vallejuelo, S. F.-O., Aramendia, J., Gómez-Nubla, L., de Diego, A., Madariaga, J. M., and Cáceres, J. O. (2022). Characterization of atmospheric aerosols in the Antarctic region using Raman Spectroscopy and Scanning Electron Microscopy. *Spectrochimica Acta Part A: Molecular and Biomolecular Spectroscopy*, 266, 120452.

Marnane, R., Elliot, D., and Coulson, S. (2006). A pilot study to determine the background population of foreign fibre groups on a cotton/polyester T-shirt. *Science & Justice*, 46(4), 215-220.

Mastrotheodoros, G. P., and Beltsios, K. G. (2022). Pigments—Iron-based red, yellow, and brown ochres. *Archaeological and Anthropological Sciences*, 14(2), 35.

Mateos-Cárdenas, A., O'Halloran, J., van Pelt, F. N., and Jansen, M. A. (2020). *Rapid fragmentation of microplastics by the freshwater amphipod Gammarus duebeni (Lillj.)*. Scientific reports, 10(1), 12799.

Materić, D. a., Kasper-Giebl, A., Kau, D., Anten, M., Greilinger, M., Ludewig, E., van Sebille, E., Röckmann, T., and Holzinger, R. (2020). Micro-and nanoplastics in alpine snow: a new method for chemical identification and (semi) quantification in the nanogram range. *Environmental science & technology*, 54(4), 2353-2359.

Mathissen, M., Scheer, V., Vogt, R., and Benter, T. (2011). Investigation on the potential generation of ultrafine particles from the tire–road interface. *Atmospheric Environment*, 45(34), 6172-6179.

Matsueda, M., Mattonai, M., Iwai, I., Watanabe, A., Teramae, N., Robberson, W., Ohtani, H., Kim, Y.-M., and Watanabe, C. (2021). Preparation and test of a reference mixture of eleven polymers with deactivated inorganic diluent for microplastics analysis by pyrolysis-GC–MS. *Journal of Analytical and Applied Pyrolysis*, 154, 104993.

Matsui, K., Ishimura, T., Mattonai, M., Iwai, I., Watanabe, A., Teramae, N., Ohtani, H., and Watanabe, C. (2020). Identification algorithm for polymer mixtures based on Py-GC/MS and its application for microplastic analysis in environmental samples. *Journal of Analytical and Applied Pyrolysis*, 149, 104834.

Mattsson, K., de Lima, J. A., Wilkinson, T., Järlskog, I., Ekstrand, E., Sköld, Y. A., Gustafsson, M., and Hassellöv, M. (2023). Tyre and road wear particles from source to sea. *Microplastics and Nanoplastics*, 3(1), 14.

Mayorga, C., Athalye, S., Boodaghidizaji, M., Sarathy, N., Hosseini, M., Ardekani, A., and Verma, M. S. (2025). Limit of detection of Raman spectroscopy using polystyrene particles from 25 to 1000 nm in aqueous suspensions. *bioRxiv*, 2025.2001. 2017.632088.

Meinhardt, T. J., YOUNG, R. J., and HARTLE, R. W. (1978). Epidemiologic investigations of styrene-butadiene rubber production and reinforced plastics production. *Scandinavian Journal of Work, Environment & Health*, 240-246.

Mikac, L., Rigó, I., Himics, L., Tolić, A., Ivanda, M., and Veres, M. (2023). Surface-enhanced Raman spectroscopy for the detection of microplastics. *Applied surface science*, 608, 155239.

Miranda-Peña, L., Buitrago-Duque, L., Rangel-Buitrago, N., Gracia, A., Arana, V. A., and Trilleras, J. (2023). Geographical heterogeneity and dominant polymer types in microplastic contamination of lentic ecosystems: implications for methodological standardization and future research. *RSC advances*, 13(39), 27190-27202.

Mizuguchi, H., Takeda, H., Kinoshita, K., Takeuchi, M., Takayanagi, T., Teramae, N., Pipkin, W., Matsui, K., Watanabe, A., and Watanabe, C. (2023a). Direct analysis of airborne microplastics collected on quartz filters by pyrolysis-gas chromatography/mass

spectrometry. *J. Anal. Appl. Pyrolysis*, 171, 105946. https://doi.org/https://doi.org/10.1016/j.jaap.2023.105946

Mizuguchi, H., Takeda, H., Kinoshita, K., Takeuchi, M., Takayanagi, T., Teramae, N., Pipkin, W., Matsui, K., Watanabe, A., and Watanabe, C. (2023b). Direct analysis of airborne microplastics collected on quartz filters by pyrolysis-gas chromatography/mass spectrometry. *Journal of Analytical and Applied Pyrolysis*, 171, 105946.

Morioka, T., Tanaka, S., Kohama-Inoue, A., and Watanabe, A. (2024). The quantification of the airborne plastic particles of 0.43–11 μm: Procedure development and application to atmospheric environment. *Chemosphere*, 351, 141131.

Moyo, S. (2022). An enigma: A meta-analysis reveals the effect of ubiquitous microplastics on different taxa in aquatic systems. *Frontiers in Environmental Science*, 10, 999349.

Mphaga, T., Mhlongo, T., Zikalala, S., and Topkin, J. (2023). Identification and quantification of microplastics in wastewater treatment plants by spectroscopic and microscopic techniques in Johannesburg East, South Africa. *Water Practice & Technology*, 18(12), 3124-3140.

Munno, K., De Frond, H., O'Donnell, B., and Rochman, C. M. (2020). Increasing the accessibility for characterizing microplastics: introducing new application-based and spectral libraries of plastic particles (SLoPP and SLoPP-E). *Analytical chemistry*, 92(3), 2443-2451.

Mutshekwa, T., Mulaudzi, F., Maiyana, V. P., Mofu, L., Munyai, L. F., and Murungweni, F. M. (2025). Atmospheric deposition of microplastics in urban, rural, forest environments: A case study of Thulamela Local Municipality. *PloS one*, 20(3), e0313840.

Nachtnebel, M., Rastel, M., Mayrhofer, C., Zankel, A., Gahleitner, M., and Poelt, P. (2017). The fracture behavior of particle modified polypropylene–3D reconstructions and interparticle distances. *Polymer*, 126, 65-73.

Nafea, T. H., Chan, F. K. S., Xu, Y., Xiao, H., and He, J. (2025). Unveiling the seasonal transport and exposure risks of atmospheric microplastics in the southern area of the Yangtze River Delta, China. *Environmental Pollution*, 367, 125567.

Nagpure, A. S., Gurjar, B. R., Kumar, V., and Kumar, P. (2016). Estimation of exhaust and non-exhaust gaseous, particulate matter and air toxics emissions from on-road vehicles in Delhi. *Atmospheric environment*, 127, 118-124.

Neukirchen, C., Saraji-Bozorgzad, M. R., Mäder, M., Mudan, A. P., Czasch, P., Becker, J., Di Bucchianico, S., Trapp, C., Zimmermann, R., and Adam, T. (2025). Comprehensive elemental and physical characterization of vehicle brake wear emissions from two different brake pads following the Global Technical Regulation methodology. *Journal of Hazardous Materials*, 482, 136609.

Ng, E.-L., Lwanga, E. H., Eldridge, S. M., Johnston, P., Hu, H.-W., Geissen, V., and Chen, D. (2018). An overview of microplastic and nanoplastic pollution in agroecosystems. *Science of the total environment*, 627, 1377-1388.

Nosratabadi, A. R., Gustafsson, M., Lovén, K., Ljunggren, S. A., Olofsson, U., Abbasi, S., Blomqvist, G., Karlsson, H., Ljungman, A. G., and Cassee, F. R. (2023). Airway contraction and cytokine release in isolated rat lungs induced by wear particles from the road and tire interface and road vehicle brakes. *Inhalation Toxicology*, 35(13-14), 309-323.

O'Brien, S., Rauert, C., Ribeiro, F., Okoffo, E. D., Burrows, S. D., O'Brien, J. W., Wang, X., Wright, S. L., and Thomas, K. V. (2023). There's something in the air: A review of sources, prevalence and behaviour of microplastics in the atmosphere. *Science of The Total Environment*, 874, 162193.

Oehlschlägel, L. M., Schmid, S., Lehmann, M., Gekle, S., and Held, A. (2024). Water–air transfer rates of microplastic particles through bubble bursting as a function of particle size. *Microplastics and Nanoplastics*, 4(1), 1.

Oh, H.-J., Han, T. T., and Mainelis, G. (2021). Potential consumer exposure to respirable particles and TiO2 due to the use of eyebrow powders. *Journal of exposure science & environmental epidemiology*, 31(6), 1032-1046.

Okoffo, E. D., O'Brien, S., O'Brien, J. W., Tscharke, B. J., and Thomas, K. V. (2019). Wastewater treatment plants as a source of plastics in the environment: a review of occurrence, methods for identification, quantification and fate. *Environmental Science: Water Research & Technology*, 5(11), 1908-1931.

Oßmann, B. E., Sarau, G., Schmitt, S. W., Holtmannspötter, H., Christiansen, S. H., and Dicke, W. (2017). Development of an optimal filter substrate for the identification of small microplastic particles in food by micro-Raman spectroscopy. *Analytical and bioanalytical chemistry*, 409, 4099-4109.

Ostle, C., Thompson, R. C., Broughton, D., Gregory, L., Wootton, M., and Johns, D. G. (2019). The rise in ocean plastics evidenced from a 60-year time series. *Nature communications*, 10(1), 1622.

Panko, J. M., Chu, J., Kreider, M. L., and Unice, K. M. (2013). Measurement of airborne concentrations of tire and road wear particles in urban and rural areas of France, Japan, and the United States. *Atmospheric Environment*, 72, 192-199.

Panko, J. M., Hitchcock, K. M., Fuller, G. W., and Green, D. (2019). Evaluation of tire wear contribution to PM2. 5 in urban environments. *Atmosphere*, 10(2), 99.

Patidar, K., Alshehri, M., Singha, W., Alrasheedi, M., Younis, A. M., Dumka, U. C., and Ambade, B. (2024). Assessing the Microplastic Pandemic: Prevalence, Detection, and Human Health Impacts in Asian Aquatic Environments. *Physics and Chemistry of the Earth, Parts A/B/C*, 103800.

Peñalver, R., Costa-Gómez, I., Arroyo-Manzanares, N., Moreno, J. M., López-García, I., Moreno-Grau, S., and Córdoba, M. H. (2021). Assessing the level of airborne polystyrene microplastics using thermogravimetry-mass spectrometry: Results for an agricultural area. *Science of The Total Environment*, 787, 147656.

Pfaff, G. (2022). Carbon black pigments. *Physical Sciences Reviews*, 7(2), 109-125.

Pfeiffer, R. (2005). Sampling for PM10 and PM2. 5 particulates. *Micrometeorology in Agricultural Systems*, 47, 227-245.

Picó, Y., and Barceló, D. (2020). Pyrolysis gas chromatography-mass spectrometry in environmental analysis: Focus on organic matter and microplastics. *TrAC Trends in Analytical Chemistry*, 130, 115964.

Pilapitiya, P. N. T., and Ratnayake, A. S. (2024). The world of plastic waste: a review. *Cleaner Materials*, 100220.

Pipkin, W., Belganeh, R., Robberson, W., Allen, H., Cook, A.-M., and Watanabe, A. (2021). Identification of microplastics in environmental monitoring using pyrolysis–GC–MS analysis. *LCGC North America,* 179–186.

Pittroff, M., Müller, Y. K., Witzig, C. S., Scheurer, M., Storck, F. R., and Zumbülte, N. (2021). Microplastic analysis in drinking water based on fractionated filtration sampling and Raman microspectroscopy. *Environmental Science and Pollution Research*, 28(42), 59439-59451.

Pivokonsky, M., Cermakova, L., Novotna, K., Peer, P., Cajthaml, T., and Janda, V. (2018). Occurrence of microplastics in raw and treated drinking water. *Science of the total environment*, 643, 1644-1651. https://doi.org/10.1016/j.scitotenv.2018.08.102

Prata, J. C. (2018). Airborne microplastics: consequences to human health? *Environmental pollution*, 234, 115-126.

Prata, J. C., Castro, J. L., da Costa, J. P., Duarte, A. C., Cerqueira, M., and Rocha-Santos, T. (2020). An easy method for processing and identification of natural and synthetic microfibers and microplastics in indoor and outdoor air. *MethodsX*, 7, 100762. https://doi.org/https://doi.org/10.1016/j.mex.2019.11.032

Prata, J. C., Padrão, J., Khan, M. T., and Walker, T. R. (2024). *Do's and don'ts of microplastic research: a comprehensive guide*. OAE Publishing Inc.

Primpke, S., Wirth, M., Lorenz, C., and Gerdts, G. (2018a). Reference database design for the automated analysis of microplastic samples based on Fourier transform infrared (FTIR) spectroscopy. *Anal Bioanal Chem*, 410, 5131-5141. https://doi.org/https://doi.org/10.1007/s00216-018-1156-x

Primpke, S., Wirth, M., Lorenz, C., and Gerdts, G. (2018b). Reference database design for the automated analysis of microplastic samples based on Fourier transform infrared (FTIR) spectroscopy. *Analytical and bioanalytical chemistry*, 410, 5131-5141.

Purwiyanto, A. I. S., Prartono, T., Riani, E., Naulita, Y., Cordova, M. R., and Koropitan, A. F. (2022). The deposition of atmospheric microplastics in Jakarta-Indonesia: The coastal urban area. *Marine pollution bulletin*, 174, 113195.

Qiu, J., Zhang, H., Liu, J., and Liu, Y. (2024). The Impact of Indoor Air Humidity on the Infiltration of Ambient Particles. *Buildings*, 14(4), 1022.

Rahman, L., Mallach, G., Kulka, R., and Halappanavar, S. (2021). Microplastics and nanoplastics science: collecting and characterizing airborne microplastics in fine

particulate matter. *Nanotoxicology*, 15(9), 1253-1278. https://doi.org/10.1080/17435390.2021.2018065

Rai, P. K., Sonne, C., Song, H., and Kim, K.-H. (2023). Plastic wastes in the time of COVID-19: Their environmental hazards and implications for sustainable energy resilience and circular bio-economies. *Science of The Total Environment*, 858, 159880.

Rangel-Buitrago, N., Ben-Haddad, M., Nicoll, K., Galgani, F., and Neal, W. J. (2024). Marine plastic pollution in the Anthropocene: A linguistic toolkit for holistic understanding and action. *Ocean & Coastal Management*, 248, 106967.

Rassaei, F. (2024). EDDS and polystyrene interactions: implications for soil health and management practices. *International Journal of Phytoremediation*, 26(4), 504-523.

Rattanakunuprakarn, S., Jin, M., Sussman, M., and Felix, P. (2024). Comparative evaluation of highways and railroads using life-cycle benefit-cost analysis. *International Journal of Sustainable Transportation*, 18(10), 803-826.

Rauert, C., Rødland, E. S., Okoffo, E. D., Reid, M. J., Meland, S., and Thomas, K. V. (2021). Challenges with quantifying tire road wear particles: recognizing the need for further refinement of the ISO technical specification. *Environmental Science & Technology Letters*, 8(3), 231-236.

Rednikin, A. R., Frank, Y. A., Rozhin, A. O., Vorobiev, D. S., and Fakhrullin, R. F. (2024). Airborne Microplastics: Challenges, Prospects, and Experimental Approaches. *Atmosphere*, 15(11), 1380.

Revell, L. E., Kuma, P., Le Ru, E. C., Somerville, W. R., and Gaw, S. (2021). Direct radiative effects of airborne microplastics. *Nature*, 598(7881), 462-467.

Reynolds, R. L., Molden, N., Kokaly, R. F., Lowers, H., Breit, G. N., Goldstein, H. L., Williams, E. K., Lawrence, C. R., and Derry, J. (2024). Microplastic and associated black particles from road-tire wear: Implications for radiative effects across the cryosphere and in the atmosphere. *Journal of Geophysical Research: Atmospheres*, 129(19), e2024JD041116.

Roblin, B., Ryan, M., Vreugdenhil, A., and Aherne, J. (2020). Ambient atmospheric deposition of anthropogenic microfibers and microplastics on the western periphery of Europe (Ireland). *Environmental science & technology*, 54(18), 11100-11108.

Rocha-Santos, T. A., and Duarte, A. C. (2017). *Characterization and analysis of microplastics.* Elsevier.

Rochman, C. M., Brookson, C., Bikker, J., Djuric, N., Earn, A., Bucci, K., Athey, S., Huntington, A., McIlwraith, H., and Munno, K. (2019). Rethinking microplastics as a diverse contaminant suite. *Environmental toxicology and chemistry*, 38(4), 703-711.

Rødland, E. S., Gustafsson, M., Jaramillo-Vogel, D., Järlskog, I., Müller, K., Rauert, C., Rausch, J., and Wagner, S. (2023). Analytical challenges and possibilities for the quantification of tire-road wear particles. *TrAC Trends in Analytical Chemistry*, 165, 117121.

Romay, F. J., and García-Ruiz, E. (2023). Design of Round-Nozzle Inertial Impactors Review with Updated Design Parameters. *Aerosol and Air Quality Research*, 23(3), 220436.

Rosso, B., Corami, F., Barbante, C., and Gambaro, A. (2023a). Quantification and identification of airborne small microplastics (< 100 μm) and other microlitter components in atmospheric aerosol via a novel elutriation and oleo-extraction method. *Environ. Pollut*, 318, 120889. https://doi.org/https://doi.org/10.1016/j.envpol.2022.120889

Rosso, B., Gregoris, E., Litti, L., Zorzi, F., Fiorini, M., Bravo, B., Barbante, C., Gambaro, A., and Corami, F. (2023b). Identification and quantification of tire wear particles by employing different cross-validation techniques: FTIR-ATR Micro-FTIR, Pyr-GC/MS, and SEM. *Environmental Pollution*, 326, 121511.

Saha, S. C., and Saha, G. (2024). Effect of microplastics deposition on human lung airways: A review with computational benefits and challenges. *Heliyon, 10(2)*.

Santos, L. H., Insa, S., Arxé, M., Buttiglieri, G., Rodríguez-Mozaz, S., and Barceló, D. (2023). Analysis of microplastics in the environment: Identification and quantification of trace levels of common types of plastic polymers using pyrolysis-GC/MS. *MethodsX*, 10, 102143.

Schefer, R. B., Koestel, J., and Mitrano, D. M. (2025). Minimal vertical transport of microplastics in soil over two years with little impact of plastics on soil macropore networks. *Communications Earth & Environment*, 6(1), 278.

Schymanski, D., Goldbeck, C., Humpf, H. U., and Furst, P. (2018). Analysis of microplastics in water by micro-Raman spectroscopy: Release of plastic particles from different packaging into mineral water. *Water Res*, 129, 154-162. https://doi.org/10.1016/j.watres.2017.11.011

Seeley, M. E., and Lynch, J. M. (2023). Previous successes and untapped potential of pyrolysis–GC/MS for the analysis of plastic pollution. *Analytical and bioanalytical chemistry*, 415(15), 2873-2890.

Shao, L., Li, J., Zhang, M., Wang, X., Li, Y., Jones, T., Feng, X., Silva, L. F., and Li, W. (2021). Morphology, composition and mixing state of individual airborne particles: Effects of the 2017 Action Plan in Beijing, China. *Journal of Cleaner Production*, 329, 129748.

Shao, L., Li, Y., Jones, T., Santosh, M., Liu, P., Zhang, M., Xu, L., Li, W., Lu, J., and Yang, C.-X. (2022a). Airborne microplastics: A review of current perspectives and environmental implications. *Journal of Cleaner Production*, 347, 131048.

Shao, L., Liu, P., Jones, T., Yang, S., Wang, W., Zhang, D., Li, Y., Yang, C.-X., Xing, J., and Hou, C. (2022b). A review of atmospheric individual particle analyses: Methodologies and applications in environmental research. *Gondwana Research*, 110, 347-369.

Sharma, S., Sharma, V., and Chatterjee, S. (2023). Contribution of plastic and microplastic to global climate change and their conjoining impacts on the environment-A review. *Science of the total environment*, 875, 162627.

Sheng, X.-y., Lai, Y.-j., Yu, S.-j., Li, Q.-c., Zhou, Q.-x., and Liu, J.-f. (2023). Quantitation of atmospheric suspended polystyrene nanoplastics by active sampling prior to pyrolysis–gas chromatography–mass spectrometry. *Environmental Science & Technology*, 57(29), 10754-10762.

Shiu, R.-F., Chen, L.-Y., Lee, H.-J., Gong, G.-C., and Lee, C. (2022). New insights into the role of marine plastic-gels in microplastic transfer from water to the atmosphere via bubble bursting. *Water Research*, 222, 118856.

Silva, A. B., Bastos, A. S., Justino, C. I., da Costa, J. P., Duarte, A. C., and Rocha-Santos, T. A. (2018). Microplastics in the environment: Challenges in analytical chemistry-A review. *Analytica chimica acta*, 1017, 1-19.

Smichowski, P., and Gómez, D. R. (2024). An overview of natural and anthropogenic sources of ultrafine airborne particles: analytical determination to assess the multielemental profiles. *Applied Spectroscopy Reviews*, 59(3), 355-381.

Smith, E., and Dent, G. (2005). *Introduction, basic theory and principles. Modern Raman spectroscopy: a practical approach*. In: Wiley, Chichester, England.

Sommer, F., Dietze, V., Baum, A., Sauer, J., Gilge, S., Maschowski, C., and Gieré, R. (2018). Tire abrasion as a major source of microplastics in the environment. *Aerosol and air quality research*, 18(8), 2014-2028.

Sridharan, S., Kumar, M., Singh, L., Bolan, N. S., and Saha, M. (2021). Microplastics as an emerging source of particulate air pollution: A critical review. *Journal of Hazardous Materials*, 418, 126245.

Stefaniak, A. B., Virji, M. A., Badding, M. A., and Cummings, K. J. (2017). Application of the ICRP respiratory tract model to estimate pulmonary retention of industrially sampled indium-containing dusts. *Inhalation toxicology*, 29(4), 169-178.

Stelson, A. W. (1990). Urban aerosol refractive index prediction by partial molar refraction approach. *Environ. Sci. Tech*, 24(11), 1676-1679.

Strady, E., Kieu-Le, T.-C., Tran, Q.-V., and Thuong, Q.-T. (2021). Microplastic in atmospheric fallouts of a developing Southeast Asian megacity under tropical climate. *Chemosphere*, 272, 129874.

Suaria, G., Achtypi, A., Perold, V., Lee, J. R., Pierucci, A., Bornman, T. G., Aliani, S., and Ryan, P. G. (2020). Microfibers in oceanic surface waters: A global characterization. *Science advances*, 6(23), eaay8493.

Sundt, P., Schulze, P.-E., and Syversen, F. (2014). *Sources of microplastic-pollution to the marine environment*. Mepex for the Norwegian Environment Agency, 86, 20.

Swinnerton, S., Su, J., and Tsai, C. S. (2024). The emission and physicochemical properties of airborne microplastics and nanoplastics generated during the mechanical recycling of plastic via shredding. *Scientific Reports*, 14(1), 24755.

Szewc, K., Graca, B., and Dołęga, A. (2021). Atmospheric deposition of microplastics in the coastal zone: Characteristics and relationship with meteorological factors. *Science of the Total Environment*, 761, 143272.

Tang, I. N. (1996). Chemical and size effects of hygroscopic aerosols on light scattering coefficients. *Journal of Geophysical Research: Atmospheres*, 101(D14), 19245-19250. https://doi.org/10.1029/96JD03003

Tang, R., Shang, J., Qiu, X., Gong, J., Xue, T., and Zhu, T. (2024). Origin, Structural Characteristics, and Health Effects of Atmospheric Soot Particles: A Review. *Current Pollution Reports*, 1-16.

Tatsii, D., Bucci, S., Bhowmick, T., Guettler, J., Bakels, L., Bagheri, G., and Stohl, A. (2023). Shape matters: long-range transport of microplastic fibers in the atmosphere. *Environmental Science & Technology*, 58(1), 671-682.

Thompson, R. C., Olsen, Y., Mitchell, R. P., Davis, A., Rowland, S. J., John, A. W., McGonigle, D., and Russell, A. E. (2004). Lost at sea: where is all the plastic? *Science*, 304(5672), 838-838.

Timmers, V. R., and Achten, P. A. (2016). Non-exhaust PM emissions from electric vehicles. *Atmospheric environment*, 134, 10-17.

Tisch Environmental, I. (2004). *OPERATIONS MANUAL of High Volume Cascade Impactors.* In. Tisch-Env.com.

Torres-Agullo, A., Karanasiou, A., Moreno, T., and Lacorte, S. (2021). Overview on the occurrence of microplastics in air and implications from the use of face masks during the COVID-19 pandemic. *Science of the total environment*, 800, 149555.

Trainic, M., Flores, J. M., Pinkas, I., Pedrotti, M. L., Lombard, F., Bourdin, G., Gorsky, G., Boss, E., Rudich, Y., and Vardi, A. (2020). Airborne microplastic particles detected in the remote marine atmosphere. *Communications Earth & Environment*, 1(1), 1-9. https://doi.org/10.1038/s43247-020-00061-y

Tsakona, M. (2021). Drowning in plastics: marine litter and plastic waste vital graphics.

Uddin, S., Fowler, S. W., Habibi, N., Sajid, S., Dupont, S., and Behbehani, M. (2022). A preliminary assessment of size-fractionated microplastics in indoor aerosol—Kuwait's baseline. *Toxics*, 10(2), 71. https://doi.org/10.3390/toxics10020071

Unice, K., Weeber, M., Abramson, M., Reid, R., Van Gils, J., Markus, A., Vethaak, A., and Panko, J. (2019). Characterizing export of land-based microplastics to the estuary-Part I: Application of integrated geospatial microplastic transport models to assess tire and road wear particles in the Seine watershed. *Science of the total environment*, 646, 1639-1649.

Valavanidis, A., Vlachogianni, T., Fiotakis, K., and Loridas, S. (2013). Pulmonary oxidative stress, inflammation and cancer: respirable particulate matter, fibrous dusts and ozone as major causes of lung carcinogenesis through reactive oxygen species mechanisms. *International journal of environmental research and public health*, 10(9), 3886-3907.

van Broekhuizen, P. (2024). *Airborne release of tyre wear particles*. Update.

Vattanasit, U., Kongpran, J., and Ikeda, A. (2023). Airborne microplastics: a narrative review of potential effects on the human respiratory system. *Science of The Total Environment*, 166745.

Verschoor, A., De Poorter, L., Dröge, R., Kuenen, J., and de Valk, E. (2016). *Emission of microplastics and potential mitigation measures: Abrasive cleaning agents, paints and tyre wear.* National Institute for Public Health and the Environment.

Verschoor, A., De Poorter, L., Roex, E., and Bellert, B. (2014). *Quick scan and prioritization of microplastic sources and emissions*. RIVM Letter report, 156, 1-41.

Vianello, A., Jensen, R. L., Liu, L., and Vollertsen, J. (2019). Simulating human exposure to indoor airborne microplastics using a Breathing Thermal Manikin. *Scientific reports*, 9(1), 8670.

Wagner, S., Hüffer, T., Klöckner, P., Wehrhahn, M., Hofmann, T., and Reemtsma, T. (2018). Tire wear particles in the aquatic environment-a review on generation, analysis, occurrence, fate and effects. *Water research*, 139, 83-100.

Wang, C.-q., Wang, H., Fu, J.-g., and Liu, Y.-n. (2015). Flotation separation of waste plastics for recycling—A review. *Waste Management*, 41, 28-38.

Wang, S., Inthavong, K., Wen, J., Tu, J., and Xue, C. (2009). Comparison of micron-and nanoparticle deposition patterns in a realistic human nasal cavity. *Respiratory physiology & neurobiology*, 166(3), 142-151.

Wang, T., Niu, S., Wu, J., and Yu, J. (2022). Seasonal and daily occurrence of microplastic pollution in urban road dust. *Journal of Cleaner Production*, 380, 135025.

Wang, T., Wang, L., Chen, Q., Kalogerakis, N., Ji, R., and Ma, Y. (2020). Interactions between microplastics and organic pollutants: Effects on toxicity, bioaccumulation, degradation, and transport. *Science of The Total Environment*, 748, 142427. https://doi.org/10.1016/j.scitotenv.2020.142427

Wang, X., Li, C., Liu, K., Zhu, L., Song, Z., and Li, D. (2020). Atmospheric microplastic over the South China Sea and East Indian Ocean: abundance, distribution and source. *Journal of hazardous materials*, 389, 121846.

Wang, Y., Zhu, Y., Guo, G., An, L., Fang, W., Tan, Y., Jiang, J., Bing, X., Song, Q., and Zhou, Q. (2024). A comprehensive risk assessment of microplastics in soil, water, and atmosphere: Implications for human health and environmental safety. *Ecotoxicology and Environmental Safety*, 285, 117154.

Waters, C. N., and Turner, S. D. (2022). Defining the onset of the Anthropocene. *Science*, 378(6621), 706-708.

Welsh, B., Aherne, J., Paterson, A. M., Yao, H., and McConnell, C. (2022). Atmospheric deposition of anthropogenic particles and microplastics in south-central Ontario, Canada. *Science of the Total Environment*, 835, 155426.

Wieland, S., Balmes, A., Bender, J., Kitzinger, J., Meyer, F., Ramsperger, A. F., Roeder, F., Tengelmann, C., Wimmer, B. H., and Laforsch, C. (2022). From properties to toxicity: comparing microplastics to other airborne microparticles. *Journal of Hazardous Materials*, 428, 128151.

Wik, A., and Dave, G. (2009). Occurrence and effects of tire wear particles in the environment–A critical review and an initial risk assessment. *Environmental pollution*, 157(1), 1-11.

Wright, S., Levermore, J., and Ishikawa, Y. (2023). Application of Infrared and Near-Infrared Microspectroscopy to Microplastic Human Exposure Measurements. *Applied Spectroscopy*, 77(10), 1105-1128.

Wright, S. L., Gouin, T., Koelmans, A. A., and Scheuermann, L. (2021a). Development of screening criteria for microplastic particles in air and atmospheric deposition: critical review and applicability towards assessing human exposure. *Microplastics and Nanoplastics*, 1(1), 6.

Wright, S. L., Gouin, T., Koelmans, A. A., and Scheuermann, L. (2021b). Development of screening criteria for microplastic particles in air and atmospheric deposition: critical review and applicability towards assessing human exposure. *Microplastics and Nanoplastics*, 1(1), 1-18.

Wright, S. L., and Kelly, F. J. (2017). Plastic and human health: a micro issue? *Environmental science & technology*, 51(12), 6634-6647. https://doi.org/https://doi.org/10.1021/acs.est.7b00423.

Wright, S. L., Levermore, J. M., and Kelly, F. J. (2019). Raman spectral imaging for the detection of inhalable microplastics in ambient particulate matter samples. *Environmental science & technology*, 53(15), 8947-8956. https://doi.org/10.1021/acs.est.8b06663

Wright, S. L., Ulke, J., Font, A., Chan, K. L. A., and Kelly, F. J. (2020). Atmospheric microplastic deposition in an urban environment and an evaluation of transport. *Environment international*, 136, 105411.

Xia, W., Rao, Q., Deng, X., Chen, J., and Xie, P. (2020). Rainfall is a significant environmental factor of microplastic pollution in inland waters. *Science of the Total Environment*, 732, 139065.

Xu, C., Zhang, B., Gu, C., Shen, C., Yin, S., Aamir, M., and Li, F. (2020). Are we underestimating the sources of microplastic pollution in terrestrial environment? *Journal of hazardous materials*, 400, 123228.

Xu, S., Cui, B., Zhang, W., Liu, R., Liu, H., Zhu, X., Huang, X., and Liu, M. (2024). Microplastics in the atmospheric of the eastern coast of China: different function

areas reflecting various sources and transport. *Environmental Geochemistry and Health*, 46(11), 461.

Yang, J., Peng, Z., Sun, J., Chen, Z., Niu, X., Xu, H., Ho, K.-F., Cao, J., and Shen, Z. (2024). A review on advancements in atmospheric microplastics research: The pivotal role of machine learning. *Science of The Total Environment*, 945, 173966.

Yang, S., Brasseur, G., Walters, S., Lichtig, P., and Li, C. W. (2025). Global atmospheric distribution of microplastics with evidence of low oceanic emissions. *npj Climate and Atmospheric Science*, 8(1), 81.

Yao, X., Luo, X.-S., Fan, J., Zhang, T., Li, H., and Wei, Y. (2022). Ecological and human health risks of atmospheric microplastics (MPs): a review. *Environmental Science: Atmospheres*, 2(5), 921-942.

Yao, Y., Glamoclija, M., Murphy, A., and Gao, Y. (2022). Characterization of microplastics in indoor and ambient air in northern New Jersey. *Environmental research*, 207, 112142.

Yoo, H., Kim, M., Lee, Y., Park, J., Lee, H., Song, Y.-C., and Ro, C.-U. (2023). Novel Single-Particle Analytical Technique for Inhalable Airborne Microplastic Particles by the Combined Use of Fluorescence Microscopy, Raman Microspectrometry, and SEM/EDX. *Analytical Chemistry*. https://doi.org/https://doi.org/10.1021/acs.analchem.3c00581

Youn, J.-S., Kim, Y.-M., Siddiqui, M. Z., Watanabe, A., Han, S., Jeong, S., Jung, Y.-W., and Jeon, K.-J. (2021). Quantification of tire wear particles in road dust from industrial and residential areas in Seoul, Korea. *Science of the Total Environment*, 784, 147177.

Yttri, K. E., Aas, W., Bjerke, A., Cape, J., Cavalli, F., Ceburnis, D., Dye, C., Emblico, L., Facchini, M., and Forster, C. (2007). Elemental and organic carbon in PM 10: a one year measurement campaign within the European Monitoring and Evaluation Programme EMEP. *Atmospheric Chemistry and Physics*, 7(22), 5711-5725.

Yukioka, S., Tanaka, S., Nabetani, Y., Suzuki, Y., Ushijima, T., Fujii, S., Takada, H., Van Tran, Q., and Singh, S. (2020). Occurrence and characteristics of microplastics in surface road dust in Kusatsu (Japan), Da Nang (Vietnam), and Kathmandu (Nepal). *Environmental Pollution*, 256, 113447.

Zhang, K., Hamidian, A. H., Tubić, A., Zhang, Y., Fang, J. K., Wu, C., and Lam, P. K. (2021). Understanding plastic degradation and microplastic formation in the environment: A review. *Environmental Pollution*, 274, 116554.

Zhang, Q., Xu, E. G., Li, J., Chen, Q., Ma, L., Zeng, E. Y., and Shi, H. (2020). A review of microplastics in table salt, drinking water, and air: direct human exposure. *Environmental science & technology*, 54(7), 3740-3751.

Zhang, T., Yang, S., Ge, Y., Wan, X., Zhu, Y., Li, J., Yin, L., Pu, Y., and Liang, G. (2022). Polystyrene nanoplastics induce lung injury via activating oxidative stress: Molecular insights from bioinformatics analysis. *Nanomaterials*, 12(19), 3507.

Zhang, X., Hu, N., Yu, Z., Du, Y., Liu, Y., Wang, H., Pu, L., He, X., Pan, D., and He, S. (2022). Research tendency of microplastics and nanoplastics based on bibliometric analysis and perspective of the influence of human health. *Environmental Research Communications*, 4(9), 095004.

Zhang, Y.-L., Kang, S.-C., and Gao, T.-G. (2022). Microplastics have light-absorbing ability to enhance cryospheric melting. *Advances in Climate Change Research*, 13(4), 455-458.

Zhang, Y., Kang, S., Allen, S., Allen, D., Gao, T., and Sillanpää, M. (2020). Atmospheric microplastics: A review on current status and perspectives. *Earth-Science Reviews*, 203, 103118.

Zhao, X., Wang, J., Yee Leung, K. M., and Wu, F. (2022). Color: an important but overlooked factor for plastic photoaging and microplastic formation. *Environmental Science & Technology*, 56(13), 9161-9163.

Zhu, X., Huang, W., Fang, M., Liao, Z., Wang, Y., Xu, L., Mu, Q., Shi, C., Lu, C., and Deng, H. (2021). Airborne microplastic concentrations in five megacities of northern and southeast China. *Environmental science & technology*, 55(19), 12871-12881. https://doi.org/https://doi.org/10.1021/acs.est.1c03618.

APPENDIX- A

MATERIALS AND METHODS

Table A.1. *Weather condition of main sampling process.*

Locations	Date	Tem_ mean(c)	Air pressure (millibar)	RH%	Wind speed (m/s)	UV index (out of 11)	PM_{10} ($\mu g/m^3$)	$PM_{2.5}$ ($\mu g/m^3$)
Industrial (Summer) (N:39°44'10,03668"(LAT), E:30°39'0,92592" (LONG), Height: 835 m)	25/07/2023	29.43	1008.6	20.67	1.82	7	23.56	4.87
	26/07/2023	34.68	1009.1	18.22	1.10	8	64.40	6.80
	27/07/2023	30.55	1009.1	39.50	3.19	9	78.90	7.33
	28/07/2023	25.33	1011	30.00	2.03	8	26.65	9.68
	29/07/2023	27.64	1012.2	25.44	1.88	7	23.32	6.35
	30/07/2023	27.60	1011.2	33.67	1.94	7	23.33	4.65
	31/07/2023	28.54	1009.1	36.33	2.34	8	47.97	5.70
	01/08/2023	28.84	1010.2	35.44	2.27	8	20.52	9.78
	02/08/2023	18.90	1013.2	78.89	0.54	8	23.29	4.37
	03/08/2023	32.60	1013.2	22.22	1.67	7	23.98	7.26
	04/08/2023	33.79	1012.2	25.67	1.42	9	54.84	14.04
	05/08/2023	35.07	1008.1	22.33	1.23	2	13.31	6.54
	06/08/2023	35.72	1007.1	20.22	1.91	9	15.79	6.78
	07/08/2023	21.56	1013.2	63.22	1.04	7	29.47	6.48
	08/08/2023	27.82	1011.2	47.67	2.69	9	37.86	7.64
Urban (Summer) (N:39°46'21,94212"(LAT), E:30°29'23,514" Height: 795 m)	09/08/2023	23	1011.7	47	3.05	8	11.95	17.6
	10/08/2023	26.50	1013.2	55.11	2.46	8	34.51	4.88
	11/08/2023	24.36	1018	52.67	2.77	8	33.04	8.39
	12/08/2023	27.84	1017.3	48.22	1.99	9	29.23	4.32
	13/08/2023	32.39	1016.3	36.78	2.31	9	37.80	11.90
	14/08/2023	33.61	1016.3	31.44	2.09	8	54.85	16.78
	15/08/2023	37.84	1015.2	20.00	2.09	8	70.84	18.30
	16/08/2023	36.31	1012.2	23.78	1.87	7	89.19	24.89
	17/08/2023	35.47	1011.2	26.67	2.28	8	92.21	44.12
	18/08/2023	35.64	1013.2	23.67	1.53	8	87.00	24.07
	19/08/2023	35.34	1013.2	24.11	1.53	8	67.47	10.01
	20/08/2023	30.44	1013.2	33.22	2.46	7	36.61	5.38
	21/08/2023	19.94	1016.3	58.44	1.86	8	45.77	4.13
	22/08/2023	19.94	1018	61.75	1.31	8	38.66	3.41
	23/08/2023	32.27	1017.3	22.22	1.61	8	60.72	9.53
Rural (Summer) (N:39°48'54,99828"(LAT), E:30°32'16.37052" (LONG).	24/08/2023	30	1015.2	25	2.77	8	17.66	16.73
	25/08/2023	31.14	1014.2	29.22	1.62	7	45.38	7.40
	26/08/2023	31.07	1016.3	24.89	1.41	8	61.48	6.68
	27/08/2023	30.64	1010.2	29.11	2.00	7	51.70	7.95
	28/08/2023	26.89	1010.2	44.67	2.67	6	37.95	8.92
	29/08/2023	29.70	1009.1	27.44	1.69	7	55.76	13.35
	30/08/2023	32.29	1011.2	24.78	1.88	7	65.91	6.30
	31/08/2023	30.03	1013.2	33.67	1.89	8	74.79	12.45
	01/09/2023	27.91	1017.3	36.67	2.24	8	42.87	5.26
	02/09/2023	26.22	1015.2	47.67	2.38	7	38.02	10.29
	03/09/2023	22.87	1016.3	59.22	1.36	7	29.92	6.69
	04/09/2023	21.88	1013.2	62.11	1.50	7	33.45	5.29
	05/09/2023	16.79	1012.2	86.67	0.37	7	35.70	4.16
	06/09/2023	18.36	1018	90.22	1.49	7	35.50	6.13
	07/09/2023	27.13	1015.2	49.78	2.04	8	40.43	10.71

Table A.1.(Continued) *Weather condition of main sampling process.*

Locations	Date	Tem_ mean(c)	Air pressure (millibar)	RH%	Wind speed (m/s)	UV index (out of 11)	PM_{10} ($\mu g/m^3$)	$PM_{2.5}$ ($\mu g/m^3$)
Rural (Winter)(N:39°48'54,99828"(LAT), E:30°32'16,37052" (LONG),	19/12/2023	5.30	1025	73.00	1.50	2	58.83	40.7
	20/12/2023	7.42	1017	87.00	3.87	2	59.05	22.03
	21/12/2023	5.45	1007	76.00	3.64	1	41.21	12.34
	22/12/2023	9.11	999.9	88.00	3.66	5	29.05	5.58
	23/12/2023	9.66	1005.4	44.00	6.90	1	18.33	4.23
	24/12/2023	9.11	1013.5	58.00	6.85	1	26.59	5.12
	25/12/2023	10.60	1018.5	55.00	2.30	1	42.63	11.41
	26/12/2023	10.88	1022	49.00	2.50	1	57.45	23.34
	27/12/2023	11.44	1023	81.00	2.00	2	54.1	38.55
	28/12/2023	8.60	1027.5	90.00	1.60	1	57.58	21.3
	29/12/2023	7.30	1023.7	75.00	2.67	2	70.35	14.96
	30/12/2023	3.40	1022	77.00	1.69	1	63.34	29.79
	31/12/2023	7.40	1021	77.00	2.20	1	78.64	51.96
	01/01/2023	5.50	1020	76.00	5.30	2	49.6	20.1

*Blue letters indicate the sampling date for night samples, and red letters show the sampling day were selected based on PM_{10} index for particle and mass-based analysis.

Table A. 2. *Weather condition and analytical samples in preparation of the sampling process.*

Locations	Date	Tem_ mean(c)	Air pressure (millibar)	RH%	Wind speed (m/s)	UV index (out of 11)	
Eskisehir Technical *University campus* *(N:39°48'54,99828"(LAT), E:30°32'16,37052"*	03/07/2022	20.6	1017	36	2.04	7	
	18/07/2022	20.5	1019	38	3.14	8	
	21/06/2023	18.12	1017	66	3.53	7	
	12/07/2023	22.5	1021	38	2.6	7	
	13/07/2023	23.18	1020	30	2.5	8	
	Date	**Stage 1**	**Stage 2**	**Stage 3**	**Stage 4**	**Stage 5**	**Backup**
	03/07/2022	10 slots optical	10 slots optical	10 slots optical	10 slots optical	10 slots optical	
	18/07/2022	10 slots optical	10 slots optical	10 slots optical	10 slots optical	10 slots optical	
	21/06/2023	1 cm^2 optical	1 cm^2 optical	1 cm^2 optical	1 cm^2 optical	SEM-EDX& 1 cm^2 optical	SEM-EDX
	12.07.2023 40 cfm (4, 8, 12, 24h)	Raman	Raman	Raman	Raman	Raman	
	12.07.2023 20 cfm (4, 8, 12, 24h)	Raman	Raman	Raman	Raman	Raman	
	13.07.2023 40 cfm (4, 8, 12, 24h)	Raman	Raman	Raman	Raman	Raman	
	13.07.2023 20 cfm (4, 8, 12, 24h)	Raman	Raman	Raman	Raman	Raman	

Table A.3. *Analytical samples in the main sampling process.*

Locations	Date	Stage 1	Stage 2	Stage 3	Stage 4	Stage 5	Backup
Industrial (Summer)	25/07/2023	-	-	-	-	-	Pyr
	26/07/2023	-	-	-	-	-	Pyr
	27/07/2023	-	-	-	-	-	Pyr
	28/07/2023	-	-	-	-	-	Pyr
	29/07/2023	-	-	-	-	-	Pyr
	30/07/2023	-	-	-	-	-	Pyr
	31/07/2023	-	-	-	-	-	Pyr
	01/08/2023	-	-	-	-	-	Pyr
	02/08/2023	Raman &Pyr	Raman &Pyr	Raman &Pyr	Raman &Pyr	Raman &Pyr	Pyr
	02/08/2023	Raman &Pyr	Raman &Pyr	Raman &Pyr	Raman &Pyr	Raman &Pyr	Pyr& SEM-EDX
	03/08/2023	-	-	-	-	-	Pyr
	04/08/2023	Raman &Pyr	Raman &Pyr	Raman &Pyr	Raman &Pyr	Raman &Pyr	Pyr& SEM-EDX
	05/08/2023	-	-	-	-	-	Pyr
	06/08/2023	Raman &Pyr	Raman &Pyr	Raman &Pyr	Raman &Pyr	Raman &Pyr	Pyr
	07/08/2023	Raman &Pyr	Raman &Pyr	Raman &Pyr	Raman &Pyr	Raman &Pyr	Pyr
Urban (Summer)	09/08/2023	Raman &Pyr	Raman &Pyr	Raman &Pyr	Raman &Pyr	Raman &Pyr	Pyr
	10/08/2023	-	-	-	-	-	Pyr
	11/08/2023	-	-	-	-	-	Pyr
	12/08/2023	-	-	-	-	-	Pyr
	13/08/2023	-	-	-	-	-	Pyr
	14/08/2023	-	-	-	-	-	Pyr
	15/08/2023	-	-	-	-	-	Pyr
	16/08/2023	-	-	-	-	-	Pyr
	17/08/2023	-	-	-	-	-	Pyr
	18/08/2023	-	-	-	-	-	Pyr
	19/08/2023	Raman &Pyr	Raman &Pyr	Raman &Pyr	Raman &Pyr	Raman &Pyr	Pyr& SEM-EDX
	20/08/2023	-	-	-	-	-	Pyr
	21/08/2023	-	-	-	-	-	Pyr
	22/08/2023	Raman &Pyr	Raman &Pyr	Raman &Pyr	Raman &Pyr	Raman &Pyr	Pyr
	23/08/2023	-	-	-	-	-	Pyr
Rural (Summer)	24/08/2023	-	-	-	-	-	Pyr
	25/08/2023	-	-	-	-	-	Pyr
	26/08/2023	-	-	-	-	-	Pyr
	27/08/2023	-	-	-	-	-	Pyr
	28/08/2023	-	-	-	-	-	Pyr
	29/08/2023	Raman &Pyr	Raman &Pyr	Raman &Pyr	Raman &Pyr	Raman &Pyr	Pyr& SEM-EDX
	30/08/2023	-	-	-	-	-	Pyr
	31/08/2023	-	-	-	-	-	Pyr

Table A.3. (Continued) *Analytical samples in the main sampling*

Locations	Date	Stage 1	Stage 2	Stage 3	Stage 4	Stage 5	Backup
Rural (Summer)	01/09/2023	-	-	-	-	-	Pyr
	02/09/2023	-	-	-	-	-	Pyr
	03/09/2023	Raman &Pyr	Raman &Pyr	Raman &Pyr	Raman &Pyr	Raman &Pyr	Pyr
	04/09/2023	-	-	-	-	-	Pyr
	05/09/2023	Raman &Pyr	Raman &Pyr	Raman &Pyr	Raman &Pyr	Raman &Pyr	Pyr& SEM-EDX
	05/09/2023	Raman &Pyr	Raman &Pyr	Raman &Pyr	Raman &Pyr	Raman &Pyr	Pyr
	06/09/2023	Raman &Pyr	Raman &Pyr	Raman &Pyr	Raman &Pyr	Raman &Pyr	Pyr
	06/09/2023	-	-	-	-	-	Pyr
	07/09/2023	-	-	-	-	-	Pyr
Rural (Winter)	19/12/2023	-	-	-	-	-	Pyr
	20/12/2023	-	-	-	-	-	Pyr
	21/12/2023	-	-	-	-	-	Pyr
	22/12/2023	-	-	-	-	-	Pyr
	23/12/2023	-	-	-	-	-	Pyr
	24/12/2023	-	-	-	-	-	Pyr
	25/12/2023	-	-	-	-	-	Pyr
	26/12/2023	-	-	-	-	-	Pyr
	27/12/2023	-	-	-	-	-	Pyr
	28/12/2023	-	-	-	-	-	Pyr
	29/12/2023	-	-	-	-	-	Pyr
	30/12/2023	-	-	-	-	-	Pyr
	31/12/2023	-	-	-	-	-	Pyr& SEM-EDX
	01/01/2023	Raman &Pyr	Raman &Pyr	Raman &Pyr	Raman &Pyr	Raman &Pyr	Pyr& SEM-EDX
	01/01/2023	Raman &Pyr	Raman &Pyr	Raman &Pyr	Raman &Pyr	Raman &Pyr	Pyr

*Blue letters indicate the sampling date for night samples, and red letters show the sampling day were selected based on PM_{10} index for particle and mass-based analysis. (20 particles from $1cm^2$ analyzed by Raman and less than 20 µg analyzed by Pyr-GC/MS, 6 particles spectra were analyzed by SEM-EDX)

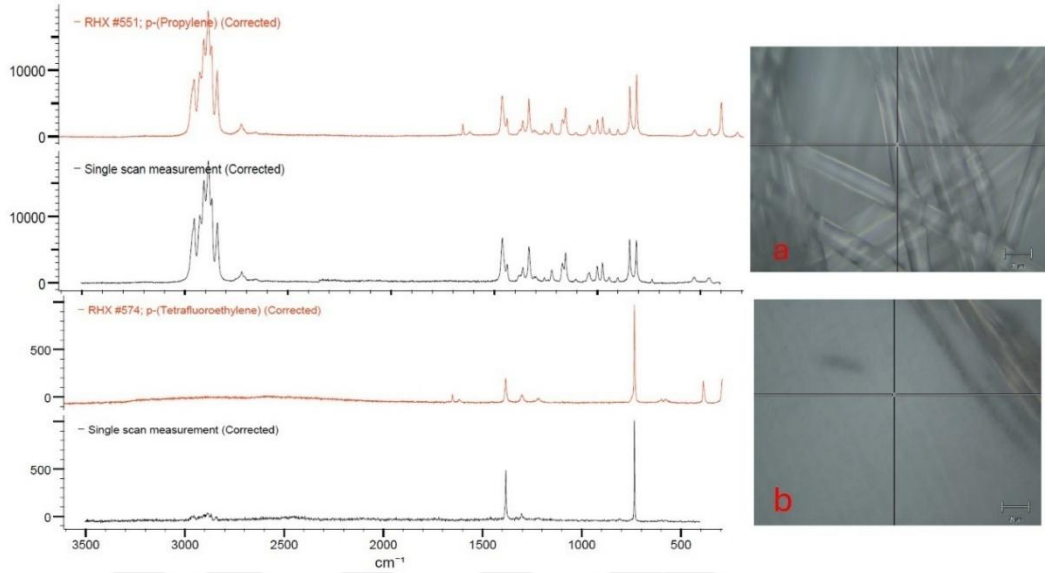

Figure A. 1. *Micro-Raman analysis of virgin the slotted Teflon filter, a) Back of Teflon filter. b) Face of Teflon filter.*

Table A. 4. *Calculation P_2/P_1 two indicators of each polymer.*

	NR				**SBR**			
Calibration	**P_2/P_1**	**Mean**	**SD**	**RSD%**	**P_2/P_1**	**Mean**	**SD**	**RSD%**
	0.160249	0.14	0.01	9.97	10.93239	10.42	1.513	14.52
	0.153186				9.65664			
	0.124603				9.07392			
	0.136805				9.59761			
	0.137472				12.83344			
	PE				**PP**			
	P_2/P_1	**Mean**	**SD**	**RSD%**	**P_2/P_1**	**Mean**	**SD**	**RSD%**
	0.39158116	0.45	0.05	11.00	0.12241	0.11	0.014	12.80
	0.46365496				0.11657			
	0.41984586				0.09207			
	0.52263802				0.11097			
	0.45110145				0.09342			
	PVC				**PS**			
	P_2/P_1	**Mean**	**SD**	**RSD%**	**P_2/P_1**	**Mean**	**SD**	**RSD%**
	3.697805	4.03	0.23	5.54	0.099834	0.15	0.032	22.23
	3.924084				0.135350			
	4.125137				0.149837			
	4.155312				0.151541			
	4.260208				0.189376			
	PC				**PET**			
	P_2/P_1	**Mean**	**SD**	**RSD%**	**P_2/P_1**	**Mean**	**SD**	**RSD%**
	3.345708	2.06	1.28	61.99	163.0208	99.80	38.566	38.64
	1.201445				110.6812			
	2.051113				75.11665			
	3.272278				76.67114			
	0.428702				73.53339			
Airborne samples	**PS, (**rural 5.09.2023, night)				**PS, (**rural 1.01.2024, night)			
	P_2/P_1	**Mean**	**SD**	**RSD%**	**P_2/P_1**	**Mean**	**SD**	**RSD%**
	1.938898	2.00	0.09	4.71	2.178203096	2.34	0.31	13.21
	1.905579				1.905765975			
	2.029989				2.645650140			
	2.114389				2.344625015			
	-				2.610131497			
	PP, (urban 12.08.2023, day, Backup)							
	P_2/P_1	**Mean**	**SD**	**RSD%**				
	0.285714	0.28	0	0				
	0.285714							

APPENDIX- B

RESULTS AND DISCUSSIONS

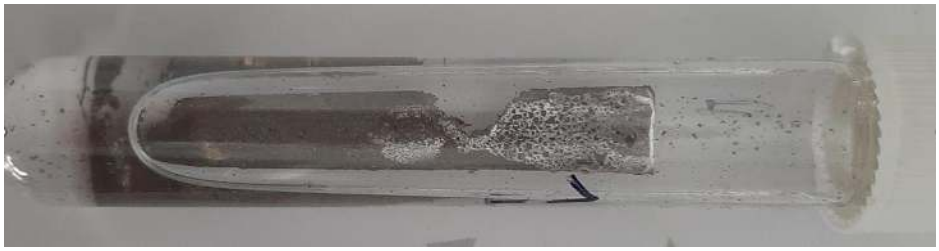

Figure B. 1. *The piece of Al filter under ultrasonic bathing.*

Table B. 1. *A comparison of the densities of airborne particulate matter (PM), constituents (<10 μm) and virgin microplastics (MPs).*

Polymer type	Density ($g\ cm^{-3}$)	PM type (2.5 -10 μm)	Density ($g\ cm^{-3}$)	Reference
Polyethylene (PE)	0.910-0.925	NH_4HSO_4	1.78	(Stelson, 1990)
Ethylene-vinyl acetate (EVA)	0.93-0.95	$(NH_4)_3H(SO_4)_2$	1.83	(Stelson, 1990)
Polyethylene (HDPE)	0.959-0.965	$(NH4)_2SO_4$	1.77	(Tang, 1996)
Polypropylene (PP)	0.90-0.91	NH_4NO_3	1.73	(Tang, 1996)
Polyamide (Nylon)	1.02-1.05	$CaSO_4$	2.3	(Horvath, 1998)
Polystyrene (PS)	1.04-1.1	$NaNO_3$	2.26	(Tang, 1996)
Acrylonitrile butadiene styrene (ABS)	1.05-1.18	NaCl	2.2	(Tang, 1996)
Acrylic	1.09-1.2	OC (organic carbon)	1.2	(Ebert et al., 2004)
Polyphenylene ether (PPE)	1.10-1.13	EC (elemental carbon)	2	(Lowenthal et al., 2000)
Polyamide (Nylon 6)	1.13-1.15	Al_2O_3	3.97	(Stelson, 1990)
Polyvinylchloride (PVC)	1.16-1.58	MgO	2.58	(Stelson, 1990)
Polymethyl methacrylate (PMMA)	1.16-1.20	Sea salts	2.20	(Horvath, 1998)
Polycarbonate (PC)	1.20_1.22	Silicates	2.60	(Horvath, 1998)
Polyurethane (PU)	1.20-1.26	Carbonates	2.70	(Horvath, 1998)
Alkyd	1.24-2.10	Biological	1.30	(Horvath, 1998)

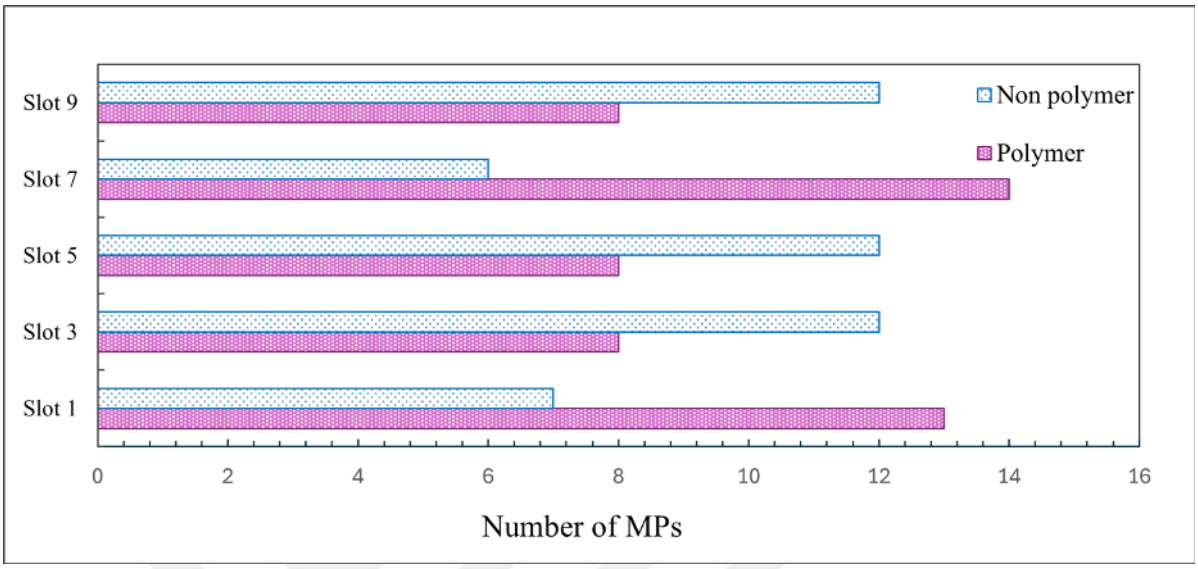

Figure B. 2. *The number of MPs identified in various slots in stage 1 by spectrometric analysis to investigate homogenous MNPs distribution.*

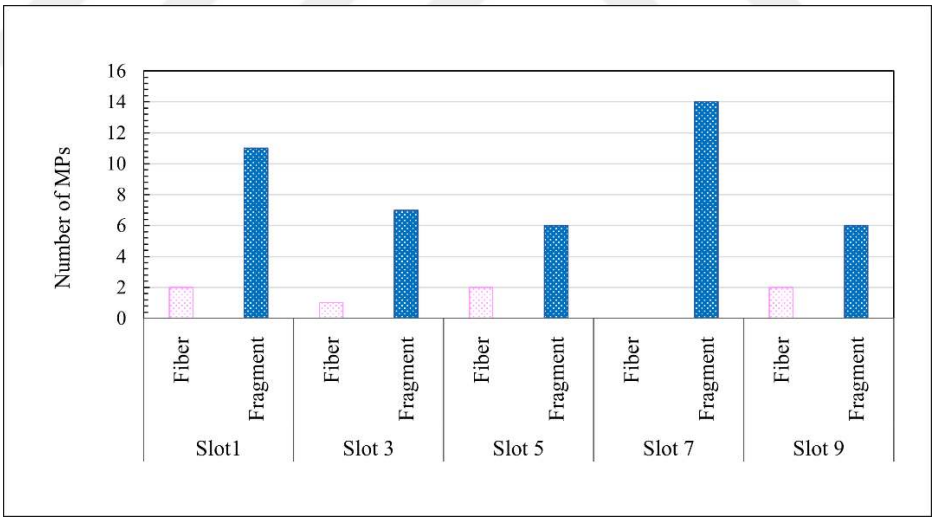

Figure B. 3. *Number of MNPs based on morphological characterization in stage 1(flow rate 40 cfm in 24 hours).*

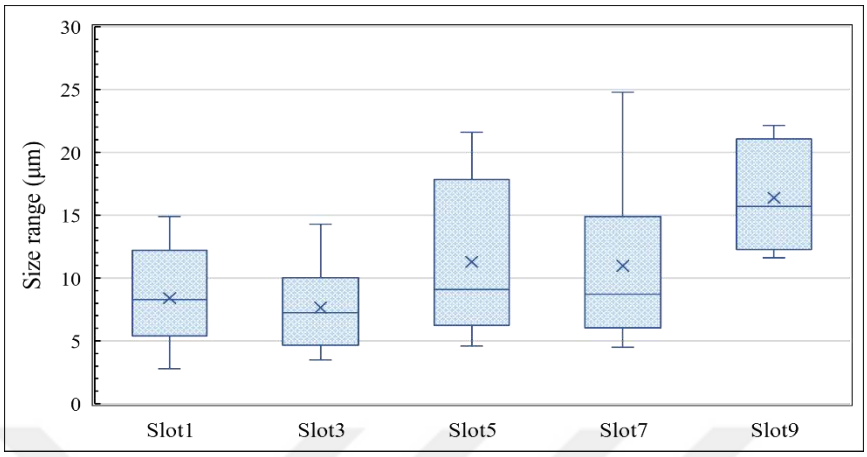

Figure B. 4. *Size distribution of MP fragments in different slots of stage 1(flow rate 40 cfm in 24 hours).*

.

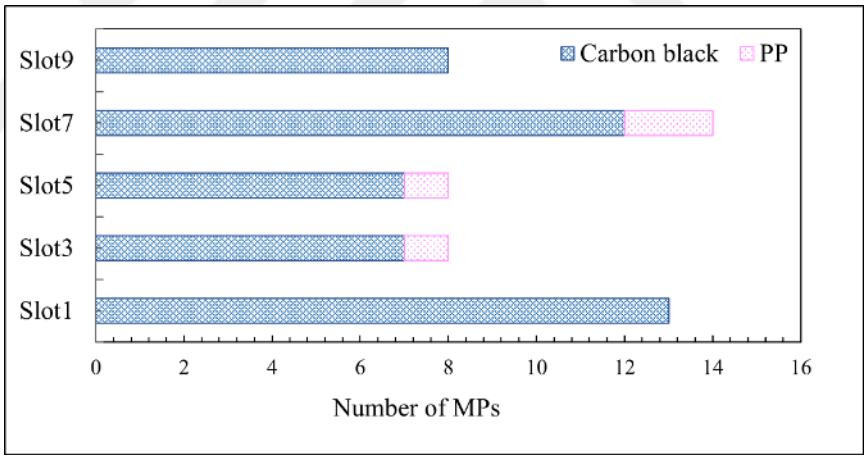

Figure B. 5. *Chemical composition of MNPs in stage 1(flow rate 40 cfm in 24 hours).*

.

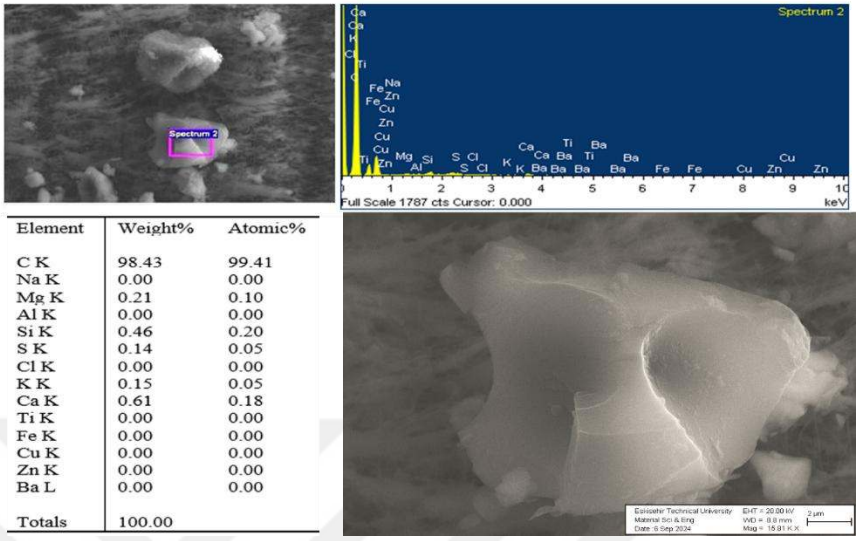

Element	Weight%	Atomic%
C K	98.43	99.41
Na K	0.00	0.00
Mg K	0.21	0.10
Al K	0.00	0.00
Si K	0.46	0.20
S K	0.14	0.05
Cl K	0.00	0.00
K K	0.15	0.05
Ca K	0.61	0.18
Ti K	0.00	0.00
Fe K	0.00	0.00
Cu K	0.00	0.00
Zn K	0.00	0.00
Ba L	0.00	0.00
Totals	100.00	

Figure B. 6. *A particle selected for chemical identification by Raman spectrometry.*

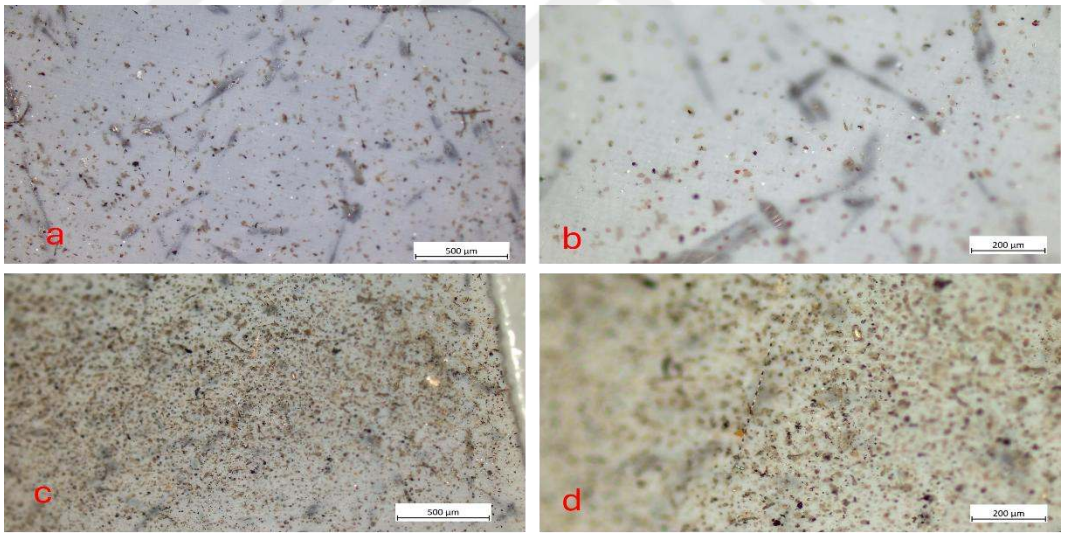

Figure B. 7. *Particles collected in two primary stages, a & b) stage 1 (x5, x10), c & d) stage 2 (x5, x10) objective.*

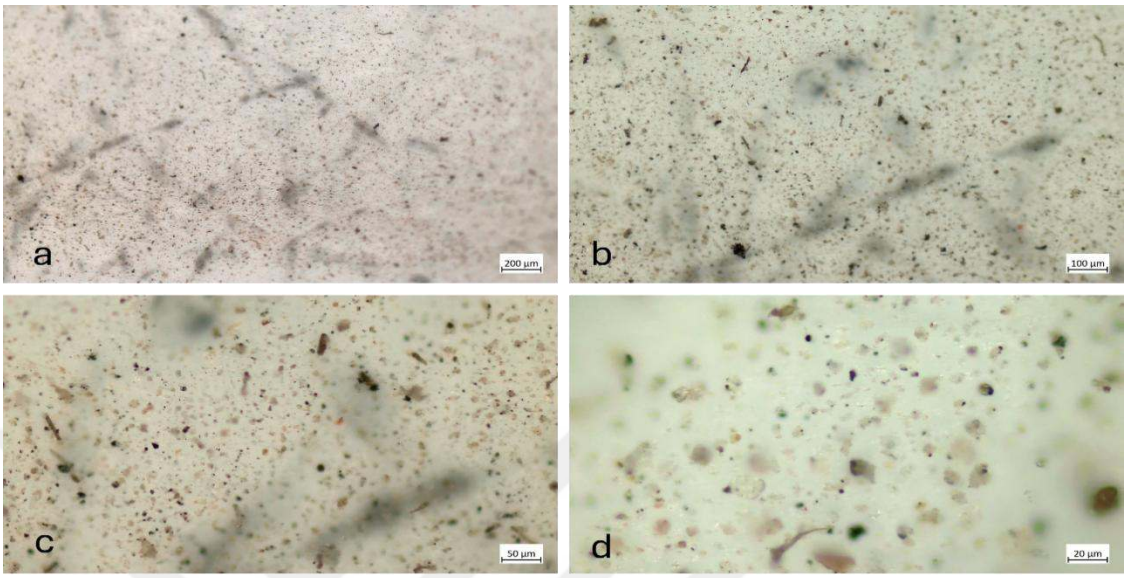

Figure B. 8. *Particles collected in stage 3 (40 cfm & 24 hours), a) x5, b) x10, c) x20, d) x50 objective*.

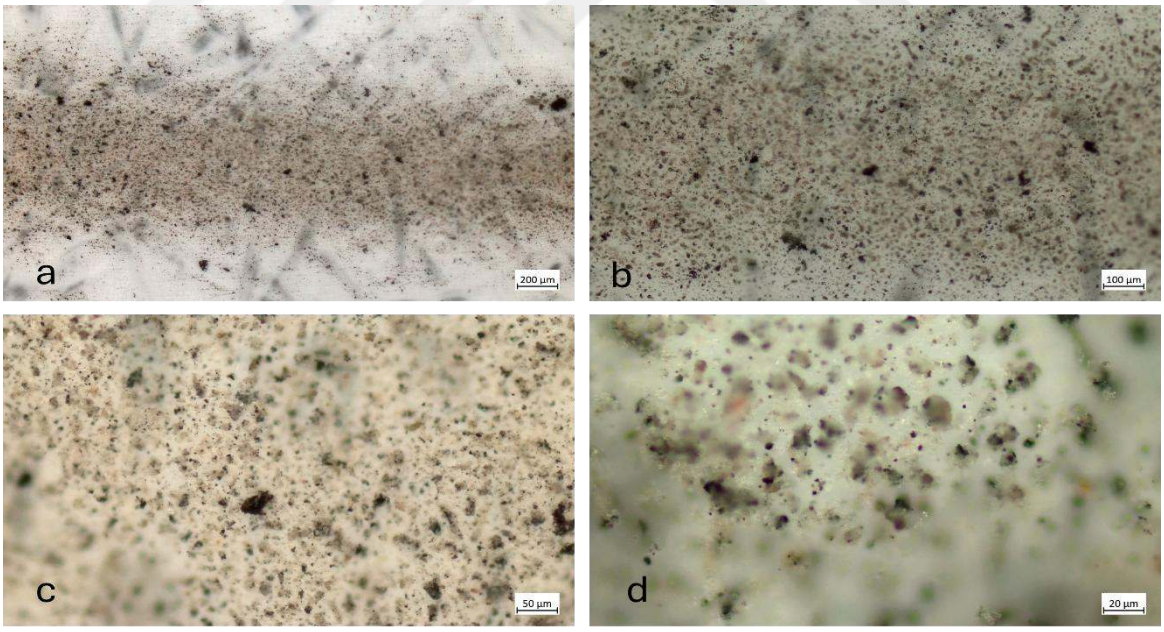

Figure B. 9. *Particles collected in stage 4 (40 cfm & 24 hours), a) x5, b) x10, c) x20, d) x50 objective.*

Table B. 2. *Particle distribution collected in stages 1, 2, 3, and 4. a-e) 5x; b, f) 10x; c, g) 20x; d, h) 50x objective.*

Stage 1 (24 hrs)		Stage 1 (12 hrs)		Stage 1 (8 hrs)		Stage 1 (4 hrs)	
20	40	20	40	20	40	20	40
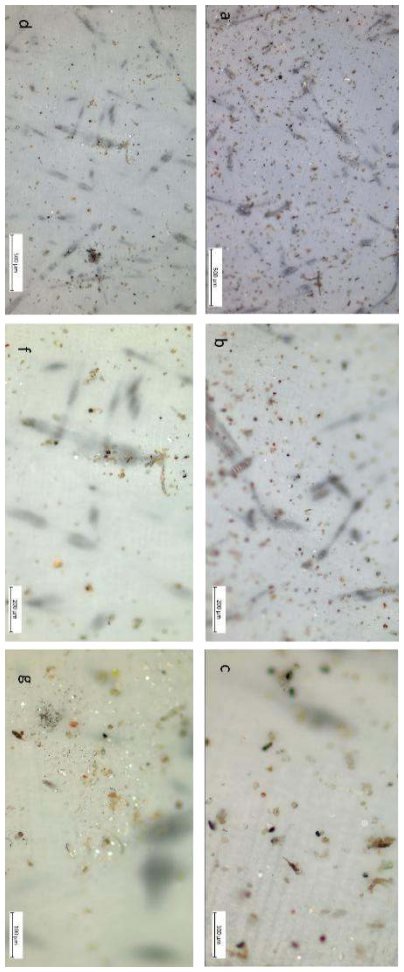		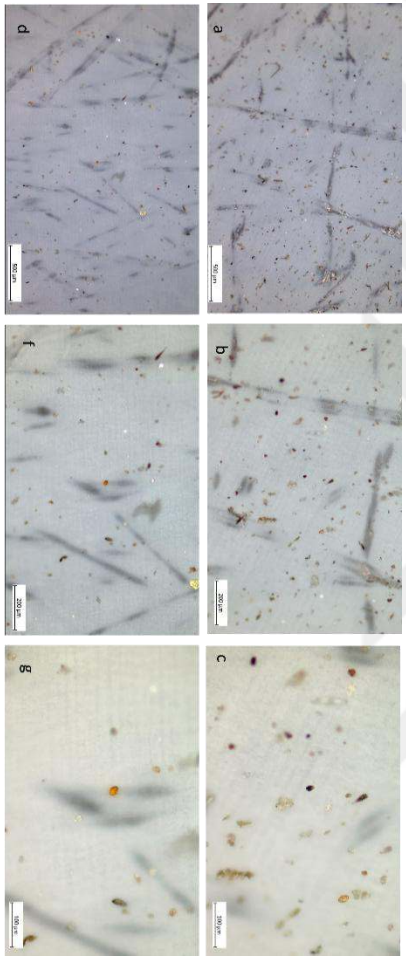		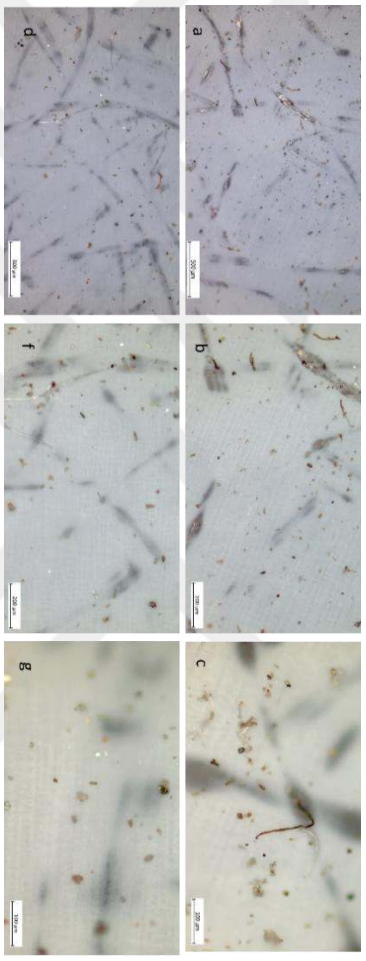		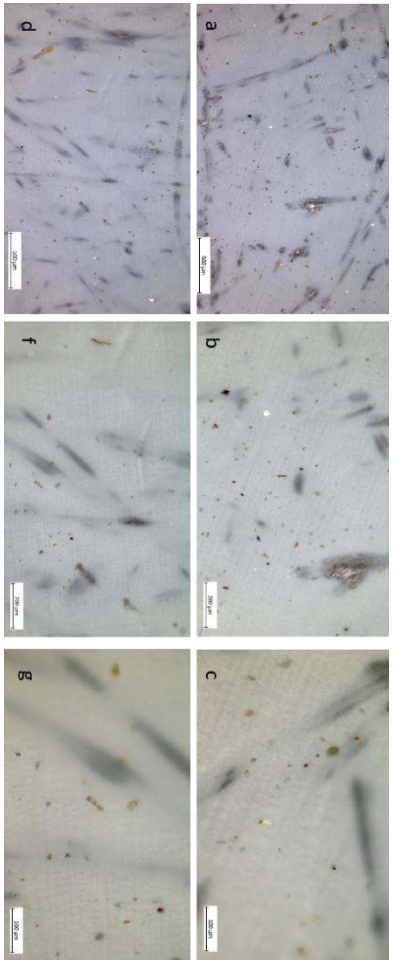	

Stage 2 (24 hrs)		Stage 2 (12 hrs)		Stage 2 (8hrs)		Stage 2 (4hrs)	
20	40	20	40	20	40	20	40
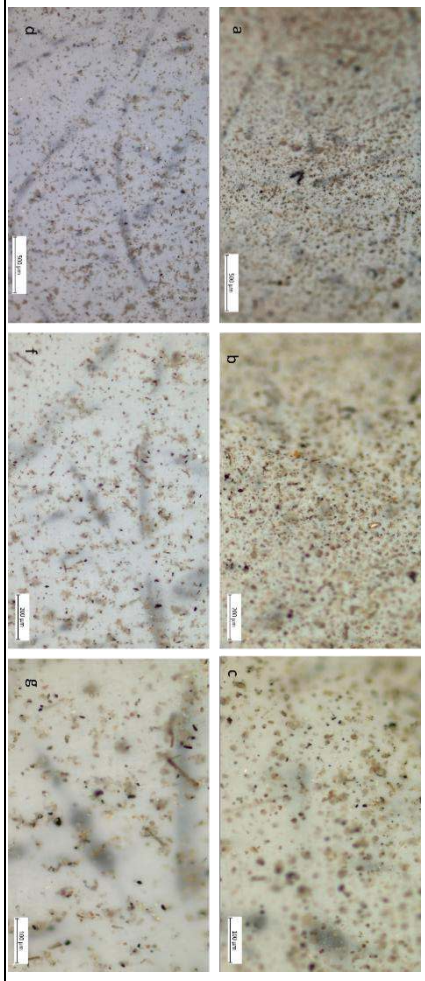		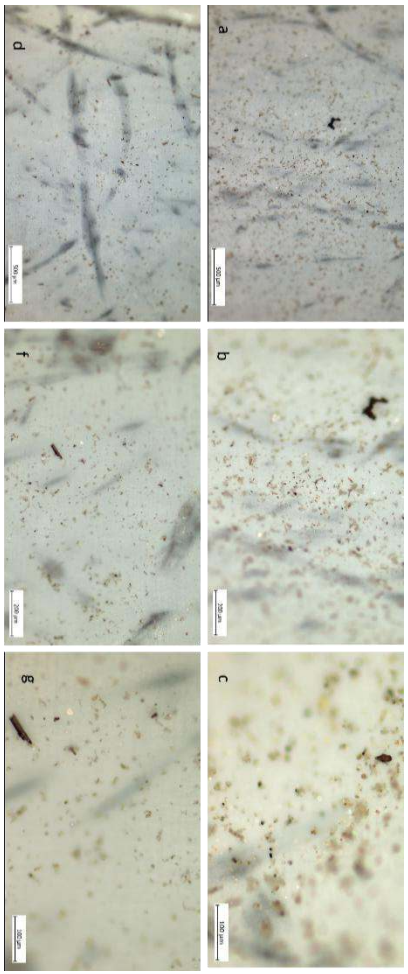		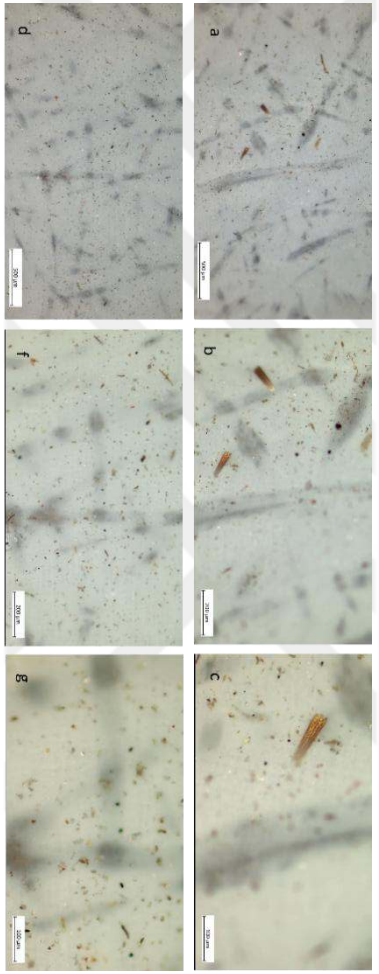		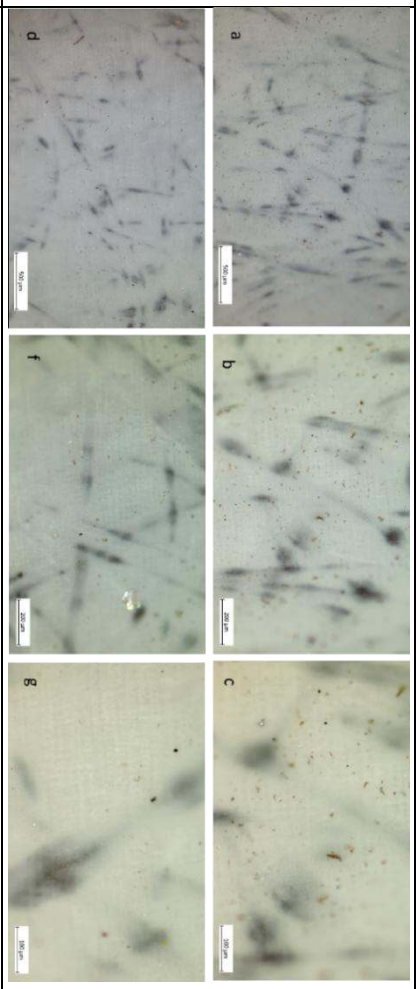	

Stage 3 (4 hrs)		Stage 3 (8 hrs)		Stage 3 (12 hrs)		Stage 3 (24 hrs)	
20	40	20	40	20	40	20	40
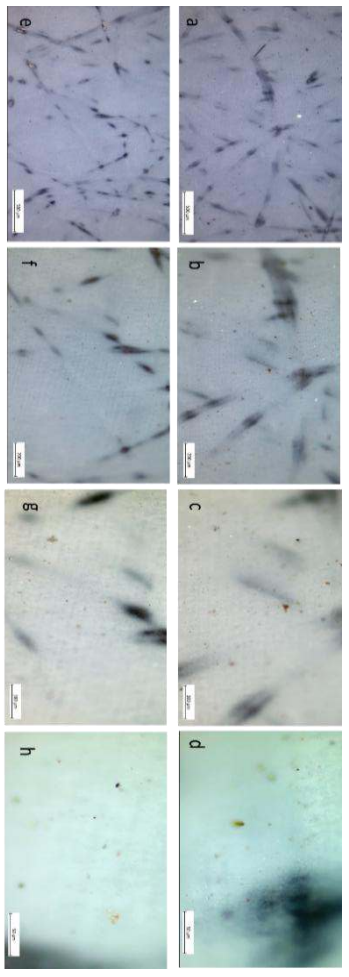		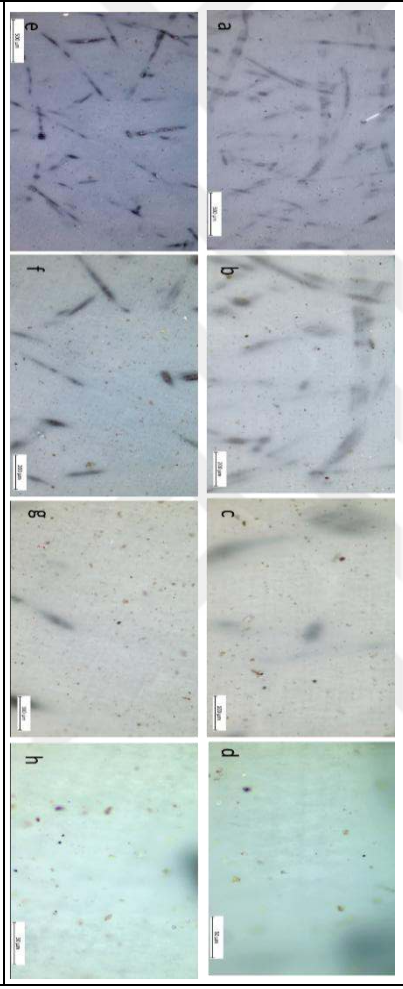		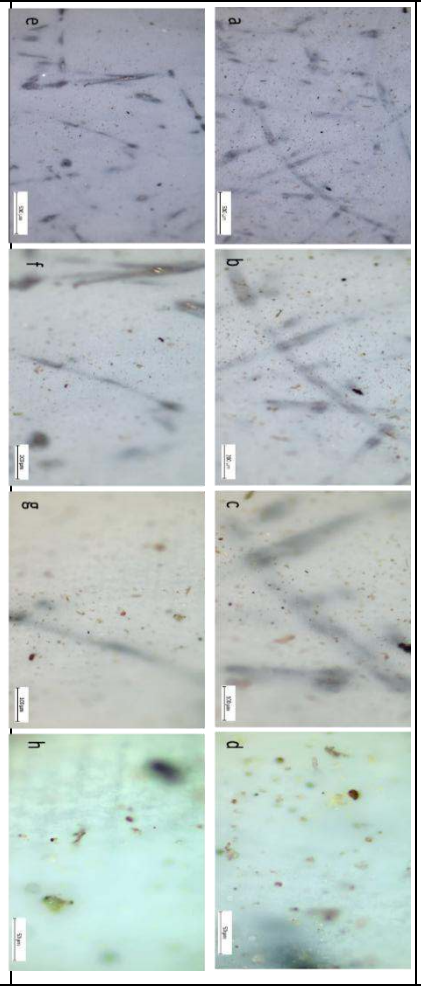		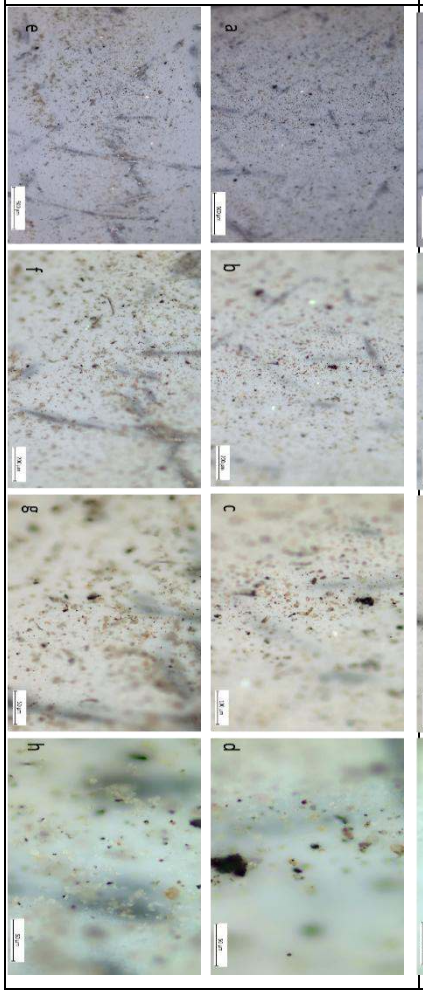	

Stage 5 (24 hrs)	Stage 5 (12 hrs)	Stage 5 (8 hrs)	Stage 5 (4 hrs)
20 40	20 40	20 40	20 40
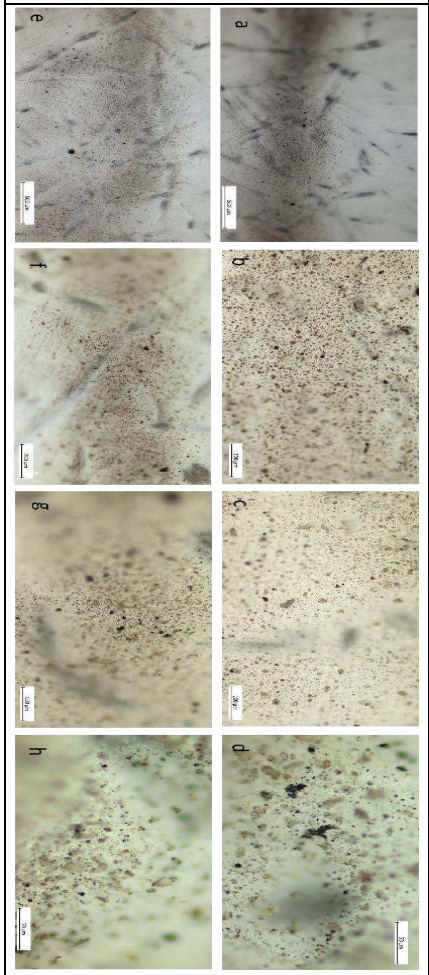	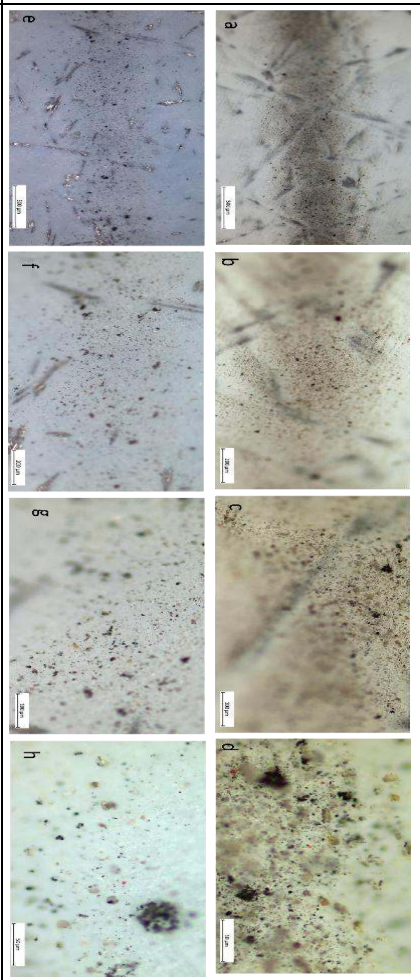	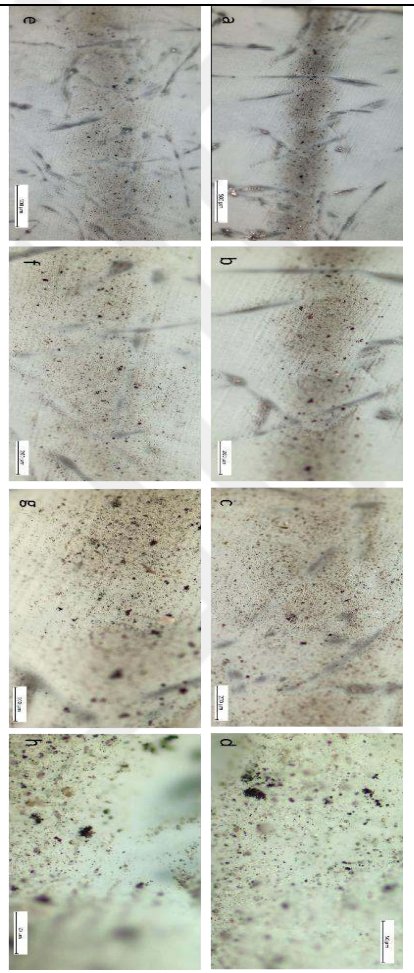	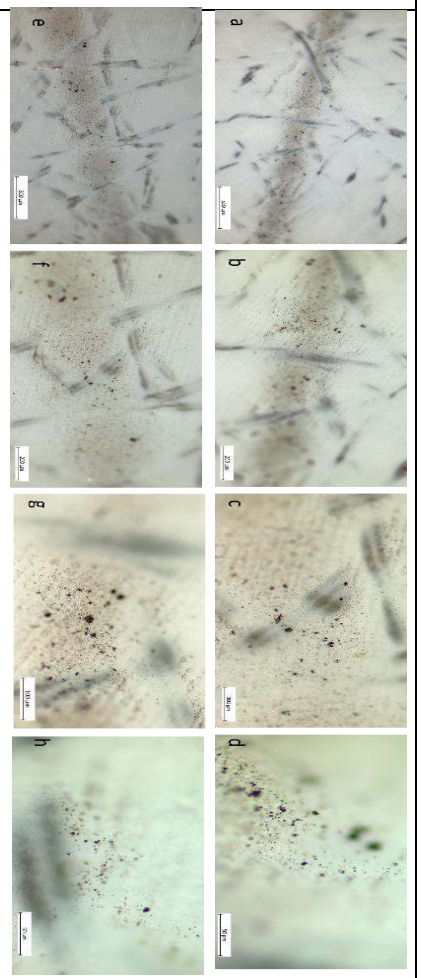

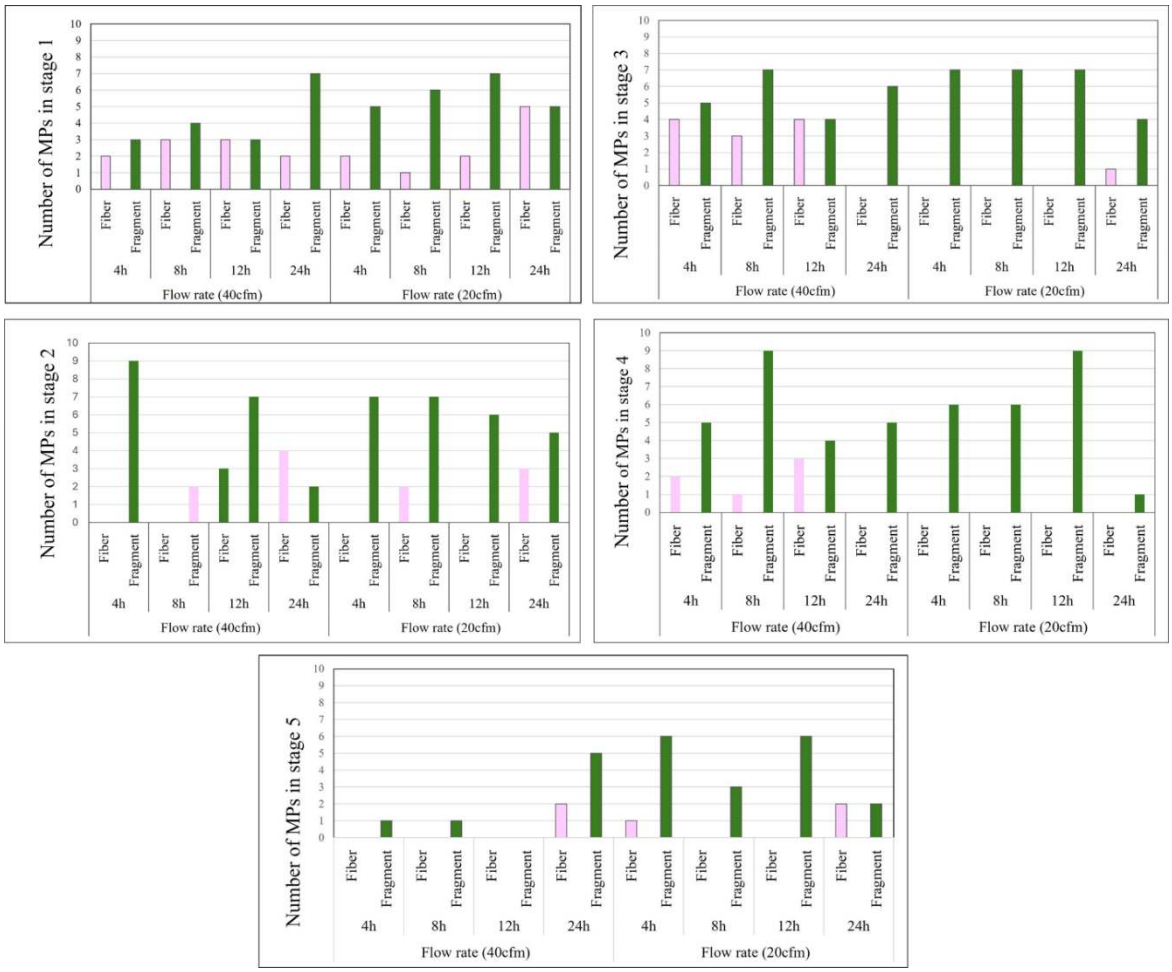

Figure B. 10. *Number of MNPs at different stages with variation of sampling parameters.*

Table B. 3. *Morphological characteristics of MNPs at different stages and different sampling parameters.*

Stage	Flow rate (cfm) & cascade size range (µm)	Sampling duration (h)	Fragment				Fiber				Total Concentration (MP/m^3)	Mean concentration (MP/m^3)	SD
			Number	Size range (µm)	Mean size (µm)	SD	Number	Size range (µm)	Mean size (µm)	SD			
1	20 (∞-10.2)	4	5	5.5-17.4	11.93	4.29	2	29-100.5	64.75	50.56	569	539	45
		8	6	5.3-22.5	12.30	7.28	1	-	39.7	-	474		
		12	7	5.3-27.7	14.35	7.58	2	37.3-69.5	53.40	22.77	569		
		24	5	13.4-23.7	18.13	3.97	5	21.7-101.6	50.52	31.94	542		
	40 (∞-7.2)	4	3	4.3-11.2	8.75	3.86	2	41.1-54.7	47.92	9.59	443	408	40
		8	4	5.6-31	18.05	10.76	3	32.8-72.5	57.93	21.79	434		
		12	3	6-13.3	8.68	4.01	3	20.4-138.7	60.88	67.41	355		
		24	7	9.8-38.1	18.29	9.14	2	27.4-59.1	43.26	22.42	399		
2	20 (10.2-4.2)	4	7	0.6-4.2	2.63	1.5	-	-	-	-	922	1123	311
		8	7	0.3-7.2	3.07	2.28	2	11.2-11.4	11.37	0.13	1581		
		12	6	3.4-18.1	8.09	5.3	-	16.7-33.2	-	_-	1054		
		24	5	4.8-18.3	9.8	5.2	3		23.52	8.66	937		
	40 (7.2-3)	4	9	4.2-31	10.36	8.38	-	-	-	-	1809	1278	636
		8	2	4.4-6.9	5.65	1.77	-	-	-	-	431		
		12	7	3.7-19.1	10.49	5.36	3	25.5-52.3	41.57	14.17	1723		
		24	2	2.7-6.5	4.6	2.69	4	12.4-30	21.7	7.26	1149		
3	20 (4.2-2.1)	4	7	1.5-3.2	2.03	0.68	-	-	-	-	2793	1808	802
		8	7	1.1-6.7	3.31	2.17	-	-	-	-	1745		
		12	7	0.9-4.3	2.67	1.06	-	-	-	-	1862		
		24	4	7.8-19.3	11.27	5.39	1	-	88.37	-	831		
	40 (3-1.5)	4	5	3-16	7.03	5.24	4	27.7-92.5	52.75	27.84	1174	1202	347
		8	7	2.4-8.8	6	2.1	3	16.5-44.7	26.83	15.55	1631		
		12	4	4.9-15.9	7.87	5.36	4	20.2-50.7	36.28	16.05	1218		
		24	6	3.8-44.8	1.6	26	-	-	-	-	783		
4	20 (2,1-1.3)	4	6	0.5-4	2.02	1.5	-	-	-	-	878	679	416
		8	6	1.1-3.3	1.92	0.78	-	-	-	-	732		
		12	9	0.8-8	2.5	2.14	-	-	-	-	1024		
		24	1	-	43.35	-	-	-	-	-	81		
	40 (1.5-0.95)	4	5	1.7-18.9	7.66	6.77	2	17-23.8	20.48	4.81	670	713	327
		8	9	1.2-18.1	8.42	5.88	1	-	25	-	1117		
		12	4	4.6-5.4	5.02	0.35	3	20.7-88.4	60.87	35.57	745		
		24	5	1.4-2	1.6	0.38	-	-	-	-	319		

Table B. 3. (Continued) *Morphological characteristics of MNPs at different stages and different sampling parameters.*

Stage	Flow rate (cfm) & cascade size range (µm)	Sampling duration (h)	Fragment				Fiber				Total Concentration (MP/m^3)	Mean concentration (MP/m^3)	SD
			Number	Size range (µm)	Mean size (µm)	SD	Number	Size range (µm)	Mean size (µm)	SD			
5	20 (1.3-0.69)	4	6	2-8.3	5.98	2.49	1	-	51.24	-	3415	1713	1188
		8	3	3.1-9.2	5.72	3.12	-	-	-	-	1016		
		12	6	1.8-7.7	4.18	2.09	-	-	-	-	1626		
		24	2	5.6-7.2	6.4	1.13	2	28.3-79	53.71	35.84	795		
	40 (0.95-0.49)	4	1	-	9.2	-	-		-	-	532	568	588
		8	1	-	18.7	-	-		-	-	355		
		12	-	-	-	-	-	-	-	-	0		
		24	5	6.1-16.8	11.32	3.9	2	35.8-46.4	41.1	7.5	1384		

Table B. 4. *Chemical characteristics of MNPs at different stages with different sampling parameter.*

Stage	Flow rate (cfm)	Sampling duration														
		4 (h)				8 (h)				12 (h)				24 (h)			
		Type	n	Mean of score (%)	SD	Type	n	Mean of score (%)	SD	Type	n	Mean of score (%)	SD	Type	n	Mean of score (%)	SD
1	40	Carbon black	5	82.57	7.1	Carbon black	5	80.8	6.07	Carbon black	5	78.33	3.47	Carbon black	4	83.91	3.59
		-	-	-	-	PTFE*	1	71.41	-	Polyacrylic	1	66.45	-	PP*	2	79.35	0.9
		-	-	-	-	-	-	-	-	-	-	-	-	PTFE	1	81.44	-
	20	Carbon black	6	81.32	16.76	Carbon black	7	85.01	11.54	Carbon black	8	71.75	15.96	Carbon black	8	76.4	15.89
		PP	1	80.96		-	-	-		PTFE	1	81.87		-	-	-	-
2	40	Carbon black	8	65.98	14.43	Carbon black	1	78.2		Carbon black	9	79.87	12.27	Carbon black	6	88.01	3.37
	20	Carbon black	7	78.87	18.48	Carbon black	9	73.52	18.48	Carbon black	6	83.05	22.95	Carbon black	8	84.62	7.95
3	40	Carbon black	9	66.2	14.51	Carbon black	10	83.77	3.41	Carbon black	8	79.19	14.82	Carbon black	6	79.12	17.72
	20	Carbon black	7	92.11	1.9	Carbon black	7	82.17	17	Carbon black	7	91.16	1.85	Carbon black	4	80.33	9.91
4	40	Carbon black	7	77.74	6.8	Carbon black	8	80.28	7.22	Carbon black	7	69.89	15.22	Carbon black	5	87.14	4.02
		-	-	-	-	PE*	2	56.92	9.5	-	-	-	-	-	-	-	-
	20	Carbon black	7	87	4.9	Carbon black	6	87.46	5.17	Carbon black	9	90.86	2.13	Carbon black	1	82.78	_
5	40	Carbon black	1	75.56	-	Carbon black	1	81.55	-	Carbon black		-	-	Carbon black	7	87.79	2.84
	20	Carbon black	6	85.02	10.02	Carbon black	1	88.07	-	Carbon black	6	72.78	14.79	Carbon black	4	86.7	14.57
		-	-	-	-	PE	2	62.93	2.8	-	-	-	-	-	-	-	-

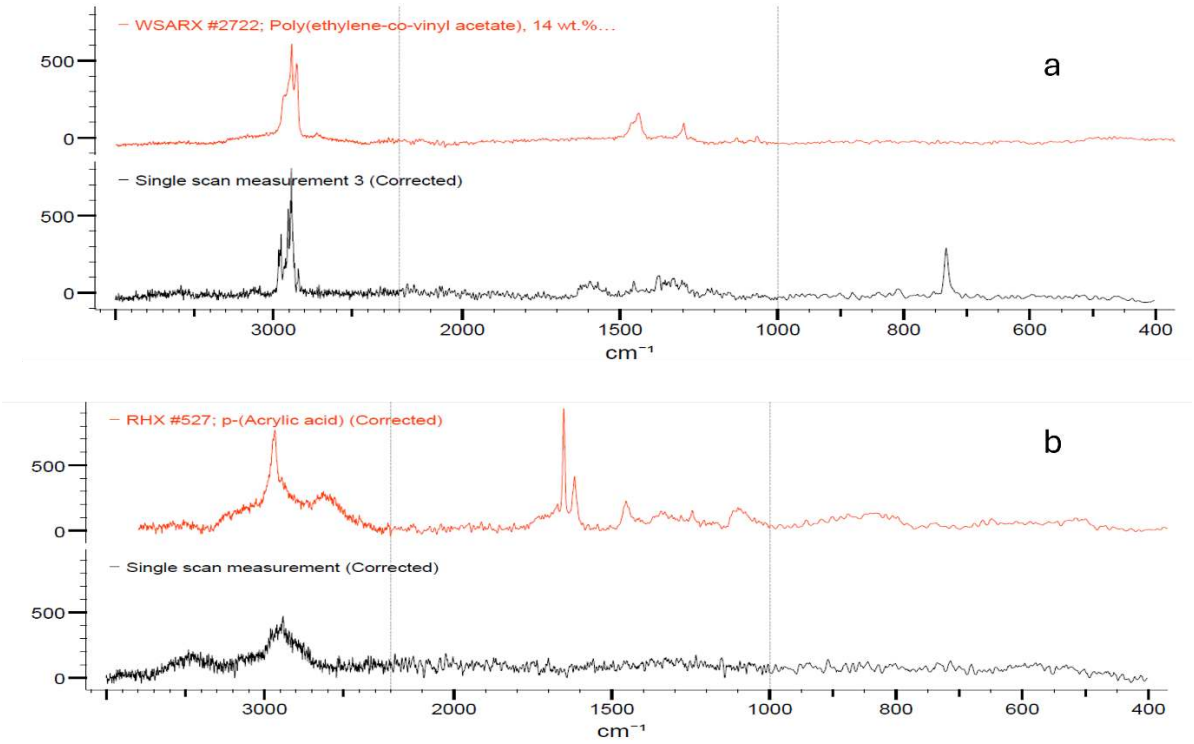

Figure B. 11. *Chemical identification of MNPs, Spectrometric peak of a) Polyethylene - matching ratio 66%, b) Polyacrylic - matching ratio 63%.*

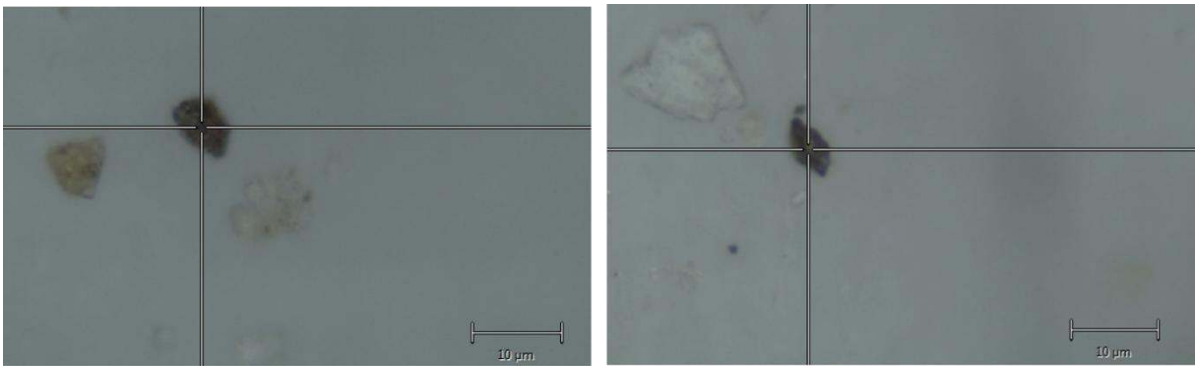

Figure B. 12. *Morphology of particles detected as Carbon black by micro-Raman.*

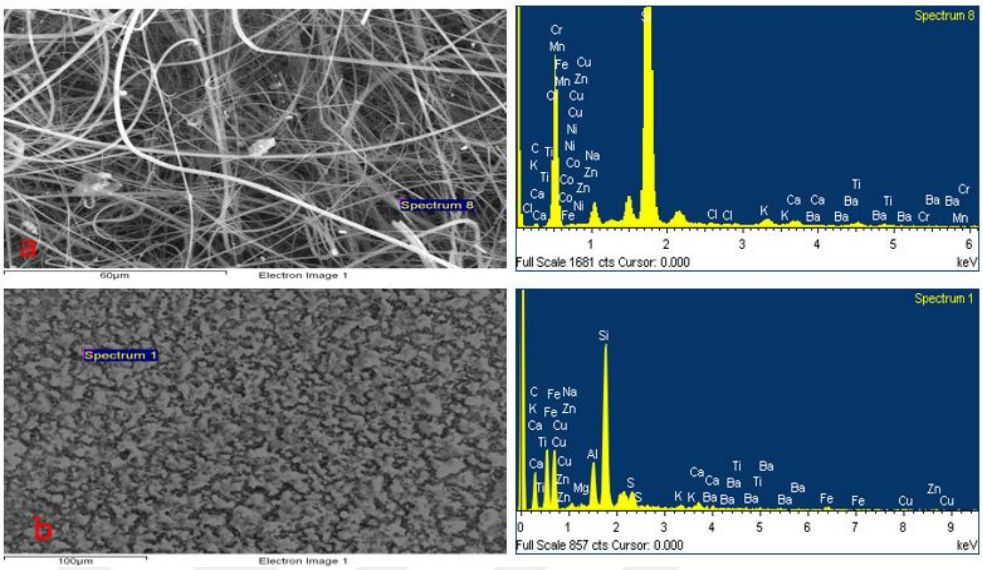

Figure B. 13. *SEM-EDS results, a) particles on the glass fiber filter in the backup stage, b) particles on the Teflon filter in stage 5.*

Table B. 5. *SEM-EDX results of backup stages in different regions.*

Element	Summer								Winter			
	Industrial		Urban		Rural				Rural			
	(02.08.2023)	(04.08.2023)	(21.08.2023)	(17.08.2023)	(05.09.2023)	(29.08.2023)	Mean	SD	(01.01.2024)	(31.12.2024)	Mean	SD
C	40.7	40.4	37.7	39.3	45.7	40.8	40.8	2.7	70.1	58.4	64.2	8.3
Na	2.7	4.4	4.2	5.9	3.3	4.1	4.1	1.1	3.5	4.9	4.2	1.0
Mg	0.9	1.1	0.8	1.0	0.4	0.8	0.8	0.3	0.2	0.0	0.1	0.1
Al	5.5	5.5	12.5	4.6	2.6	6.1	6.1	3.3	2.4	1.9	2.2	0.3
Si	21.9	28.4	28.4	31.0	20.1	25.9	25.9	4.2	13.1	20.4	16.8	5.2
S	0.0	0.0	0.0	1.1	0.0	0.2	0.2	0.4	0.8	0.2	0.5	0.4
Cl	0.0	0.1	0.2	0.0	0.4	0.1	0.1	0.1	2.7	1.3	2.0	1.0
K	2.9	3.7	2.9	3.2	2.0	2.9	2.9	0.5	2.2	4.1	3.2	1.3
Ca	18.1	7.6	8.3	4.7	19.1	11.6	11.6	5.9	0.9	2.1	1.5	0.8
Ti	0.1	0.1	0.4	0.2	0.5	0.3	0.3	0.1	0.0	0.3	0.1	0.2
Fe	3.3	3.1	1.2	2.2	0.3	2.0	2.0	1.1	0.1	0.3	0.2	0.1
Cu	0.1	0.2	0.3	0.2	0.7	0.3	0.3	0.2	0.3	0.3	0.3	0.0
Zn	1.6	2.0	1.6	2.6	2.1	2.0	2.0	0.4	1.8	3.3	2.5	1.1
Ba	2.3	3.3	2.1	4.1	3.3	3.0	3.0	0.7	1.8	3.9	2.8	1.5

- *The unit amount of elements is weight*

Table B. 6. *Morphological characteristics of MNPs in industrial zone.*

Location	Date	Time	Stage	Fragment				Fiber				Total
				Number	Range size(µm)	Mean size(µm)	SD size(µm)	Number	Range size(µm)	Mean size(µm)	SD size(µm)	Concentration (MP/m^3)
Industrial	02.08.2023	Day	Stage 1	4	2.2 - 10.7	6.1	3.7	-	-	-	-	773
			Stage 2	10	1.6 - 7.2	3.6	2	-	-	-	-	2685
			Stage 3	8	1.2 - 4.7	3	1	-	-	-	-	1627
			Stage 4	8	1.8 - 8.3	3.9	2	-	-	-	-	1114
			Stage 5	4	1 - 1.3	1.2	0.1	-	-	-	-	1768
	02.08.2023	Night	Stage 1	4	6.2 - 16.4	9.8	4.5	-	-	-	-	773
			Stage 2	2	13.1 - 13.3	13.2	0.1	-	-	-	-	537
			Stage 3	8	4.3 - 16.3	8.6	3.8	-	-	-	-	1627
			Stage 4	10	0.7 - 8.6	1.9	2.4	-	-	-	-	1392
			Stage 5	6	0.7 - 1.6	1.1	0.4	-	-	-	-	2652
	07.08.2023	Day	Stage 1	7	1.5 - 6.7	3.9	2.2	2	8.4 - 10.8	9.6	1.7	1740
			Stage 2	7	1.1 -5.3	3.2	1.5	-	-	-	-	1880
			Stage 3	12	1.5 -2.8	2.9	1.4	-	-	-	-	2440
			Stage 4	12	1.2 - 4.1	2	0.9	1		10.4		1810
			Stage 5	17	0.9 - 5.3	2.1	1	-	-	-	-	7514
	07.08.2023	Night	Stage 1	5	5.7 - 12.1	7.5	2.7	1		53.4	53.4	1160
			Stage 2	6	2.2 - 11.7	6.2	3.5	2	56.5-70.4	63.5	9.8	2148
			Stage 3	11	1.2 - 6.4	3.6	1.3	-	-	-	-	2236
			Stage 4	13	0.6 - 3.2	1.3	0.8	-	-	-	-	1810
			Stage 5	10	0.7 -1.3	1.1	0.4	-	-	-	-	4420
	04.08.2023	Based on PM_{10} (High)	Stage 1	13	1.4 - 8.2	4.5	2.5	-	-	-	-	2514
			Stage 2	13	1.4 - 7.1	2.8	1.5	-	-	-	-	3491
			Stage 3	5	1 - 3.1	2	0.9	-	-	-	-	1017
			Stage 4	14	0.8 - 5.5	2.7	1.3	-	-	-	-	1949
			Stage 5	16	1 - 4.1	2.3	0.8	-	-	-	-	7072
	06.08.2023	Based on PM_{10} (Low)	Stage 1	9	2.2 - 5.5	3.9	1.1	-	-	-	-	1740
			Stage 2	10	1.5 - 8.2	2.9	2	-	-	-	-	2685
			Stage 3	7	1.1 - 4.1	2.5	1.1	1		8.3		1627
			Stage 4	16	1.3 - 3.8	2.1	0.7	-	-	-	-	2228
			Stage 5	15	1.1 - 5.2	2.7	1	-	-	-	-	6630

Table B. 7. *Morphological characteristics of MNPs in urban zone.*

Location	Date	Time	Stage	Fragment				Fiber				Total
				Number	Range size(µm)	Mean size(µm)	SD size(µm)	Number	Range size(µm)	Mean size(µm)	SD size(µm)	Concentration (MP/m^3)
Urban	21.08.2023	Day	Stage 1	9	2.2 - 9.6	4.6	2.3	1		16.4		1552
			Stage 2	10	1.5 - 4.3	3	1	3	11.6- 21.5	15.5	5.3	2801
			Stage 3	8	1 - 3.2	1.8	0.7	4	9.4 - 16.4	11.2	3.5	1958
			Stage 4	12	1.8 - 10.1	3.5	2.4					1341
			Stage 5	9	0.6 - 5.5	2.3	2.1					3192
	21.08.2023	Night	Stage 1	8	0.7 - 12.4	5.3	4					1241
			Stage 2	8	1.4 - 5.4	3.4	1.5					1724
			Stage 3	8	1.2 - 3.6	2.7	0.8					1305
			Stage 4	6	0.9 - 2.2	1.4	0.5					670
			Stage 5	9	0.6 - 5.5	2.3	2.1					3192
	22.08.2023	Day	Stage 1	9	0.9 - 9.4	5.9	3.1	1		9		1552
			Stage 2	14	1.6 - 5	2.9	1.1					3016
			Stage 3	15	1.2 - 5.3	2.5	1.1	1		23.6		2610
			Stage 4	16	1.5 - 6.8	3	1.4					1787
			Stage 5	18	1.6 - 5.1	2.7	1					6384
	22.08.2023	Night	Stage 1	11	1.8 - 13.5	5.8	4					1707
			Stage 2	5	1 - 8.6	4.9	2.8					1077
			Stage 3	7	0.6 - 2.8	1.5	0.9					1142
			Stage 4	6	0.4 - 1.4	1	0.4					670
			Stage 5	4	0.3 - 2.7	1.3	1.1					1419
	17.08.2023	Based on PM_{10} (High)	Stage 1	14	2.8 - 10.5	5.5	2.2	1		45.1		2327
			Stage 2	9	1.9 - 7.1	3.9	1.8					1939
			Stage 3	13	1.1 - 3.5	2.1	0.7	2	12.5 - 22.6	17.6	7.1	2427
			Stage 4	7	1.6 - 4.1	2.8	0.8					782
			Stage 5	8	1.1 - 3.9	2.3	0.9					2837
	20.08.2023	Based on PM_{10} (Low)	Stage 1	10	1.6 - 6.1	4.4	1.4					1552
			Stage 2	14	1.8 - 7.2	4	1.9	1		14.9		3016
			Stage 3	14	1.2 - 4.3	2.2	0.8	1		13.1		2447
			Stage 4	16	1.2 - 8.8	2.7	1.9	1		7.7		1899
			Stage 5	13	1.4 - 3.6	2.4	0.6					4610

Table B. 8. *Morphological characteristics of MNPs in rural zone (summer & winter).*

Location	Date	Time	Stage	Fragment				Fiber				Total
				Number	Range size(μm)	Mean size(μm)	SD size(μm)	Number	Range size(μm)	Mean size(μm)	SD size(μm)	Concentration (MP/m^3)
Rural (summer)	05.09.2023	Day	Stage 1	9	1.7-10.6	4.8	2.9	1	-	19.9		1552
			Stage 2	7	1.8-3.8	2.6	0.8	2	-	16.5	6	1939
			Stage 3	10	1-8.7	3.2	2.5	1	-	9.7	-	1794
			Stage 4	10	1.2-4.5	2.3	1	-	-	-	-	1117
			Stage 5	6	1.3-5.7	4.1	1.6	-	-	-	-	2128
	05.09.2023	Night	Stage 1	8	0.98-10.3	5.9	3.2	2	19.8-50.3	35.1	21.6	1552
			Stage 2	8	1.06-6.9	4.9	2.1	-	-	-	-	1724
			Stage 3	9	0.9-4.9	2.5	1.2	1	-	10.5	-	1631
			Stage 4	9	1.2-2.03	1.6	0.3	-	-	-	-	1005
			Stage 5	3	1.2-1.7	1.4	0.3	-	-	-	-	1064
	06.09.2023	Day	Stage 1	6	1.3-7.1	3.7	2.5	-	-	-	-	931
			Stage 2	10	1.1-2.1	2	1.1	-	-	-	-	2154
			Stage 3	12	0.9-3.1	1.7	0.8	1	-	24	-	2121
			Stage 4	12	1.3-3.8	2.4	0.7	-	-	-	-	1341
			Stage 5	13	1.4-2.6	1.9	0.4	-	-	-	-	4610
	06.09.2023	Night	Stage 1	2	6.9-8.1	7.5	0.8	1	-	24.3		465
			Stage 2	11	1.4-3.9	2.4	0.8	-	-	-	-	2370
			Stage 3	11	1.5-15.3	5.5	4.9	-	-	-	-	1794
			Stage 4	8	0.8-4.8	2.1	1.3	-	-	-	-	894
			Stage 5	8	1.1-3.3	2.1	0.9	-	-	-	-	2837
	29.08.2023	Based on PM_{10} (High)	Stage 1	10	2.1-9.2	5.3	2.2	-	-	-	-	1552
			Stage 2	16	2.5-7.3	4.3	1.5	-	-	-	-	3447
			Stage 3	13	1.2-5.5	2.9	1.2	-	-	-	-	2121
			Stage 4	18	1.6-5.6	3.1	1.1	-	-	-	-	2011
			Stage 5	10	1.5-3.6	2.2	0.8	-	-	-	-	3546
	03.09.2023	Based on PM_{10} (Low)	Stage 1	6	1.8-5.3	3.4	1.4	-	-	-	-	931
			Stage 2	11	1.4-9.1	3.6	2.1	2	7.6-19.4	13.5	8.3	2801
			Stage 3	17	1.6-4.9	3	1	1	-	8.2	-	2936
			Stage 4	15	1.3-4.8	2.4	1	1	-	11.5	-	1787
			Stage 5	10	1.3-4.7	2.3	1.2	-	-	-	-	3546

Table B. 8. **(Continued)** *Morphological characteristics of MNPs in rural zone (summer & winter)*.

Location	Date	Time	Stage	Fragment				Fiber				Total
				Number	Range size(µm)	Mean size(µm)	SD size(µm)	Number	Range size(µm)	Mean size(µm)	SD size(µm)	Concentration (MP/m^3)
Rural (winter)	01.01.2024	Day	Stage 1	7	3-12.8	6.1	3.6					1862
			Stage 2	10	2.2-6.1	3.8	1.1	2	25.9-48.4	37.2	15.9	1939
			Stage 3	12	1.8-5.1	3.3	1.1	-	-	-	-	2610
			Stage 4	13	1.4-2.7	1.9	0.4	-	-	-	-	1452
			Stage 5	12	0.9-2.9	1.5	0.6	-	-	-	-	2482
	01.01.2024	Night	Stage 1	12	1.2- 7.8	3.4	1.4	-	-	-	-	1086
			Stage 2	9	1.4- 5.2	2.7	1.2	-	-	-	-	2585
			Stage 3	16	1.3- 10.4	2.6	2.2	-	-	-	-	1958
			Stage 4	13	1.1-2.1	1.4	0.3	-	-	-	-	1452
			Stage 5	7	0.9-3	1.9	0.7	-	-	-	-	4256
			Stage 5	10	1.5-3.6	2.2	0.8	-	-	-	-	3546

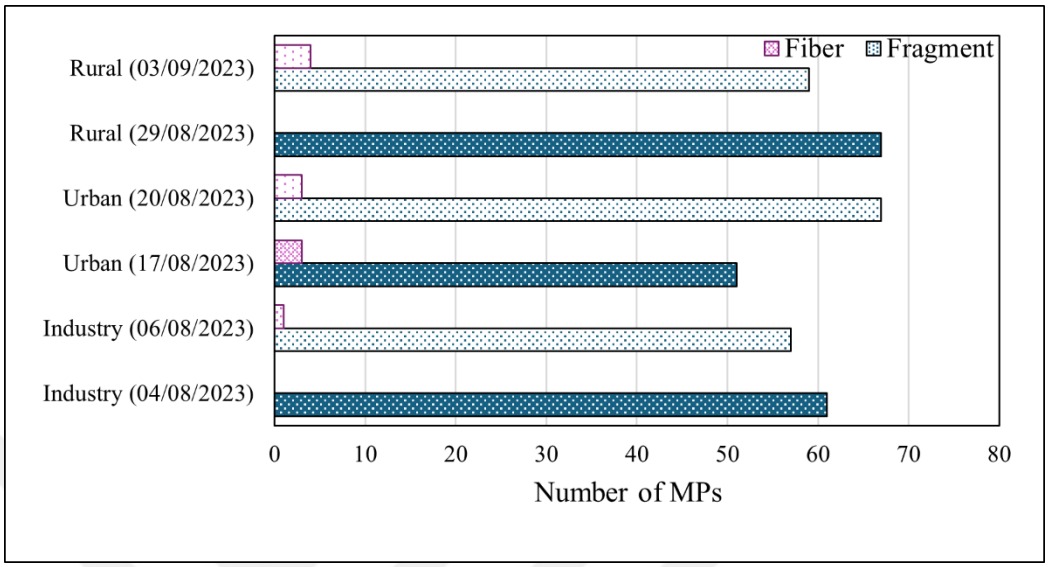

Figure B. 14. *Morphological number of MNPs in three sampling locations (dark color: day that PM_{10} was high, and light color: day PM_{10} was low.*

Table B. 9. *Chemical characteristics MNPs with matching ratio > 70%.*

Location	Stage1				Stage 2				Stage 3				Stage 4				Stage 5			
	Type of MP	Number	Mean Score (%)	SD	Type of MP	Number	Mean Score (%)	SD	Type of MP	Number	Mean Score (%)	SD	Type of MP	Number	Mean Score (%)	SD	Type of MP	Number	Mean Score (%)	SD
Industrial (02 .08.2023 Day)	Carbon black	4	92.8	3	Carbon black	10	89.9	6.3	Carbon black	8	90.5	5	Carbon black	8	86.3	6.3	Carbon black	4	81.2	1
Industrial (02 .08.2023 Night)	Carbon black	4	82.4	8.4	Carbon black	2	75.9	0.3	Carbon black	8	86.7	4	Carbon black	10	89.4	3.3	Carbon black	6	85.5	8.3
Industrial (07 .08.2023 Day)	Carbon black	7	82.8	6	Carbon black	7	89.4	5.4	Carbon black	12	88.4	5.3	Carbon black	13	85.7	3.2	Carbon black	17	84.6	4.8
Industrial (07 .08.2023 Night)	Carbon black	6	86.2	4.2	Carbon black	8	86.8	2.7	Carbon black	11	91.1	4	Carbon black	13	90.8	5.6	Carbon black	10	88.9	5.3
Industrial (04 .08.2023 Day)	Carbon black	13	85.3	5.2	Carbon black	13	85.9	5.7	Carbon black	5	83.8	6.9	Carbon black	14	86.9	5.6	Carbon black	16	84.9	4.3
Industrial (06 .08.2023 Day)	Carbon black	10	86.2	5.3	Carbon black	10	84.6	5.6	Carbon black	8	85	6.5	Carbon black	16	88.2	5.1	Carbon black	15	86.2	4.5
Urban (21.08.2023-Day)	Carbon black	10	90.7	4	Carbon black	13	88.1	4.8	Carbon black	12	89.6	6.7	Carbon black	12	90	6.1	Carbon black	9	85.9	5.7
Urban (21.08.2023-Night)	Carbon black	8	89.3	5	Carbon black	7	92.3	3.6	Carbon black	8	92.9	2.2	Carbon black	8	90.5	4.3	Carbon black	6	85.2	3.6
Urban (22.08.2023-Day)	Carbon black	10	86.4	3.4	Carbon black	15	85.9	5.6	Carbon black	16	84.6	5.2	Carbon black	16	85.3	5	Carbon black	18	85.4	5
Urban (22.08.2023-Night)	Carbon black	11	91.5	2.8	Carbon black	5	85.7	5.5	Carbon black	7	90.1	4	Carbon black	6	93.1	2.3	Carbon black	4	85.4	6.6

Table B. 9. (Continued) *Chemical characteristics MNPs with matching ratio > 70%.*

Location	Stage1				Stage 2				Stage 3				Stage 4				Stage 5			
	Type of MP	Number	Mean Score (%)	SD	Type of MP	Number	Mean Score (%)	SD	Type of MP	Number	Mean Score (%)	SD	Type of MP	Number	Mean Score (%)	SD	Type of MP	Number	Mean Score (%)	SD
Urban (17.08.2023-Day)	Carbon black	14	86.8	5	Carbon black	10	87.3	5.1	Carbon black	15	83.3	5	Carbon black	7	84.2	4.9	Carbon black	8	83.1	6.8
Urban (20.08.2023-Day)	Carbon black	10	89.1	4.5	Carbon black	15	89.6	3.3	Carbon black	14	90	4.3	Carbon black	17	88.2	5.5	Carbon black	13	84.9	3.8
Rural (05.09.2023-Day)	Carbon black	10	88.4	6	Carbon black	9	84.3	7.9	Carbon black	11	84.4	7.4	Carbon black	10	88.7	3.7	Carbon black	6	86	5.9
Rural (05.09.2023-Night)	Carbon black	10	89.6	5.4	Carbon black	8	92.7	1.9	Carbon black	10	91.8	1.6	Carbon black	9	90.3	3.2	Carbon black	3	80.5	4.3
Rural (06.09.2023-Day	Carbon black	5	87.2	2.9	Carbon black	10	88.8	5.2	Carbon black	13	88.7	5.5	Carbon black	12	85.4	6.1	Carbon black	13	83.7	4.9
	PTFE	1	71										Carbon black	8	87.8	5.6	Carbon black	8	85.4	6.4
Rural (06.09.2023-Night)	Carbon black	3	84.9	2.3	Carbon black	11	89.5	4.1	Carbon black	11	90.2	3.3	Carbon black	18	86.3	4.4	Carbon black	10	82.8	4
Rural (29.08.2023-Day	Carbon black	10	88.1	3.7	Carbon black	16	87.5	4.1	Carbon black	13	89	3.3	Carbon black	16	88	3.2	Carbon black	9	83.3	4.6
Rural (03.09.2023-Day	Carbon black	6	81.5	5.2	Carbon black	13	88.6	2.7	Carbon black	18	88.5	3	Carbon black	13	87.3	3.1	Carbon black	12	85.1	2.5
Rural (01.01.2024-Day	Carbon black	7	86.7	4.8	Carbon black	12	84.9	5.4	Carbon black	12	87.8	5.9	Carbon black	13	85.5	2.7	Carbon black	7	85.5	2
Rural (01.01.2024-Night)	Carbon black	12	87.2	5.4	Carbon black	9	85.6	3.9	Carbon black	16	87.6	3.4	Carbon black	13	88.2	2.5	Carbon black	12	85.3	2.8

Table B. 9. (Continued) *Chemical characteristics MNPs with matching ratio > 70%.*

Location	Stage1				Stage 2				Stage 3				Stage 4				Stage 5			
	Type of MP	Number	Mean Score (%)	SD	Type of MP	Number	Mean Score (%)	SD	Type of MP	Number	Mean Score (%)	SD	Type of MP	Number	Mean Score (%)	SD	Type of MP	Number	Mean Score (%)	SD
Rural (31.12.2023-Day	Carbon black	8	88.2	2.3	Carbon black	14	88.8	3.3	Carbon black	14	89.2	3.8	Carbon black	16	85.3	5	Carbon black	18	85.4	5
	PTFE	1	75.1										Carbon black	6	93.1	2.3	Carbon black	4	85.4	6.6

Table B. 10. *Chemical characteristics MNPs in industrial zone with matching ratio > 40% (another materials pigments…).*

Location	Stage1			Stage 2			Stage 3			Stage 4			Stage5		
	Type of MP	Number	Score%	Type of MP	Number	Score%	Type of MP	Number	Score%	Type of MP	Number	Score%	Type of MP	Number	Score%
Industrial (2 August Day)	Graphite	1	91.8				Nylon 6	1	54.3						
	Burnt Umber	1	62				p- (Acrylic acid)	1	60.8						
	Iron Chromium Oxide	1	64.8				Graphite	1	87.9						
	Astra Blue Base		63.6												
	Carbon Black	2	59.8 /66.9	Carbon Black	2	50.5/66	-	-	-	Carbon Black	1	68	Carbon Black	2	49.8/ 43.1
	-	-	-	Poly (m-phenylene terephthalamide	1	46.6	Poly (m-phenylene terephthalamide	1	46.1	Unknown	1	-	-	-	-
	Burnt Umber	1	62.7				Astra Blue Base	1	80.1	Astra Blue Base	1	80.4			
Industrial (7August Day)	Astra Blue Base	1	80.4												
	Carotene	1	76										Terre Verte(green)	1	49.7
	Cadmium Yellow	1	82.7										Polypropylene	1	50.8
Industrial (7August Night)										Pigment Yellow	1	73.4			
Industrial (4August Day)	Carotene	1	69.7				PTFE	1	69.3	Irgalith Blue	1	74.9	Irgalith Blue	1	69.9
Industrial (6August Day)	Carotene	1	60.3				PP	1	59.6						
Urban (21 August Day)	Carbon Black	1	51.8	Sphalerite	1	56.2				Carbon Black	1	67.4			
				Carbon Black	1	67.9									

Table B. 10. (Continued) *Chemical characteristics MNPs in industrial zone with matching ratio > 40% (another materials pigments…).*

Location	Stage1			Stage 2			Stage 3			Stage 4			Stage5		
	Type of MP	Number	Score%	Type of MP	Number	Score%	Type of MP	Number	Score%	Type of MP	Number	Score%	Type of MP	Number	Score%
Urban (21 August Night)							-	-	-				Carbon Black	1	62.17
Urban (22 August Night)							Hematite		58.7				Carbon Black	1	68.4
Urban (17 August Day)	Composite Spectrum		75.2	Irgalith Blue	1	65.4				Irgalith Blue	1	65.9	Hostopen violet	1	70.6
										Pigment Red	1	56.5			
Urban (20 August Day)							Carotene	1	61.9						
Rural (5 September Day)	Cadmium Orange Medium	1	62.5							Carbon Black	1	57.7	Carbon Black	1	67.8
Rural (5 September Night)	Carotene	1	63.9	Nitrazine Yellow		63.1				PTFE	1	54.5			
										Hematite		60.1			
Rural (6 September Day)	Carotene	1	71.7	Carotene	1	73.5	p-(Arylетherketone)	1	58.8						
	Carotene		54	Hematite	2	68.3	Carotene		70.3	Carotene	1	81			
							Carotene		87						
Rural (6 September Night)				Carbon Black	2	68.1/ 66.4	Carbon Black	2	68.8 /67.4	Carbon Black	1	69.7			
Rural (29 August Day)	Carotene		54				Carotene		70.3						
Rural (3 September Day)													Irgalith Blue	1	65.9

Table B. 10. (Continued) *Chemical characteristics MNPs in industrial zone with matching ratio > 40% (another materials pigments…).*

Location	Stage1			Stage 2			Stage 3			Stage 4			Stage5		
	Type of MP	Number	Score%	Type of MP	Number	Score%	Type of MP	Number	Score%	Type of MP	Number	Score%	Type of MP	Number	Score%
Rural (1 January Night)	Sphalerite		73.9	Irgalith Blue		72.9									
Rural (31 Desember Day)							Carotene		70.3						

Table B. 11. *Mass concentration of MNPs regarding mass-based analysis in industrial zone.*

Location	Date	Stage	Type of polymer (µg/m³)								Total Concentration	
			NR	PC	PE	PET	PP	PS	PVC	SBR	∑MNP (µg/m³)	PM* (µg/m³)
Industrial	Day (02.08.2023)	1	0.08189	-	-	-	-	-	-	-	0.08189	10.9576
		2	0.03398	-	-	-	-	-	-	-	0.03398	9.7974
		3	0.03574	-	-	-	-	-	-	-	0.03574	5.0829
		4	0.02640	-	-	-	-	-	-	0.00868	0.03508	2.1731
		5	0.05118	-	-	-	-	-	-	0.29167	0.34284	5.6354
		b	-	-	-	-	-	-	-	1.78887	1.78887	35.1565
	Night (02.08.2023)	1	0.05651	-	-	-	-	-	-	-	0.05651	11.67587
		2	-	-	-	-	-	-	-	-	-	7.67956
		3	-	-	-	-	-	-	-	-	-	3.86740
		4	-	-	-	-	-	-	-	-	-	26.39042
		5	-	-					0.53867	0.04001	0.57868	3.59116
		b	-	-	5.23020	6.27624				0.53801	12.04446	20.92081
	Day (07.08.2023)	1	-	-	1.41436	-	-	-	-	-	1.41436	7.0718
		2	-	-	1.64641	-	-	-	-	-	1.64641	8.2320
		3	-	-	0.81031	-	-	-	-	-	0.81031	4.0516
		4	-	-	-	-	-	-	-	-	-	3.3149
		5	-	-	1.11971	-	-	-	-	-	1.11971	2.7993
		b	-	-	-	-	-	-	-	-	-	24.4936
	Night (07.08.2023)	1	-	-	-	-	-	-	-	-	-	57.21915
		2	-	-	-	-	-	-	-	-	-	5.58011
		3	-	-	-	4.55985	-	-	-	-	4.55985	11.39963
		4	0.00592	-	-	-	-	-	-	-	0.00592	1.47330
		5	0.56745	-	-	-	-	-	-	-	0.56745	49.15285
		b	0.06928	-	3.18232		1.59116		0.79558	0.09801	5.73634	15.91160

- The difference between secondary weight and primary weight of filter

Table B. 12. *Mass concentration of MNPs regarding mass-based analysis in urban zone.*

Location	Date	Stage	Type of polymers (µg/m³)								Concentration	
			NR	PC	PE	PET	PP	PS	PVC	SBR	∑MNP (µg/m³)	PM* (µg/m³)
Urban	Day (21.08.2023)	1	0.01531	-		-	-	-	-	-	0.01531	1.9337
		2	-	-	1.09576	-	-	-	0.21915	-	1.31492	2.1915
		3	0.21303	-	11.55157	-	-	-	-	-	11.76460	46.2063
		4	0.00631	-		-	-	-	-	0.00507	0.01138	1.1050
		5	0.03165	-	0.78821	-	-	-	-	-	0.81987	1.9705
		b		-	8.48619		1.06077		2.12155	0.02842	11.69693	21.2155
	Night (21.08.2023)	1	0.01362	-	-	-	-	-	-	-	0.01362	2.65193
		2	-	-	-	-	-	-	-	-	-	2.76243
		3	-	-	-	-	-	-	-	-	-	3.77532
		4	0.01335		0.58195	-	-	-	-	-	0.59530	1.45488
		5				-	-	-	-	-	-	3.03867
		b	0.40510		9.66851		3.86740			1.13849	15.07950	19.33702
	Day (22.08.2023)	1	-	-	0.23573	-	-	-	-	-	0.23573	0.5893
		2	-	-	0.45580	-	-	-	-	-	0.45580	1.8232
		3	-	-	-	-	-	-	-	-	-	1.2707
		4	-	-	-	-	-	-	-	-	-	0.8287
		5	0.01049		0.49724	-	-	-	-	-	0.50773	2.4862
		b	-	-	-		2.01105		1.00552	0.02694	3.04352	20.1105
	Night (2208.2023)	1	-	-	-	-	-	-	-	-	-	2.28361
		2	-	-	-	-	-	-	-	-	-	3.77532
		3	-	-	-	-	-	-	-	0.00180	0.00180	2.28361
		4	-	-	-	-	-	-	-	-	-	2.19153
		5	-	-	-	-	-	-	-	-	-	2.55985
		b	-	-	4.90608		2.45304	-	-	-	7.35912	24.53039

- The difference between secondary weight and primary weight of filter.

Table B. 13. *Mass concentration of MNPs regarding mass-based analysis in rural zone.*

Location	Date	Stage	Type of polymer (µg/m³)								Concentration	
			NR	PC	PE	PET	PP	PS	PVC	SBR	∑MNP (µg/m³)	PM* (µg/m³)
Rural (summer)	Day (05.09.2023)	1		-	0.14733	-	-	-	-	-	0.14733	0.7366
		2	0.02287	-	0.79190	-	-	-	-	-	0.81476	3.1676
		3	0.00650	-	0.37937	-	-	-	-	-	0.38588	1.8969
		4	-	-		-	-	-	-	-	-	2.2652
		5	-	-	2.12891	-	-	-	-	-	2.12891	5.3223
		b	0.09696	-	6.06262	-	-		1.51565	-	7.67523	15.1565
	Night (05.09.2023)	1	-	-		-	-	0.64899	-	0.67178	1.32077	1.62063
		2	0.01448					0.52389		1.97794	2.51631	2.72560
		3	-	-		-	-	0.86875	-	1.71340	2.58215	2.87293
		4	-	-		-	-	0.07517	-	0.30415	0.37932	1.36280
		5	0.02146					0.62119		2.55306	3.19571	3.35175
		b	0.03198	-	1.88582	3.30018	0.47145	-	-	-	5.68944	9.42910
	Day (06.09.2023)	1	0.04077	-		-	-	-	-	-	0.04077	6.0405
		2	-	-		-	-	-	-	-	-	2.0074
		3	-	-	0.24401	-	-	-	-	-	0.24401	0.9761
		4	0.00314	-	0.18048	-	-	-	-	-	0.18362	0.9024
		5	-	-	0.36832	-	-	-	-	-	0.36832	1.8416
		b	-	-	2.82505	-	-	-	0.70626	-	3.53131	14.1252
	Night (06.09.2023)	1	0.00340	-	-	-	-	-	-	-	0.00340	1.10497
		2	0.00376	-	-	-	-	-	-	-	0.00376	1.06814
		3	0.00848	-	-	-	-	-	-	-	0.00848	2.39411
		4	0.00332	-		-	-	-	-	-	0.00332	1.12339
		5	0.00457	-	0.22099	-	-	-	-	-	0.22556	1.10497
		b		-	-	-	-	-	-	-	-	8.45304
		4		-	-	-	-	0.52384	-	-	0.52384	5.48803
		5	0.02355	-	-	-	-	0.29680	-	0.68595	1.00631	4.19890
		b	-	-	-	-	-	1.84909	-	10.64041	10.64041	11.34438

Table B. 13. **(Continued)** *Mass concentration of MNPs regarding mass-based analysis in rural zone.*

Location	Date	Stage	Type of polymer (µg/m³)								Concentration	
			NR	PC	PE	PET	PP	PS	PVC	SBR	∑MNP (µg/m³)	PM* (µg/m³)
Rural (winter)	Day (01.01.2024)	1	0.01721	-	-	-	-	-	-	-	0.017205	1.988950
		2		-	-	-	-	0.13820	-	1.81159	1.94979	3.86740
		3	0.01671	-	-	-	-	0.01092	-	-	0.02764	2.22836
		4		-	-	-	-	0.52384	-	-	0.52384	5.48803
		5	0.02355	-	-	-	-	0.29680	-	0.68595	1.00631	4.19890
		b	-	-	-	-	-	1.84909	-	10.64041	10.64041	11.34438
	Night (01.01.2024)	1	-	-	-	-	-	0.01518	-	0.24001	0.25520	2.08103
		2	-	-	-	-	-	-	-	-	0.00000	3.51750
		3	0.01105	-	-	-	-	0.01148	-	0.15571	0.17824	3.05709
		4	0.01209	-	-	-	-	-	-		0.01209	3.77532
		5	0.02036	-	-	-	-	0.10590	-	1.17459	1.30085	5.69061
		b		-	-	-	-	-	-	-	-	10.99448

- The difference between secondary weight and primary weight of filter.

Table B. 14. *Mass concentration of MNPs regarding mass-based analysis based on PM_{10} in three zones.*

Location	Date	Stage	Type of polymers (µg/m³)								Concentration	
			NR	PC	PE	PET	PP	PS	PVC	SBR	∑MNP (µg/m³)	PM* (µg/m³)
Industrial	High PM_{10} (04.08.2023)	1	-	-	-	2.8425	-		0.4061	0.00004	3.2487	8.122
		2	-	-	-	7.3297	-		-	-	7.3297	29.319
		3	-	-	-		-	0.2565	-	0.00010	0.2566	19.282
		4	0.0090	-	-		-	-	-	-	0.0090	3.315
		5	-	-	-	1.6519	-	-	0.2753	-	1.9273	5.506
		b	0.0875		8.6050	12.0470	-	-	1.7210	0.00017	22.4606	34.420
	Low PM_{10} (06.08.2023)	1	-	-	-	-	-	-	-	-	0.0000	6.317
		2	0.0137	-	-	-	-	-	0.3269	-	0.3405	6.538
		3	-	-	-	-	-	-	-	-	-	3.628
		4	-	-	-	-	-	-	-	-	-	39.042
		5	-	-	-	-	-	-	-	0.00003	0.00003	5.414
		b	0.1055	-	11.7219	14.0663	-	-	4.6888		30.5824	46.888
Urban	High PM_{10} (17.08.2023)	1	0.0127	-	-	-	-	-	-	-	0.0127	2.615
		2	0.0081	-	-	-	-	-	-	-	0.0081	3.241
		3	0.0052	-	-	-	-	-	-	-	0.0052	1.971
		4	-	-	-	-	-	-	-	-	-	3.646
		5	-	-	-	-	-	-	-	-	-	4.917
		b	-	-	3.6501	-	0.9125	-	-	-	4.5626	18.250
	Low PM_{10} (20.08.2023)	1	0.0116	-	-	-	-	-	-	-	0.0116	4.088
		2	-	-	-	-	-	-	-	-	-	5.046
		3	0.0059	-	-	-	-	-	0.0985	-	0.1045	1.971
		4	0.0030	-	-	-	-	-	-	-	0.0030	0.902
		5	-	-	-	-	-	-	-	-	-	2.762
		b	-	-	4.4494	-	2.2247	-	-	-	6.6740	22.247
Rural	High PM_{10} (29.08.2023)	1	-	-	-	-		-	-	-	-	3.886
		2	-	-	-	-		-	-	-	-	9.779
		3	-	-	-	-		-	-	-	-	3.573
		4	0.0051	-	-	-		-	-	-	0.0051	1.897
		5	-	-	-	2.3020		-	-	-	2.3020	4.604
		b	-	-	9.0976	-	4.5488	-	-	-	13.6464	22.744
	Low PM_{10} (03.09.2023)	1	0.00001	-	-	-		-	-	-	0.00001	1.713
		2	-	-	-	-		-	-	-	-	4.107
		3	-	-	-	-		-	-	-	-	1.805
		4	-	-	-	-		-	-	-	-	2.044
		5	-	-	-	-		-	-	-	-	3.573
		b	0.0426	-	3.4291	-	1.7145	-	-	-	5.1862	17.145

- The difference between secondary weight and primary weight of filter.

Table B. 15. *Mass concentration of NPs in back-up stage.*

Location	Date	Type of polymers (µg/m³)								Total Concentration	
		NR	PC	PE	PET	PP	PS	PVC	SBR	∑MNP (µg/m³)	PM* (µg/m³)
Industrial	25.07.2023	-	-	5.5248		2.20994	-	1.10497		8.8398	22.099
	26.07.2023	-	-	8.3333	1.6667	5	-	1.66667	0.19424	16.860	33.333
	27.07.2023	-	-		-	-	-	1.66667	0.41576	2.0824	33.333
	28.07.2023	0.1654	-	7.1381	-	-	-	1.78453	0.01070	9.0988	17.845
	29.07.2023	0.1691	-	-	-	-	0.18876	4.98711	1.12636	6.4713	24.935
	30.07.2023	0.1851	-	-	-	-	-	2.21547	-	2.4006	22.154
	31.07.2023	-	-	-	10.475	-	-	-	-	10.475	34.917
	01.08.2023	-	-	7.3885	11.082	12.9300	-	1.84715	-	33.248	36.942
	02.08.2023	-	-	-	-	-	-	-	1.78887	1.7888	35.156
	03.08.2023	0.0862	-	-	-	-	-	-	0.53154	0.6178	24.769
	04.08.2023	0.0875	-	8.6050	12.047	-	-	1.7210	0.00017	22.460	34.420
	05.08.2023	0.1192	0.0493	5.9852		10.4742	-	1.49632	0.23132	18.355	29.926
	06.08.2023	0.1055	-	11.721	14.066		-	4.6888	-	30.582	46.888
	07.08.2023	-	-				-	-	-	-	24.493
	08.08.2023	0.3070	-	8.4272		4.21363	-	4.21363	0.53410	17.695	42.136
Urban	09.08.2023	0.0847	-		5.2578	-	-	1.05157	-	6.3942	21.031
	10.08.2023	0.0107	-	0.4751		-	-	0.11878	-	0.6046	2.3757
	11.08.2023	-	-	3.9779		-	-	0.99448	-	4.9724	19.889
	12.08.2023	0.0577	-	3.1602	3.1602	7.11050	-	-	-	13.488	15.801
	13.08.2023	0.0399	-	3.5506	-	1.77532	-	-	-	5.3659	17.753
	14.08.2023	0.1646	-	11.91160	-	5.95580	-	-	0.37125	18.403	29.779
	15.08.2023	0.1222	-	5.3885	-	2.69429	-	1.34714		9.5523	26.942
	16.08.2023	-	-	-	-		-	-	0.21708	0.2171	28.287
	17.08.2023	-	-	3.6501	-	0.9125	-	-		4.5626	18.250

Table B. 15. (Continued) *Mass concentration of NPs in back-up stage.*

Location	Date	Type of polymers (µg/m^3)								Total Concentration	
		NR	PC	PE	PET	PP	PS	PVC	SBR	∑MNP (µg/m^3)	PM* (µg/m^3)
Rural	18.08.2023	0.02720	-	4.53775	-	2.82873	-	1.134438	0.01891	8.5470	11.3444
	19.08.2023	-	-	5.11602	-	8.95304	-	-	-	14.0691	25.5801
	20.08.2023	-	-	4.4494	-	2.2247	-	-	-	6.6740	22.247
	21.08.2023	-	-	8.48619	-	1.06077	-	2.12155	0.02842	11.6969	21.2155
	22.08.2023	-	-		-	2.01105	-	1.00552	0.02694	3.04352	20.1105
	23.08.2023	-	-	5.20810	-	-	0.02003	-	0.51491	5.7430	26.0405
	24.08.2023	0.12314	-	9.55801	-	19.11602	-	-	0.07390	28.8711	47.7901
	25.08.2023	0.07002	-	6.34899	-	-	-	-	-	6.4190	25.3959
	26.08.2023	0.05396	-		-	-	-	-	-	0.0540	24.8250
	27.08.2023	0.08660	-	4.91713	-	1.22928	-	-	-	6.2330	24.5856
	28.08.2023	0.07651	-	7.14180	-	3.57090	-	-	-	10.7892	35.7090
	29.08.2023	-	-	9.0976	-	4.5488	-	-	-	13.6464	22.744
	30.08.2023	-	-		-	2.97974	-	1.48987	-	4.4696	29.7974
	31.08.2023	-	-	5.75506	-	2.30203	-	-	-	8.0571	23.0203
	01.09.2023	0.09881	-		-		-	1.37293	-	1.4717	27.4586
	02.09.2023	0.05500	-	4.55341	-	1.82136	-	0.91068	0.25584	7.5963	18.2136
	03.09.2023	0.0426	-	3.4291	-	1.7145	-	-		5.1862	17.145
	04.09.2023	-	-		-	-	0.002080	-	0.10434	0.1064	11.6206
	05.09.2023	0.09696	-	6.06262	-	-	-	1.51565	-	7.67523	15.1565
	06.09.2023	-	-	2.82505	-	-	-	0.70626	-	3.53131	14.1252
	07.09.2023	-	-		-	-	-		-	-	14.6593

• The difference between secondary weight and primary weight of filter.

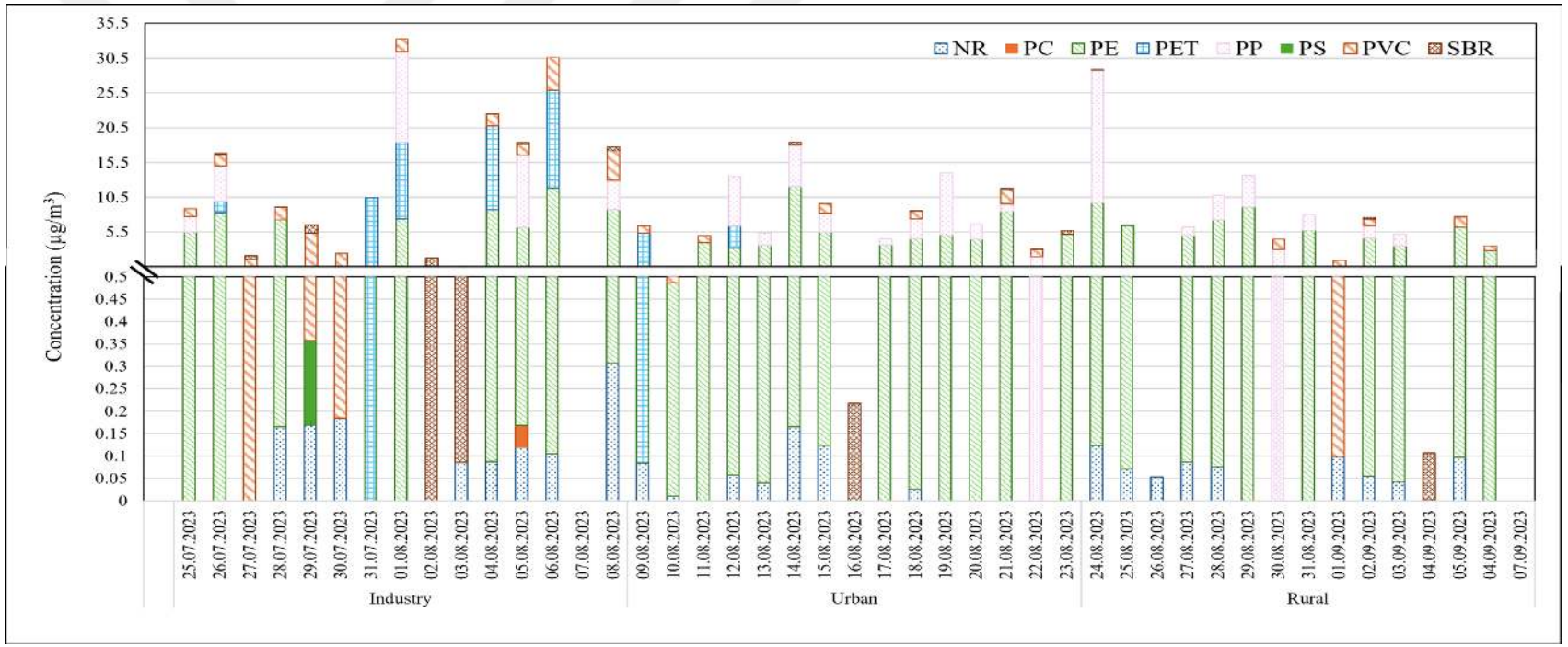

Figure B. 15. *Comparison spatial mass concentration of MNPs nano-fraction stage.*

CURRICULUM VITAE

ORCID ID: **0000-0002-7756-1821**

Name Surname: **Parisa AKBARI DANA**

Foreign Language: **English**

Education and Professional Background:

Eskişehir Technical University — Türkiye, Eskişehir

Ph.D. in Environmental Engineering, GPA:(3.77/4) — Jul 2019-June 2025

Thesis title: "Analysis Methodology, Distribution, and Health Risk Assessment of Size Segregated Airborne Micro(nano)plastics".

Islamic Azad University, Tehran Science & Research Branch — Iran, Tehran

M.Sc. in Health, Safety and Environment, GPA: (18.38/20) — Sep 2014 – Jul 2017

Thesis title: "Assessment of safety climate hospital based on Sammer's Model".

Shahid Beheshti Medical Sciences and Health Services — Iran, Tehran

B.Sc. in Occupational Health Engineering GPA: (17.92/20) — Sep 2003 – Mar 2007

Publications and/or Scientific Activities:

Journal Papers:

- ✓ Akbari Dana P, Gaga O, E, Gedik K., "Micro(nano)plastics in size-segregated atmospheric particles in Eskişehir, Türkiye: Optimization of sampling parameters", Water, Air, & Soil Pollution, 2025, 236(9), 1-18.
- ✓ Gachayzade Z, Akbari Dana P, Mizik E, Gedik K, Çelik Y, Zehra Yiğit Avdan, Kadir Gedik. "Matrix preparation and workflow for microplastics analysis in soil", Chemosphere, 2025, 376, 144284.
- ✓ Akbari Dana P, Gaga O, E, Gedik K. "Analytical challenges and strategies for particle-based analysis of airborne micro(nano)plastics in size-fractionated samples using

microscopy, SEM/EDX, and Raman spectroscopy", Analytical Chemistry, 2024, 96, 20622−20634.

- ✓ Jahangiri K, Akbari Dana P, Borgheipour H, Tehrani GM. Hospital safety climate assessment toward attitude's nurses based on sammer's model case study: an academic general and a specialized hospital in Tehran (Iran). Iranian Journal of Health, Safety and Environment, 2020, 7(1), 1384-1394.

Projects:

- ✓ Microplastic Pollution from Air to Soil: Investigation of Behavior, Transport, Vectorial Interaction with Organic Pollutants and Genotoxic Effects. The Scientific and Technological Research Council of Türkiye (TÜBİTAK) (No:121Y142), Scholarship, 2021-2024.
- ✓ Evaluation of Health Risks Due to Inhalation Exposure to Heavy Metal-Loaded Microplastics with an In Vitro Approach. Eskişehir Technical University (Scientific Research Project: 21GAP088), Scholarship, 2021-2023.
- ✓ Development of a filter analysis method for atmospheric microplastics sampled with a cascade separator. Eskişehir Technical University (Scientific Research Project: 24ADP056), Scholarship, 2024-Continuing.
- ✓ Investigation of micro(nano)plastics in nasal solutions containing sea/ocean water in their formulation. Karamanoğlu Mehmetbey University (Scientific Research Project: 43-M-24), Researcher, 2024-Continuing.
- ✓ Evaluation of Microplastic Releases of Different Toothbrush Brands During Brushing. İstanbul Medipol University (Scientific Research Project), Researcher, 2024-Continuing.

Book Chapters:

- ✓ Gedik K, Dogan N, Akbari Dana P, Gachayzade Z. Bölüm 1: Antroposen çağın kirleticileri, Mikroplastiklerden Nanoplastiklere, PLASTİK KİRLETİCİLER (Chapter 1: Pollutants of the Anthropocene, From Microplastics to Nanoplastics, PLASTIC POLLUTANTS). 2023, pages 1-20.
- ✓ Akbari Dana P, Gachayzade Z, Gedik K. The fixtures of life: Polymers, plastics, microplastics, nanoplastics. In: Toygar H, Balcı N, eds. Exposure to Microplastics in Life and Dentistry. 1st ed. Ankara: Türkiye Klinikleri; 2024. p.1-11.

Congress or Conferences:

- ✓ Akbari Dana P, Gaga O, E, Gedik K. "What to choose when analyzing airborne micro(nano)plastics: Mass- or particle-based analytical techniques?", oral

presentation, the 6th International Environmental Chemistry Congress, (5 to 8 November 2024), Trabzon, Türkiye.

- ✓ Akbari Dana P, Şensoy Gün B, Gurbanov R, Gaga E, Gedik K. "A Methodological Approach for The Direct Analysis of Airborne Plastic Particles by Pyrolysis-GC/MS", oral presentation, 7th International Agriculture, Environment and Health Congress, (30 May to 1 June 2024), Bursa, Türkiye.
- ✓ Çam H, Gachayzade Z, Akbari Dana P, Gedik K." Effect of Household Cleaning Products on Microplastic Morphology and Structure", oral presentation, 7th International Agriculture, Environment and Health Congress, (30 May to 1 June 2024), Bursa, Türkiye.
- ✓ Şimşek M, Gachayzade Z, Akbari Dana P, Gedik K." Could Faucet Aerators Indicate Microplastics in Drinking Water?", oral presentation, 7th International Agriculture, Environment and Health Congress. (30 May to 1 June 2024), Bursa, Türkiye.
- ✓ Akbari Dana P, Gaga O, E, Gedik K. "Insights from microscopy to spectroscopy: Size-segregated analysis of airborne microplastics (<10 µm)", oral presentation, 2nd International Forum on Environmental Science and Applications, (April 11-13, 2024), in Munich, Germany.
- ✓ Akbari Dana P, Gaga O, E, Gedik K. "Sample Pretreatment to Determine Inhalable Microplastics in Atmospheric Size Segregated Particles (<10 µm)", oral presentation, the 5th International Environmental Chemistry Congress, (30 October to 2 November 2023), Antalya, Türkiye.
- ✓ Akbari Dana P, Gaga O, E, Selimoğlu G, Gedik K. "Performance of Collection Substrates for Airborne Microplastics (<10 µm) in a Cascade Impactor", oral presentation, the 5th International Environmental Chemistry Congress, (30 October to 2 November 2023), Antalya, Türkiye.
- ✓ Gachayzade Z, Akbari Dana P, Mizik E, Gedik K, Avdan Z. "Microplastic Analysis in Soil: Basis for Establishing an Operating Procedure", oral presentation, the 5th International Environmental Chemistry Congress, (30 October to 2 November 2023), Antalya, Türkiye.
- ✓ Öztürk Ç, Akbari Dana P, Gachayzade Z, Balcı N, Aksak N, Toygar H, Gedik K. "Evaluation of Microplastic Releases by Brushing Different Toothbrush Brands", oral presentation, Turkish Society of Periodontology 52nd Scientific Congress and 30th Scientific Symposium, (21 to 23 September 2023), İzmir, Türkiye.

Awards:

- ✓ The São Paulo School of Advanced Sciences has accepted my candidacy for participation in the Emerging Pollutants event, a highly competitive program that received a total of 214 applications from 35 different countries.

- ✓ Top student in Master level in Islamic Azad university- Tehran Science & Research Branch, Iran (2016).
- ✓ Full tuition waiver scholarship in Bachelor from Health in Shahid Beheshti Medical Sciences and Health Services, Iran.
- ✓ Top student in Bachelor level, Awarded by the Minister of Health in Shahid Beheshti Medical Sciences and Health Services (National University of Iran) in May 2009.
- ✓ Top student in Bachelor level, Awarded by the Head of Health school in Faculty Health of Shahid Beheshti Medical Sciences and Health Services (National University of Iran) in November 2008.